A MECHANISTIC MODEL FOR CARBON STEEL CORROSION RATE IN AQUEOUS CARBONATED SOLUTION OF ACTIVATED MDEA AND ACTIVATED DEA

LUBNA GHALIB ABDULKHALEQ

FACULTY OF ENGINEERING
UNIVERSITY OF MALAYA
KUALA LUMPUR

2016

A MECHANISTIC MODEL FOR CARBON STEEL CORROSION RATE IN AQUEOUS CARBONATED SOLUTION OF ACTIVATED MDEA AND ACTIVATED DEA

LUBNA GHALIB ABDULKHALEQ

THESIS SUBMITTED IN FULFILLMENT
OF THE REQUIREMENTS
FOR THE DEGREE OF DOCTOR OF
PHILOSOPHY

FACULTY OF ENGINEERING
UNIVERSITY OF MALAYA
KUALA LUMPUR

2016

UNIVERSITY OF MALAYA

ORIGINAL LITERARY WORK DECLARATION

Name of Candidate: LUBNA GHALIB ABDULKHALEQ

Registration/Matric No: KHA120124

Name of Degree: Doctor of Philosophy

Title of Thesis: A MECHANISTIC MODEL FOR CARBON STEEL CORROSION RATE IN AQUEOUS CARBONATED SOLUTION OF ACTIVATED MDEA AND ACTIVATED DEA

Field of Study: Chemical Reaction Engineering

I do solemnly and sincerely declare that:

(1) I am the sole author/writer of this Work;
(2) This Work is original;
(3) Any use of any work in which copyright exists was done by way of fair dealing and for permitted purposes and any excerpt or extract from, or reference to or reproduction of any copyright work has been disclosed expressly and sufficiently and the title of the Work and its authorship have been acknowledged in this Work;
(4) I do not have any actual knowledge nor do I ought reasonably to know that the making of this work constitutes an infringement of any copyright work;
(5) I hereby assign all and every rights in the copyright to this Work to the University of Malaya ("UM"), who henceforth shall be owner of the copyright in this Work and that any reproduction or use in any form or by any means whatsoever is prohibited without the written consent of UM having been first had and obtained;
(6) I am fully aware that if in the course of making this Work I have infringed any copyright whether intentionally or otherwise, I may be subject to legal action or any other action as may be determined by UM.

Candidate's Signature Date:

Subscribed and solemnly declared before,

Witness's Signature Date:

Name:

Designation:

ABSTRACT

Corrosion constitutes a major operational difficulty in CO_2 absorption plants using aqueous amine solutions and has a significant impact on the plant's economy. It is a complex phenomenon in which transport, electrochemical and chemical processes occur simultaneously and interactively. It is difficult to control corrosion problems in a cost-effective manner as knowledge of corrosion in this system is limited and inconclusive. Thus, the purpose of this work is to obtain a better understanding of corrosion process in an aqueous activated amine based CO_2 environment.

A mechanistic corrosion model was built using Matlab software, to predict corrosion rate of carbon steel in the carbon dioxide (CO_2) absorption processes using aqueous solutions of activated Methyl-di-ethanolamine and activated Diethanolamine, to identify the oxidizing agents responsible for corrosion reactions when no protective films are present. The developed corrosion model takes into account the effects of fluid flow on the corrosion process. The electrochemical corrosion model takes into account charge transfer and diffusion of oxidizing agents.

This work provides comprehensive information on the corrosion behavior of carbon steel in an aqueous carbonated solution of activated Methyl-di-ethanolamine and activated Diethanolamine systems. The model comprises two main models, i.e. Vapor-liquid equilibrium model and electrochemical corrosion model. The rigorous electrolyte-NonRandom Two Liquid model was built into the model in order to determine the concentrations of chemical species in the bulk solution. The speciation results from electrolyte-nonrandom two liquid equilibrium model were subsequently used for generating polarization curve and predict the corrosion rate taking place at the metal surface.

The direct impact of the important process parameters were investigated by conducting corrosion modeling using electrochemical polarization technique under a wide range of input conditions. Corrosion rates are predicted based on the input data required for model simulation such as solution temperature, CO_2 partial pressure, amine concentration, electrode rotating speed and pipe diameter. The output from the model simulation can be presented as species concentration in the bulk solution, CO_2 loading, corrosion potential, corrosion rate, and polarization curves. Predictions of the present corrosion model were compared to the experimental corrosion data from literature and generally good agreement was achieved.

Simulation results show that the corrosivity order of CO_2 amines in carbon steel was governed mainly by their CO_2 loading; higher CO_2 absorption capacity such absorption led to higher corrosion rate. For activated amine mixtures, the data showed that a reduction in carbon steel corrosion rate of MDEA-PZ system when keeping the total amine concentration at 2 M and varying the activator and the base amine concentrations. However, for DEA-PZ the data showed an increase in carbon steel corrosion rate, the corrosion rates were evaluated under the same operating conditions (CO_2 loading, solution temperature and amine concentration) for both systems. At low CO_2 loading, low solution temperature, and low activator concentration, the order of the corrosivity of the systems is as follows: MDEA-PZ is greater than that of DEA-PZ. Whereas at high conditions of CO_2 loading, solution temperature and activator concentration, the corrosivity ranked is opposite to that of lower conditions.

ABSTRAK

Hakisan merupakan penyumbang utama kepada permasalahan operasi loji penyerapan CO_2 yang menggunakan larutan cecair amina serta memberi kesan ekonomi yang mendalam terhadap loji tersebut. Ia merupakan satu fenomena kompleks yang menyebabkan pengangkutan, elektrokimia dan proses kimia terhasil secara serentak serta interaktif. Kesukaran mengawal hakisan dapat diperhatikan melalui keberkesanannya terhadap penjimatan kos, oleh kerana pengetahuan berkaitan hakisan pada sistem ini terbatas dan kurang meyakinkan. Oleh itu, tujuan penyelidikan ini adalah untuk mendalami proses hakisan di dalam larutan cecair amina yang diaktifkan oleh persekitaran karbon dioksida (CO_2).

Model hakisan mekanik, dibentuk menngunakan perisian MATLAB, bagi meramalkan kadar hakisan keluli karbon di dalam proses penyerapan CO_2 menggunakan larutan cecair Methyl-di-ethanolamine dan Diethanolamine yang diaktifkan. Ini bertujuan mengenalpasti agen oksida yang menyebabkan berlakunya tindakbalas penghakisan terutamanya semasa ketiadaan filem pelindung. Model hakisan yang dibentuk mengambil kira kesan pengaliran cecair terhadap proses hakisan. Model hakisan berlandaskan elektrokimia juga menekankan perubahan terhadap pemindahan dan penyebaran agen pengoksidaan.

Penyelidikan ini memberikan maklumat yang komprehensif terhadap keluli karbon di dalam sistem cecair berkarbonat Methyl-di-ethanolamine dan Diethanolamine yang diaktifkan. Model tersebut terbahagi kepada dua model utama iaitu gabungan gas-cecair (VLE) dan hakisan elektrokimia. Model pengimbang elektrolit - tidak rawak dua cecair dibentuk bersama bagi mngukur kepekatan spesies kimia di dalam larutan pukal. Keputusan spesies yang diperolehi daripada model pengimbang elektrolit - tidak rawak dua cecair akan digunakan untuk menghasilkan lengkungan polarisasi dan meramalkan

kadar hakisan pada permukaan berlogam. Kesan langsung terhadap parameter yang penting di dalam proses ini juga diselidiki melalui pembentukan model hakisan menggunakan teknik polarisasi elektrokimia melibatkan keadaan input yang meluas. Kadar hakisan pula dapat diramalkan berdasarkan maklumat input dari model yang disimulasikan seperti suhu larutan, tekanan separa CO_2, kepekatan amina, putaran kelajuan elektrod dan diameter paip. Bahan yang keluar dari model yang disimulasikan itu merupakan spesies kepekatan di dalam larutan pukal, bebanan CO_2, potensi hakisan, kadar hakisan dan lengkungan polarisasi.

Ramalan model hakisan semasa ini dibandingkan dengan maklumat hakisan yang diperolehi daripada sumber literature dan perbandingan yang memuaskan diperolehi secara keseluruhannya. Selain itu, keputusan simulasi menunjukkan turutan hakisan amina CO_2 di dalam keluli karbon dipengaruhi oleh bebanan CO_2; jika kadar penyerapan CO_2 meningkat, maka kadar hakisan juga akan meningkat. Bagi campuran amina yang diaktifkan pula, penurunan kadar hakisan terhadap keluli karbon bagi sistem MDEA-PZ ditunjukkan melalui data dengan mengekalkan keseluruhan kepekatan amina kepada 2M dan mengubah bahan pengaktif serta dasar kepekatan amina. Walaupun begitu, data bagi DEA-PZ menunjukkan peningkatan kadar hakisan terhadap keluli karbon, sungguhpun kedua-dua penyelidikan dijalankan pada keadaan yang sama (bebanan CO_2, suhu larutan dan kepekatan amina). Pada keadaan bebanan CO_2, suhu larutan dan kepekatan bahan aktif yang rendah, turutan hakisan terhadap sistem tersebut adalah seperti berikut: MDEA-PZ melebihi DEA-PZ. Namun begitu, pada keadaan bebanan CO_2, suhu larutan dan kepekatan bahan aktif yang tinggi pula, kadar hakisan berlainan dapat diperhatikan.

ACKNOWLEDGEMENTS

First of all, I am thankful to Almighty Allah that has given me the strength, patience and courage to complete this work to the best of my ability. I would like to take this opportunity to express my special gratitude and sincere appreciation to my supervisor, Dr. Brahim Si Ali, for his constant concern, patience, guidance and invaluable suggestions. I am thankful to him for his contained patience in helping me to improve the quality of my PhD work. Also, I would like to extend my sincerest thanks to Prof. Dr. Wan Mohd Ashri Bin Wan Daud for his unselfish assistance and continuous support in helping complete the work. This work could not have occurred without his extensive help, for which I am really grateful.

I would like to gratefully acknowledge my parents. They have instilled many admirable qualities in me and laid the good foundation with which I can meet the challenges of my life courageously. They have taught me hard work and self-respect. I would like to thank my husband, Ahmed. He has been very understanding during the whole duration of my studies and has been a constant source of encouragement.

I would like to express my sincere gratitude to my friends Shaukat Mazari, Idris Mohamed, Maha abduljabar for their help, support, friendship and encouragement throughout my stay in Malaysia.

Finally, I gratefully acknowledge the financial support provided by the Ministry of Higher Education & Scientific Research of Iraq. I also would like to thank the Material Engineering Department at University of Mustansiriyah for giving me the wonderful opportunity of pursing my PhD.

TABLE OF CONTENTS

LIST OF FIGURES

LIST OF TABLES

LIST OF SYMBOLS

A_ϕ : Debye-Hückel parameter

A : surface area (cm^2)

a : Activity, or anodic Tafel constant

a : Atomic weight

b : Cathodic Tafel constant

C : Concentration of species (mol/l)

CR : Corrosion rate (mm/year)

d : Solvent density or diameter

D : Dielectric constant or diffusion coefficient of species (m^2/sec)

e : Electron charge (coulombs).

D_i : Diffusion coefficients of the i^{th} species (m^2/Sec)

D_{ref} : Diffusion coefficient at reference state (m^2/Sec)

E : Electrode potential (V)

E^o : standard electrode potential (V)

E_a : Activation energy (kJ/mol)

E_{corr} : Corrosion potential (V)

E_{rev} : Equilibrium potential (or Reversible potential) (V)

F : Faraday’s constant (C/mol)

f : Correction factor of the i^{th} key influencing variable

ΔG^o : Standard change in Gibbs free energy (kJ/mol)

ΔG : Change in Gibbs free energy at non-standard state (kJ/mol)

H : Henry’s constant

ΔH^o : Standard change in enthalpy of formation (kJ/mol)

I : Ionic strength or net current in (A)

i_0 : The exchange current density (A/m^2)
i_a : Anodic current density (A/m^2)
i_c : Cathodic current density (A/m^2)
i_{corr} : Corrosion current density (A/m^2)
i_{lim} ; Limiting current density (A/m^2)
k : Boltzmann constant (J/K) or rate constant (m/s)
k_m : Mass transfer coefficient
K : Equilibrium constant
m : Mass of substance
M : Molarity ($kmol/m^3$) or (mol/liter)
M_S : Solvent molecular weight (kg/kmol)
MW : Molecular weight (kg/kmol)
N_A : Avogadro’s number
N or n : Mole number or number of electrons or flux of species
P : Pressure (kPa)
P^0 : Saturation pressure (vapor pressure) of the solvent mixture
Q : Charge passed (coulombs) or instantaneous reaction rate constant of CO_2 in water
r : Born radius (m)
r_b : Rate of backward reaction
r_f : Rate of forward reaction
R : Universal gas constant (J/K mol)
t : Time
T : Temperature (K) or (° C) as noted
V : Partial molar volume (m^3/mol)
w : Element’s equivalent weight or weight fraction of amine

x : Liquid phase mole fraction

y : Vapor phase mole fraction

Z or z : Absolute value of the ionic charge or the numbers of electrons transferred in the anodic and cathodic reactions.

GREEK LETTERS

α : Transport constant or NRTL non-randomness factor or symmetry factor.

α_{CO_2} : Loading (Mol CO_2/Mol alkalinity)

ß$_a$: Anodic Tafel slope (mV/decade of current density)

ß$_c$: Cathodic Tafel slope (mV/decade of current density)

η : Over-potential (V)

γ : Activity coefficient

ρ : Closest approach parameter of the Pitzer-Debye-Hückel equation or density of the corroding species (g/cm^3).

τ : NRTL interaction parameter (energy parameter)

Ø : Vapor-phase fugacity coefficient

η : The over potential (V)

δ : Diffusion layer thickness

ξ : Specific parameter for solvent

μ : Dynamic viscosity (Ns/m)

ν : Kinematic viscosity

ω : Rotation speed or acentric factor

SUPERSCRIPTS

∞ : Infinite dilution

ex : Excess property

o : Standard state or saturation

* : Equilibrium or excess or activation or asymmetric convention

SUBSCRIPTS

a, a', a" : Anion or anode

b : Bulk

corr : Corrosion

c, c', c" : Cation or cathode

e : Electron

i, j, k : Any species

m,m' : Molecular species or mixed

Me : Metal

mm/yr : Millimeters per year

rev : Reversible

t : Total

w : Water

s : Surface

cm : Critical mixture

rm : Reduced mixture

o : Oxidant

L : Limiting

Sat : Saturation

RA : Racket

ct	:	Charge transfer

CHEMICAL SPECIES

MDEA	:	N, methyl-di-ethanolamine
$MDEAH^+$	:	Protonated MDEA
DEA	:	Diethanolamine
$DEAH^+$	:	Protonated DEA
$DEACOO^-$	:	Diethanolamine-carbamate
PZ	:	Piperazine
PZH^+	:	Protonated piperazine
$PZCOO^-$	:	Piperazine carbamate
H^+PZCOO^-	:	Protonated piperazine carbamate
$PZ(COO^-)_2$	:	Piperazine di-carbamate
H_2O	:	Water
CO_2	:	Carbon dioxide
H_2CO_3	:	Carbonic acid
HCO_3^-	:	Bicarbonate
CO_3^{2-}	:	Carbonate
OH-	:	Hydroxide
H_3O^+	:	Hydronium

CHAPTER 1: INTRODUCTION

1.1 Background

Carbon dioxide (CO_2) is known as a major greenhouse gas released to the atmosphere and its quantity has been increased in the recent years by rapid industrialization and urbanization, enormous number of industrial and anthropogenic activities. Greenhouse gases tend to accumulate in the atmosphere, introducing problems such as: climate change and global warming. This is linked with the tendency of these gases to behave as a heat barrier in the atmosphere that absorbs and reflects heat back to the earth surface, ultimately leading to rapid increase in global average temperature (Wattanaphan, 2012). The main sources of anthropogenic CO_2 emissions are related to generation of flue gases from coal-fired power plants, cement manufacturing plants, and oil refineries. To reduce CO_2 emissions, carbon capture and sequestration (CCS) is considered as an effective strategy and immediate technological solution. CCS techniques are mainly divided into three categories: post-combustion CO_2 capture, pre-combustion CO_2 capture, and oxy-combustion (Figueroa *et al.*, 2008). Post combustion CO_2 capture is primarily applied to sequester CO_2 from flue gases produced from coal-fired power plants. The flue gases after air driven combustion consist of a higher percentage of nitrogen (N_2) and have lower percentages of CO_2 present (< 15%).

Pre-combustion CO_2 capture is mostly applied to gasification processes. A primary fuel is chemically reacted with either steam or oxygen to generate synthesis gas containing mainly hydrogen (H_2), carbon dioxide (CO_2), and trace gases. Later on, the synthesis gas is further processed through a water-gas-shift reaction (WGS) to produce a CO_2/H_2 (40%/55%) rich stream. Since carbon dioxide in the synthesis gas has high partial pressure, it is easy to remove, usually by physical or physical/chemical absorption (Blomen *et al.*, 2009). In oxy-combustion, fossil fuel is burnt in a highlypurified oxygen (O_2) stream, typically produced using cryogenic air separation units (ASU), which results in a very high carbon dioxide concentration flue gas.

The concept of post- combustion CO_2 capture and sequestration has received wide attention from researchers. This concept involves sequestration of CO_2 from flue gas prior to their release into the environment, without affecting the fossil fuel combustion processes and more importantly the utilization of recovered CO_2 in various applications, such as in enhanced oil recovery operations or storing it in depleted oil/gas reservoirs and deep oceans.

There are various ways to recover or capture CO_2 from industrial flue gas. The most practical and promising way is the absorption process using aqueous solutions of alkanolamines, often mentioned as amine treating process. Amine treating process has been applied in gas processing industry for decades to remove acidic impurities such as: CO_2 and hydrogen sulfide (H_2S) from natural gas streams. However, the perspective of applying amine treating process for CO_2 capture from industrial flue gas opens new prospects for practitioners as there is a difference in the operating conditions and compositions of natural gas and industrial flue gas (Soosaiprakasam, 2007).

1.2 CO_2 Absorption Process

An amine treating unit is regarded as an absorption process in which aqueous solutions of alkanolamines are used as an absorbent to separate acid gases, carbon dioxide (CO_2) and hydrogen sulfide (H_2S) from industrial gas streams. The unit is considered essential for many industrial operations including natural gas processing, sweetening of liquefied petroleum gas (LPG), coal gasification, and in the manufacturing of hydrogen and ammonia. The purpose of this unit is to enhance the quality of gas products and avoid operational difficulties that may occur during the gas processing steps. In addition to these industrial applications, the amine treating unit can potentially be used for capturing CO_2, which is the largest contributor to greenhouse gas emissions, from industrial point sources particularly the coal-fired power plants (Kohl & Nielsen, 1997). A generalized process flow diagram for a typical amine-based CO_2 capture unit is shown in Figure 1.1. The main components of this process are the absorber, regenerator, rich-lean heat exchanger, reboiler, cooler and overhead condenser.

The first step in the processing of flue gases produced from power plant is the initial treatment in a direct contact cooler. In this cooler, the initial temperature of the flue gas 100 °C is brought down to around 40 °C to enhance the absorption efficiency. The flue gas is transported with the assistance of a gas blower to the absorber unit to overcome the pressure drop induced by the absorber.

The flue gas stream entering from the bottom of the absorber is counter-currently contacted with the lean alkanolamine solution flowing down from the top of absorber. CO_2 from the gas stream is absorbed into the lean alkanolamine solution through reversible chemical reactions. The treated gas from the absorber top passes through a water wash unit to recover the volatile amine component and eventually is released to the atmosphere while the alkanolamine solution leaves the absorber bottom as rich alkanolamine solution loaded with CO_2. It is then sent through a heat exchanger, where the rich alkanolamine solution is pre-heated by the lean amine solution from the stripper bottom.

The rich solution is then fed to the top of the stripper, where its temperature is further elevated to 100 – 120°C by heat exchange from a stream of hot gaseous mixture that contains water vapour, CO_2, and alkanolamine and are produced from the reboiler. This results in the reversal of the chemical equilibrium between the amine and CO_2. The stripped CO_2 along with water vapors leaves the stripper and enters in the overhead condenser. The condensed water is recycled back to the stripper and the produced CO_2 gas is compressed for transportation and storage purposes. The lean alkanolamine solution is cooled by the heat exchanger to reduce its temperature before reaching the top of the absorber for the next cycle of CO_2 absorption.

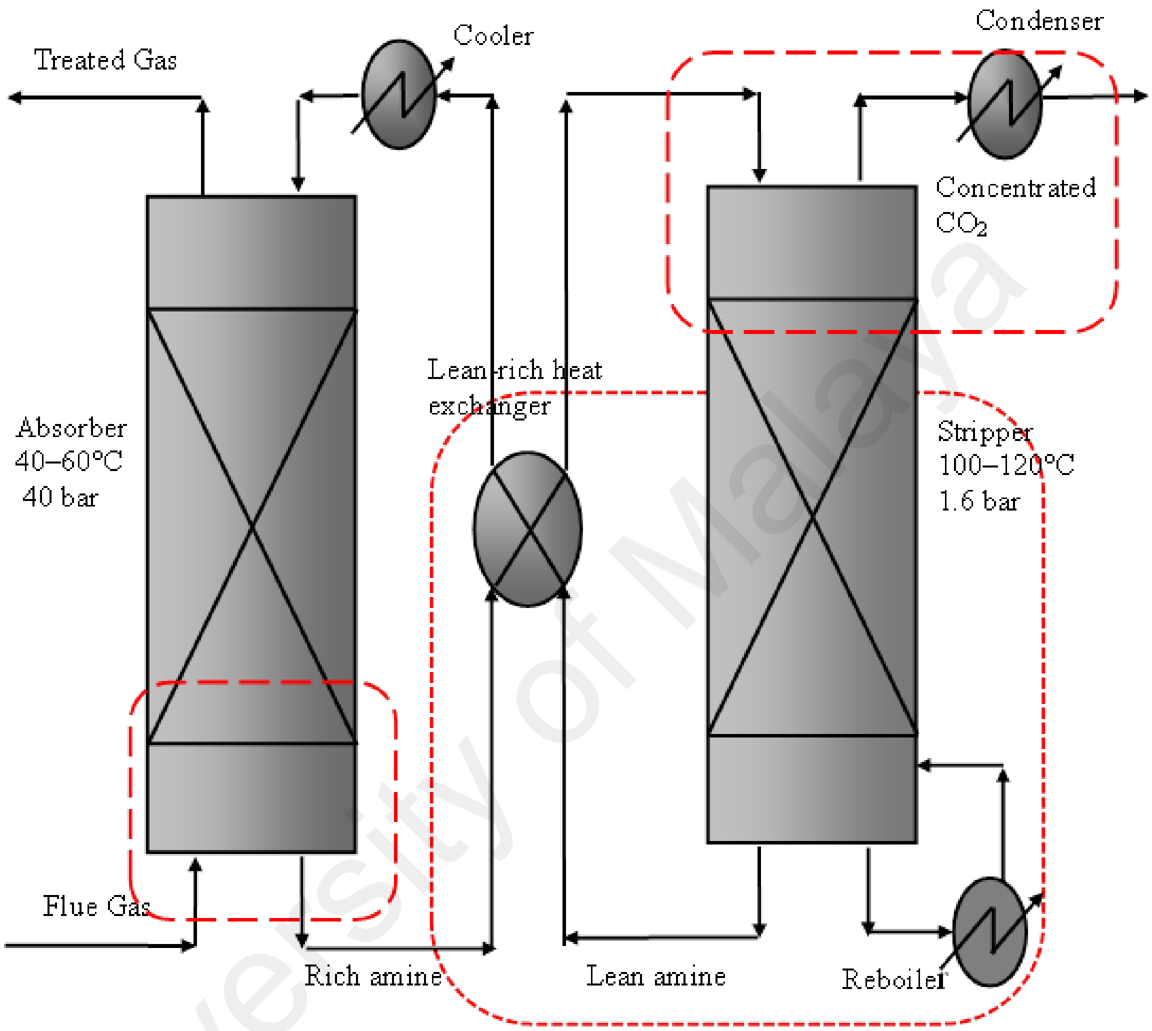

Figure 1.1: A Schematic diagram of the alkanolamine-based acid gas treating plant

1.3 CO_2 Absorption Solvents

Amines chemically react with carbon dioxide (CO_2) to form water soluble compounds; which are able to capture CO_2 even at a low partial pressure within a flue gas. However, capturing capacity of amines are normally equilibrium limited (Mandal *et al.*, 2001). Amines are considered to typically exist in three forms: primary, secondary, and tertiary amines. Alkanolamine solutions are well known to be one of the most important solvents for CO_2 absorption. This is dedicated to the fact that it either provides high reactivity with CO_2 or simply has satisfactory removal capacity (Chakma, 1997). A hydroxyl group in an alkanolamine is considered to have an important influence over the reduction of vapor pressure and in the increase of the water solubility, while an amino group provides the necessary alkalinity in aqueous solution for CO_2 absorption (Kohl & Nielsen, 1997).

These amines are broadly classified into primary (e.g., monoethanolamine (MEA), diglycolamine (DGA)), secondary (e.g., diethanolamine (DEA), diisopropanolamine (DIPA), and piperazine (PZ)), tertiary (e.g., triethanolamine (TEA), methyldiethanolamine (MDEA)), and sterically hindered amines (e.g., 2-amino-2-methyl-1-propanol (AMP), 2–piperidine ethanol (PE)) based on the number of substitutions on the nitrogen atom. Their molecular structures are described in Table 1.1. MEA, DEA, and MDEA have drawn a major commercial interest in the application of gas purification processes (Kohl & Nielsen, 1997).

Among all the above mentioned amines, MEA is the most widely applied solvent and estimates showed that in 1990, its market share in the solvent industry was 40% (DuPart *et al.*, 1993). The main characteristic of MEA are its high reactivity, considerably low cost, and its ability to absorb CO_2 at a low partial pressure, which makes it a suitable option for its application in post-combustion as the percentage of CO_2 in a typical coal-fired flue gas is usually less than 15% (Chakma, 1995).

It is important to mention that even though MEA seems to be an ideal candidate based on a reaction rate point of view, its absorption capacity is usually limited by equilibrium stoichiometry at about 0.5 CO_2 loading (mole of CO_2 per mole of amine), in which carbamate is the final product of the reaction (Mandal *et al.*, 2001; Mofarahi *et al.*, 2008). Moreover, from an energy perspective, MEA is not the most appealing solvent because it requires slightly higher energy consumption in the solvent regeneration process due to higher heat of vaporization compared to other alkanolamines (Chakma, 1997). In addition, if the concentration of MEA is restricted by the equilibrium limit, it directly affects the energy requirement for solvent regeneration, as a lower weight percentage of MEA in an aqueous solution will require higher energy in the solvent regeneration process (Chakma, 1995). Although, MDEA has a lower heat of reaction with CO_2 but the rate of reaction with CO_2 is lower, which increases its capital cost due to the requirement of a larger size of absorber. PZ is a cyclic diamine and is generally used in small concentrations as a promoter or as an activating agent with other amines due to its relatively higher rate of reaction with CO_2. In recent years, there has been several studies on the application of PZ alone as an absorption solvent for CO_2 capture (Bishnoi & Rochelle, 2000; Derks *et al.*, 2006; Kadiwala *et al.*, 2010; Samanta & Bandyopadhyay, 2007). The kinetic studies on CO_2 absorption using concentrated PZ (8 molarity) have revealed its rapid rate of CO_2 absorption, higher resistant to thermal degradation, lower oxidaative degradation rate, and lower equivalent work requirement for stripping compared to 7 molarity MEA (Freeman, Dugas, *et al.*, 2010).

involving PZ, AMP, MEA, MDEA and other solvents have been reported in the literature (Dang, 2000; Dash & Bandyopadhyay, 2013, 2016).

1.4 Activated amines

Another remarkable development in the amine absorption process is the use of so called activated amines. Activated amines are regarded as a conventional amine solvent promoted by the addition of small amounts of “activator”, which are known for their very fast reaction rate with CO_2. Piperazine is one of the most widely used activator to enhance CO_2 absorption rate with amines. Piperazine is a cyclic secondary diamine that is known to be very reactive with CO_2 (Dash & Bandyopadhyay, 2013; Freeman, Davis, *et al.*, 2010; Freeman, Dugas, *et al.*, 2010). In fact, reaction of CO_2 with PZ is about ten times faster than reaction of MEA with CO_2 (Dang & Rochelle, 2003). Therefore, the addition of very small amount PZ to aqueous amine accelerates reaction kinetics considerably. The addition of small amount of PZ to amines does not only accelerate the reaction kinetics but it also increases the CO_2 absorption capacity. The increase in the absorption capacity is attributed to the fact that PZ is a diamine that contains two CO_2- reactive amine groups, which consequently increases the CO_2 absorption capacity per molecule. Piperazine has been known in the gas sweetening industry since the 1980’s when it was first patented by BASF to activate the tertiary amine MDEA. Since then, MDEA/PZ solvent, also called ″a MDEA″ (activated MDEA), became a major solvent used in the ammonia synthesis gas purification and other applications that requires bulk CO_2 removal (Ali & Aroua, 2004; Bishnoi & Rochelle, 2002; Closmann *et al.*, 2009). The second order reaction rate constants for MEA, DEA, TEA, MDEA and PZ applied for CO_2 absorption reaction at 25°C are presented in Table 1.2.

Table 1.2: The overall forward rate constant for CO_2-amine reactions at 25 °C (Chakma, 1997).

Solvent	Reaction rate constant (mol/l·s)
MEA	7600
DEA	1500
TEA	16.8
DEA	9.2
PZ	59000

The comparison of the reaction rate constants indicates that PZ has a rate constant that is several magnitudes greater than MEA reaction constant, which has the highest rate constant amongst other amines (Mondal *et al.*, 2012). Nevertheless, PZ has some limitations and disadvantages such as its limited solubility in aqueous phase (Nainar & Veawab, 2009; Samanta & Bandyopadhyay, 2007). Also, PZ is highly volatile even more volatile than MEA (PZ b.p: 146°C, MEA b.p: 170°C). In terms of cost, PZ is 2 to 3 times more expensive than MEA (Bishnoi & Rochelle, 2000). Due to all the mentioned limitations, the addition of PZ to amines does not usually exceed 8wt.% maximum (Rinprasertmeechai *et al.*, 2012).

1.5 Corrosion in alkanolamine plants

CO_2 absorption process using aqueous alkanolamine solutions can have a number of factors that can cause operational difficulties, such as corrosion, alkanolamine loss, foaming, and plugging of the equipment. However, corrosion is the chief influencing factor from an economic perspective (Kohl & Nielsen, 1997). Corrosion can greatly influence both the economics and safety associated with the CO_2 absorption process. The occurrence of corrosion leads to unscheduled downtime of plants, production losses, reduced equipment life and possibly injury or death (DuPart *et al.*, 1993).

Corrosion is regarded as a serious issue in amine-based gas treating plants that has been reported in the literature, notably when carbon steel is used for plant construction. The corrosion of carbon steel is primarily caused by CO_2 in alkanolamine solutions but not alkanolamine alone or its mixture with water (DuPart *et al.*, 1993).

Severe corrosion was observed in CO_2 absorption plant in both uniform and localized forms and the most common locations for corrosion occurrence were the absorber bottom, rich-lean heat exchanger, regenerator areas (trays and valves) and in some cases reboiler, and associated piping area are also susceptible to serve corrosion (DuPart *et al.*, 1993). Corrosion in the alkanolamine-based CO_2 absorption process can be classified into two categories: 1) wet acid gas corrosion or CO_2 corrosion and 2) alkanolamine solution corrosion. Their brief descriptions will be provided in the following section.

1.5.1 Wet acid gas corrosion

Wet CO_2 corrosion occurs predominantly in the process areas, where CO_2 reacts with carbon steel in an aqueous CO_2 environment with little or no alkanolamine (Kohl & Nielsen, 1997). The absence of alkanolamine makes the solution of CO_2 and water highly acidic which is highly corrosive. As illustrated in Figure 1.1, the wet acid gas corrosion occurs in the overhead sections of the regenerator and at the bottom of the absorber in situations where feed gas is water saturated (Kohl & Nielsen, 1997). This type of corrosion can be minimized by spraying or wetting the surface of the regenerator top with alkanolamine to increase the pH. Such alkanolamine wash should be ensured to have a result of 0.5 wt.% of alkanolamine in the reflux condensed water (Kohl & Nielsen, 1997). The absorber bottom can also be protected from wet acid gas corrosion by wetting the wall of the absorber with alkanolamine. This can be achieved effectively by immersing the inlet gas distributor in the alkanolamine solution. Drilling weep holes around the perimeter of the bottom tray support ring would be an alternative solution and far better than to submerged gas distributor since it avoids the entrainment of gas in the rich alkanolamine solution. In cases, where the CO_2 is the only acid gas, the bottom tray of the absorber made of carbon steel will corrode and this will propagate to the upper trays as well. This problem can be solved by using stainless steel trays (Najumudeen, 2012).

1.5.2 Alkanolamine solution corrosion

Pure alkanolamines and aqueous alkanolamine solutions are not corrosive. However, when alkanolamines contain a certain amount of CO_2, they have the tendency to become corrosive (Kohl & Nielsen, 1997). This type of corrosion is called alkanolamine solution corrosion. As illustrated in Figure 1.1, alkanolamine solution corrosion occurs predominantly in the piping sections of the rich solution from the bottom of the absorber to the regenerator, the rich alkanolamine side of the lean-rich heat exchanger, and the hot bottom part of the regenerator.

1.6 Factors affecting corrosion

Corrosiveness of the amine solutions loaded with CO_2 depends on a number of factors, such as: type and concentration of alkanolamine solution, higher temperature in the regenerator, oxygen ingression, alkanolamine degradation products, high CO_2 loading, and solution contamination. Apart from these described issues, plant design, plant metallurgy, poor operating practices, and improper fabrication can also lead to severe corrosion (Kohl & Nielsen, 1997). In the following section, influence of several parameters will be discussed in detail.

1.6.1 Effect of CO_2 loading or CO_2 partial pressure

CO_2 loading plays an important role in the corrosiveness of aqueous amine-CO_2 system. The corrosion rates are seen to increase with the increase of CO_2 loading in the amine solution. Because of the increase in CO_2 loading, the direct reduction of bicarbonates also increases due to the increase in HCO_3^- and H^+ ion concentration in the solution. This is supported by the fact that the rich amine (high loading) solutions are more corrosive than the lean amine (low loading) solution (Kohl & Nielsen, 1997). de Waard & Milliams (1975) studied the effect of CO_2 partial pressure on steel under varying conditions of pressure and temperature. They reported that the corrosion rate increases proportionally with P_{CO2} raised to the power of 0.67. Similar power laws between corrosion rates and P_{CO2} were reported in another study with the exponent ranging from 0.5 to 0.8 (Feng *et al.*, 2012).

1.6.2 Effect of solution temperature

Temperature has a significant impact on corrosion as higher temperature tends to increase the rate of corrosion (DuPart *et al.*, 1991; Helle, 1995; Keller *et al.*, 1992; Veawab *et al.*, 1999). As a general rule, an increase in the solution temperature increases all electrochemical and chemical processes involved in the amine solution by increasing reaction rates and mass transport. Because the operating temperature in amine treating plants varies from 40 to as high as 120 °C, a great variety of corrosion rates can be found throughout the plant.

1.6.3 Effect of amine concentration

The most important factor that affects the corrosion rate is the concentration of amine solution. In general, an increase in the amine concentration results in an increase in corrosion rate (Chakma & Meisen, 1986; DuPart *et al.*, 1991; Veawab *et al.*, 1999). According to Tanthapanichakoon & Veawab (2003), the industry preferred to use a high amine concentration rather than lower one concentration of amine. The reason for using higher amine concentration is justified by energy saving. Several investigators offered recommendations for the amine concentrations that keep the corrosion within acceptable limits.

1.6.4 Effect of solution velocity

The solution velocity affects the corrosiveness of the amine solution by increasing the transfer of oxidizing agents between the metal surface and the carbonated solution. Where, there is no evidence of film formation, the corrosion rate is completely controlled by the solution velocity (Videm & Dugstad, 1989). While in the presence of corrosion inhibitor or corrosion product formed, the solution velocity may remove the film leading to an increase in corrosion rate (Nešić, 2007). However, as the main corrosion resistance in the presence of a protective film is not only due to the species transfer but also to the film layer itself, thus the effect of flow is not as great as in the condition without film formation.

1.7 Mechanism of solution corrosion

1.7.1 Wet CO_2 corrosion mechanism

When CO_2 is dissolved in water to form carbonic acid (H_2CO_3) (reaction (1.1), which, in turn, ionizes partially to form hydrogen ion (H^+) and bicarbonate on (HCO_3^-) (reaction (1.2) (Nešić *et al.*, 2002; Nyborg, 2002).

$$\mathrm{CO_2 + H_2O \rightleftharpoons H_2CO_3} \tag{1.1}$$

$$\mathrm{H_2CO_3 \rightleftharpoons H^+ + HCO_3^-} \tag{1.2}$$

The increase in H^+ ions plays a major role in the wet CO_2 corrosion of carbon steel, where the H^+ accepts electrons from iron (Fe), thereby oxidizing it to ferrous ions (Fe^{2+}) and forming hydrogen (H_2) as expressed in reaction (1.3).

$$\mathrm{2H^+ + Fe \rightarrow Fe^{2+} + H_2} \tag{1.3}$$

At a pH values higher than 4, bicarbonate ions are further reduced to carbonate ions (CO_3^{2-}) thereby producing more hydrogen ions and increasing the corrosion rate Reaction (1.4) (Nesic *et al.*, 2001).

$$\mathrm{HCO_3^- \rightleftharpoons CO_3^{2-} + H^+} \tag{1.4}$$

There will be an increase in the corrosion rate with the increase in temperature and CO_2 partial pressure following this mechanism (Kohl & Nielsen, 1997).

1.7.2 Alkanolamine-CO_2 corrosion mechanism

The mechanism of alkanolamine solution corrosion differs from the mechanism of wet CO_2 corrosion and is yet not fully understood. A number of researchers have speculated about the mechanism responsible for this type of corrosion. Riesenfeld & Blohm, (1950) were the first to suggest that an evolution of acid gases from rich amine solutions contribute to corrosion. CO_2 can react directly with an iron surface in the presence of water to form iron carbonate ($FeCO_3$) as shown below.

$$\mathrm{Fe + CO_2 + H_2O \rightarrow FeCO_3 + H_2} \tag{1.5}$$

Kosseim et al. (1984) suggested that corrosion mechanism involves the release of the proton from the alkanolamine solution needed for carbon steel corrosion reactions (1.6) and (1.7).

$$\mathrm{CO_2 + R_3N + H_2O \rightleftharpoons R_3NH^+ + HCO_3^-} \tag{1.6}$$

$$\mathrm{CO_2 + 2R_2NH \rightleftharpoons R_2NH_2^+ + R_2NCO_2^-} \tag{1.7}$$

Alkanolamines ions ($R_2NH_2^+$ and R_3NH^+) are acidic in nature and have the ability to provide protons for the corrosion reaction. The corroding carbon steel will react with the most plentiful acid in the solution. In alkanolamine solutions, the numbers of the protonated ions are higher compared to the hydrogen ions. Thus, the chemical reaction between carbon steel and protonated alkanolamine can be expressed in the reactions (1.8) and (1.9).

$$\mathrm{Fe + 2R_3NH^+ \rightleftharpoons Fe^{+2} + H_2 + 2R_3N} \tag{1.8}$$

$$\mathrm{Fe + 2R_2NH_2^+ \rightleftharpoons Fe^{+2} + H_2 + 2R_2NH} \tag{1.9}$$

Generally, it is suggested that the corrosion rate will increase with the corresponding increase in the concentration of protonated amine as expressed in the reaction (1.8) and (1.9). Moreover, it is considered that richer solutions have higher corrosive potential compared to lean solution, provided the other parameters are equal (Kohl & Nielsen, 1997). However, (Austgen *et al.*, 1991) had a different view about the corrosion mechanism of alkanolamine solutions. They reported that carbamate ions in the solutions are responsible for iron corrosion. (DuPart *et al.*, 1993) suggested carbamate ions could be one of the oxidizing agents because tertiary alkanolamine solutions do not form carbamate ions and are reported to be less corrosive than primary and secondary alkanolamine solutions. Although there are different views regarding the way in which carbon steel corrodes in amine service, further studies are needed to identify the corrosion mechanism in these systems.

Veawb & Aroonwilas, (2002) developed a mechanistic model to identify major oxidizing agents in MEA-based CO_2 absorption process. They concluded that HCO_3^- and H_2O are the major oxidizing agents not the H_3O^+ ions. Same oxidizing agents are reported by (Benamor & Al-Marri, 2014) in the aqueous DEA-based CO_2 absorption process. (Choi *et al.*, 2012) suggested that $MDEAH^+$ and HCO_3^- ions are stronger oxidizing agents than H_2O and H_3O^+ ions in the MDEA-based CO_2 absorption process. This also confirmed by (Duan *et al.*, 2013) when they studied the effects of all oxidizing agents in aqueous solution of MDEA-CO_2 system to understand general mechanism of carbon steel. They concluded that the contribution of H_2O as an oxidizing agent is low for this high pH condition and the dominant cathodic reactions in the system are HCO_3^- reduction and $MDEAH^+$ reduction reactions.

1.8 Plant Experiences

Plant experiences with respect to corrosion problems have been reported in the literature (Dingman *et al.*, 1966; Krawczyk *et al.*, 1984; Russell *et al.*, 1999; Smith & Younger, 1972; Williams & Leckie, 1968). As summarized in Table 1.3 a variety of solvents, such as: MEA, DEA, MDEA, and sulfinol, have been used to sequester CO_2 from natural gas. Uniform corrosion was detected throughout the entire plant, while localized corrosion, such as pitting and erosion corrosion, were reported at the bottom of the absorber by (DuPart *et al.*, 1993) and stress corrosion cracking (SCC) was reported by Safruddin (2000) in both the absorber and regenerator (Figure 1.1). Common corrosion mitigation methods include modification of process and equipment design, use of corrosion inhibitors, use of alternative solvents that are less corrosive, use of corrosion resistant materials, and application of chemical passivation onto the process equipment and piping made of steel before plant operation. In most cases, a combination of two or more of these methods are applied (Najumudeen, 2012).

Table 1.3: Summary of plant experiences on corrosion in the acid treating plants (Najumudeen, 2012)

Reference	Plant	Acid gas	Solvent	Corrosion detected	Corrosion mitigation
Rodriguez and Edwards (1999)	Acid gas treating plant (natural gas processing)	CO_2	DEA - MDEA blend	* Corrosion rate (50 – 60 mpy) in the lean side of the lean-rich heat exchanger	* Addition of sulfur-based corrosion inhibitor (reduced corrosion rate to less than 5 mpy)
DeHart et al. (1999)	Acid gas treating plant (CO_2 recovery plant)	3% CO_2	30% MEA	* Uniform and galvanic corrosion found in the bottom of the absorber and in the regenerator	* Hot solvent with copper based corrosion Inhibitor was re-circulated for 16 hours before the plant operation for passive film formation.
Veldman (2000)	Acid gas treating plant (natural gas processing)	25% CO_2	Sulfinol	* Heavy $FeCO_3$ deposition in heat Exchanger * Iron oxide (FeO) and hematite (Fe_2O_3) deposition	* Injection of 2 to 4 L/d of oxygen scavenging inhibitors (reduced Fe^{2+} content from 50 to 5 ppm)
		Mainly H_2S	DEA	* Iron sulphide (FeS) fouling and reboiler corrosion	* Injection of 0.5 L/d of corrosion inhibitor
Sutopo and Safruddin (2000)	Acid gas treating plant (natural gas treating)	5.88 to 8% CO_2 and trac of H_2S	MEA and later Formulated MDEA	* Stress Corrosion Cracking (SCC) with MEA * Erosion corrosion with MDEA – Type A	* MEA was replaced with MDEA Type-A and then to MDEA Type-B to avoid SCC and erosion corrosion, respectively.

Table 1.3 (continued) : Summary of plant experiences on corrosion in the acid treating plants (Najumudeen, 2012)

Reference	Plant	Acid gas	Solvent	Corrosion detected	Corrosion mitigation
Rodriguez and Edwards (1999)	Acid gas treating plant (natural gas processing)	CO_2	DEA - MDEA blend	* Corrosion rate (50 – 60 mpy) in the lean side of the lean-rich heat exchanger	* Addition of sulfur-based corrosion inhibitor (reduced corrosion rate to less than 5 mpy)
eHart et al. (1999)	Acid gas treating plant (CO_2 recovery plant)	3% CO_2	30% MEA	* Uniform and galvanic corrosion found in the bottom of the absorber and in the regenerator	* Hot solvent with copper based corrosion Inhibitor was re-circulated for 16 hours before the plant operation for passive film formation.
Veldman (2000)	Acid gas treating plant (natural gas processing)	25% CO_2	Sulfinol	* Heavy $FeCO_3$ deposition in heat Exchanger * Iron oxide (FeO) and hematite (Fe_2O_3) deposition	* Injection of 2 to 4 L/d of oxygen scavenging inhibitors (reduced Fe^{2+} content from 50 to 5 ppm)
		Mainly H_2S	DEA	* Iron sulphide (FeS) fouling and reboiler corrosion	* Injection of 0.5 L/d of corrosion inhibitor
Sutopo and Safruddin (2000)	Acid gas treating plant (natural gas treating)	5.88 to 8% CO_2 and trac of H_2S	MEA and later Formulated MDEA	* Stress Corrosion Cracking (SCC) with MEA * Erosion corrosion with MDEA – Type A	* MEA was replaced with MDEA Type-A and then to MDEA Type-B to avoid SCC and erosion corrosion, respectively.

1.9 Corrosion prediction

Corrosion prediction is essential for the design of process equipment. The knowledge of corrosion prediction for wet CO_2 corrosion is more common than for alkanolamine solution corrosion. A number of studies on corrosion prediction modeling for wet CO_2 corrosion are available in the literature, whereas only a few studies were found on corrosion prediction modeling for alkanolamine solution corrosion.

1.9.1 CO_2 corrosion models

The corrosion prediction models for CO_2 corrosion date back to as early as 1975, one of the most well-known and widely applied models is de Waard and Milliams. This model was proposed by de Waard and his coworkers (de Waard & Lotz, 1993; de Waard *et al.*, 1995; de Waard *et al.*, 1991; de Waard & Milliams, 1975) is the most widely accepted CO_2 corrosion model in oil and gas industry for the past two decades. This mechanistic model is based on the assumption of direct reduction of H_2CO_3 and the correlation with glass cell laboratory data. The initial model only incorporated the effect of CO_2 partial pressure and temperature as shown in equation (1.10):

$$\log(\mathrm{CR}) = 7.96 - \frac{2320}{\mathrm{T} + 273} - 0.00555\,\mathrm{T} + 0.67\log(\mathrm{P_{CO_2}}) \tag{1.10}$$

where CR describes the corrosion rate (mmpy), T is the temperature (°C) and P_{CO2} denotes the CO_2 partial pressure (Bard & Faulkner). The temperature function in the above equation was determined by assuming Arrhenius type dependence for a charge transfer controlled process. On the other hand, CO_2 partial pressure function was obtained by assuming that all the H^+ ions in solution originate by the dissociation of carbonic acid, which is only valid for pure saturated CO_2 solution in the absence of brines. Moreover, the model falsely assumed that the anodic dissolution of iron is strongly influenced by concentration of OH^- ions. However, this well-known pH dependent mechanism (Bockris *et al.*, 1961) is only valid in strong acidic solutions (pH<4) (Lee., 2004).

This model was improved by de Waard et al. in 1991, to include the effects of other factors on corrosion rate, such as pH, flow velocity, protective iron carbonate ($FeCO_3$) film formation, steel composition, and mass transport, which were incorporated into the model using a nomogram. The corrosion rate was predicted by the equation (1.11) and fitted on the nomogram. The corrected corrosion rate was calculated using the nomogram. Following is the improved semi-empirical CO_2 corrosion model (de Waard *et al.*, 1991):

$$\log(\mathrm{CR}) = 5.8 - \frac{1710}{\mathrm{T}} + 0.67 \log(\mathrm{P}_{CO_2}) \tag{1.11}$$

Mishra et al. (1997) developed an empirical corrosion prediction equation based on reaction kinetic principles where the corrosion rate was expressed as a function of temperature, pH (concentration of H^+) and CO_2 partial pressure (equation (1.12)).

$$\mathrm{CR} = \mathrm{C}\,[\mathrm{H}^+]^{1.33}\,\mathrm{P}_{\mathrm{CO_2}}^{0.67}\,\mathrm{e}^{-\mathrm{Q}/_{\mathrm{kT}}} \tag{1.12}$$

Where *CR* is the corrosion rate (mm/yr), *C* is a constant, $[H^+]$ is the concentration of H^+ ions (kmol/m^3), P_{CO2} denotes the partial pressure of CO_2 in (N/m^2), *Q* is the instantaneous reaction rate constant of CO_2 dissolution in water, *k* is the Boltzmann constant (J/K).

In 1999, Anderko and Young developed a mechanistic corrosion model composed of thermodynamic and electrochemical components to provide realistic speciation of aqueous system, as well as anodic and cathodic processes at the metal surface. The model was validated against experimental results and used to analyze parametric effects on corrosion rate, such as temperature, CO_2 partial pressure, solution composition, and flow velocity.

In 2001, a mechanistic corrosion model for aqueous CO_2 developed by Nesic et al. This model incorporates electrochemical reactions at the metal surface, diffusion of chemical species between bulk and metal surface, diffusion of chemical species across porous $FeCO_3$ corrosion films, electro-migration of ions under the influence of the established potential gradients, and the chemical reactions taking place in the bulk solution. This model allows users to specify $FeCO_3$ film thickness and to study its effect on the corrosion rate.

Later, in 2003, Nesic and Lee improved the previous model by incorporating the growth of $FeCO_3$ films into the model. The $FeCO_3$ precipitation starts when the solution is supersaturated with Fe^{2+} and CO_3^{2-} ions. It was found from the simulation results that $FeCO_3$ films are formed at high pH values, high temperature, high CO_2 partial pressure, and high Fe^{2+} concentration.

In 2009, Nesic et al. developed a mechanistic model that uses species transport equations to solve for speciation. This model includes the effects of H_2S, O_2 and organic acids on corrosion rate. Transport equations were written using Fick's first and second laws, and electro-neutrality was added as a constraint to solve for speciation. This specific model can predict corrosion rates at various CO_2 partial pressures, temperatures, velocities, $FeCO_3$ film thicknesses, and flow velocities.

1.9.2 Corrosion model for alkanolamine solution corrosion

The model for alkanolamine solution corrosion by Veawab & Aroonwilas, (2002) was developed specifically for $MEA-H_2O-CO_2$ environments. It accounts for thermodynamic equilibrium of chemical species in bulk solution and electrochemical reactions on the metal-solution interface. The electrolyte Non-Random Two Liquid (NRTL) model was employed for the estimation of equilibrium concentrations of the chemical species present in the solution. The mixed potential theory was applied to represent kinetics of electrochemical reactions on the metal-solution interface during corrosion processes. HCO_3^- and H_2O were identified as the major oxidizing agents, whereas H_3O^+ ions were found to play only a minor role in corrosion rate.

In 2008, Nouri et al. developed a semi-empirical corrosion prediction model for DEA-H_2O-CO_2 systems. This predictive model was a modification of the de Waard and Milliams model (1975). The corrosion rate obtained from the de Waard and Milliams model was fixed as the base corrosion rate (CR_{base}), and the modified corrosion rate (CR_{modified}) was the product of the base corrosion rate and the individual correction factors for the effects of all key influencing variables, such as partial pressure of CO_2, partial pressure of H_2S, H_2S/CO_2 ratio, temperature, pH, presence of protective films, free water, water composition, oil wetting, presence of glycol and methanol, addition of corrosion inhibitors, and material type. The base corrosion rate prediction is calculated using the equation (1.13), while the modified corrosion rate is expressed in the form of equation (1.14).

$$\log \mathrm{CR} = 5.8 - \frac{1710}{\mathrm{T}} + 0.67 \log \mathrm{P}_{\mathrm{CO_2}} \tag{1.13}$$

$$\mathrm{CR}_{\mathrm{modified}} = \mathrm{CR}_{\mathrm{base}} \prod_{\mathrm{i}=1}^{\mathrm{n}} f_{\mathrm{i}} \tag{1.14}$$

Where n is the total number of key influencing variables and f_i is the correction factor of the i^{th} key influencing variable. The correction factors for all the key influencing parameters were obtained either from plant data or laboratory experiments.

Najumudeen (2012) developed a mechanistic corrosion model of Veawab and Aroonwilas (2002) for carbon steel based on MEA-CO_2 capture plants for flue gas treatment that incorporated three factors into the model, dissolved O_2, heat-stable salts and in the presence of $FeCO_3$ film on the metal surface. He used the vapor-liquid equilibrium e-NRTL sub-model in the developed corrosion model to calculate the thermodynamic equilibrium concentration of chemical species present in the solution. The results indicated that H_3O^+ ions contributes the least to the corrosion in aqueous MEA-CO_2 compared to other oxidizing agents, including H_2O and HCO_3^- environments. The variations in the temperature and CO_2 loading change kinetics of corrosion reaction and they affect corrosion in higher magnitudes than MEA concentration. Furthermore, he reported that the presence of dissolved O_2 and acetic acid (tested as the HSSs) in aqueous MEA-CO_2 environments do not affect corrosion of carbon steel.

Choi et al. (2012) developed a model to prdict the corrosion of carbon steel in aqueous MDEA-CO_2 systems based on modeling of solution speciation and key electrochemical reactions. This model is applicable to uniform corrosion in the absence of protective films. They observed that the corrosion rate increased with the increase of $MDEAH^+$ concentration and HCO_3^- concentration.

1.10 Motivation of the research

Current knowledge of corrosion prediction for alkanolamine solution corrosion is very limited. Few researchers attempted to predict the corrosion rate of carbon steel in single alkanolamine-based acid gas treating plants. For blended system, a very limited scarce data on modeling is available in the literature.

The limitations of the work done by Veawb & Aroonwilas (2002) are that the model did not account for a protonated amine as oxidizing agents, the electrochemical kinetics parameters were specifically for aqueous solutions of MEA. Furthermore, the model was built only for single amine solutions and did not study the effect of different blended alkanolamine. The corrosion predictive model developed by Nouri et al. (2008) was built in the form of a semi-empirical model that was regressed from plant corrosion data and the operating conditions specifically of acid gas treating plants using aqueous solutions of DEA. There are two main limitations of this model. First, the model might not be applicable to flue gas treatment operations, of which the process conditions differ from acid gas treating plants. Second, the model might not be applicable to other solvents. To extend the knowledge of corrosion prediction for activated alkanolamine solution corrosion, this work aims at developing a mechanistic corrosion model of carbon steel for activated MDEA and activated DEA-based CO_2 capture plants for flue gas treatment that this work implements a mechanistic-type of model, not a semi-empirical model, for two main reasons: firstly, the mechanistic model can be extended to other solvents by altering the vapour-liquid equilibrium data without modification of the model structure. Secondly, the mechanistic model does not require for model regression a significant quantity of corrosion data from plant operations, which are currently not available for flue gas treatment operations. This gives the motivation for this work to further expore the promise of this solvent in with respect to potential corrosion reduction.

1.10.1 Scope of the research

The research will investigate corrosion rate of carbon steel in CO_2 absorption process using aqueous carbonated solution of activated MDEA and activated DEA in several solution temperature, CO_2 loading, amine concentration and type of amine. Disscusion of various parameters in the model related to the corrosion mechanism will be based on the available published experimental data. The scopes of this research are:

1. Develop the corrosion model mechanistically.
2. Study the effect of parameters using simulations results.
3. Compared the results obtained between corrosion models with the experimental methods.

1.10.2 Research objectives

Activated MDEA and activated DEA were chosen as the CO_2 absorption solvent for this work because of its promise as a cost-effective solvent for CO_2 capture in flue gas treatment applications and as a representative for CO_2 absorption solvents due to its common use in gas treating plants, as well as in post-combustion CO_2 capture units. The following objectives have to be achieved:

1. To determine species concentration for different activated amine solution.
2. To develop mechanistic corrosion rate model for Piperazine/Methyl-di-ethanolamine and Piperazine/Di-ethanolamine carbonated solution.
3. To study the effect of activator on the corrosion rate.

1.11 Structure of the thesis

This thesis consists of five chapters;

Chapter 1

This chapter provides an overview of the literature, and describes previous research achieved concerning the carbon dioxide absorption into alkanolamine solutions, their vapor liquid equilibrium (VLE) modeling, and their corrosivity. It also defines the scope and aims of this thesis.

Chapter 2

This chapter provides general background on electrochemistry for the corrosion studies, a literature review on available vapour-liquid equilibrium models, and the kinetics of aqueous corrosion modeling. The corrosion prediction models for amine-CO_2 aqueous solution are also described.

Chapter 3

This chapter describes the speciation and electrochemical model methodology development and their implementation. It emphasizes the criteria upon which such thermodynamic model was selected, and the description of its parameters, and their formulae are also outlined in this chapter. The uses of the model for identify oxidizing agents that are responsible for the corrosion in the carbonated aqueous solution of activated MDEA and activated DEA systems, are also presented.

Chapter 4

This chapter presents and discusses the simulation results. The results, comparison, and discussion, of (VLE) modeling and speciation predictions are presented, the important parameters influencing speciation predicted in activated carbonated aqueous solutions are also subject of discussion in this chapter. This chapter presents the carbonated activated MDEA and activated DEA corrosivity results, comparison, and discussion. The effects of CO_2 loading, solution temperature and activator concentration polarization curves and corrosion rate of carbon steel are also discussed.

Chapter 5

Chapter 5 presents the conclusions and provides recommendations for future work in this area.

Appendix A

Appendix presents the Matlab codes for activated MDEA and activated DEA, the computer Matlab code used in the corrosion model.

Appendix B

Appendix presents the tables for comparison between published and predicted CO_2 loading in aqueous solutions of activated MDEA and activated DEA.

Appendix C

Appendix presents the tables for comparison between published and predicted solution pH for aqueous carbonated solution of activated MDEA and activated DEA.

CHAPTER 2: LITERATURE REVIEW

This chapter deals with the acid gas removal using alkanolamines and describs the reaction mechanisms of CO_2 with aqueous activated secondary and tertiary amines. It also presents the basic of corrosion, corrosion kinetics and electrochemical techniques. Furthermore, vapor-liquid equilibrium models, the kinetics of aqueous corrosion models, type of corrosion prediction models are also presented.

2.1 Electrochemical nature of corrosion

Electrochemical mechanism controls the corrosion of metal and alloys metals in aqueous solution or in any other ionically conducting medium. A metallic corrosion process is electrochemical in nature and involves transfer of electrons at the metal-solution interface. It consists of anodic and cathodic reactions. An anodic reaction (oxidation) occurs when any chemical species donates an electron (e^-) to acquire a more positive charge. A cathodic reaction (reduction) occurs when any chemical species accepts an (e^-) to acquire a more negative charge (Yang, 2008) .

2.1.1 Electrode potentials

Electrochemical thermodynamics deals with the energy changes involved in the electrochemical reactions. This energy change is directly related to the driving force for electrode (or corrosion) reactions and dictates reaction spontaneity. Though thermodynamics can predict the feasibility of any corrosion reaction, it cannot predict the rate of the corrosion reaction. Actual corrosion rate is governed by the kinetics of electrochemical reactions (Yang, 2008). When a conducting metal is immersed in an electrolyte that has ionic conductivity, two half-cell reactions will occur, one is anodic and the other is cathodic. Each reaction has its inherent electrode potential called its half-cell electrode potential or electromotive force (emf). The difference in the potential of the two half-cell reactions constitutes the electrochemical potential or the cell potential (E) as given equation (2.1):

$$\mathrm{E} = \mathrm{E_a} + \mathrm{E_c} \tag{2.1}$$

Where; E_a and E_c represent anodic and cathodic half-cell electrode potentials, respectively. According to thermodynamics, for any electrochemical reaction there is always a change of free energy associated with it. The fundamental relationship between the free-energy change, ΔG, and the electrochemical potential, E, is expressed as in equation (2.2):

$$\Delta\mathrm{G} = -\mathrm{nFE} \tag{2.2}$$

Where n denotes the number of electrons exchanged in the reaction, F is the Faraday's constant, 96,485 coulombs per mole, ΔG is the Gibb's free energy change (kJ/mol) and E is the electrochemical potential (V) (Bard & Faulkner, 1980).

2.1.2 Nernst equation

Consider the following reaction where A, B, C, and D describe the chemical species involved in the reaction, and a, b, c, and d; are the number of moles of the reacting chemical species, respectively.

$$\mathrm{aA} + \mathrm{bB} \leftrightharpoons \mathrm{cC} + \mathrm{dD} \tag{2.3}$$

The corresponding changes in Gibbs free energy for reactions under the standard conditions are represented by the following equation:

$$\Delta\mathrm{G^o} = (\mathrm{c\,G_C^o} + \mathrm{d\,G_D^o}) - (\mathrm{a\,G_A^o} + \mathrm{b\,G_B^o}) \tag{2.4}$$

Where; superscript o denotes the Gibbs free energy at standard conditions (25 ^{o}C). However, for nonstandard conditions, equation (2.4) can be expressed as:

$$\Delta G = (c\,G_C + d\,G_D) - (a\,G_A + b\,G_B) \tag{2.5}$$

The change of free energy from standard to non-standard state can be determined by equation (2.6).

$$\Delta G - \Delta G^o = c(G_c - G_c^o) + d(G_d - G_d^o) - a(G_a - G_a^o) - b(G_b - G_b^o) \tag{2.6}$$

Each term on the right-hand side of equation (2.6) can be expressed in terms of activity for estimating the change in Gibbs free energy with respect to the standard state. Taking the chemical specie A as an example and using its concentration [A], the following relationship can be written:

$$a(G_A - G_A^o) = RT \ln [A]^a \tag{2.7}$$

Where; R is the universal gas constant (J/mol.K) and T is the absolute temperature (K). By writing the same relation for the other three chemical species, the following expression can be written:

$$\Delta G - \Delta G^0 = RT \ln \frac{[C]^c[D]^d}{[A]^a[B]^b} \tag{2.8}$$

Using the relationship between changes in Gibbs free energy and electrode potential (i.e. $\Delta G^o = -nFE^o$ and $\Delta G = -nFE$ yields (Yang, 2008):

$$E = E^0 - \frac{RT}{nF} \ln \frac{[C]^c[D]^d}{[A]^a[B]^b} \tag{2.9}$$

Where; E^o is the standard electrode potential (V). Equation (2.9) is the general form of Nernst's equation which can be applied to determine the electrode potential at nonstandard conditions of any electrochemical reaction.

2.1.3 Electrochemical kinetic

Electrochemical reactions are described as reactions in which they lose or accept electrons. Thus, the rate of the electron flow can be termed as the reaction rate. The rate of electron flow is conveniently measured as current (I) in amperes, where one ampere is equal to one coulomb of charge per second. The proportionality between the current and mass of the substance that reacts electrochemically *(m)* is given by Faraday's laws (Jones, 1992).

The first Faraday's law states that during the electrolysis process the mass of substance transformed at an electrode is directly proportional to the quantity of electricity transferred *(Q)* at that particular electrode. The measurement of electricity transferred referred also as the quantity of electrical charge is expressed by coulombs and the relationship is described by the following equation.

$$\mathrm{m} \propto \mathrm{Q} \tag{2.10}$$

The above expression can be rewritten in terms of current and time as given below:

$$\mathrm{m} \propto \mathrm{It} \tag{2.11}$$

The second Faraday's law describes the directly proportional relationship between the mass (m) altered at an electrode and to the element's equivalent weight (z). This equivalent weight (z) is the ratio of its atomic weight (a) to its valence (n). The relationship between these two quantities is described below:

$$\mathrm{m} \propto \mathrm{Z} \tag{2.12}$$

After substituting $\left(Z = \frac{a}{n}\right)$ into equation (2.12) and combining equations (2.11) and (2.12), the following expression can be written:

$$\mathrm{m} = \frac{\mathrm{Ita}}{\mathrm{nF}} \tag{2.13}$$

Where; *F* is the proportionality constant, called Faraday's constant (F = 96485 C/mol). The expression for corrosion rate can be arrived at by dividing equation (2.13) by time (t) and surface area (A) as given below (Jones, 1992):

$$\mathrm{CR} = \frac{\mathrm{m}}{\mathrm{tA}} = \frac{\mathrm{ai}}{\mathrm{nF}} \tag{2.14}$$

Where; i is the current density (A/cm2) and is written as current per unit area $\left(i = \frac{I}{A}\right)$. Corrosion rate can be calculated as a function of current density. The current density is in the range of 10^{-9} up to several A/cm^2. The corrosion rate can be conveniently expressed in terms of penetration as shown below (Jones, 1992).

$$\mathrm{CR} = 0.00327 \frac{\mathrm{ai}}{\mathrm{nD}} \tag{2.15}$$

Where *CR* is the corrosion rate (mm/yr) and *D* is the density of the metal (g/cm^3).

2.1.4 Exchange current density

The exchange current density (i_0) is the characteristic of a reversible electrode reaction. It is referred to the current density at the equilibrium condition, at which the rate of the forward half-cell reaction becomes equal to the rate of the backward half-cell reaction. At equilibrium, there is no net current flow in the system. The relationship between the exchange reaction rate and the current density can be stated from Faraday's law equation (2.16).

$$r_f = r_b = \frac{i_0 a}{nF} \tag{2.16}$$

Where; r_f and r_b are the oxidation and reduction reaction rate at equilibrium, i_o is the exchange current density (A/m^2), "a" is the atomic weight in g/mol, n is the number of electrons exchanged, F is Faraday's constant (96485 C/equivalent), where; i_0 is defined as (Bockris & Reddy, 1970):

$$\mathrm{i_0} = \mathrm{Fk_c C_A exp}\left(\frac{\alpha \mathrm{FE_{rev}}}{\mathrm{RT}}\right) \tag{2.17}$$

where k_c is the reaction rate constant, c_A is the concentration of the reactant (kmol/m^3) ,α is the symmetry factor, and E_{rev} is the equilibrium potential (V). It is not possible to measure the absolute values of i_0 by any instrument, since there is no net transfer of electrons. The theoretical calculation of i_0 is limited by the lack of knowledge of reaction rate constant, k_c and the polarization curves.

2.1.5 Electrochemical polarization

Electrochemical polarization is the deviation in electrochemical potential from the equilibrium potential, where equilibrium potential is exhibited by the electrode in the absence of an external current, and it is conveniently measured in volts (V) or millivolts (mV). The potential change ($E-E_{rev}$) is typically defined as polarization (η). Two modes of electrochemical polarization are discussed: cathodic polarization and anodic polarization. Cathodic polarization is caused by an addition of electrons resulting in a negative charge buildup at the cathode. Anodic polarization occurs by the removal of electrons resulting in a positive charge buildup at the anode (Bockris & Reddy, 1970).

The electrochemical polarization can be categorized into two types: activation polarization and concentration polarization. The activation polarization occurs when the rate of electron transfer at the metal-solution interface is lower than the rate of chemical species transport from the bulk solution to the interface. This causes the corrosion rate of the metal to depend mainly on the rate of electron transfer at the interface. On the contrary, concentration polarization occurs when the rate of electron transfer at the metal-solution interface is greater than the rate of chemical species transport from the bulk solution to the interface. The corrosion takes place almost instantaneously, and the corrosion rate depends mainly on the rate of chemical species transfer from the bulk solution to the interface. Note that, in some cases, both activation and concentration polarizations are present at the electrode surface. This type of polarization is called as combined polarization (Oldham and Maryland, 1993 and Jones, 1992).

2.2 Vapor-liquid equilibrium models

Before going into the details of VLE models, a physical model is introduced first. Acid gases and alkanolamines are considered weak electrolytes, which have the characteristics of dissociating partially in the aqueous phase to form a complex mixture of nonvolatile solvent species (alkanolamine), highly volatile molecular species (such as CO_2), and nonvolatile ionic species.

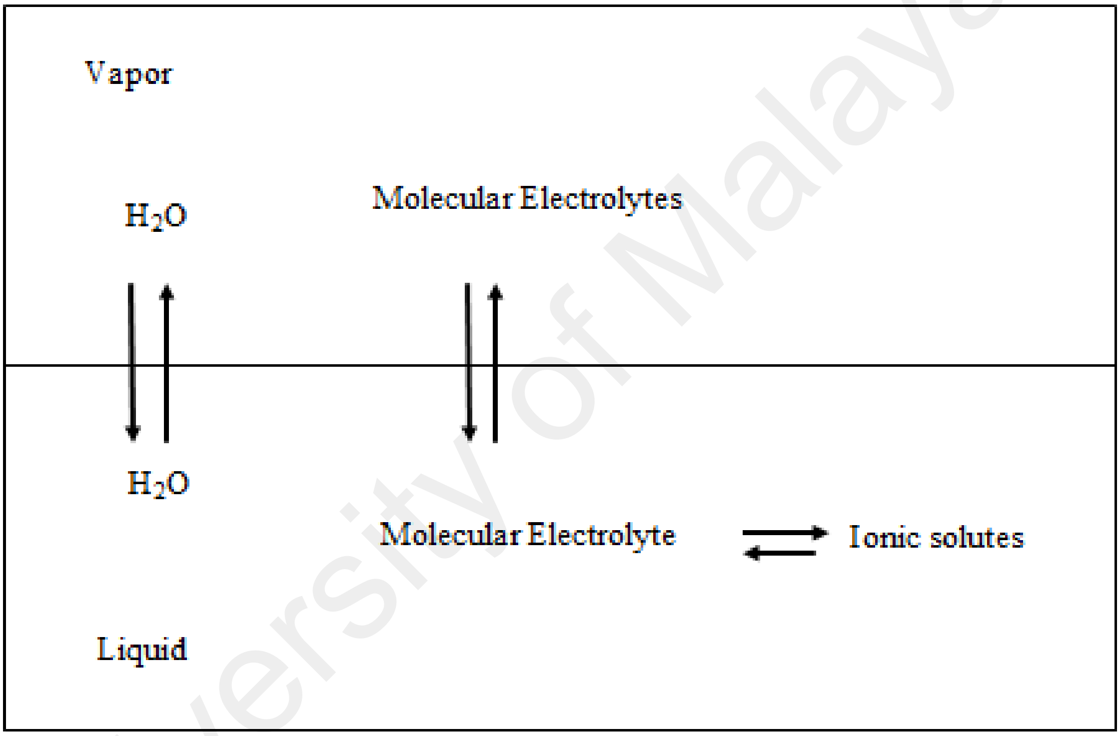

Figure 2.1: Chemical and physical equilibria in a closed aqueous weak electrolyte system.

Figure 2.1 illustrates the phase and chemical equilibria of a weak electrolyte system (i.e., the acid gas-alkanolamine-water system). In a closed system having constant temperature and pressure conditions, the phase equilibrium governs the distribution of molecular species between the liquid and vapor phases, while chemical reactions occur in the liquid phase between acid gases and alkanolamines to produce a number of ionic species. As shown Figure 2.1, phase and chemical equilibria are highly coupled in this system so that the degree of dissociation of the weak electrolytes in the liquid phase is influenced by the partial pressure of acid gases in the vapor phase and vice versa. Hence, representation of the vapor-liquid equilibrium behavior of acid gas-alkanolamine in the aqueous systems is quite complicated due to large number of chemical reactions occurring in the system. Therefore, representation of phase equilibria for such systems requires that both phase and chemical equilibria are taken into account.

In the early stage of developing VLE models for weak electrolyte solutions, most models assume the activity coefficients for all species to be unity. There are several models for aqueous electrolyte systems such as: semi-empirical excess Gibbs energy models or activity coefficients models for aqueous electrolyte systems. Moreover, several thermodynamic models have been presented also to describe the solubility of acid gases like CO_2 and H_2S in blended amine solutions. There are three main types of VLE models that have played important roles in simulating the aqueous alkanolamine-CO_2 systems.

The first type is the empirical approach as introduced by Kent and Eisenberg (1976), which follows a regression-based approach. The equilibrium constants are fitted into the CO_2 partial pressure and solubility data. Kent and Eisenberg (1976) presented the first equilibrium model which was based on pseudo-equilibrium constants and Henry's law and was extensively applied for many systems. The pseudo-equilibrium constants for amine protonation and carbamate reverse reactions for MEA and DEA systems were regressed to match with experimental vapor-liquid equilibrium data. This leads to the generation of model having only two parameters per acid gas to measure the ionic strength dependencies of the acid gas partial pressure. The limitation of this model was that it works perfectly for loading values greater than 0.1 but was inappropriate for lower loading values due to the manipulations of amine equilibrium constants.

Furthermore, this model was not able to measure ionic species concentrations. Another drawback of this model is the combination of activity coefficients and species mole fractions, which makes it impossible for the model for independent determinations. In their paper, only MEA and DEA systems were studied and reported a reasonable predictive agreement with mixed acid gases data.

The second type studies the application of excess Gibbs energy model to determine the activity coefficients of all chemical species in terms of excess Gibbs energy. Another thermodynamically rigorous model was proposed by Deshmukh-Mather (1981) based on extended Debye-Huckel theory and the work of Edwards *et al.* (1975, 1978) and Beutier and Renon (1978). The important feature of their model was that they have only one term to account for electrostatic forces by Debye-Huckel law, while for short range interactions they have another term with adjustable parameters.

Later on, more sophisticated models were proposed, such as the rigorous physical-chemical model developed by Austgen (1989) to investigate the liquid phase chemical equilibria of acid gas-alkanolamine-water systems. The model framework demands an input of the equilibrium constant for all solution reactions, Henry's constant for gases, and binary interaction parameters for all important solution species. Austgen and Rochelle (1991) used the electrolyte-NRTL equation to correlate most of available data on acid gas equilibria in aqueous solution of common alkanolamines. To determine the model parameters for the acid gas-alkanolamine-water system, the authors did a regression on amine-water total pressure data to obtain amine-water parameters, and regressed acid gas solubility data to evaluate the interaction parameters of bisulfide or bicarbonate salt with water. The remaining activity parameters were set to their default values. The electrolyte-NRTL model assumes water to have non-ideal behavior, and the binary interaction parameters between all chemical species (including water) were taken into account to predict the activity coefficients. The model is accurate in predicting speciation, since it calculates the actual activity coefficients of all chemical species in the system (Austgen *et al.*, 1989; Mock *et al.*, 1986).

The third type of VLE model is an equation of state model, which was applied to represent both liquid and vapour phases of the system. The main advantage of this equation of state models over the excess Gibbs energy models is that the equation of state model is effective to predict the activity coefficients of chemical species at a wide range of temperatures and pressures for both binary and multi-component vapour-liquid equilibrium. The vapor phase fugacity coefficients were determined by Peng-Robinson equation of state. They assumed the activity coefficient of water to be 1. In fact, the water coefficient can be different from 1 and is highly correlated with the amine activity coefficient. A 5% change in water coefficient can result in a large change in the amine activity coefficient. To simplify their regression, the species having small concentrations were removed from the mass balances and their parameters were set to zero to eliminate their influence on the model. These assumptions leave questions about the validity of the model at the low loadings where the above neglected species are important.

2.3 Modeling the kinetics of aqueous corrosion

Aqueous corrosion is described as an electrochemical process involving the charge transfers at metal-solution interface, which is referred as heterogeneous process comprise on the following fundamental steps:

1. The reactions occurring in the bulk aqueous environment,
2. The transportation of reactant to the metal surface.
3. The occurrence of charge transfer reaction at the metal surface to form products.
4. The release of formed products from the surface.

5. The transportation of products into the bulk environment.

The main objective of aqueous corrosion kinetics study it to determine the relationship between the rate of electrochemical corrosion and external conditions, varying flow conditions, also to have in-depth view on the influence of chemistry and metallurgical characteristics of the corroding interface.

Corrosion rate and corrosion potential are two important parameters that are determined from electrochemical modeling. The determination of corrosion rate assists one to simulate general corrosion pattern and also the rate of dissolution in obstructed environments such as: pits or crevices. Corrosion potential has an important role to determine the type of corrosion damage as there is often a relationship between the corrosion potential and type of corrosion damages.

This generalized observation applies to all the localized corrosion types including pitting, crevice corrosion, inter-granular and stress corrosion cracking.

Therefore, corrosion model should have the ability to provide simultaneously a reasonable corrosion rate and corrosion potential. The computational studies on the corrosion potential are of interest for predicting other form of corrosion rate than modeling general corrosion (Anderko, 2010).

2.3.1 Modeling of charge transfer

A number of authors including (Vetter, 2013), (Bockris & Reddy, 1970), (Kaesche, 1985), (Bockris & Khan, 2013), and (Gileadi, 1993) have reviewed the well-developed theory of charge transfer reactions. In this section, the key relationships that lay foundation for the modeling of charge kinetics will be discussed in detail.

In a simple reaction, transfer of electrons between two species leads to produce a reduced from "Red" and an oxidized form named as "Ox":

$$\mathrm{Red} \underset{r_c}{\overset{r_a}{\rightleftharpoons}} \mathrm{Ox} + ne \tag{2.18}$$

The current density for this reaction is determined by the difference between the anodic rate v_a and cathodic rate v_c, multiplied by nF:

$$i = \mathrm{nF}(\mathrm{v_a} - \mathrm{v_c}) \tag{2.19}$$

In the theory of electrochemical kinetics, Vetter (2013) states that the rates of anodic and cathodic reactions are related to the potential and the concentration of the reacting species at the phase boundary described by equations (2.20) and (2.21).

$$i_a = nFv_a = nFk_aC_{r,s}^{x,r}exp\left(\frac{\alpha_a nFE}{RT}\right) \tag{2.20}$$

$$i_c = nFv_c = -nFk_cC_{o,s}^{x,o}exp\left(-\frac{\alpha_c nFE}{RT}\right) \tag{2.21}$$

Where; the anodic and cathodic rate constants are denoted by k_a and k_c while α_a and α_c denotes anodic and cathodic electrochemical transfer coefficients. The concentration of the reduced (r) and oxidized (o) formed at the interface are described by $C_{r,s}$ and $C_{o,s}$, respectively. While, x,r and x,o describe the order of reaction for the reduced and oxidized species. The anodic and cathodic electrochemical transfer for an individual redox process is described as $\alpha_c = 1 - \alpha_a$. The total current density for reaction (2.18) is determined as in equation (2.22).

$$i = nFk_aC_{r,s}^{x,r}exp\left(\frac{\alpha_a nFE}{RT}\right) - nFk_cC_{o,s}^{x,o}exp\left(-\frac{\alpha_c nFE}{RT}\right) \tag{2.22}$$

The current density *i* is set equal to zero at equilibrium described as E_{rev}.

In the absence of the a net current, the concentrations of chemical species at the surface become equal to the respective bulk concentrations (i.e., $C_{r,s}$= $C_{r,b}$ and $C_{o,s}$= $C_{o,b}$) and similarly the current density of anodic process, which is described as the exchange current density i_0 by equation (2.23).

$$i_0 = nFk_a C_{r,s}^{x,r} exp\left(\frac{\alpha_a nFE_{rev}}{RT}\right) - nFk_c C_{o,s}^{x,o} exp\left(-\frac{\alpha_c nFE_{rev}}{RT}\right) \tag{2.23}$$

Using equation (2.23), the equation for current density (2.22) can be expressed in terms of the exchange current density and the overvoltage η = E-E_{rev} :

$$i = i_0 \left(\frac{C_{r,s}}{C_{r,b}}\right)^{x,r} e^{\left(\frac{\alpha_a nF(E-E_{rev})}{RT}\right)} - i_0 \left(\frac{C_{o,s}}{C_{o,b}}\right)^{x,o} e^{\left(-\frac{\alpha_c nF(E-E_{rev})}{RT}\right)} \tag{2.24}$$

The transport of reactants and products to the metal surface and the colliding interface gives us the values of the ratios $C_{r,s}/C_{r,b}$ and $C_{o,s}/C_{o,b}$. The surface concentration of the species is different from those in the bulk in the case where mass transport is slow compared to charge transfer. On the other hands, when the charge transfer rate is low compared to mass transfer of species, the reaction rate is influenced by charge control and the ratios become equal to unity not only at the equilibrium potential. In such cases, the equation (2.24) minimized to a simpler form and is regarded as Butler-Volmer equation for charge transfer reactions:

$$i = i_0\, e^{\left(\frac{\alpha_a nF(E-E_{rev})}{RT}\right)} - i_0 e^{\left(-\frac{\alpha_c nF(E-E_{rev})}{RT}\right)} \tag{2.25}$$

The charge transfer reaction mechanism control the electrochemical transfer coefficient α. There are several reactions in which its value can obtained simply from mechanistic consideration; however, this cannot be generalized as it requires being determined empirically. One way to determine the transfer coefficient α is from the slop of plot between potential and logarithm of current density which is also called empirical Tafel coefficients as described in equations (2.26) through (2.28).

$$\beta_a = \frac{\mathrm{d}E}{\mathrm{d}\ln i_a};\ \beta_c = \frac{\mathrm{d}E}{\mathrm{d}\ln i_c} \tag{2.26}$$

$$\beta_a = \frac{RT}{\alpha_a nF};\ \beta_c = \frac{RT}{\alpha_c nF} \tag{2.27}$$

Or, in a more traditional decimal logarithm form:

$$\mathrm{b_a} = \frac{2.303\ \mathrm{RT}}{\alpha_\mathrm{a}\mathrm{nF}};\ \mathrm{b_c} = \frac{2.303\ \mathrm{RT}}{\alpha_\mathrm{c}\mathrm{nF}} \tag{2.28}$$

The equation described above contains both the anodic and cathodic process for a certain redox couple. However, in practice either only a cathodic or anodic partial current for a given redox process is sufficient for corrosion modeling.

Moreover, there are certain specific cases in which the cathodic or anodic partial process can be neglected, for example in metal ion reaction cathodic partial process can be neglected because the deposition of metal ion is typically not of much significance in corrosion. Similarly, anodic partial process can be ignored in the case of oxidizing agents as we are only interested in their reduction for corrosion studies.

2.3.2 Modeling of mass transport

The rate of mass transport controls the concentration of reactants and products at the surface and any point either in the bulk or on the interface. Three mechanisms are considered to contribute to the mass transport of species called diffusion, migration, and convection.

There are situations in which either of these mechanism has more influence over the system or the other becomes less significant. For example, in the case of transport of neutral molecules and also for the transport of charged species migration mechanism can be neglected. However, in ionic systems migration mechanism become important as there is no supporting electrolyte.

Furthermore, in cases where the mass transfer is controlled by the diffusion and convection, the relationship can be described by the concept of Nernst diffusion layer, in which the environment near the corroding surface can be divided into two regions referred as inner region and outer region. In the inner region, diffusion mechanism is the major controlling mechanism and convection is negligible and this is also regarded as Nernst diffusion layer. While in the outer region, concentrations of the species are considered to be uniform and equal to those in the bulk solution. Hence, the concentration of species is observed to change linearly from the surface to bulk region over a certain distance δ, here δ denotes the thickness of diffusion layer. In such a model, the flux of a species *i* in the vicinity of a corroding interface given by Fick's law

$$\mathrm{N_i} = -\mathrm{D_i}\left(\frac{\partial \mathrm{C_i}}{\partial \mathrm{z}}\right)_{\mathrm{z}=0} \tag{2.29}$$

Where; D_i is the diffusion coefficient of species *i* and z in the direction perpendicular to the surface. Integration of equation (2.29) over the thickness of the diffusion layer gives:

$$\mathrm{N_i} = -\mathrm{D_i}\,\frac{\mathrm{C_{i,b}} - \mathrm{C_{i,s}}}{\delta_\mathrm{i}} \tag{2.30}$$

It is important to mention here that the diffusion layer thickness is not a general physical property of the system and is regarded as a convenient mathematical construct which makes it easy to distinguish the influence of diffusion and convection. It depends on the flow conditions, properties of the environments, and the diffusion coefficient of individual species and thus has different values for different species.

The significance of equation (2.30) is that it can be applied to both reactants entering into the electrochemical reaction and corrosion products leaving the interface. Later on it can be combined with Faraday's law to obtain the current density and for oxidant O, equation (2.30) gives rise to the expression for a catholic current density:

$$i_c = nFN_O = -\mathrm{nFD_O}\frac{\mathrm{C_{O,b}} - \mathrm{C}_{\mathrm{O},s}}{\delta_\mathrm{O}} \tag{2.31}$$

According to equation (2.31) the current density exhibits a maximum limiting values as the surface concentration $C_{o,s}$ approaches zero. This condition was described as the limiting current density

$$i_{c,L} = -\frac{\mathrm{nFD_O C_{O,b}}}{\delta_\mathrm{O}} \tag{2.32}$$

For corrosion product (e.g., Me ions), an analogous equation can be written for anodic current density

$$i_a = nFN_{Me} = -nFD_{Me}\frac{\mathrm{C_{Me,b}} - \mathrm{C_{Me,s}}}{\delta_\mathrm{Me}} \tag{2.33}$$

The surface concentration becomes limited due to the solubility of corrosion products derived from equation (2.33). Hence, as the surface concentration of metal ions corresponds to the metal solubility a limiting anodic current density can be achieved described in equation (2.34):

$$i_a = -nFD_{Me}\frac{\mathrm{C_{Me,b}} - \mathrm{C_{Me,sat}}}{\delta_\mathrm{Me}} \tag{2.34}$$

The theory of metal corrosion or also referred as the mixed potential theory assist one to model the behavior of the corroding surface, which is the sum of all partial anodic currents is equal to the sum of all partial cathodic currents (Wagner & Traud, 1938). It is also assumed that the electrical potential of the metal at both anodic and cathodic sites are equal, and this assumption is made to fulfill the requirement of no charge accumulation within a metal. This leads to the conclusion that the electrons produced as result of oxidation process surely will be consumed in the reduction process.

$$\sum_j A_a i_{a,j} = \sum_j A_c i_{c,j} \ \text{ at } E = E_{corr} \tag{2.35}$$

Where; A_a and A_c describes the areas over which the anodic and cathodic reactions are taking place, respectively. The corrosion potential E_{corr} can be determined from equation (2.35).

Later on, the corrosion current density and the corrosion rates can be computed with the anodic current density derived from metal dissolution at certain corrosion potential given by equation (2.36).

$$i_{corr} = i_{a,Me}(E_{corr}) \tag{2.36}$$

The predicted current can be estimated by the potential that deviates from the corrosion potential. Hence, these computed current versus potential relationship can be used for comparison purpose with the experimentally determined polarization behavior.

2.3.3 Diffusion of amines and ions

In situations for fast kinetics, it is believed that the diffusion of the amine and products formed at the gas-liquid interface may limit the overall reaction rate. Moreover, it is suggested that under condition where high fluxes are present, concentration gradient will exist in the boundary layer. Therefore, it is very important to have precise prediction of the diffusion coefficient of the investigated components (organic and ionic) in aqueous solution.

Stokes-Einstein relation describes the diffusion of molecules in the simplest form and also it has been exhibited that at conditions of infinite dilution, molar volume of the solute and diffusion coefficient of the amine are related.

The relationship between the diffusion coefficient as a function of solvent viscosity, temperature and solvent specific parameters is described by a more sophisticated model known as Wilke-Chang correlation (Wilke & Chang, 1955).

$$D^{o} = 1.17 \times 10^{-13} \frac{(\xi_{sol} MW_{sol})^{0.5}}{V_{Am}^{0.6} \mu_{sol}} T \tag{2.37}$$

Where; D^o denote diffusion coefficient of the amine at infinite dilution in water, V indicates molar volume. MW_{sol} is the molecular weight of the solvent, and ξ_{sol} represents the solvent specific parameter which is equal to 2.6 for the solvent water. The prediction of the diffusion coefficient (< 10%) of the various components such as amines and organic molecules (i.e., carboxylic acids) is executed with Wilke-Chang correlation.

Versteeg & Swaalj, (1988) suggested a modified Stokes-Einstein relation for the estimation of amine diffusion coefficient based on the solutions viscosity descrie by equation (2.38). The study by (Snijder *et al.*, 1993) showed that this relation has the ability to predict the diffusion coefficient of various alkanolamines over a wide range of temperature and concentration.

$$D^o = D_{Am}^{\infty} \left(\frac{\mu_w}{\mu}\right)^{0.6} \tag{2.38}$$

Where; μ_w, μ denotes the viscosity of pure water and alkanolamine solution, respectively. While, D^o denotes the diffusion coefficient at infinite dilution.

2.3.4 Modeling mass transport using mass transfer coefficients

The prediction of the diffusion layer thickness δ_i or, equivalently, the limiting current density is necessary to calculate the mass transport effect on electrochemical kinetics. Empirical approaches are opted for most practical application as theoretical formulas for the quantities cannot be derived for arbitrary flow conditions. Levich (1962) proposed a theoretical solution for rotating disk electrode and his solution preceded experimental results. The thickness of the diffusion layer on a rotating disk electrode is calculated by following equation (2.39).

$$\delta_i = 1.61\, D_i^{1/3} \nu^{1/6} \omega^{-1/2} \tag{2.39}$$

Where; D_i is the diffusion coefficient of the reacting species in cm^2/s, ω is the rotation rate in rad/s, and ν is the kinematic viscosity in cm^2/s, which is the ratio of dynamic viscosity and density, that is

$$\nu = \eta/\rho \tag{2.40}$$

The relationship for the limiting current density can be expressed as in equation (2.41);

$$i_{c,L} = -0.6205 nF C_{O,b} D_O^{2/3} \nu^{-1/6} \omega^{1/2} \tag{2.41}$$

Mass transport can be calculated using empirical correlations expressed in terms of the mass transfer coefficients k_m defined as in equation (2.42);

$$k_m = \frac{\text{Reaction rate}}{\text{Concentration driving force}} \tag{2.42}$$

The electrochemical reaction rate is expressed by the current density and equation (2.30) for mass-transport limited reaction can be modified in terms of mass transfer coefficient k_m and expressed by following equation (2.43);

$$N_i = \frac{i_i}{n_i F} = -D_i \frac{C_{i,b} - C_{i,s}}{\delta_i} = -k_{m,i}(C_{i,b} - C_{i,s}) \tag{2.43}$$

This equation indicates a relationship between diffusion layer thickness (δ_i) and k_m, expressed as in equation (2.44);

$$k_{m,i} = \frac{D_i}{\delta_i} \tag{2.44}$$

The mass transfer coefficient k_m is also presented in Sherwood number *Sh*, which is defined as in equation (2.45);

$$Sh = \frac{k_m d}{D} \tag{2.45}$$

Where; d is a characteristic dimension (e.g., a pipe or rotating disk diameter); *D* diffusion coefficient for reacting species *i*. Sh; Sherwood number can be correlated with Reynolds number (Re) and Schmidt number (Sc), described by in equations (2.46) and (2.47);

$$Re = \frac{Vd}{\nu} \tag{2.46}$$

$$Sc = \frac{\nu}{D} \tag{2.47}$$

Where; V is the linear velocity. The dimensional analysis showed that *Sh* is a function of *Re* and *Sc*. This function is expressed in the following form (Poulson, 1983, 1993):

$$Sh = constant \times Re^{x} \times Sc^{y} \tag{2.48}$$

They theoretically derived results for a rotating disk can be written as

$$Sh = 0.6205\ Re^{0.5}\ Sc^{0.33} \tag{2.49}$$

For rotating cylinder, the correlation of (Eisenberg *et al.*, 1954) is widely used in equation (2.50);

$$Sh = 0.0791\ Re^{0.7}\ Sc^{0.356} \tag{2.50}$$

Several correlations have been proposed for single-phase flow in a straight pipe. However, Berger & Hau, (1977) correlation has found widespread application in a number of corrosion modeling studies:

$$Sh = 0.0165\ Re^{0.86}\ Sc^{0.33} \tag{2.51}$$

Poulson, (1983) reviewed the earlier pipe formula and more recent equation has been discussed by (Lin *et al.*, 1996). However, the limitations of these equations are that they cannot be applied for multiphase flow. There are correlation available for stratified flow (Wang & Nesic, 2003), but there is not a single comprehensive correlation available for various regimes of multiphase flow.

2.4 Corrosion prediction models

There are three types of corrosion prediction models available in the literature. They are empirical, semi-empirical, and mechanistic models. Although aqueous CO_2 environments can cause pitting corrosion, mesa attack, flow-induced corrosion, and uniform corrosion (Fosbøl *et al.*, 2009), due to the predominance of uniform corrosion and the complexity of model development for localized corrosion, all corrosion prediction models for aqueous CO_2 environments to date were developed for uniform corrosion. The three types of corrosion prediction models are discussed in the following sections.

2.4.1 Empirical model

The empirical predictive corrosion models are the simplest to develop. It is purely data driven and requires a large amount of corrosion data that are either obtained from actual plant operations or from laboratory experiments. The model can be expressed, with little or no significant difference, as a linear or non-linear mathematical correlation of the corrosion rates and the variables. The major drawbacks of this type of model are that they require a large set of data for various operating conditions that affect the corrosion rate, their confidence intervals are low, and they cannot be extended to other systems easily. The slight change in the operating conditions leads to a large deviation in the corrosion rate prediction. They extrapolate poorly outside the conditions present in their database (Fosbøl *et al.*, 2009). An example of an empirical corrosion model for an aqueous CO_2-H_2S-O_2 environment is the model developed by (Schutt & Lyle, 1998) as presented in equation (2.52):

$$\begin{aligned} CR &= 8.6988 + 9.856\times10^{-3}[O_2] - 1.48\times10^{-7}[O_2]^2 \\ &-1.30865\,pH + 0.04934[CO_2][H_2S] - 4.8231\times10^{-5}[CO_2][O_2] \\ &-2.372\times10^{-3}[H_2S][O_2] - 1.113\times10^{-3}[O_2]pH \end{aligned} \tag{2.52}$$

Where; CR is the corrosion rate (mpy), $[O_2]$ is the concentration of oxygen in gas phase (ppmv), $[H_2S]$ is the concentration of hydrogen sulfide in the gas phase (psi), and $[CO_2]$ is the concentration of carbon dioxide in gas phase (psi).

2.4.2 Semi-empirical model

The semi-empirical model is the mathematical correlation that consists of two components: an empirical correlation for base corrosion rate and correction factors. The empirical correlation is regressed from the corrosion data either from plant operations or experiments. The correction factors represent physical or chemical phenomena involved in corrosion process, such as $FeCO_3$ film formation, flow velocity, pH, and/or the presence of inhibitors. An example of the semi-empirical corrosion model is the model developed by Nouri *et al*., (2008) as previously described in equation (1.14). The main drawback of the empirical model is that it relies on a large set of corrosion data. The semi-empirical model, however, can be used to predict corrosion rate outside the variable ranges used during model development with higher confidence than the empirical model. This is because its correction factors are represented by parameters from physical chemistry. This type of model is preferred by industries since it is less time consuming and simpler to develop than the purely theory-driven mechanistic models. In addition, it can extrapolate better than the empirical models (Fosbøl *et al.*, 2009); (de Waard & Milliams, 1975);(de Waard *et al.*, 1991).

2.4.3 Mechanistic model

Mechanistic corrosion models differ from the empirical and semi-empirical models in a sense that they are built on the theory of corrosion processes and do not require any corrosion data for model development. These models have good extrapolation capabilities and can be modified to simulate other systems. However, they require better understanding of fundamental science related to kinetics, thermodynamics, heat transfer and mass transfer, these type of models are usually developed at educational institutions (Fosbøl *et al.*, 2009; Nesic *et al.*, 2001).

2.5 Limitations of the current knowledge

Although corrosion is recognized as the major operational problem in amine treating plants, the current knowledge of corrosion phenomena taking place in the system is very limited. The following are highlited limitations.

2.5.1 Lack of corrosion data

There are a limited number of data on corrosion in amine treating plants avaialable in the open literature. They were reported according to process parameters such as solution temperature, amine concentration, and CO_2 loading, which vary significantly from place to place in the process. These available data are rather scattered because they were generated and gathered from different sources under different test environments using different corrosion measuring techniques. As a result, such information can only be useful for describing corrosion behavior qualitatively, i.e. the corrosion trend in respect of process parameters. In addition, the data in most cases were reported without a complete list of essential operating or test conditions. This makes the task of data integration formidable, and also prevents complete understanding of the role of process parameters on corrosion behavior. Therefore, to understand the corrosion behavior, comprehensive corrosion data generated under well-controlled environments are necessary.

2.5.2 Weakness of knowledge of corrosion mechanism

Several corrosion mechanisms have been used to characterize the corrosion phenomena taking place in amine treating plants (Comeaux, 1962; Martin et al., 1977; Parkins and Foroulis, 1988; DuPart et al., 1993; Tomoe *et al.*, 1996). It is speculated in most cases that corrosion reactions are governed by one of the three oxidizing agents which are commonly present in the CO_2 - water system, i.e. hydrogen ion (H^+), undissociated carbonic acid (H_2CO_3) and bicarbonate ion (HCO_3^-). However, no theoretical study currently exists that focuses on the identification of the actual corrosion mechanism in the aqueous amine - CO_2 system in order to verify such speculation. Consequently, the mechanism of CO_2 - alkanolamine corrosion is not yet well understood and remains inconclusive.

CHAPTER 3: MODEL DEVELOPMENT

This chapter employs two sub models, i.e., vapor-liquid equilibrium model and electrochemical corrosion model to generate polarization curve and calculate corrosion rate of carbon steel. For this work the most rigorous Electrolyte-NRTL model (accounting for real gas and real solution) has been selected for the representation of vapor liquid equilibrium in carbon dioxide absorption using activated alkanolamine systems. The electrochemical model takes into account the following electrochemical reactions: hydronium reduction, bicarbonate reduction, water reduction, protonated amine reduction, protonated activator amine reduction and the iron dissolution. The electrochemical cathodic reactions are quantified using the rate equation that takes into account the effect of resistance to both charge and mass transfer. Exchange current densities are evaluated based upon the species bulk concentrations. Mass transfer coefficients from established correlation for electroactive species are used in the electrochemical model. Corrosion rate are calculated based on the mixed potential theory.

3.1 Scheme of the corrosion process

The corrosion process constitutes a number of activities occurring in three layers connected in series: bulk solution, diffusion layer and metal surface. In the bulk solution, a number of chemical species exist as a result of carbon dioxide absorption into the aqueous solution of activated MDEA and activated DEA. These chemical species are dissociated water, dissolved carbon dioxide, bicarbonate ion, carbonate ion, hydronium ion, hydroxyl ion, piperazine, protonated piperazine, piperazine carbamate, piperazine di-carbamate, and protonated carbamate piperazine. In the case of activated MDEA, these species are methyl-di-ethanolamine and protonated methyl-diethanolamine, while for activated DEA these species are di-ethanolamine, protonated di-ethanolamine, and di-ethanolamine carbamate.

It is believed that electrochemical corrosion takes place at the interface and concentration gradients play a major key role to assist the diffusion of chemical species between the bulk solution and the metal surface layer. Furthermore, electrochemical corrosion reactions occur at the metal surface and oxidizing agents are assumed to consist of H_2O, HCO_3^-, H_3O^+ ions and protonated alkanolamines, undergo reduction reactions by oxidizing iron (Fe) and accepting electrons, while the metal undergoes oxidation reactions, producing ferrous ions (Fe^{2+}). The produced Fe^{2+} ions travel from the diffusion layer to the bulk solution. Figure 3.1 depicts the overall corrosion process that was modeled in this work.

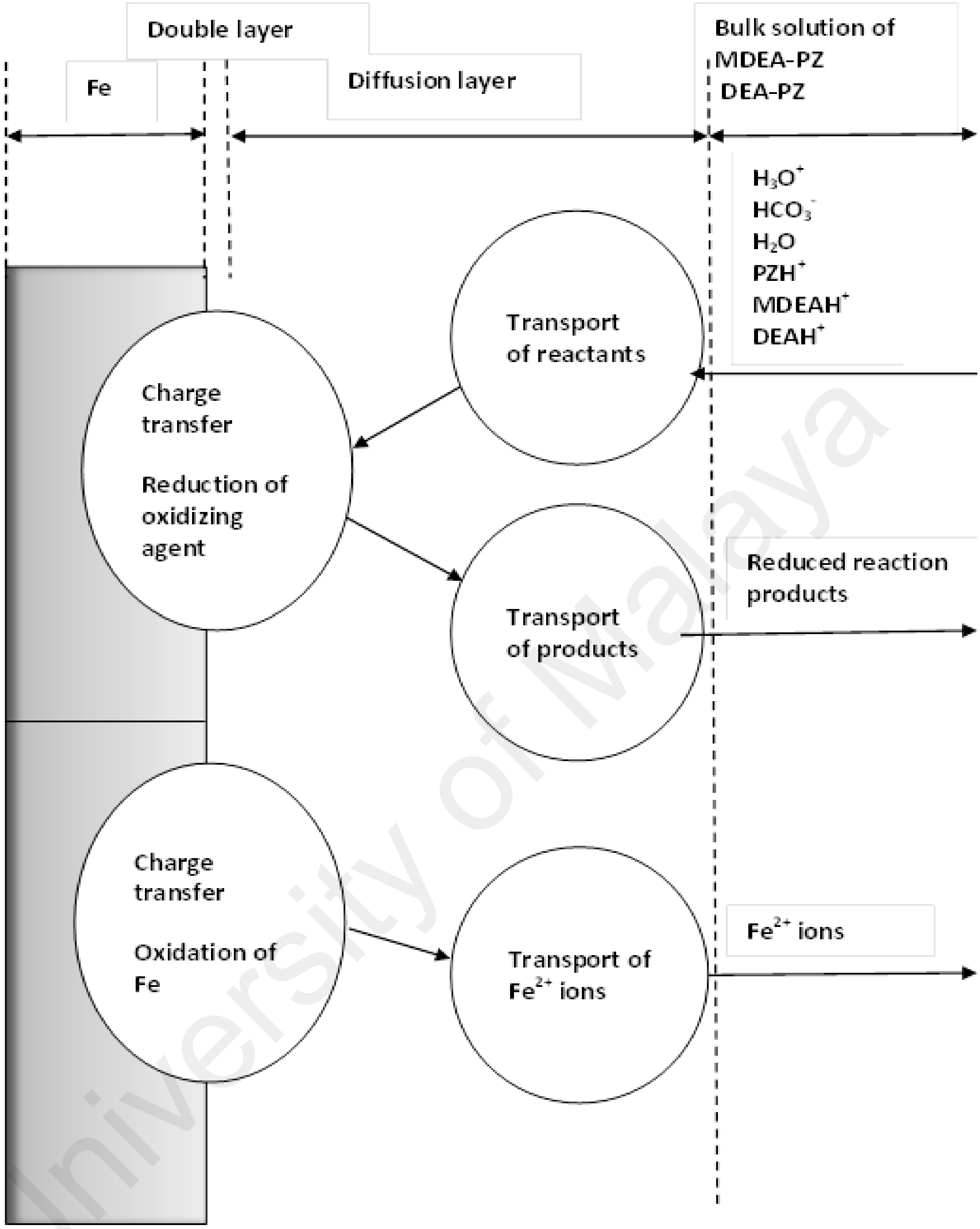

Figure 3.1: Schematic representation of reaction steps during the corrosion process of the carbon steel in the aqueous carbonated alkanolamine environments (Landolt, 2007)

3.2 Thermodynamic framework

The thermodynamic framework comprises three main model components: input, calculation models, and output, as illustrated in Figure 3.2. The input requires information of typical operating conditions of the activated MDEA and activated DEA based CO_2 absorption process, including solution temperature, amine and activator concentrations, and CO_2 partial pressure. The calculation model consists of two sub models: vapour liquid equilibrium model and electrochemical corrosion model. The vapour liquid equilibrium model is used for predicting the solution speciation of all chemical species exist in the bulk solution and the simulated results for VLE were validated using the experimental data obtained from literature. A VLE model for multi-components system is composed of water, PZ, MDEA and DEA as a solvent and dissolved CO_2 should consider the following equations; 1) phase equilibria of each components; 2) equilibrium of chemical reactions occurring in the bulk solution (i.e. dissolution of solvents and electrolyte and the reactions between electrolyte and/or products of their dissolution; 3) mass balance of carbon dioxide atoms and amines; 4) electro-neutrality of solution. In estimating the concentration of each species, e-NRTL model was used for the calculation of activity coefficient. The e-NRTL model considers interactions among chemical species in the bulk solution, which causes the departure from the unity activity coefficients. The bulk concentrations of chemical species obtained from the VLE model are subsequently used in the electrochemical corrosion model. The electrochemical corrosion model accounts for the electrochemical reactions (oxidation of metal and reduction of oxidizing agents) occurring on the metal surface, which are represented by mixed potential theory. The simulation results can be presented as species concentrations in the bulk solution, the concentration of oxidizing agents at the metal surface, polarization curve, and corrosion rate.

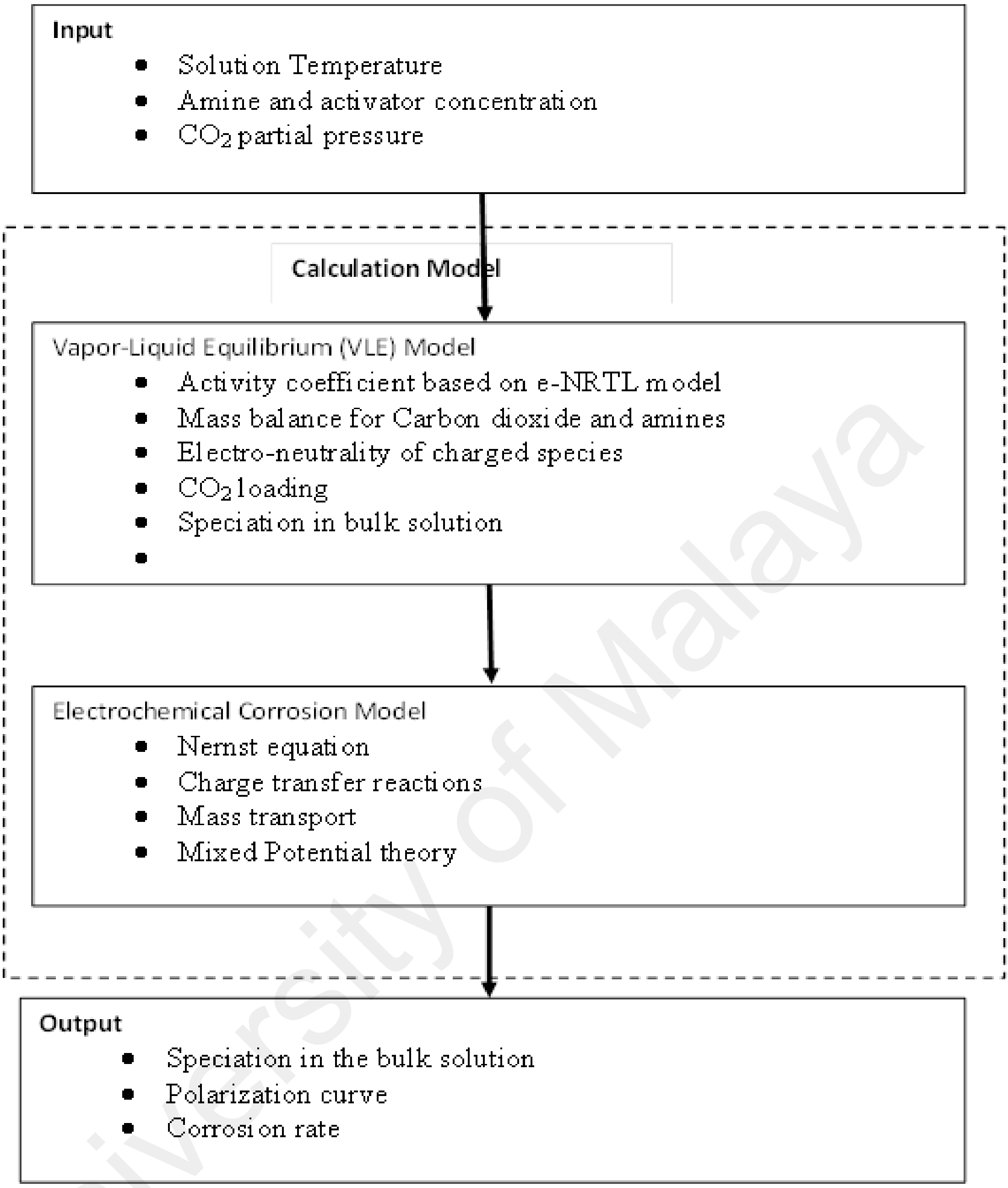

Figure 3.2: Framework of the mechanistic corrosion model

3.3 Vapor-liquid equilibrium model

There are two kinds of equilibria in the alkanolamine aqueous solution: phase equilibrium and chemical equilibrium.

3.3.1 Phase equilibrium

The phase equilibrium governs the distribution of molecular species between the liquid phase and gas phase and represented by Henry's law:

R1: Carbon dioxide phase change:

$$CO_2(g) \overset{H_{co_2}}{\longleftrightarrow} CO_2(l) \tag{3.1}$$

$$H_{CO_2} = \frac{P_{CO_2}}{x_{CO_2}} \tag{3.2}$$

Where, H_{CO_2} is the Henry's law constant of CO_2 in alkanolamine solution, P_{CO_2} is the equilibrium partial pressure of CO_2 in the gas phase, $x_{CO_2}$is the mole fraction of CO_2 molecules in the liquid phase.

3.3.2 Chemical equilibrium

Equilibrium reactions determine speciation in the liquid phase. Most of these equilibrium reactions can be written as chemical dissociation. The reaction mechanism for blends involving aqueous carbonated PZ+MDEA or PZ+DEA in the bulk solution is expressed as :(Austgen *et al.*, 1989; Bishnoi & Rochelle, 2002)

R2: Dissociation of water:

$$2H_2O \overset{K_{H_2O}}{\longleftrightarrow} H_3O^+ + OH^- \tag{3.3}$$

R3: Dissociation of CO_2:

$$CO_2 + 2H_2O \overset{K_{CO_2}}{\longleftrightarrow} HCO_3{}^- + H_3O^+ \tag{3.4}$$

R4: Dissociation of bicarbonate ions:

$$HCO_3^- + H_2O \overset{K_{HCO_3^-}}{\longleftrightarrow} CO_3^{2-} + H_3O^+ \tag{3.5}$$

R5: Dissociation of protonated piperazine:

$$PZH^+ + H_2O \overset{K_{PZH^+}}{\longleftrightarrow} PZ + H_3O^+ \tag{3.6}$$

R6: Formation of piperazine carbamate:

$$PZ + CO_2 + H_2O \overset{K_{PZCOO^-}}{\longleftrightarrow} PZCOO^- + H_3O^+ \tag{3.7}$$

R7: Dissociation of zwitterion (protonated carbamate):

$$H^+PZCOO^- + H_2O \overset{K_{H^+PZCOO^-}}{\longleftrightarrow} PZCOO^- + H_3O^+ \tag{3.8}$$

R8: Formation of piperazine dicarbamate:

$$PZCOO^- + CO_2 + H_2O \overset{K_{PZ(COO^-)_2}}{\longleftrightarrow} PZ(COO^-)_2 + H_3O^+ \tag{3.9}$$

The above reactions (R1-R8) are used for both activated MDEA and activated DEA systems. Thereafter, the reaction mechanism differs between tertiary and secondary amines, where the secondary amines follow zwitterion mechanisms, and tertiary amines does not follow zwitterion mechanisms. The reaction mechanism for MDEA and CO_2 is expressed as in R9:

R9: Dissociation of protonated methyl-di-ethanolamine:

$$MDEAH^+ + H_2O \overset{K_{MDEAH^+}}{\longleftrightarrow} MDEA + H_3O^+ \tag{3.10}$$

DEA can directly react with CO_2 to form carbamate according to the following set of reactions (Austgen *et al.*, 1989):

R10: Dissociation of protonated diethanolamine:

$$DEAH^+ + H_2O \overset{K_{DEAH^+}}{\longleftrightarrow} DEA + H_3O^+ \tag{3.11}$$

R11: Diethanolamine carbamate reversion to bicarbonate:

$$DEACOO^- + H_2O \xleftrightarrow{K_{DEACOO^-}} DEA + HCO_3{}^- \tag{3.12}$$

Where; K_i is the equilibrium constant for reversible reaction at equilibrium, and its value obtained from the literature on a mole fraction basis as exhibited in Table 3.1. Equilibrium constant for the above reactions can also be expressed in terms of activity coefficient (γ_i) and mole fraction chemical species (x_i) as given in equation (3.13) through (3.22):

$$\mathrm{K}_{\mathrm{H_2O}} = \frac{\left(\gamma_{\mathrm{H_3O^+}} x_{\mathrm{H_3O^+}}\right)\left(\gamma_{\mathrm{OH^-}} x_{\mathrm{OH^-}}\right)}{\left(\gamma_{\mathrm{H_2O}} x_{\mathrm{H_2O}}\right)^2} \tag{3.13}$$

$$\mathrm{K}_{\mathrm{CO_2}} = \frac{\left(\gamma_{\mathrm{HCO_3^-}} x_{\mathrm{HCO_3^-}}\right)\left(\gamma_{\mathrm{H_3O^+}} x_{\mathrm{H_3O^+}}\right)}{\left(\gamma_{\mathrm{CO_2}} x_{\mathrm{CO_2}}\right)\left(\gamma_{\mathrm{H_2O}} x_{\mathrm{H_2O}}\right)^2} \tag{3.14}$$

$$\mathrm{K}_{HCO_3^-} = \frac{\left(\gamma_{\mathrm{CO_3^{2-}}} x_{\mathrm{CO_3^{2-}}}\right)\left(\gamma_{\mathrm{H_3O^+}} x_{\mathrm{H_3O^+}}\right)}{\left(\gamma_{\mathrm{HCO_3^-}} x_{\mathrm{HCO_3^-}}\right)\left(\gamma_{\mathrm{H_2O}} x_{\mathrm{H_2O}}\right)} \tag{3.15}$$

$$K_{PZH^+} = \frac{\left(\gamma_{\mathrm{PZ}} x_{\mathrm{PZ}}\right)\left(\gamma_{\mathrm{H_3O^+}} x_{\mathrm{H_3O^+}}\right)}{\left(\gamma_{\mathrm{PZH^+}} x_{\mathrm{PZH^+}}\right)\left(\gamma_{\mathrm{H_2O}} x_{\mathrm{H_2O}}\right)} \tag{3.16}$$

$$K_{PZCOO^-} = \frac{\left(\gamma_{\mathrm{PZCOO^-}} x_{\mathrm{PZCOO^-}}\right)\left(\gamma_{\mathrm{H_3O^+}} x_{\mathrm{H_3O^+}}\right)}{\left(\gamma_{\mathrm{PZ}} x_{\mathrm{PZ}}\right)\left(\gamma_{\mathrm{CO_2}} x_{\mathrm{CO_2}}\right)\left(\gamma_{\mathrm{H_2O}} x_{\mathrm{H_2O}}\right)} \tag{3.17}$$

$$K_{H^+PZCOO^-} = \frac{\left(\gamma_{\mathrm{PZCOO^-}} x_{\mathrm{PZCOO^-}}\right)\left(\gamma_{\mathrm{H_3O^+}} x_{\mathrm{H_3O^+}}\right)}{\left(\gamma_{\mathrm{H^+PZCOO^-}} x_{\mathrm{H^+PZCOO^-}}\right)\left(\gamma_{\mathrm{H_2O}} x_{\mathrm{H_2O}}\right)} \tag{3.18}$$

$$K_{PZ(COO^-)_2} = \frac{\left(\gamma_{\mathrm{PZ(COO^-)_2}} x_{\mathrm{PZ(COO^-)_2}}\right)\left(\gamma_{\mathrm{H_3O^+}} x_{\mathrm{H_3O^+}}\right)}{\left(\gamma_{\mathrm{PZCOO^-}} x_{\mathrm{PZCOO^-}}\right)\left(\gamma_{\mathrm{CO_2}} x_{\mathrm{CO_2}}\right)\left(\gamma_{\mathrm{H_2O}} x_{\mathrm{H_2O}}\right)} \tag{3.19}$$

$$K_{MDEAH^+} = \frac{\left(\gamma_{\mathrm{MDEA}} x_{\mathrm{MDEA}}\right)\left(\gamma_{\mathrm{H_3O^+}} x_{\mathrm{H_3O^+}}\right)}{\left(\gamma_{\mathrm{MDEAH^+}} x_{\mathrm{MDEAH^+}}\right)\left(\gamma_{\mathrm{H_2O}} x_{\mathrm{H_2O}}\right)} \tag{3.20}$$

$$\mathrm{K}_{\mathrm{DEAH^+}} = \frac{\left(\gamma_{\mathrm{DEA}} x_{\mathrm{DEA}}\right)\left(\gamma_{\mathrm{H_3O^+}} x_{\mathrm{H_3O^+}}\right)}{\left(\gamma_{\mathrm{DEAH^+}} x_{\mathrm{DEAH^+}}\right)\left(\gamma_{\mathrm{H_2O}} x_{\mathrm{H_2O}}\right)} \tag{3.21}$$

$$\mathrm{K}_{\mathrm{DEACOO^-}} = \frac{\left(\gamma_{\mathrm{DEA}} x_{\mathrm{DEA}}\right)\left(\gamma_{\mathrm{HCO_3^-}} x_{\mathrm{HCO_3^-}}\right)}{\left(\gamma_{\mathrm{DEACOO^-}} x_{\mathrm{DEACOO^-}}\right)\left(\gamma_{\mathrm{H_2O}} x_{\mathrm{H_2O}}\right)} \tag{3.22}$$

The quantification of the concentration of all chemical species in the bulk solution requires additional equation as described in equation (3.23) through (3.28):

Electro-neutrality balance:

$$\mathrm{AmH^+ + PZH^+ + H_3O^+ = HCO_3^- + OH^- + 2\,CO_3^{-2} + PZCOO^-} \\ \mathrm{+2PZ(COO^-)_2} \qquad (3.23)$$

Mole balance for piperazine:

$$\mathrm{PZ + PZH^+ + PZCOO^- + H^+PZCOO^- + PZ(COO^-)_2 = PZ}_{Total} \qquad (3.24)$$

Mole balance for methyl-di-ethanolamine:

$$\mathrm{MDEA + MDEAH^+ = MDEA_{\,Total}} \qquad (3.25)$$

Mole balance for diethanolamine:

$$\mathrm{DEA + DEAH^+ + DEACOO^- = DEA_{Total}} \qquad (3.26)$$

Total mole fraction:

$$\sum_{i=1}^{\mathrm{i=N}} \mathrm{x_i} = 1.0 \qquad (3.27)$$

Mole balance for carbon dioxide:

$$\mathrm{CO_2 + HCO_3^- + CO_3^{2-} + PZCOO^- + H^+PZCOO^- + PZ(COO^-)_2} \\ \mathrm{+AmCOO^- = \alpha_{CO_2}[total\ Amine]_{alk}} \qquad (3.28)$$

Where; $\mathrm{AmH^+}$ is the protonated amine ($\mathrm{MDEAH^+}$ in the MDEA-PZ system and $\mathrm{DEAH^+}$ in the DEA-PZ system), N is the number of chemical species in the solution, $\mathrm{AmCOO^-}$ is carbamate of amine and it appears only in the DEA-PZ system because MDEA does not form carbamate, therefore, it is omitted from the equation (3.28) for MDEA-PZ system.

Table 3.1: Temperature dependence of equilibrium constants and Henry's constant.

Constant	C_1	C_2	C_3	C_4	T(K)	Reference
Equilibrium constant: $\ln \boldsymbol{K_i} = \boldsymbol{C_1} + \frac{\boldsymbol{C_2}}{\boldsymbol{T}} + \boldsymbol{C_3} \ln \boldsymbol{T} + \boldsymbol{C_4 T}$						
K_{H_2O}	132.9	-13446	-22.48	0.0	273-498	(Posey & Rochelle, 1997)
K_{CO_2}	231.4	-12092	-36.78	0.0	273- 98	(Posey & Rochelle, 1997)
$K_{HCO_3^-}$	216.0	-12432	-35.48	0.0	273-498	(Posey & Rochelle, 1997)
K_{PZH^+}	-9.6416	-5008.4	0.0	0.0	270-350	(Moioli & Pellegrini, 2015)
K_{PZCOO^-}	466.497	1614.5	-97.540	0.2471	273-343	(Dash *et al.*, 2011)
$K_{H^+PZCOO^-}$	6.822	-6066.9	-2.290	0.0036	273-343	(Dash *et al.*, 2011)
$K_{PZ(COO^-)_2}$	-11.563	1769.4	-1.467	0.0024	373-343	(Dash *et al.*, 2011)
K_{MDEAH^+}	-83.49	-819.7	10.9756	0.0	278-368	(Derks *et al.*, 2010)
K_{DEAH^+}	-13.337	-4218.7	0.0	0.0098	313-353	(Austgen *et al.*, 1989)
K_{DEACOO^-}	16.5027	-4068.7	-1.5027	0.0	313-353	(Austgen *et al.*, 1989)
Henry's constant: $\ln \boldsymbol{H_{co_2}} = \boldsymbol{C_1} + \boldsymbol{C_2}/\boldsymbol{T} + \boldsymbol{C_3} \ln \boldsymbol{T} + \boldsymbol{C_4 T}$						
H_{co_2}	170.71	8477.7	-21.95	0.005781	273-373	(Austgen *et al.*, 1989)

The mixed solvent system (symmetric reference state) was produced by the various solvents (water, PZ, DEA and MDEA) and the chosen reference state for ionic solutes and molecular solutes is considered as the ideal infinitely diluted aqueous solution at the system temperature and pressure (asymmetric reference state).

3.3.3 Vapor-liquid equilibrium calculations

The fugacity of each component either in liquid or vapor phase is considered equal provided that the phase equilibrium is established. Equation (3.29) deals with the distribution of CO_2 molecules between the liquid and vapor phase at equilibrium condition, whereas equation (3.30) deals with solvent species (water, PZ, DEA, and MDEA) as per the activity coefficient approach (Poling *et al.*, 2001).

$$\emptyset_{co_2}^{v} y_{co_2} P = \gamma_{co_2}^{*} x_{co_2} H_{CO_2} \exp\left(\frac{\upsilon_{co_2}^{\infty}(P - P_s^{\circ})}{RT}\right) \tag{3.29}$$

$$\emptyset_i^{v} y_i P = \gamma_i x_i P_i^{\circ} \emptyset_i^{\circ} \exp\left(\frac{\upsilon_i (P - P_i^{\circ})}{RT}\right) \tag{3.30}$$

Where; y_i and x_i are concentration of species in the vapour phase and liquid phase, respectively, $\upsilon_{CO_2}^{\infty}$ is the partial molar of CO_2 infinitely diluted in water and υ_i is the partial molar volume of pure liquid solvent calculated by Racket equation of state (Spencer & Danner, 1973). The vapor phase fugacity coefficients in equations (3.29) and (3.30) are calculated using the Soave–Redlich-Kwong (SRK) equation of state (Soave, 1972) and the liquid phase activity coefficients were calculated using the e-NRTL model.

3.3.4 Molar volume

The partial molar volume of CO_2 is taken from the original work of Brelvi and O’Connell (Brelvi & O'connell, 1972). The molar volumes of alkanolamine and water solvents are estimated by the modified Rackett equation. The modified Rackett equation is an empirical expression for calculating the saturated liquid density of pure liquids as a function of temperature. For mixtures, the modified Rackett equation as in equation (3.31):

$$\frac{1}{\rho_m} = \left(\frac{RT_{cm}}{P_{cm}}\right) Z_{RAm}^{[1+(1-T_{rm})^{1/7}]} \tag{3.31}$$

Where; ρ_m is the mixed solvent density, T_{cm} and P_{cm} are the critical temperature and pressure of the mixture, T_{rm} is the reduced temperature of the solvent mixture, and Z_{Ram} is an empirical parameter for mixture. The mixing rules adopted by Spencer and Danner for mixture critical constant are as follow:

$$Z_{RAm} = \sum_i x_i \, Z_{RAi} \tag{3.32}$$

$$V_{cm} = \sum_i x_i \, V_{ci} \tag{3.33}$$

$$T_{cm} = \frac{1}{V_{cm}^2} \sum_i \sum_j x_i x_j V_{ci} V_{cj} \left(T_{ci} T_{cj}\right)^{1/2} \left(1 - k_{ij}\right) \tag{3.34}$$

$$T_{rm} = \frac{T}{T_{cm}} \tag{3.35}$$

$$\frac{T_{cm}}{P_{cm}} = \sum_i x_i \frac{T_{ci}}{P_{ci}} \tag{3.36}$$

$$k_{ij} = 1 - \left[\frac{\left(V_{ci}^{1/3} V_{cj}^{1/3}\right)^{1/2}}{\left(\frac{V_{ci}^{1/3} + V_{cj}^{1/3}}{2}\right)} \right]^3 \tag{3.37}$$

The molar volumes of pure species are calculated by substituting pure component parameters in equation (3.31).

3.3.5 Fugacity coefficient model

The modification of the Redlich-Kwong equation of state done by Soave's (Soave, 1972) is used to represent the vapor phase equilibrium. Soave changed the temperature dependence term a/T$^{0.5}$ by making the constant "a" as a function of temperature and the acentric factor. The soave Redlich-Kwong equation of state is given by equation (3.38):

$$P = \frac{RT}{V - b} - \frac{a\alpha}{V(V + b)} \tag{3.38}$$

Where T and P represent the temperature and pressure of the vapor phase and R represents the gas constant. The attraction between the molecules and dependence on their size are represented in the equation by the parameters *a* and b, respectively.

$$a = \frac{0.4274R^2T_c^2}{P_c} \tag{3.39}$$

Where;

$$\alpha = [1 + m_i(1 - T_r^{0.5})]^2 \tag{3.40}$$

$$m_i = (0.48508 + 1.55171\omega_i - 0.15613\omega_i^2) \tag{3.41}$$

The terms α and m_i were determined empirically to fit known vapor pressures. The parameter *b* is calculated similarly as in the original Redlich-Kwong equation (3.42):

$$b = \frac{0.08664RT_c}{P_c} \tag{3.42}$$

Where; T_c and P_c represent the critical temperature and pressure, respectively.

Expressions for *a* and b for gas mixtures are included in the model.

$$\mathrm{a\alpha} = \sum\sum \mathrm{y_i y_j (a\alpha)_{ij}} \tag{3.43}$$

$$\mathrm{b} = \sum \mathrm{y_i b_i} \tag{3.44}$$

$$\mathrm{(a\alpha)_{ij}} = \left(1 - \mathrm{k_{ij}}\right)\sqrt{\left[\left((\mathrm{a\alpha})_i\right)\left((\mathrm{a\alpha})_j\right)\right]} \tag{3.45}$$

k_{ij} = interaction parameter between molecule i and j. The calculation of vapor phase fugacity coefficient is done by the application of mixing rules using the SRK equation of state (equation (3.46)). Critical constants for all the relevant molecular species are reported in Table 3.3.

$$\ln(\phi_i) = \frac{b_i}{b}(z-1) - ln\left[z\left(1 - \frac{b}{V}\right)\right] + \frac{a\alpha}{bRT}\left[\frac{b_i}{b} - \frac{2}{a\alpha}\sum y_i(a\alpha)_{ij}\right] ln\left(1 + \frac{b}{V}\right) \tag{3.46}$$

Where;

$$Z = \frac{PV}{RT} \tag{3.47}$$

3.3.6 Activity coefficient model

The Electrolyte Non-Random Two-Liquid (e-NRTL) equation was used in this work to calculate excess Gibbs energy calculated by equation (3.48) (Austgen *et al.*, 1989; Chen & Evans, 1986; Mock *et al.*, 1986; Renon & Prausnitz, 1968):

$$\frac{G^{ex}}{RT} = \frac{G^{ex,PDH}}{RT} + \frac{G^{ex,Born}}{RT} + \frac{G^{ex,lc}}{RT} \tag{3.48}$$

$$\frac{G^{\ ex,PDH}}{RT} = -\sum_k x_k \left(\frac{1000}{M_s}\right)^{0.5} \left(\frac{4A_\phi I_x}{\rho}\right) \ln\left(1 + \rho {I_x}^{0.5}\right) \tag{3.49}$$

Where; Dedye-Huckel parameter, A_ϕ and ionic strength of solvent, I_x are given by equation (3.50) and equation (3.51) respectively.

$$A_\phi = \frac{1}{3}\left(\frac{2\pi N_A d_s}{1000}\right)^{\frac{1}{2}} \left(\frac{e^2}{DkT}\right)^{\frac{3}{2}} \tag{3.50}$$

$$I_x = \frac{1}{2}\sum_i x_i Z_i^2 \tag{3.51}$$

The Born correction term for the excess Gibbs energy is given by equation (3.52):

$$\frac{G^{ex,Born}}{RT} = \left(\frac{e^2}{2kT}\right)\left(\frac{1}{D_s} - \frac{1}{D_w}\right)\left(\sum_i \frac{x_i {z_i}^2}{r_i}\right) \times 10^{-2} \tag{3.52}$$

The mixed solvent dielectric constant, D_s, is calculated by a simple mass fraction average (Mock *et al.*, 1986). The dielectric constants of all solvent components are given in Table 3.2. The dielectric constant is related to the components ability to stabilize ions in solution. As the dielectric constant increases, the tendency for ions to form and remain as ionic species also increases. The temperature dependence for H_2O, MDEA, DEA and PZ on dielectric constants is represented in this work using equations (3.53) and (3.54):

$$D = a_1 + b_1/T(K)\left[\frac{1}{T(K)} - \frac{1}{T^{ref}(K)}\right] \tag{3.53}$$

Where; T^{ref} is the reference temperature (273.15 K). For mixed solvent, the dielectric constant is calculated based on the following expression:

$$D_m = \sum_i w_{mi}^{sf} D_i \tag{3.54}$$

Where : w_{mi}^{sf} is the solute free, solvent fraction.

Table 3.2: Coefficients for dielectric constant of PZ, MDEA, DEA and water.

Species	$\mathbf{a_1}$	$\mathbf{b_1}$	Source
H_2O	88.36	33030	(Bishnoi & Rochelle, 2002)
PZ	36.76	14836	(Bishnoi & Rochelle, 2002)
MDEA	24.76	8989	(Bishnoi & Rochelle, 2002)
DEA	28.01	9277	(Austgen *et al.*, 1989)

The local electrolyte NRTL expression for the short range interactions is described as:

$$\frac{G^{ex,lc}}{RT} = \sum_m X_m \frac{\sum_j X_j G_{jm}\tau_{jm}}{\sum_k X_k G_{km}} + \sum_c X_c \sum_{a'}\left(\frac{X_{a'}}{\sum_{a''} X_{a''}}\right) \frac{\sum_j X_j G_{jc,a'c}\ \tau_{jc,a'c}}{\sum_k X_k G_{kc,a'c}} + \sum_a X_a \sum_{c'}\left(\frac{X_{c'}}{\sum_{c''} X_{c''}}\right)\left(\frac{\sum_j X_j G_{ja,c'a}\ \tau_{ja,c'a}}{\sum_k X_k G_{ka,c'a}}\right) \tag{3.55}$$

$$G_{im} = \exp(-\alpha_{im}\,\tau_{im}) \tag{3.56}$$

$$G_{ca,m} = \exp(-\alpha_{ca,m}\,\tau_{ca,m}) \tag{3.57}$$

$$G_{jc,a'c} = \exp(-\alpha_{jc,a'c}\,\tau_{jc,a'c}) \tag{3.58}$$

$$G_{ja,c'a} = \exp(-\alpha_{ja,c'a}\,\tau_{ja,c'a}) \tag{3.59}$$

$$G_{cm} = \frac{\sum_a X_a G_{ca,m}}{\sum_{a'} X_{a'}}, \qquad G_{am} = \frac{\sum_c X_a G_{ca,m}}{\sum_{c'} X_{c'}} \tag{3.60}$$

$$\alpha_{cm} = \frac{\sum_a X_a \alpha_{ca,m}}{\sum_{a'} X_{a'}}, \qquad \alpha_{am} = \frac{\sum_c X_a \alpha_{ca,m}}{\sum_{c'} X_{c'}} \tag{3.61}$$

$$\tau_{ma,ca} = \tau_{ma} - \tau_{ca,ma} - \tau_{m,ca} \tag{3.62}$$

$$\tau_{mc,ac} = \tau_{cm} - \tau_{ca,m} - \tau_{m,ca} \tag{3.63}$$

Where; X_j is the effective liquid-phase mole fraction, $X_j=x_j.C_j$ ($C_j=Z_j$ for ions and 1 for molecules). α_{ij} is the e-NRTL non-randomness parameter, τ_{ij} is the binary energy interaction parameter. Both α and τ are considered as adjustable parameters of the electrolyte NRTL expression. Equation (3.64) expressing the partial derivate of the excess Gibbs energy was applied to calculate the activity coefficient for any species (ionic or molecular, solute or solvent).

$$ln\,\gamma_i = \frac{1}{RT}\left[\frac{\partial(n_t G^{ex})}{\partial n_i}\right]_{T,P,n_{j\neq i}} \tag{3.64}$$

3.3.7 Vapour-liquid equilibrium model parameters

There are several pure components and binary parameters are involved in vapor liquid equilibrium model developed above such as: critical constants, acentric factor, compressibility factor and Brelvi-O'Connell parameter. Moreover, to solve the Antoine equation the constants for vapor pressure of various molecular species are taken from literature and presented in Table 3.3 and Table 3.4. The non-randomness parameter was fixed at 0.2 for molecule-molecule interaction and water-ion pair interactions following Chen and Evan (1986). Non-randomness factors for alkanolamine-ion pair and CO_2-ion pair interactions were fixed at 0.1 as suggested by the study of Mock *et al.* (1986); for non-aqueous solutions of electrolytes. Binary interaction parameters for molecule-molecule, molecule-ion pair and ion pair-ion pair are expressed as a function of temperature as described by equation (3.65) trough (3.66):

$$\tau_{m,ca} = A_{ca,m} + \frac{B_{m,ca}}{T} \tag{3.65}$$

$$\tau_{ca,m} = A_{ca,m} + \frac{B_{ca,m}}{T} \tag{3.66}$$

Following the study of Austgen *et al.* (1989) the ion pair-ion pair parameters are considered insignificant and were assigned a value of zero by setting all other parameters values to their default as presented in the Table 3.5. Pitzer, (1980) suggested to fix the distance of closest approach term at 14.9 and the default value of 3 angstroms was set for ionic radii.

Table 3.3: Pure component physical properties for VLE model.

Properti	**H_2O**	**CO_2**	**PZ**	**DEA**	**MDEA**
MW	18.02	44.01	86.136	105.14	119.16
T_c(K)	647.3	304.2	638.0	715.0	677.79
P_c(kPa)	22048	7376	6870	3270	876
V_c(m^3/kmol)	0.0559	0.0939	0.23	0.349	0.39
Acentric factor (ω)	0.344	0.23	0.8	1.046	1.24
Racket Z_{RA}	0.2432	0.2736	0.2	0.	.19
Brelvi-O'Connell parameter	0.0464	0.0939			
Source	(Austgen, 1989)	(Austgen, 1989)	(Bishnoi & Rochelle, 2002)	(Austgen, 1989)	(Austgen, 1989)

Table 3.4: Antoine equation coefficients of molecular species.

Components	**H_2O**	**CO_2**	**PZ**	**MDEA**	**DEA**	**Ions**
A	75.55	72.82912	70.503	29.137	286. 1	-1.00E+20
B	-7206.7	-3403.28	-7914.5	-7588.5	-20360	0
C	0	0	0	0	0	0
D	0	9.49E-03	0	0	0	0
E	-7.1385	-8.56034	-6.6461	0	-40.4	0
F	4.05E-06	2.91E-16	5.21E-18	0	0.032378	0
G	2	6	6	0	1	0
$\ln(p_i^o(\mathrm{pa}) = A + \frac{B}{(T(K)+C)} + D\,T(K) + E\ln\big(T(K)\big) + F\big(T(K)\big)^G$						

Table 3.5: Default values of pair parameters for e-NRTL model.

Parameter	$A_{m,ca}$	$B_{m,ca}$	$A_{ca,m}$	$B_{ca,m}$	α_{ij}
τ (H_2O- ion pair)	8.045	0.0	-4.072	0.0	0.2
τ (CO_2-ion pair)	15	0.0	-8.00	0.0	0.1
τ(molecule-ion pair)	10	0.0	-2	0.0	0.1

3.3.8 Mathematical solving for speciation

A Matlab program was developed for calculating bulk concentration of species in the carbonated aqueous solution of MDEA-PZ and DEA-PZ systems based on the above discussed equations. Concentrations of all species were unknown and defined as dependent variables, except the concentration of CO_2, which was calculated from the equation (3.2) for both systems. For aqueous solution of MDEA-PZ, thirteen equations with thirteen variables need to be solved. Equations (3.13) - (3.20) and (3.13) - (3.27) can be reduced to a single seventh order polynomial equation in terms of hydronium ion concentration [H_3O^+], initial amine concentration and equilibrium constants of reactions corresponding to the species. For aqueous solution of DEA-PZ, fourteen equations with fourteen variables need to be solved. In this case, Equations (3.23) - (3.27), except equations for MDEA (3.20) and (3.25), can be reduced to a single eight order polynomial equation in terms of hydronium ion concentration [H_3O^+], initial amine concentration and equilibrium constants. The value of [H_3O^+] is associated with the pH of the solution at equilibrium. There is more than one possible root for each CO_2 partial pressure. However, only one value of [H_3O^+] is valid and should lie between 10^{-6} mol/L and 10^{-12} mol/l, which correspond to the pH values of a carbonated alkanolamine solution and commercial application normally reside in the range of 6 - 12 respectively. The concentrations of other species can also be calculated by combination of equations above. Equations were solved simultaneously using the iteration process of non-linear equation. The obtained outputs are concentration and activity coefficients for the chemical species in the bulk solution. The CO_2 loading in absorption systems is evaluated using equation (3.28).

3.3.9 Implementation of vapour-liquid equilibrium model

The simulation was carried out by varying input parameters (solution temperature, CO_2 partial pressure and amine concentration). Calculate the equilibrium constants and Henry's constant using values in the Table 3.1 at a given temperature. Concentrations of all species were unknown and defined as independent variable except the concentration of carbon dioxide, which was calculated using equation (3.2) at a given partial pressure. The equations were reduced to a single seventh order polynomial for MDEA-PZ system and eighth order polynomial for DEA-PZ system in terms of hydronium ion concentration $[H_3O^+]$, initial amine concentration and equilibrium constants. The concentration of hydronium ion is related to the pH of equilibrium solution. For each CO_2 partial pressure there is more than one possible root to solve the polynomial. However, one value of hydronium ion is valid, which lie between 10^{-6} and 10^{-12} mol/l corresponding to the pH of aqueous carbonated amine solution values for a commercial application is in range of 6 to 12. Calculate the initial guess for speciation $[x_i]$ according to equations (3.13) - (3.27) using equilibrium constants and $[H_3O^+]$. Then, resolve the polynomial equation for determining $[H_3O^+]$ using activity coefficients values. The concentrations species were used to iterate for the next value of concentration $[x_{i+1}]$. The program was stopped when the relative error was less than 1E-02. The obtained output is the concentration of chemical species in the bulk solution, activity coefficients and CO_2 loading in the solution. The implementation steps of the model to estimate the CO_2 loading and species concentration at equilibrium are simplified and shown in Figure 3.3.

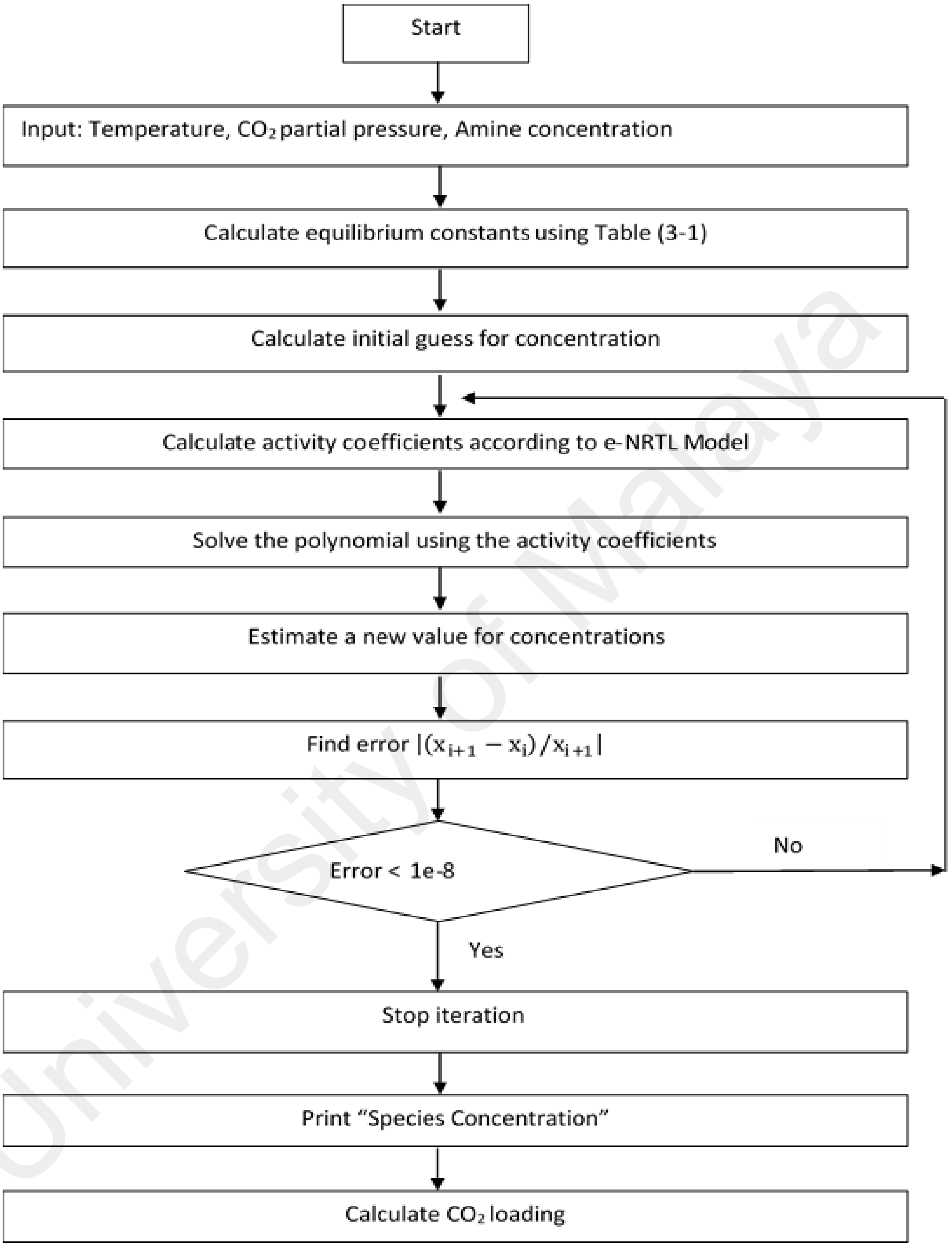

Figure 3.3: Simplified flow chart for the simulation steps to solve for speciation

3.4 Electrochemical corrosion model

3.4.1 Electrochemical reactions

The electrochemical reactions occurring simultaneously at the metal-solution interface are considered as oxidation of metal (iron dissolution) and reduction of oxidizing agents. Generally, iron (Fe) at the anode site donates electrons to the cathodic site and dissolves in the solution as ferrous (Fe^{2+}). The electrons simultaneously attract oxidizing agents to the interface for reduction reactions. Four possible reduction reactions that were considered in this work include: 1) hydronium ion, 2) bicarbonate ion 3) water and 4) protonated alkanolamine. Six electrochemical reactions are considered to occur in the MDEA-PZ and DEA-PZ systems, i.e., one anodic and five cathodic reactions at the metal solution surface as described below:

Oxidation of iron:

$$\mathrm{Fe} \rightleftharpoons \mathrm{Fe}^{2+} + 2\mathrm{e}^{-} \tag{3.67}$$

Reduction of hydronium ion:

$$2\mathrm{H_3O^+} + 2\mathrm{e}^{-} \rightleftharpoons 2\mathrm{H_2O} + \mathrm{H_2} \tag{3.68}$$

Reduction of bicarbonate ion:

$$2\mathrm{HCO_3^-} + 2\mathrm{e}^{-} \rightleftharpoons 2\mathrm{CO_3^{2-}} + \mathrm{H_2} \tag{3.69}$$

Reduction of water:

$$2\mathrm{H_2O} + 2\mathrm{e}^{-} \rightleftharpoons 2\mathrm{OH^-} + \mathrm{H_2} \tag{3.70}$$

Reduction of protonated piperazine ion:

$$2\mathrm{PZH^+} + 2\mathrm{e}^{-} \rightleftharpoons 2\mathrm{PZ} + \mathrm{H_2} \tag{3.71}$$

Reduction of protonated methyl-di-ethanolamine ion:

$$2\mathrm{MDEAH^+} + 2\mathrm{e}^{-} \rightleftharpoons 2\mathrm{MDEA} + \mathrm{H_2} \tag{3.72}$$

Reduction of protonated diethanolamine ion:

$$2\mathrm{DEAH}^{+} + 2\mathrm{e}^{-} \rightleftharpoons 2\mathrm{DEA} + \mathrm{H}_2 \tag{3.73}$$

Carbonic acid is considered to be “weak acid” because of its partial dissociation in water to produce H^+ ions and HCO_3^- ion.

$$2H_2CO_3 + 2e^{-} \rightleftharpoons 2HCO_3^{-} + H_2 \tag{3.74}$$

Since carbonated solutions of aqueous activated MDEA and activated DEA system are alkaline and the contribution of H_2CO_3 reduction reaction is negligible due to the very low concentration in the solution compared to other species.

3.4.2 Mathematical corrosion model

The mixed potential theory was incorporated into the corrosion model to determine the E_{corr} (corrosion potential). It states that the sum of the rate of the oxidation reactions is equal to the sum of the rate of reduction reactions. In carbonated aqueous solution of MDEA-PZ and DEA-PZ environment, it was assumed that the oxidation reaction deals with the conversion of Fe to Fe^{2+}, while the reduction reactions involve five reactions due to the presence of five oxidizing agents including H_3O^+,HCO_3^-, H_2O, PZH^+ and $MDEAH^+$/$DEAH^+$.

$$\sum i_{oxidation} = \sum i_{reduction} \tag{3.75}$$

Since iron dissolution is the only oxidation reaction in this system, the oxidation rate was expressed as in equation (3.76):

$$\sum i_{oxidation} = i_{Fe/Fe^{2+}} \tag{3.76}$$

The iron dissolution was considered to be under activation control (charge transfer) because of the unlimited supply of Fe. In this case, the relationship between the current density (*i*) and potential (E) was described as in equation (3.77):

$$i_{Fe/Fe^{2+}} = i_{o,Fe/Fe^{2+}} \times e^{\left(\frac{\alpha_a nF}{RT}\left(E-E_{rev,Fe/Fe^{2+}}\right)\right)} \tag{3.77}$$

For the reduction, potential reactions participating in corrosion process are H_3O^+, HCO_3^-, H_2O, PZH^+ and $MDEAH^+$/$DEAH^+$, which function as oxidizing agents. If all five are the actual oxidizing agents in aqueous carbonated MDEA-PZ and DEA-PZ environment, the total reduction rate will be as in equation (3.78):

$$\sum i_{reduction} = i_{H_3O^+/H_2} + i_{HCO_3^-/CO_3^{2-}} + i_{H_2O/OH^-} + i_{PZH^+/PZ} + i_{AmH^+/Am} \tag{3.78}$$

Where; AmH^+ and Am describe protonated alkanolamine and activated amine, respectively. For reduction reactions on the surface of the metal, the cathodic part of the general rate equation takes into account the effect of resistance to charge transfer and mass transfer, which are considered to be under mixed control. Since water molecules are present in unlimited quantities at the carbon steel surface, it can be assumed that the reduction rate of H_2O is controlled by the charge transfer control:

$$i_{H_3O^+/H_2} = -i_{o,H_3O^+/H_2} \times \left\{\frac{[H_3O^+]_s}{[H_3O^+]_b} \times \mathrm{e}^{\left(-\frac{\alpha_c nF}{RT}\left(E-E_{rev,H_3O^+/H_2}\right)\right)}\right\} \tag{3.79}$$

$$i_{HCO_3^-/CO_3^{2-}} = -i_{o,HCO_3^-/CO_3^{2-}} \times \left\{\frac{[HCO_3^-]_s}{[HCO_3^-]_b} \times \mathrm{e}^{\left(-\frac{\alpha_c nF}{RT}\left(E-E_{rev,HCO_3^-/CO_3^{2-}}\right)\right)}\right\} \tag{3.80}$$

$$i_{H_2O/OH^-} = -i_{o,H_2O/OH^-} \times \mathrm{e}^{\left(-\frac{\alpha_c nF}{RT}\left(E-E_{rev,H_2O/OH^-}\right)\right)} \tag{3.81}$$

$$i_{PZH^+/PZ} = -i_{o,PZH^+/PZ} \times \left\{\frac{[PZH^+]_s}{[PZH^+]_b} \times \mathrm{e}^{\left(-\frac{\alpha_c nF}{RT}\left(E-E_{rev,PZH^+/PZ}\right)\right)}\right\} \tag{3.82}$$

$$i_{AmH^+/Am} = -i_{o,AmH^+/Am} \times \left\{\frac{[AmH^+]_s}{[AmH^+]_b} \times e^{\left(-\frac{\alpha_c nF}{RT}\left(E - E_{rev,AmH^+/Am}\right)\right)}\right\} \quad (3.83)$$

Where; *i* is the current density of a reaction (A/m^2), $[j]_s$ is the surface concentration of *j* species (mol/l), $[j]_b$ is the bulk concentration of *j* species (mol/l), E is the applied potential (V), α is the symmetry factor, n is the number of electrons transferred in the reduction reaction and F is the Faraday's constant(C/mol). The surface concentration on electrode can be determined from the mass-transport equation:

$$i_{H_3O^+/H_2} = -nFD_{H_3O^+}\left\{\frac{[H_3O^+]_b - [H_3O^+]_s}{\delta_{H_3O^+}}\right\} \quad (3.84)$$

$$i_{HCO_3^-/CO_3^{-2}} = -nFD_{HCO_3^-}\left\{\frac{[HCO_3^-]_b - [HCO_3^-]_s}{\delta_{HCO_3^-}}\right\} \quad (3.85)$$

$$i_{PZH^+/PZ} = -nFD_{PZH^+}\left\{\frac{[PZH^+]_b - [PZH^+]_s}{\delta_{PZH^+}}\right\} \quad (3.86)$$

$$i_{AmH^+/Am} = -nFD_{AmH^+}\left\{\frac{[AmH^+]_b - [AmH^+]_s}{\delta_{AmH^+}}\right\} \quad (3.87)$$

Solving equations (3.79) – (3.83) and (3.84) – (3.87) for determining the surface concentrations, after manipulation, the final current density vs. potential relationship for H_3O^+, HCO_3^-, PZH^+ and AmH^+ reduction is:

$$\frac{1}{i_{H_3O^+/H_2}} = \frac{1}{i_{ct,H_3O^+/H_2}} + \frac{1}{i^d_{\mathrm{L},H_3O^+/H_2}} \quad (3.88)$$

$$\frac{1}{i_{HCO_3^-/CO_3^{-2}}} = \frac{1}{i_{ct,HCO_3^-/CO_3^{-2}}} + \frac{1}{i^d_{\mathrm{L},HCO_3^-/CO_3^{-2}}} \quad (3.89)$$

$$\frac{1}{i_{PZH^+/PZ}} = \frac{1}{i_{ct,PZH^+/PZ}} + \frac{1}{i^d_{\mathrm{L},PZH^+/PZ}} \quad (3.90)$$

$$\frac{1}{i_{AmH^+/Am}} = \frac{1}{i_{ct,AmH^+/Am}} + \frac{1}{i^d_{\mathrm{L},AmH^+/Am}} \quad (3.91)$$

Where i_{L}^{d} is the diffusion limiting current density (A/m^2) and i_{ct} is the charge transfer contribution to the current density in the absence of mass transfer resistance.

$$i_{ct,H_3O^+/H_2} = i_{o,H_3O^+/H_2} \times 10^{\left(-\frac{\left(E-E_{rev,H_3O^+/H_2}\right)}{\beta_c}\right)} \tag{3.92}$$

$$i_{ct,HCO_3^-/CO_3^{-2}} = i_{o,HCO_3^-/CO_3^{2-}} \times 10^{\left(-\frac{\left(E-E_{rev,HCO_3^-/CO_3^{2-}}\right)}{\beta_c}\right)} \tag{3.93}$$

$$i_{ct,H_2O/OH^-} = i_{o,H_2O/OH^-} \times 10^{\left(-\frac{\left(E-E_{rev,H_2O/OH^-}\right)}{\beta_c}\right)} \tag{3.94}$$

$$i_{ct,PZH^+/PZ} = i_{o,PZH^+/PZ} \times 10^{\left(-\frac{\left(E-E_{rev,PZH^+/PZ}\right)}{\beta_c}\right)} \tag{3.95}$$

$$i_{ct,AmH^+/Am} = i_{o,AmH^+/Am} \times 10^{\left(-\frac{\left(E-E_{rev,AmH^+/Am}\right)}{\beta_c}\right)} \tag{3.96}$$

Where; i_{o} is the equilibrium exchange current density of a reaction (A/m^2), E$_{\mathrm{rev}}$ is the reversible electrode potential (V), β_{c} and β_{a} are the cathodic and anodic Tafel slope, respectively. The values of i_{o}, E$_{\mathrm{rev}}$ and β exhibit the characteristics for a practical electrochemical reaction and exhibit dependence on the temperature and the concentration of species involved in the reaction at the metal surface. Some of these parameters are usually not available in the literature and must be obtained from the experimental study. The calculations of these parameters are summarized in Table 3.6:

$$\beta_c = \frac{2.303\,RT}{\alpha_c nF} \qquad \beta_a = \frac{2.303\,RT}{\alpha_a nF} \tag{3.97}$$

$$i_{o,Fe} = i_{o,Fe,ref}\left(\frac{C_{HCO_3^-}}{C_{HCO_3^-,ref}}\right)^{a_1}\left(\frac{C_{H_3O^+}}{C_{H_3O^+,ref}}\right)^{a_2} e^{-\frac{E_a}{R}\left(\frac{1}{T}-\frac{1}{T_{ref}}\right)} \tag{3.98}$$

$$i_{o,H_3O^+} = i_{o,H_3O^+,ref}\left(\frac{C_{H_3O^+}}{C_{H_3O^+,ref}}\right)^{a_3} e^{-\frac{E_a}{R}\left(\frac{1}{T}-\frac{1}{T_{ref}}\right)} \tag{3.99}$$

$$i_{o,HCO_3^-} = i_{o,HCO_3^-,ref}\left(\frac{C_{HCO_3^-}}{C_{HCO_3^-,ref}}\right)^{a_4} e^{-\frac{E_a}{R}\left(\frac{1}{T}-\frac{1}{T_{ref}}\right)} \quad (3.100)$$

$$i_{o,H_2O} = i_{o,H_2O,ref}\left(\frac{C_{H_2O}}{C_{H_2O,ref}}\right)^{a_5} e^{-\frac{E_a}{R}\left(\frac{1}{T}-\frac{1}{T_{ref}}\right)} \quad (3.101)$$

$$i_{o,PZH^+} = i_{o,PZH^+,ref}\left(\frac{C_{PZH^+}}{C_{PZH^+,ref}}\right)^{a_6} e^{-\frac{E_a}{R}\left(\frac{1}{T}-\frac{1}{T_{ref}}\right)} \quad (3.102)$$

$$i_{o,MDEAH^+} = i_{o,MDEAH^+,ref}\left(\frac{C_{MDEAH^+}}{C_{MDEAH^+,ref}}\right)^{a_6} e^{-\frac{E_a}{R}\left(\frac{1}{T}-\frac{1}{T_{ref}}\right)} \quad (3.103)$$

$$i_{o,DEAH^+} = i_{o,DEAH^+,ref}\left(\frac{C_{DEAH^+}}{C_{DEAH^+,ref}}\right)^{a_6} e^{-\frac{E_a}{R}\left(\frac{1}{T}-\frac{1}{T_{ref}}\right)} \quad (3.104)$$

Where; C_j is the concentration of j^th species (mol/l), a_i is the reaction order, E_a is the activation energy (J/mol), which was assumed independent of temperature, R is the universal gas constant (J/mol K), T_{ref} is the reference temperature (K) and T is the absolute temperature (K). Data and mechanisms were found in the open literature for the reactions which were considered in the present study only the exchange current density for PZH^+ and $DEAH^+$ reduction reaction which were assumed same as $MDEAH^+$ reduction.

Table 3.6: Electrochemical kinetic parameters for the exchange current density included in the model

Reaction	**$i_{o,ref}$ (A/m^2)**	**E$_a$ (kJ/mol)**	**$C_{H_3O^+,re}$ (mol/l)**	**$C_{HCO_3^-,re}$ (mol/l)**	**$C_{AmH^+,re}$ (mol/l)**	**Reaction order**	**Source**
Fe oxidation	0.53	37.5	$10^{-9.1}$	1	-	a_1=2, a_2=-0.5	(Choi *et al.*, 2012)
H_3O^+ reduction	0.05	30	10^{-4}	-	-	a_3=0.5	(Nešić *et al.*, 1996)
HCO_3^- reduction	0.15	50	-	0.5	-	a_4=0.5	(Choi *et al.*, 2012)
H_2O reduction	3.0E-5	30	10^{-4}	-	-	a_5=0.5	(Nešić *et al.*, 1996)
PZH^+ reduction	0.15	20	-	-	0.63	a_6=1	--------
$MDEAH^+$ reduction	0.1	20	-	-	0.63	a_7=1	(Choi *et al.*, 2012)
$DEAH^+$ reduction	0.15	20	-	-	0.63	a_8=1	--------

The reversible potential E_{rev} (V) for each reaction was calculated from the Nernst equation as shown in equation (3.105):

$$E_{rev,j} = E_{T,j}^{o} + \frac{RT}{nF}\ln\left(\frac{a_{oxid}}{a_{red}}\right) \qquad (3.105)$$

Where; E_T^o is the standard electrode potential (V) at any temperature, R is the universal gas constant (J/mol.K), T is the absolute temperature (K), n is the number of electrons taking part in the reaction, a_{oxid} and a_{red} are the activities of oxidized and reduced species, respectively, obtained by the product of activity coefficient and mole fraction, F is the Faraday's constant (C/mol). The calculation of E_T^o value is performed from as in equation (3.106):

$$\Delta G_T^o = -\, n_i F E_T^o \qquad (3.106)$$

Where ΔG_T^o is the Gibbs free energy of formation for any compound at any given temperature, which can be calculated using equation (3.107):

$$\Delta G_T^o = T\left[\frac{\Delta G_r^o}{298.15} + \Delta H_r^o\left(\frac{1}{T} - \frac{1}{298.15}\right)\right] \tag{3.107}$$

Where ΔG_r^o and ΔH_r^o are standard Gibbs free energy of reaction (kJ/mol) and standard enthalpy of reaction (kJ/mol) at 298.15 K, respectively, and T is the system temperature (K). The values of ΔG_r^o and ΔH_r^o are given in Table 3.7.

Table 3.7: Gibbs free energy and enthalpy of reaction at standard state (298.15 K)

Reaction	**ΔG_r^o (kJ/mol)**	**ΔH_r^o (kJ/mol)**	**Source**
Oxidation of Fe	84.9	87.9	(Veawab, 2001)
Reduction of H_3O^+	0.0	0.0	(Veawab, 2001)
Reduction of HCO_3^-	118	29.8	(Veawab, 2001)
Reduction of H_2O	159.8	111.6	(Veawab, 2001)
Reduction of $MDEAH^+$	98.46	73.8574	(Sadegh, 2012)
Reduction of PZH^+	111.09	85.78	(Goldberg *et al.*, 2002)
Reduction of $DEAH^+$	101.364	85.6	(Bower *et al.*, 1962)

According to equations (3.88) - (3.91), the current density reaches maximum limiting values provided the surface concentration decreases to zero. This condition is expressed as the limiting current density and can be written in terms of mass transfer coefficient as in equations (3.108) trough (3.112):

$$i_{L,H_3O^+}^d = -nFk_m[H_3O^+]_b \tag{3.108}$$

$$i_{L,HCO_3^-}^d = -nFk_m[HCO_3^-]_b \tag{3.109}$$

$$i_{L,PZH^+}^d = -nFk_m[PZH^+]_b \tag{3.110}$$

$$i_{L,MDEAH^+}^d = -nFk_m[MDEAH^+]_b \tag{3.111}$$

$$i_{L,DEAH^+}^d = -nFk_m[DEAH^+]_b \tag{3.112}$$

Where k_m is the mass-transfer coefficient of a reaction (1/s) and is introduced into Sherwood number (*Sh)*, for rotating disk electrode, the laminar mass transport correlation is given by Levich (1962):

$$Sh = \frac{k_m d}{D_i} = 0.621\, Re^{0.5}\, Sc^{0.33} \tag{3.113}$$

Where; d is the diameter of rotating disk diameter (m); D_i is a diffusion coefficient of reacting species in m^2/s; Re and Sc are Reynolds and Schmidt numbers, respectively, described as in equation (3.114) through (3.116) :

$$\mathrm{Re} = \frac{\mathrm{u\ d}}{\nu} \tag{3.114}$$

$$\mathrm{Sc} = \frac{\nu}{\mathrm{D}} \tag{3.115}$$

$$\nu = \mu/\rho \tag{3.116}$$

Where; u is the linear velocity; and ν is the kinematic viscosity of solution, μ and ρ are the dynamic viscosity and density of aqueous carbonated solution of activated MDEA and activated DEA, respectively. The limiting current density in terms of readily obtained parameters is given as in equations (3.117) through (3.121):

$$\mathrm{i}_{\mathrm{L,H_3O^+}} = -0.621\ \mathrm{nFD}_{\mathrm{H_3O^+}}^{2/3}[\mathrm{H_3O^+}]_{\mathrm{b}}\nu^{-1/6}\omega^{1/2} \tag{3.117}$$

$$\mathrm{i}_{\mathrm{L,HCO_3^-}} = -0.621\ \mathrm{nFD}_{\mathrm{HCO_3^-}}^{2/3}[\mathrm{HCO_3^-}]_{\mathrm{b}}\nu^{-1/6}\omega^{1/2} \tag{3.118}$$

$$\mathrm{i}_{\mathrm{L,PZH^+}} = -0.621\ \mathrm{nFD}_{\mathrm{PZH^+}}^{2/3}[\mathrm{PZH^+}]_{\mathrm{b}}\nu^{-1/6}\omega^{1/2} \tag{3.119}$$

$$\mathrm{i}_{\mathrm{L,MDEAH^+}} = -0.621\ \mathrm{nFD}_{\mathrm{MDEAH^+}}^{2/3}[\mathrm{MDEAH^+}]_{\mathrm{b}}\nu^{-1/6}\omega^{1/2} \tag{3.120}$$

$$\mathrm{i}_{\mathrm{L,DEAH^+}} = -0.621\ \mathrm{nFD}_{\mathrm{DEAH^+}}^{2/3}[\mathrm{DEAH^+}]_{\mathrm{b}}\nu^{-1/6}\omega^{1/2} \tag{3.121}$$

The diffusion coefficient is a function of temperature and can be calculated using Stokes-Einstein relation for various species:

$$\mathrm{D} = \mathrm{D_{ref}} \times \frac{\mathrm{T}}{\mathrm{T_{ref}}} \times \frac{\mu_{\mathrm{ref}}}{\mu} \tag{3.122}$$

Where; D_{ref} is the diffusion coefficient of species in water at a reference temperature (T_{ref}), μ_{ref} is the dynamic viscosity of mixed alkanolamine solutions at T_{ref} and μ is the viscosity of mixed alkanolamine solutions at any temperature (T).

The diffusion coefficient values for ionic species are provided in Table 3.8 and the diffusion coefficient for the protonated amine have been assumed equal to that of molecular amine (Critchfield, 1988).

Table 3.8: Diffusion coefficients of ionic species in water at 298.15 K

Species	Diffusion coefficient (m^2/s)	Sources
H_3O^+	9.31E-09	(Najumudeen, 2012)
HCO_3^-	1.11E-09	(Najumudeen, 2012)
$MDEAH^+$	2.35E-10	(Rowley *et al.*, 1997)
PZH^+	5.66E-10	(Derks *et al.*, 2008)
$DEAH^+$	1.56E-10	(Rowley *et al.*, 1998)

The Weiland equation can be expressed for the carbonated aqueous mixed solutions as in equation (3.123):

$$\mu_{mix} = \frac{w_1}{w_1 + w_2}\mu_{1,\alpha} + \frac{w_2}{w_1 + w_2}\mu_{2,\alpha} \tag{3.123}$$

Where; μ_{mix} is the viscosity of carbonated aqueous MDEA-PZ and DEA-PZ solutions, μ_1 and μ_2 are the viscosities of the single alkanolamines in water at loading α and w_i is the mass fraction of amine *i*. The viscosity of single alkanolamine (Ns/m^2) can be determined from the following equation (Weiland *et al.*, 1998):

$$\mu_i = \mu_{H_2O}\, e^{\left(\frac{[(a_i w_1 + b_i)T + (c_i w_1 + d_i)][\alpha(e_i w_1 + f_i T + g_i) + 1]w_1}{T^2}\right)} \tag{3.124}$$

Where; μ_{H_2O} is the viscosity of water (kg/m.s) at any given temperature T, T is the given temperature (K), α is the CO_2 loading (mol CO_2 /mol amine), w_1 is the mass percent of amine, and the values of constant (a,b,c,d,e,f, and g) are given in Table 3.9. The value of μ_{H_2O} was determined as a function of the temperature shown in equation (3.125) (Najumudeen, 2012) :

$$\mu_{H_2O} = \mu_{H_2O,20\,^oC} \times 10^{\left(\frac{1.3277(20 - T) - 0.001053(T - 20)^2}{T - 105}\right)} \tag{3.125}$$

Where $\mu_{H_2O,20\,^oC}$ is the viscosity of water at 20 °C (0.001002 NS/m^2).

Table 3.9: Parameters for MDEA and DEA viscosity

Constant	a	b	c	d	e	f	g	source
MDEA	-0.1944	0.4315	80.684	2889.1	0.0106	0	-0.2141	(Weiland *et al.*, 1998)
DEA	-0.0724	-3.4363	54.319	3628	-0.0015	0	0.2104	(Weiland *et al.*, 1998)
PZ	0.1156	8.444	-9.074	3.224	0.7412	0.0225	-9.074	(Fu *et al.*, 2013)

3.4.3 Implementation of electrochemical corrosion model

The present electrochemical model was implemented in Matlab software 2013a to exploit the user friendly interface and the advanced graphical capabilities. The model required input: temperature (K), species concentration of oxidizing agents (mol/l), and the hydrodynamic parameters which are the rotating speed (rad/sec) and disc diameter (m). Once the input parameters are determined, the model calculates individual and total cathodic and anodic currents rates. The intersection of the total cathodic curve with the anodic curve gives us the corrosion potential (E_{corr}) by solving equation (3.75). Corrosion current density (i_{corr}) is calculated from the anodic reaction current equation (3.77) at $E=E_{corr}$. The corrosion rate of carbon steel (mm/yr) was determined from the value of corrosion current density i_{corr} in (A/m^2), as shown in equation (3.126):

$$\mathrm{CR} = \frac{\mathrm{i_{corr}M_{Fe}}}{\mathrm{\rho_{Fe}nF}} \tag{3.126}$$

Equation (3.126) can be applied for carbon steel (MW= 55.854 kg/kmol, ρ = 7800 kg/m^3) accompanied with 2 moles of electron transferred. Moreover, this equation can be easily converted to more convenient and traditional sets of units exhibited as in equation (3.127):

$$CR = 1.155 \times i_{corr}(A/\mathrm{m}^2) \tag{3.127}$$

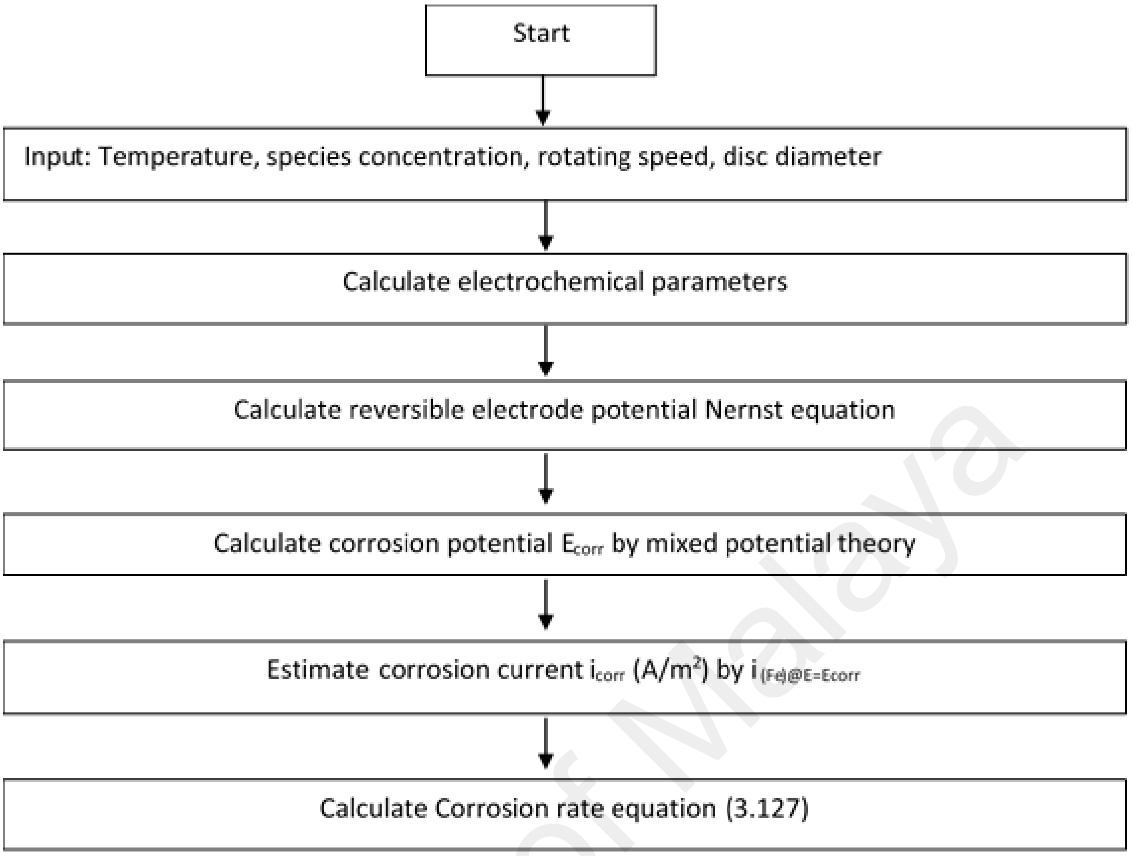

Figure 3.4: Simplified flow chart for the simulation steps to calculate corrosion rate and generate polarization curve.

3.5 Generate polarization curve

Simulated anodic and cathodic polarization curves were established on the basis of calculated species concentrations in order to investigate the theoretical oxidation and reduction behavior. It is important to note that all polarization curves begin at coordinate (i_o, E_{rev}) and proceed in the direction where the current density (i) increases. The behavior of Iron dissolution and reduction of oxidizing ions (j) simulated polarization curve following the expressed equations (3.128) and (3.129):

$$i_{ox} = i_{o,Fe/Fe^{+2}} \times e^{\frac{2.303(E-E_{rev,Fe/Fe^{+2}})}{\beta_a}} \tag{3.128}$$

$$i_{red,j} = \frac{i_{o,j} e^{\left(\frac{-2.303(E-E_{rev,j})}{\beta_c}\right)}}{1 - \frac{i_{o,j}}{i_{L,j}} e^{\left(\frac{-2.303(E-E_{rev,j})}{\beta_c}\right)}} \tag{3.129}$$

At any potential, i_{ox} will not be equal to i_{red}, and the net current density is described as in equation (3.130):

$$i_{net} = i_{ox} - \sum_{j=1}^{j=N} i_{red} \tag{3.130}$$

The values of net current density (i_{net}) and applied potential (E) obtained from equation (3.130) plotted as E verses $\log|i_{net}|$ to produce the polarization curve. It should be noted that i_{net} has been described in equation (3.130), where i_{ox} and i_{red} are always positive quantities. Therefore, the sign of i_{net} will reveal whether the net reaction is oxidation ($i_{net}>0$) or reduction ($i_{net}<0$) reaction. This convention is consistent with external current measurement, wherein positive values reflect net oxidation at the working electrode and negative values net reduction. At higher values of $\log|i_{net}|$, the branches become linear and correspond to the Tafel lines but as values of $\log|i_{net}|$ approaches zero, the polarization curve become a asymptotic to the corrosion potential, E_{corr}.

CHAPTER 4: SIMULATION RESULTS AND DISCUSSION

A mechanistic corrosion model for carbon steel corrosion rate in an aqueous activated MDEA and activated DEA solutions based CO_2 absorption process was developed in this work. The model is an integration of two main models that employ the principle of vapor-liquid equilibrium (VLE) and electrochemical corrosion. The reliability of speciation model in determining the concentrations of chemical species for activated MDEA and activated DEA was verified by comparing the developed VLE model with published data for these systems. The speciation results from VLE model were subsequently used for the generation of polarization curves, as well as relevant corrosion data, of the carbonated aqueous MDEA-PZ and DEA-PZ system under given conditions, which were compared with those from literature. The developed corrosion model was later used to simulate corrosion data under different conditions to study the effects of the activator (PZ) on corrosion rate of carbon steel in the investigated media. Details of the model verification and corrosion simulation are given in the following sections.

4.1 Simulation results of the speciation model

4.1.1 Model verification

In order to validate the VLE model, the CO_2 loading and solution pH were compared to those from the experimental work. The comparison was executed under a wide range of operating conditions, as listed in Table 4.1 and 4.2. As shown in Table 4.1, the amounts of CO_2 absorbed into the solution from experimental work and from this model are compared, with a less than 13.16 % deviation. This difference might result from the interaction parameters between ions and molecules, which were taken as a default parameter from the study of (Austgen *et al.*, 1989). This can be dedicated to the fact that

Henry's constant were used in this work, taken from the work of (Austgen *et al.*, 1989) in that they used Henry's law for CO_2 in the solvent water only, which differs from that of MDEA-PZ and DEA-PZ. Low CO_2 partial pressure data is subject to large relative errors due to limitations in the usual experimental technique employed to evaluate the CO_2 gas equilibrium partial pressure. At higher CO_2 partial pressure, accuracy is often limited by the technique used, to measure CO_2 concentration in the liquid phase.

Table 4.1: Data sets for model development and absolute average deviation, % for predicting values of solubility of solution in the MDEA, DEA, MDEA-PZ and DEA-PZ systems

Reference	MDEA (mol/l)	DEA (mol/l)	PZ (mol/l)	T (K)	P_{CO_2} (kPa)	N	AAD%[a]
(Ali & Aroua, 2004)	2 1.98 1.9 1.8		0 0.01 0.05 0.1	313-353	0.01-100	60	1 .48
(Liu *et al.*, 1999)	1.53 1.35 3.15 2.8 4.77 3.75		0.17 0.35 0.35 0.7 0.53 1.55	303-363	17.18-935.3	78	16.21
(Derks *et al.*, 2010)	4 2.8 0.5		0.6 0.7 1.5	303-333	0.25-110	85	24.53
(Vahidi *et al.*, 2009)	2 2.5 3		1.36 0.86 0.36	313.15-343.15	27.8-3938.4	103	11.14
(Sidi-Boumedine *et al.*, 2004)		6.825		298.13-348.07	2.46-4662.7	25	12.47
(Haji-Sulaiman *et al.*, 1998)		2 4		303-323	0.09-104.73	24	6.8

^{a}AAD% $= \frac{\left|\alpha_{co_2(Cal.)} - \alpha_{co_2(Exp.)}\right|}{\alpha_{co_2(Exp.)}} \times 100$; N: number of data point

Table 4.1 (continued): Data sets for model development and absolute average deviation, % for predicting values of solubility of solution in the MDEA, DEA, MDEA-PZ and DEA-PZ systems

Reference	MDEA (mol/l)	DEA (mol/l)	PZ mol/l)	T (K)	P_{CO_2} (kPa)	N	AAD%^{a}
(Dawodu & Meisen, 1994)		4.2		373.2	93-3742	6	5.9
(Lee *et al.*, 1972)		0.525 2.47 5.22 9.41 16.7 33		273.15-413.2	0.6895-6895	308	13.62
(Ali, 2007)		2 1.98 1.9 1.8	0 0.01 0.05 0.1	313-353	0.01-100	60	14.59
(Mondal, 2009)		3.2-0.8	0.02-0.8	313-353	10.13-20.265	44	0.68

$^a\text{AAD\%} = \frac{\left|\alpha_{co_2(Cal.)}-\alpha_{co_2(Exp.)}\right|}{\alpha_{co_2(Exp.)}} \times 100$; N: number of data point

Table 4.2: Data sets for model development and absolute average deviation, % for predicting values of pH of solution in the MDEA, DEA, MDEA-PZ and DEA-PZ systems

Reference	MDEA (mol/l)	DEA (mol/l)	PZ (mol/l)	T (°C)	P_{CO_2} (kPa)	N	AAD%^{b}
(Ali, 2007)	2 1.98 1.9 1.8		0 0.01 0.05 0.1	313-353	0.01-100	60	7.26
(Derks *et al.*, 2010)	4 2.8 0.		0.6 0.7 1.5	303-323	0.25-110	84	9.24
(Ali, 2007)		2 1.98 1.9 1.8	0 0.01 0.05 0.1	313-353	0.01-100	48	6.18

$^bAAD\% = \frac{\left|\text{pH}_{co_2(Cal.)}-\text{pH}_{co_2(Exp.)}\right|}{\text{pH}_{co_2(Exp.)}} \times 100$; N: number of data point

4.1.2 Speciation results

After verification, the developed VLE model was used to determine equilibrium concentration of all chemical species in the bulk MDEA-PZ and DEA-PZ solutions under a wide range of operating conditions of the activated alkanolamine-based CO_2 absorption process. These data were plotted against three operating parameters: CO_2 loading in the solution, solution temperature, and PZ concentration, for the study of parametric effects on speciation.

4.1.2.1 Effect of CO_2 loading on the solution

The speciation was simulated for partial pressure of CO_2 values from 0.001 to 100 kPa, while the amine concentration and solution temperature were kept constant. The main species of the reaction, in the activated alkanolamine are the base alkanolamine not the species of the activator, with respect to the activator concentrations. However, there is an impact on the overall behavior of the solution speciation.

Figure 4.1 represents the predicted speciation concentration for the carbonated aqueous solution of (1.8M MDEA + 0.1M PZ) at low absorption temperature. Figure 4.1 shows an abrupt decrease in PZ concentration at low CO_2 loading due to the reaction of PZ with CO_2, which is much faster than that of the MDEA reaction with CO_2. Furthermore, PZ forms carbamates and MDEA does not. Protonated piperazine PZH^+, and piperazine carbamate $PZCOO^-$ showed a sudden increase until CO_2 loading point of 0.05 moles per mole alkalinity. Both species concentration further increase slowly, to reach their maximum concentration at CO_2 loading of around 0.1 moles per mole alkalinity. The piperazine carbamates further reacts with CO_2 to produce piperazine di-carbamate and reaches its maximum concentration at CO_2 loading of 0.70 (mole CO_2/mole alkalinity). There was a decrease in the concentration of the protonated piperazine and piperazine carbamate with the increase of the piperazine di-carbamate and the protonated piperazine carbamate concentrations. The behavior of MDEA species in the mixture is similar to that of aqueous carbonated MDEA. However, at very low CO_2 loadings, MDEA concentration seems to be invariant. This is due to the fact that MDEA reaction with CO_2 is slower compared to that of piperazine with CO_2. It is important to note that the behavior of piperazine species in the mixture MDEA/PZ are different from the behavior of same species in carbonated aqueous solution of piperazine especially at low CO_2 loadings.

Figure 4.2 represents the predicted speciation for the carbonated aqueous solution of 1.8M DEA+0.1M PZ at absorption temperature of 313.15 K. Both DEA and PZ form carbamate species. PZ reacts faster with CO_2 than DEA reacting with CO_2, for DEA speciation prediction in the mixture, there is no difference in species behaviors with that of carbonated aqueous solution of DEA alone. Piperazine speciation prediction within the mixture presents a small difference compared to that of aqueous carbonated solution of piperazine alone, particularly at low CO_2 loadings. The behavior of the PZ species concentration is similar to the MDEA-PZ system, except in this case the reaction of DEA with CO_2 is faster compared to that of MDEA with CO_2. In general, the formation of bicarbonate allows a high CO_2 loading, but because of the formation of little carbamate, the kinetics of the reaction is slow. A higher free amine concentration partially counteracts the slow kinetics, but the overall rate of absorption may be slower than secondary amines.

As shown in Figure 4.1 and 4.2, the bulk concentration of H_3O^+, HCO_3^-, $MDEAH^+$,$DEAH^+$, $DEACOO^-$,PZH^+ ,$PZCOO^-$, $PZ(COO^-)_2$ and H^+PZCOO^- increases with CO_2 loading. However, the concentration of H_3O^+ and HCO_3^-, is much more sensitive to CO_2 loading than that of MDEA, DEA and PZ species concentration which exhibit dependence on the concentration of alkanolamine in the solution.

As shown in Figure 4.1 and 4.2, the bulk concentration of H_3O^+, HCO_3^-, $MDEAH^+$,$DEAH^+$, $DEACOO^-$,PZH^+ ,$PZCOO^-$, $PZ(COO^-)_2$ and H^+PZCOO^- increases with CO_2 loading. However, H_3O^+, and HCO_3^- , is much more sensitive to the CO_2 loading than MDEA, DEA and PZ species which exhibit dependence on the concentration of alkanolamine in the solution. With the common knowledge that corrosion increase with CO_2 loading, this suggests that H_3O^+ and HCO_3^- could play a more significant role in corrosion. It should be noted that HCO_3^- is likely to have more influence on corrosion rate than H_3O^+, since the quantity of HCO_3^- is much higher in the solution than H_3O^+ (i.e. the concentration of HCO_3^- is 0.0044 – 1.41 while the concentration of H_3O^+ is 4.5E-11 – 2.6E-08 in the 1.8M MDEA+0.1M PZ).

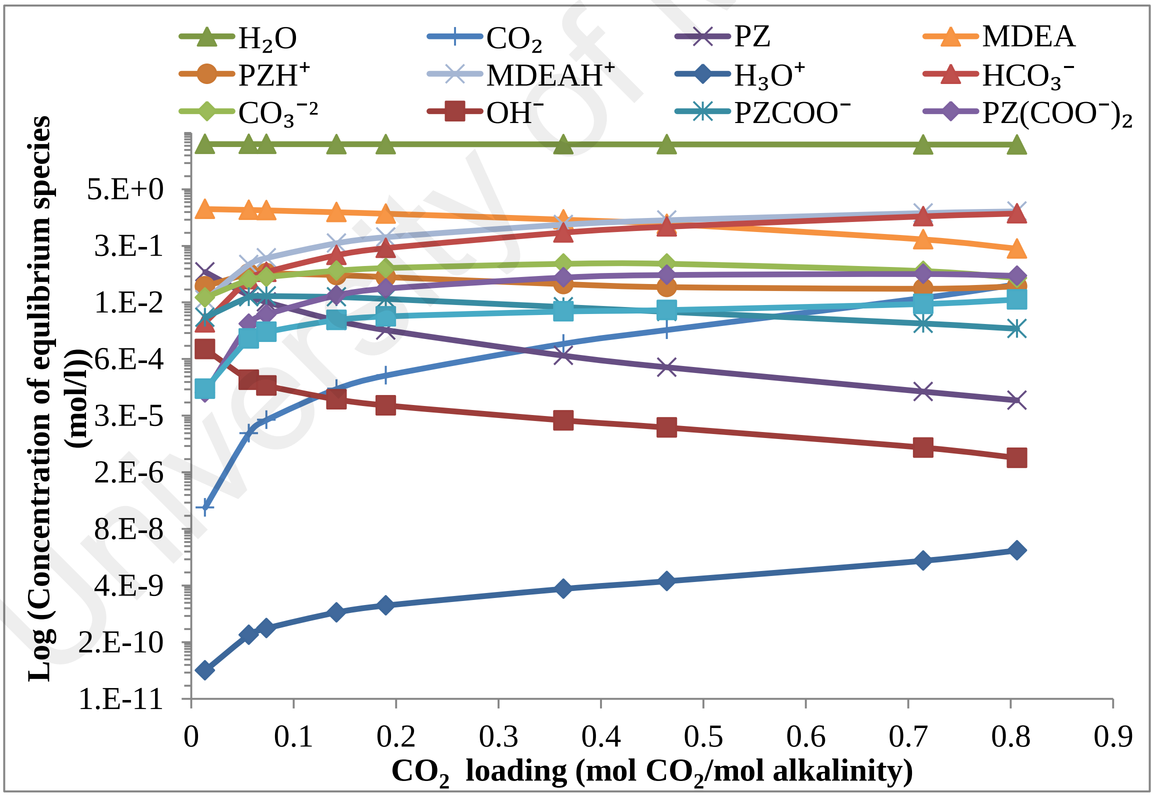

Figure 4.1: Effect of CO_2 loading on speciation in the bulk MDEA-PZ solution (1.8 + 0.1) M; 40 °C.

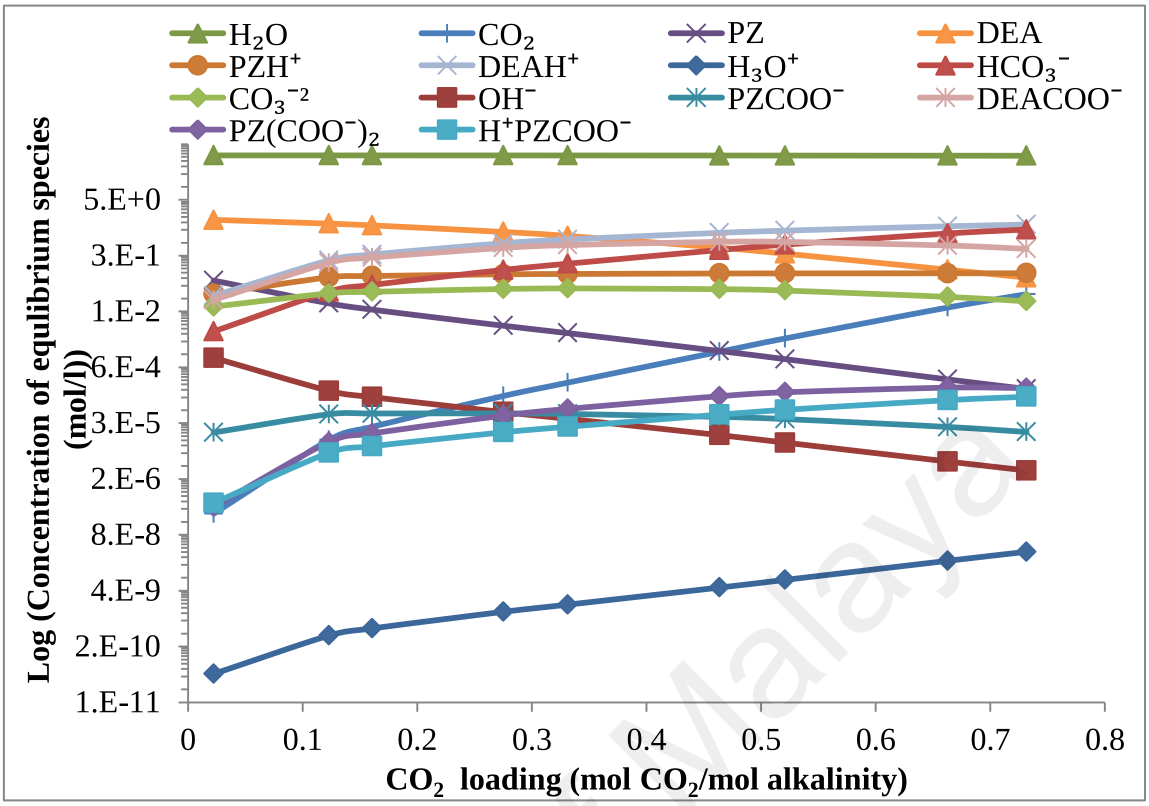

Figure 4.2: Effect of CO_2 loading on speciation in the bulk DEA-PZ solution (1.8 + 0.1) M; 40 °C.

4.1.2.2 Effect of solution temperature

The speciation was simulated for various solution temperatures ranging from 40 to 120 °C with an interval of 10 °C, while keeping total amine concentration and CO_2 partial pressure constant. The general observation that the increase in solution temperature at fixed CO_2 partial pressure, will lead to the decrease in the CO_2 solubility as molecular alkanolamine increases in the solution. This phenomenon is linked to the decreasing rate of reaction for CO_2 capture. As expected, the higher amine concentration will lead to the higher ionic species concentration. There is no significant temperature dependency on speciation concentration. Figure 4.3 and 4.4 showed that as the solution temperature increased, the bulk concentrations of equilibrium species decreased. The PZ species concentration was more sensitive to the change in solution temperature than MDEA and DEA species. However, the concentration ranges of HCO_3^-, MDEAH+ and DEAH+ in the bulk solution were greater than activator species. This suggests that $DEAH^+$, PZH^+, $MDEAH^+$ and HCO_3^- are oxidizing agents participating in the corrosion process.

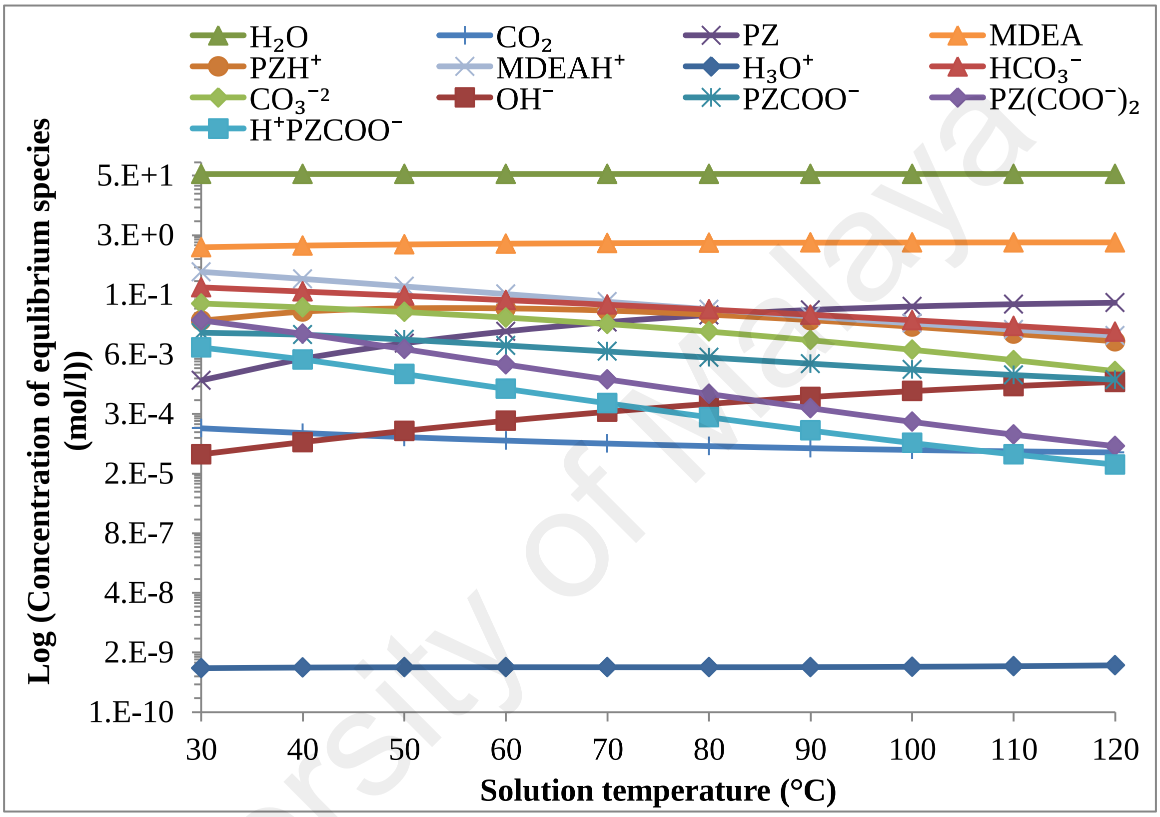

Figure 4.3: Effect of solution temperature on speciation in the bulk (1.8M MDEA + 0.1M PZ) solution; P_{CO2} =0.5 kPa.

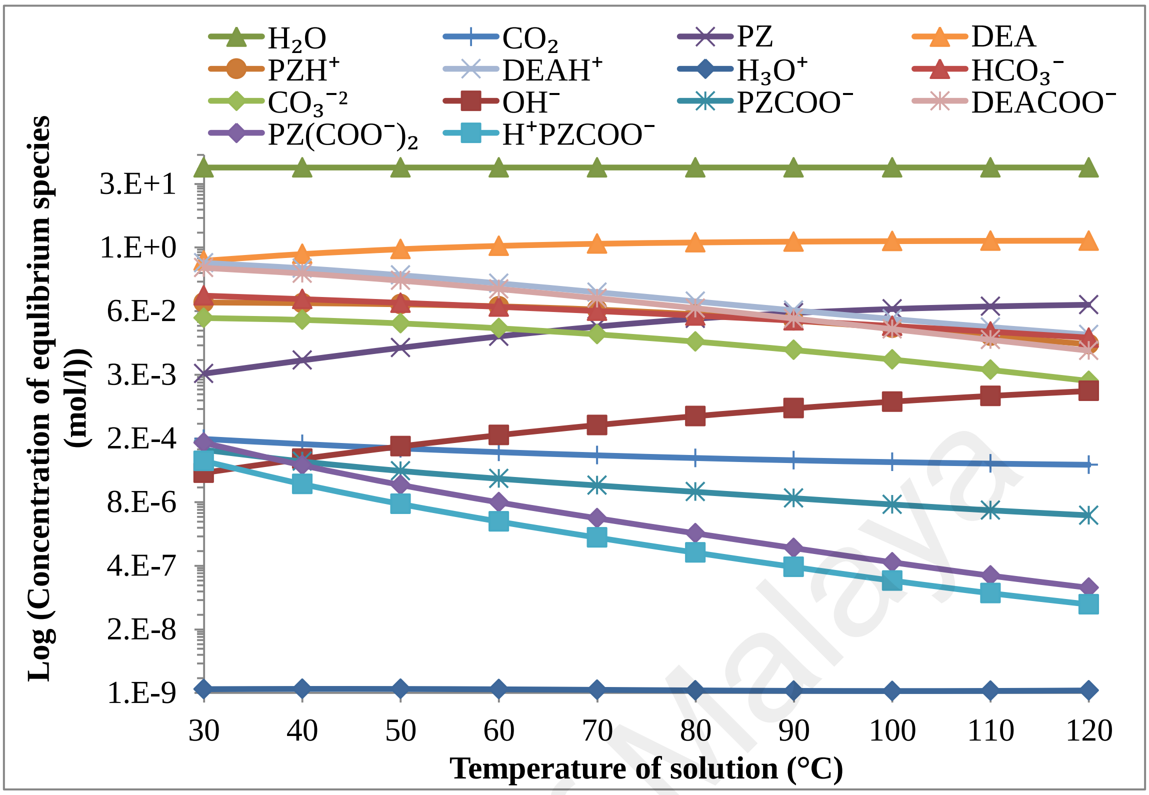

Figure 4.4: Effect of solution temperature on speciation in the bulk (1.8M DEA + 0.1M PZ) solution; P_{CO2} =0.5 kPa.

4.1.2.3 Effect of Activator Concentration

The speciation was simulated for various activator concentrations (PZ) ranging from 0 to 1M for the total amine solution by keeping the temperature and CO_2 partial pressure constant at 40 °C and 0.5 kPa, respectively. Moreover, the total alkalinity of solution was adjusted at 2 M in both MDEA-PZ and DEA-PZ systems. Figures 4.5 and 4.6 showed that the bulk concentration of all chemical species vary, except for that of HCO_3^- and H_3O^+, remained unchanged when changing amine (MDEA/DEA) concentration by PZ concentration. In the MDEA-PZ system, the concentration of HCO_3^- was slightly decreased with the increase of PZ concentration (Figure 4.5). This was dedicated to the decrease in MDEA concentration as it is dissociating to form $MDEAH^+$ and HCO_3^-. On the other hand, there was an increase in the HCO_3^-

concentration for DEA-PZ system with the increase of PZ concentration as exhibited in Figure 4.6.

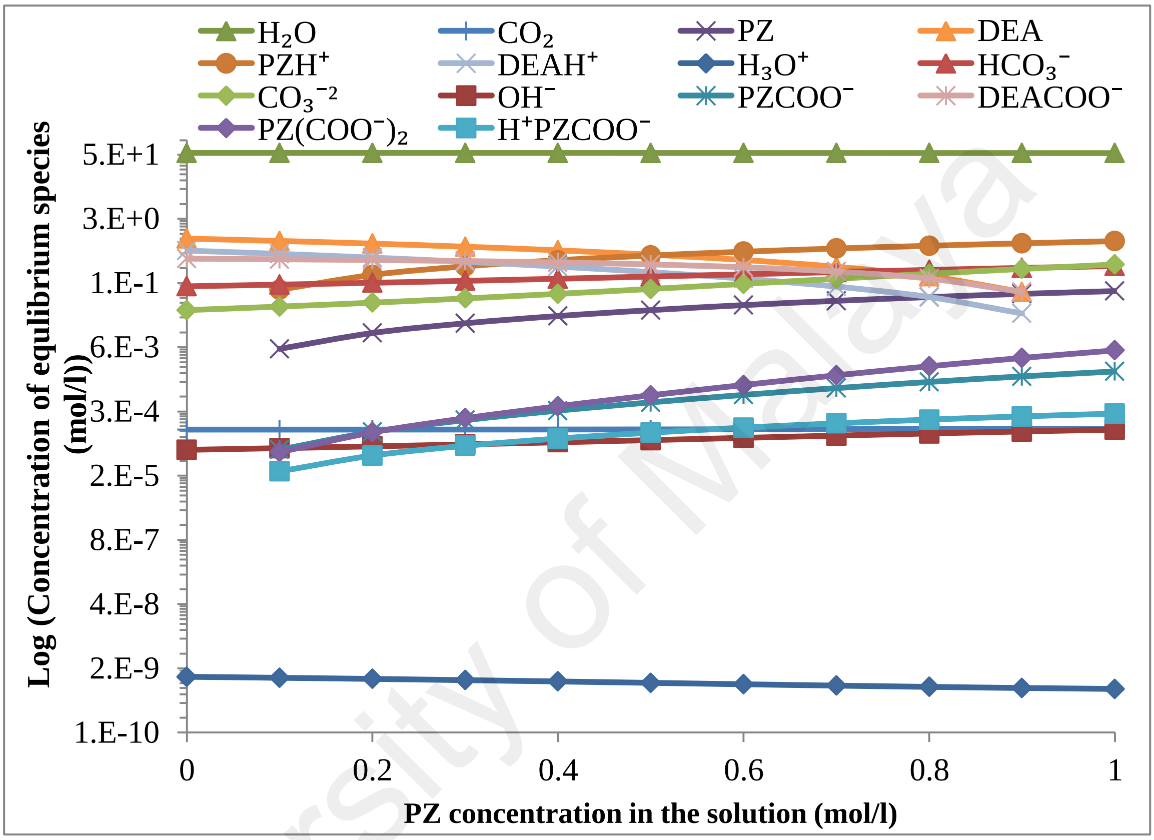

Figure 4.5: Effect of PZ concentration on species in the bulk MDEA-PZ solution at P_{CO2} = 0.5 kPa; 40 °C.

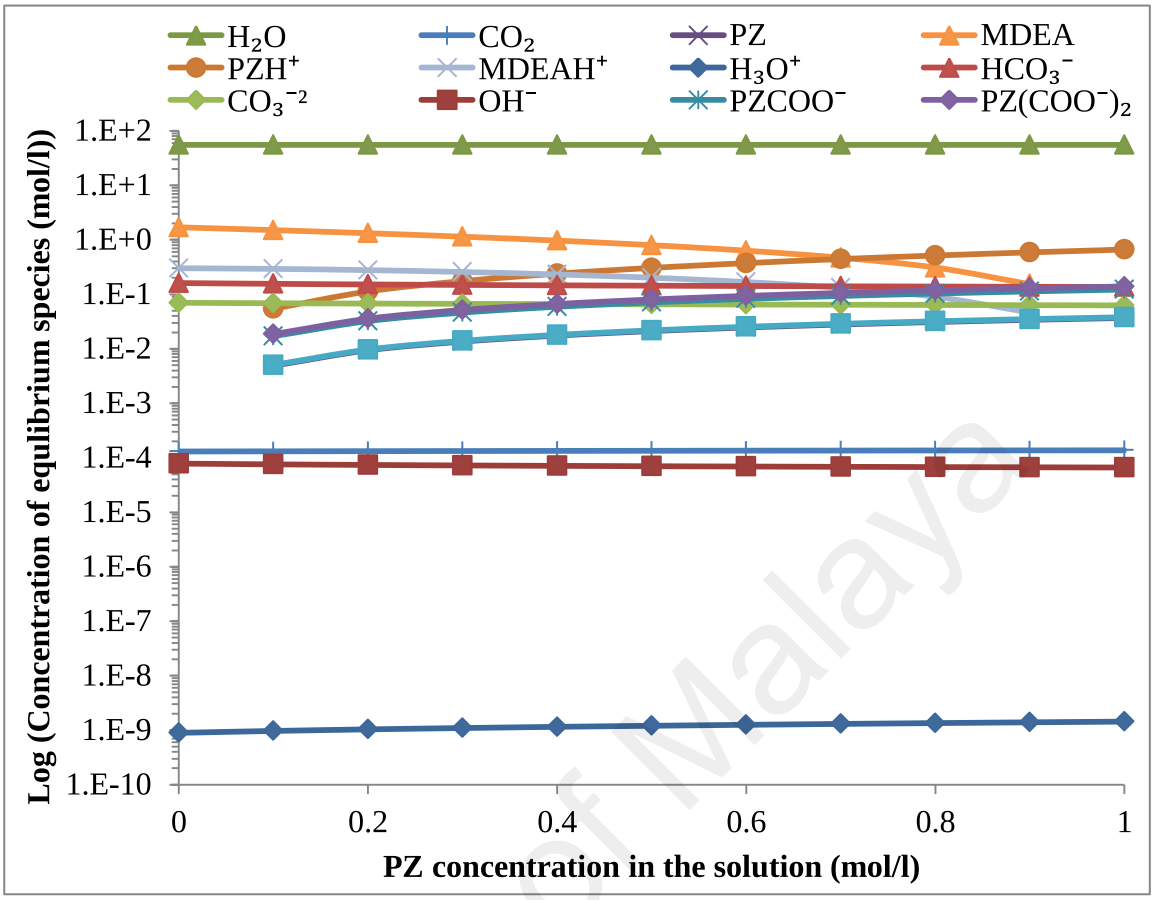

Figure 4.6: Effect of PZ concentration on species in the bulk DEA-PZ solution at P_{CO2} = 0.5 kPa; 40 °C.

4.2 Simulation results of generated polarization curve

4.2.1 Comparison of polarization curve with data from the literature

Prior to the corrosion modeling, it is necessary to validate the polarization curve generated from the model in order to ensure the reliability of the simulation results to be obtained. The generated polarization curve based on the model were compared with the experimental polarization curve data obtained from Brahim (2007).The developed polarization curve model was used to simulate the corrosion process and predicts corrosion rates of carbon steel in aqueous carbonated solution of activated MDEA and activated DEA environments. The simulation conditions were chosen from the study Brahim, (2007).

From Figures 4.7-4.14 and Table 4.3 and 4.4, most of the simulated polarization curves from the model are similar to the experimental polarization curves. However, the simulated curves shifted slightly in the direction of greater current densities (i_{corr}) and smaller corrosion potential (E_{corr}). This means the predicted corrosion rates are greater than the corrosion rates obtained from the experiments. The deviation of the simulated polarization curves might be due to the value of iron concentration in the bulk solution, which was taken from Sun *et al.* (2009) as a function of ionic strength and temperature. The polarization curves produced from the model are closer to the experimental curves. The lower corrosion rates predicted in the DEA-PZ system from the model resulted from the exchange current density of protonated piperazine and protonated di-ethanolamine values used in this model similar to protonated methyl-di-ethanolamine.

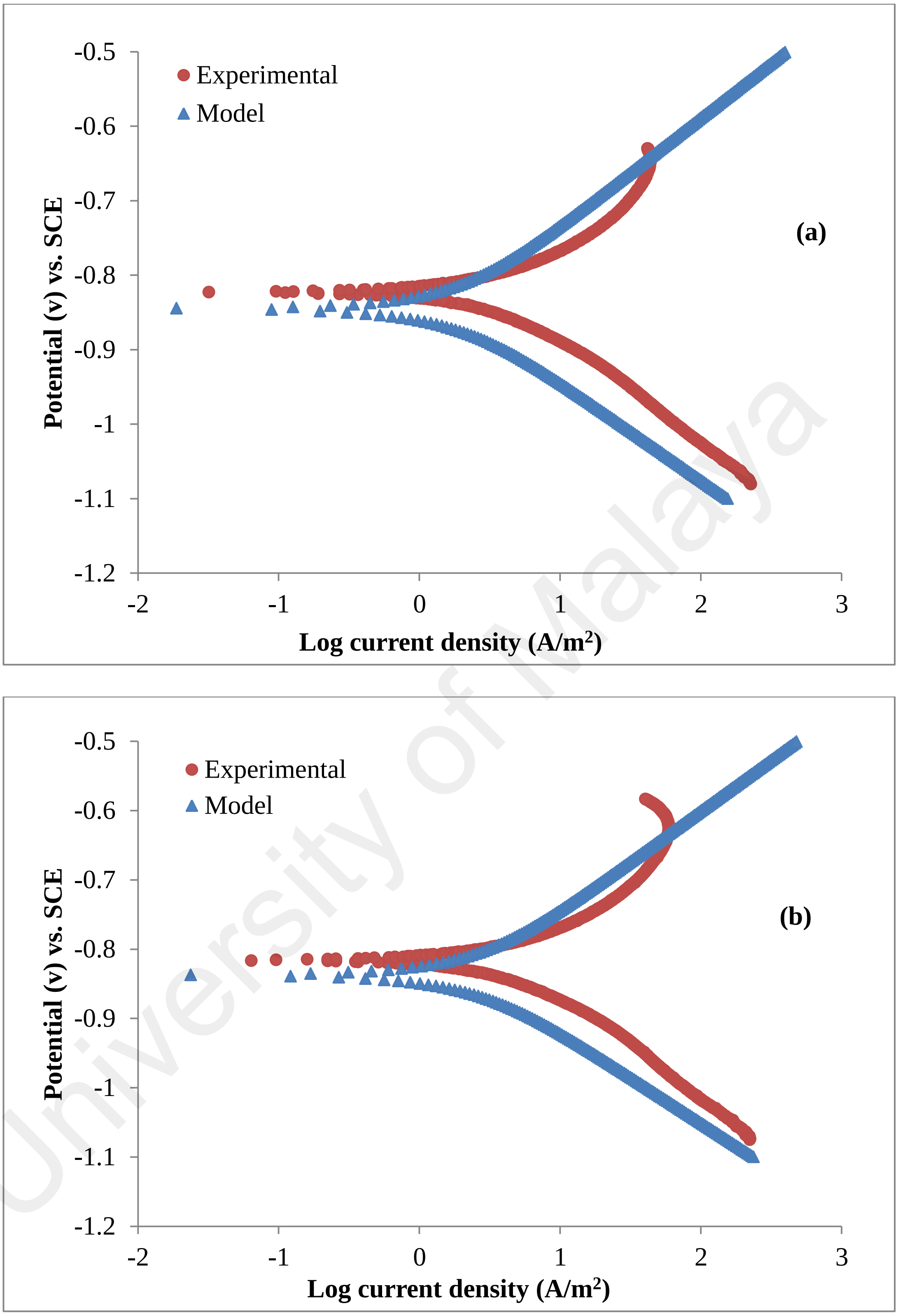

Figure 4.7: Comparison of simulated and experimental (Brahim, 2007) polarization curves (a) 2 M MDEA with CO_2 loading = 0.24 (mol CO_2/ mol Alkalinity) at 60 °C (b) 2M MDEA with CO_2 loading = 0.45 (mol CO_2/ mol Alkalinity) at 60 °C

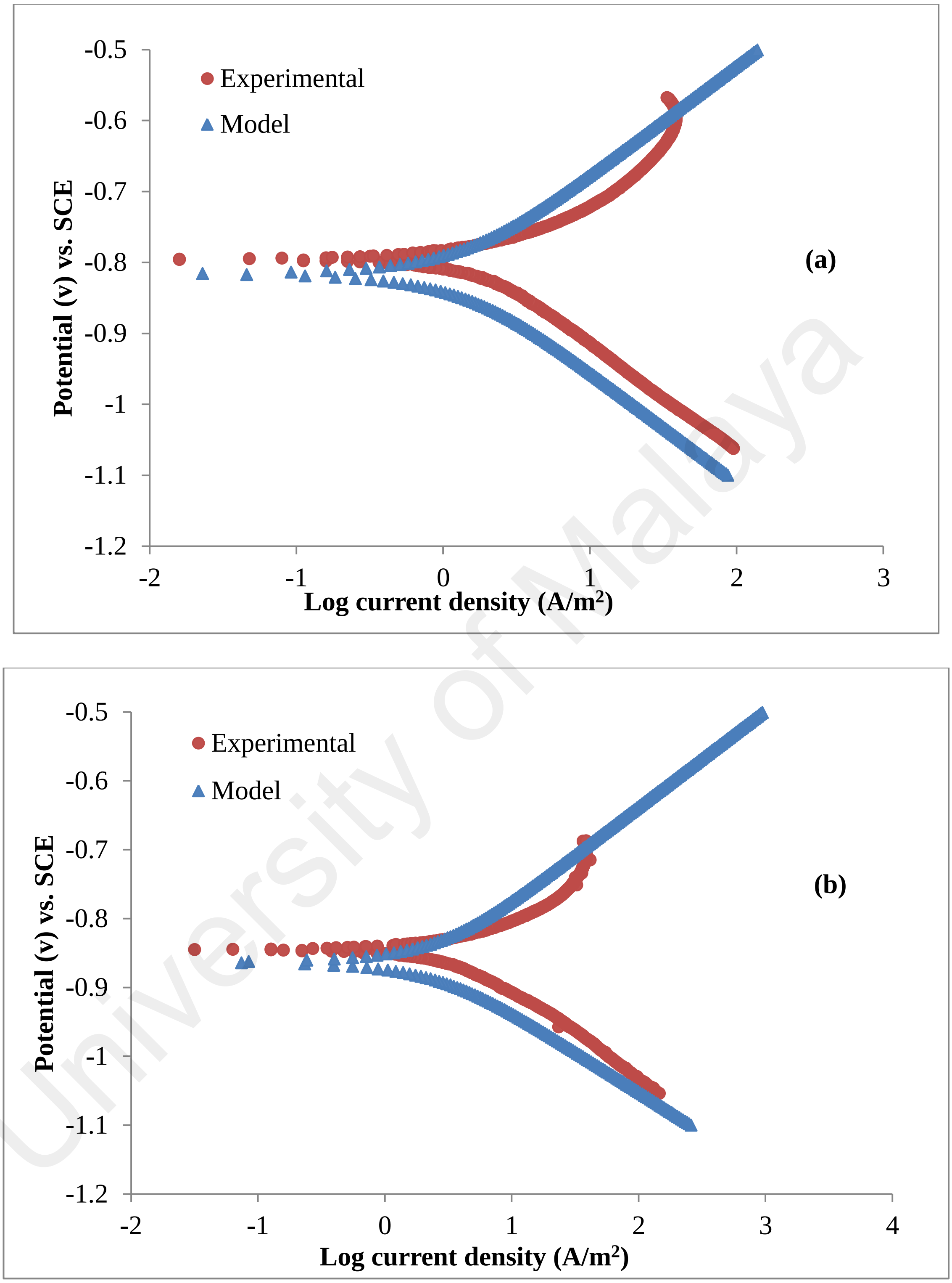

Figure 4.8: Comparison of simulated and experimental (Brahim, 2007) polarization curves (a) 2 M MDEA with CO_2 loading =0.73 (mol CO_2/ mol alkalinity) at 40 °C (b) 2M MDEA with CO_2 loading = 0. 34 (mol CO_2/ mol alkalinity) at 80 °C

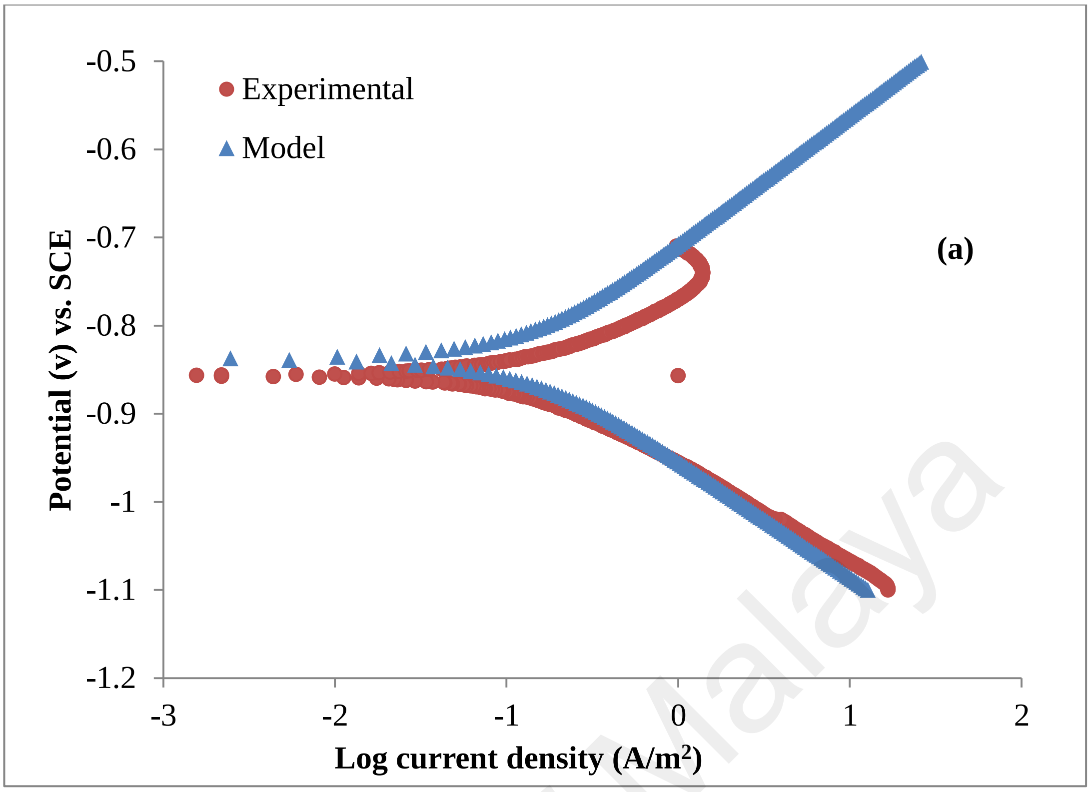

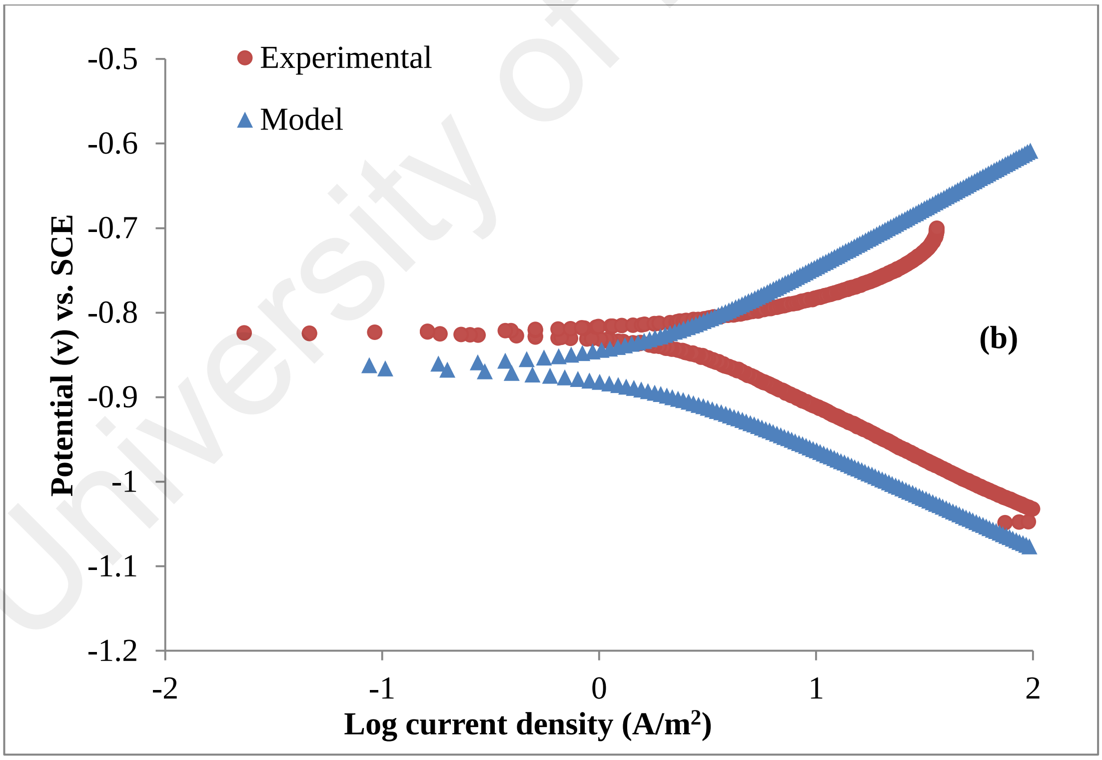

Figure 4.9: Comparison of simulated and experimental (Brahim, 2007) polarization curves (a) 1.98M MDEA + 0.01M PZ with CO_2 loading =0.10 (mol CO_2/ mol alkalinity) at 60 °C (b) 1.98M MDEA + 0.01M PZ with CO_2 loading =0.25 (mol CO_2/ mol alkalinity) at 80 °C

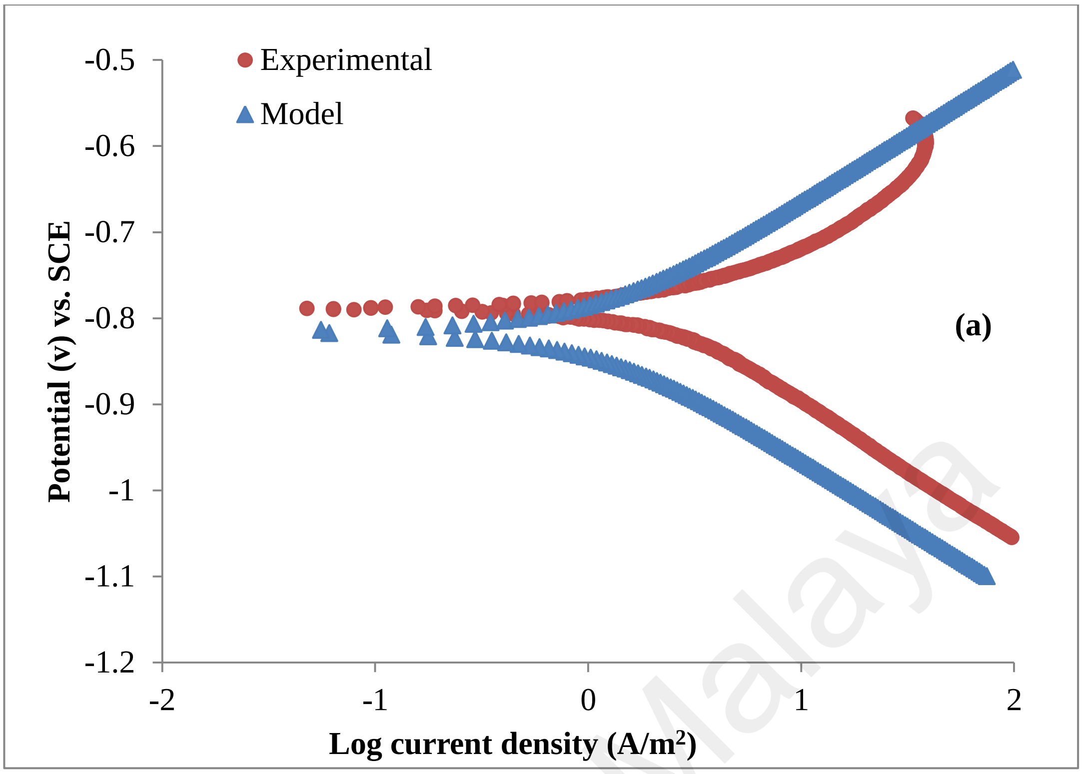

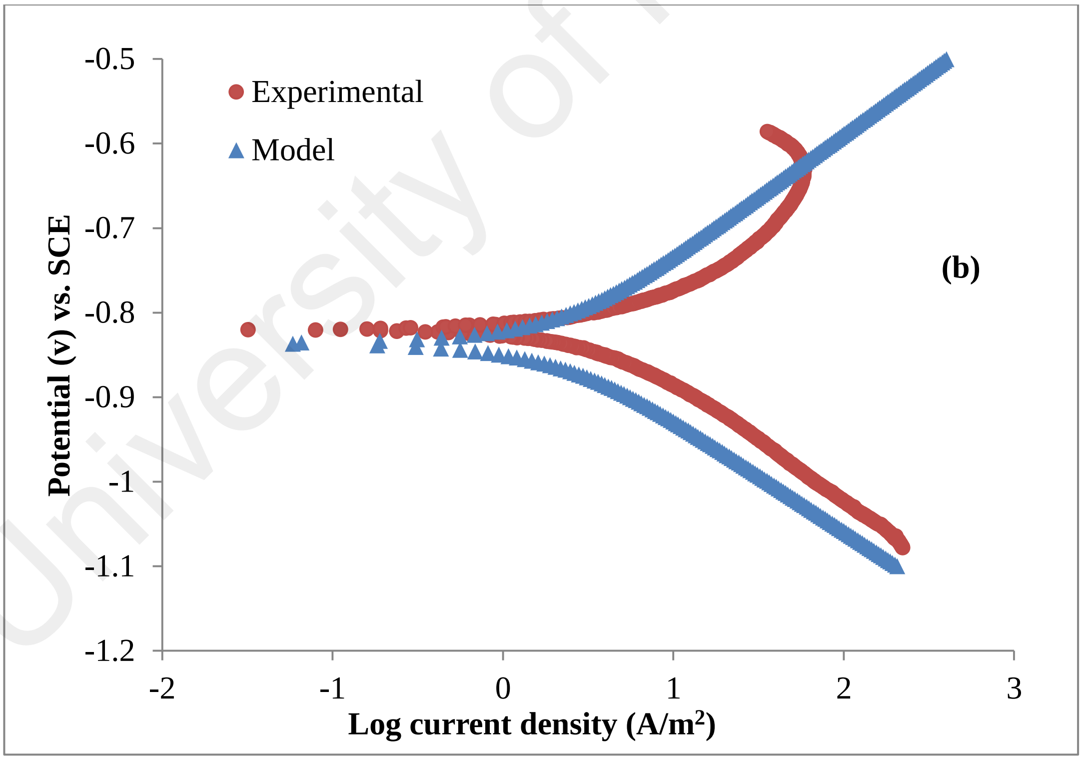

Figure 4.10: Comparison of simulated and experimental (Brahim, 2007) polarization curves (a) 1.9M MDEA + 0.05M PZ with CO_2 loading =0.75 (mol CO_2/ mol alkalinity) at 40 °C (b) 1.9M MDEA + 0.05M PZ with CO_2 loading =0.62 (mol CO_2/ mol alkalinity) at 60 °C

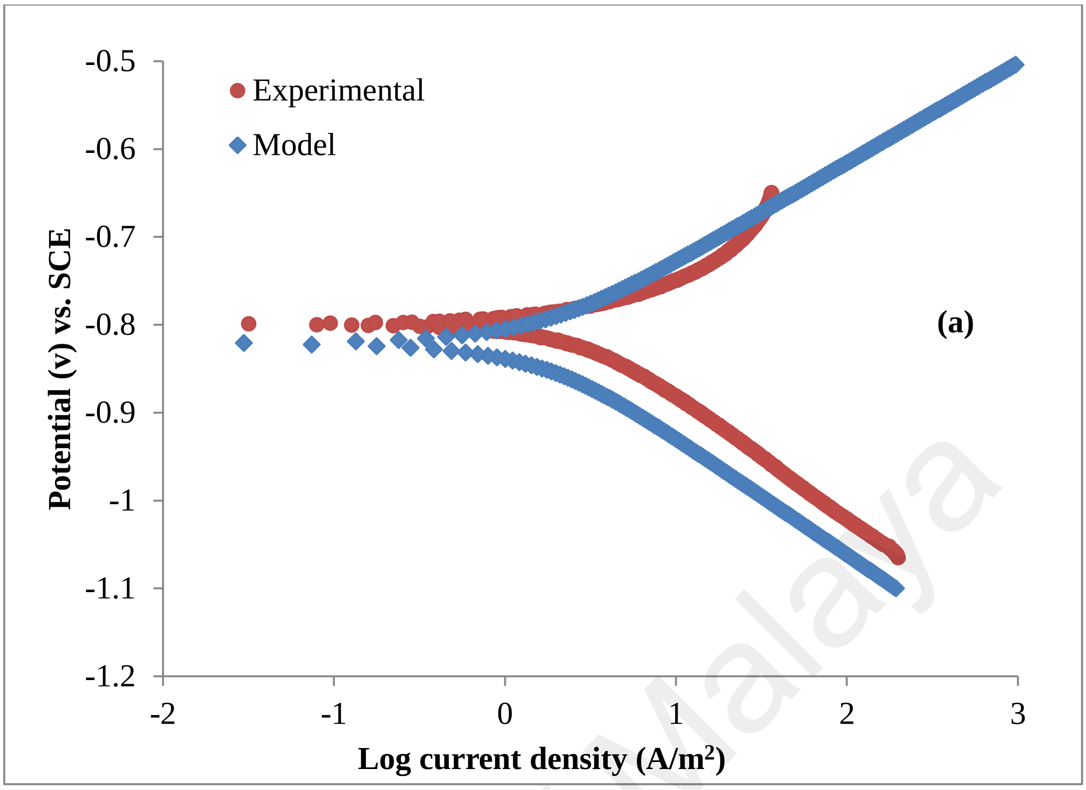

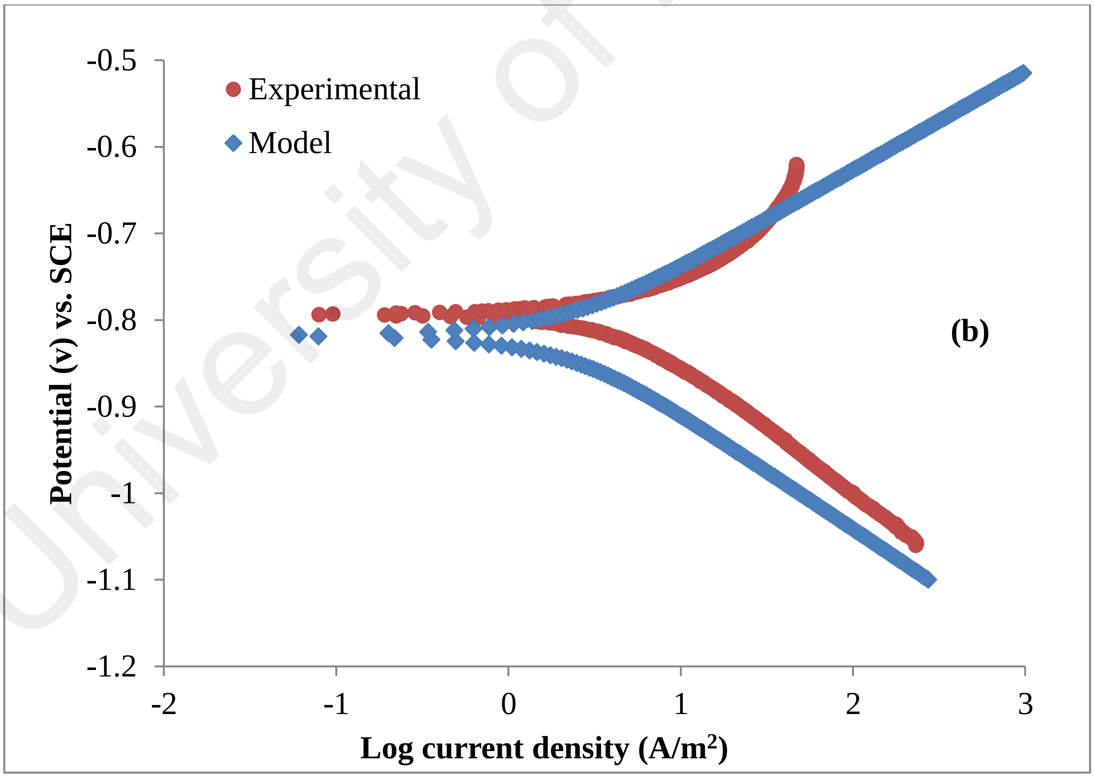

Figure 4.11: Comparison of simulated and experimental (Brahim, 2007) polarization curves (a) 2 M DEA with CO_2 loading = 0.58 at 60 °C (b) 2M DEA with CO_2 loading = 0.68 (mol CO_2/ mol Alkalinity) at 60 °C

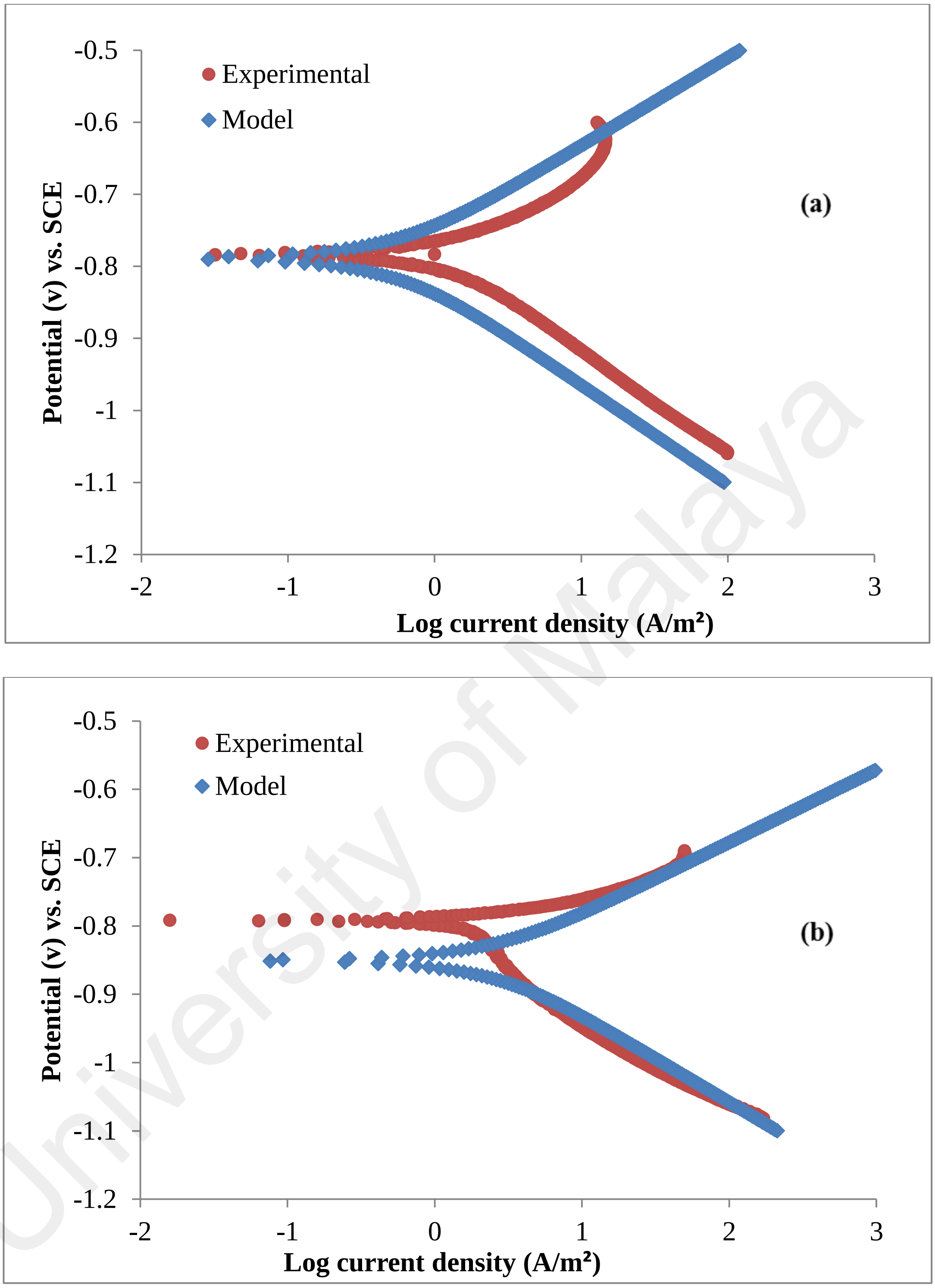

Figure 4.12: Comparison of simulated and experimental (Brahim, 2007) polarization curves. (a) 2M DEA with CO_2 loading =0.57 (mol CO_2/ mol alkalinity) at 40 °C (b) 2M DEA with CO_2 loading = 0.48 (mol CO_2/ mol alkalinity) at 80 °C

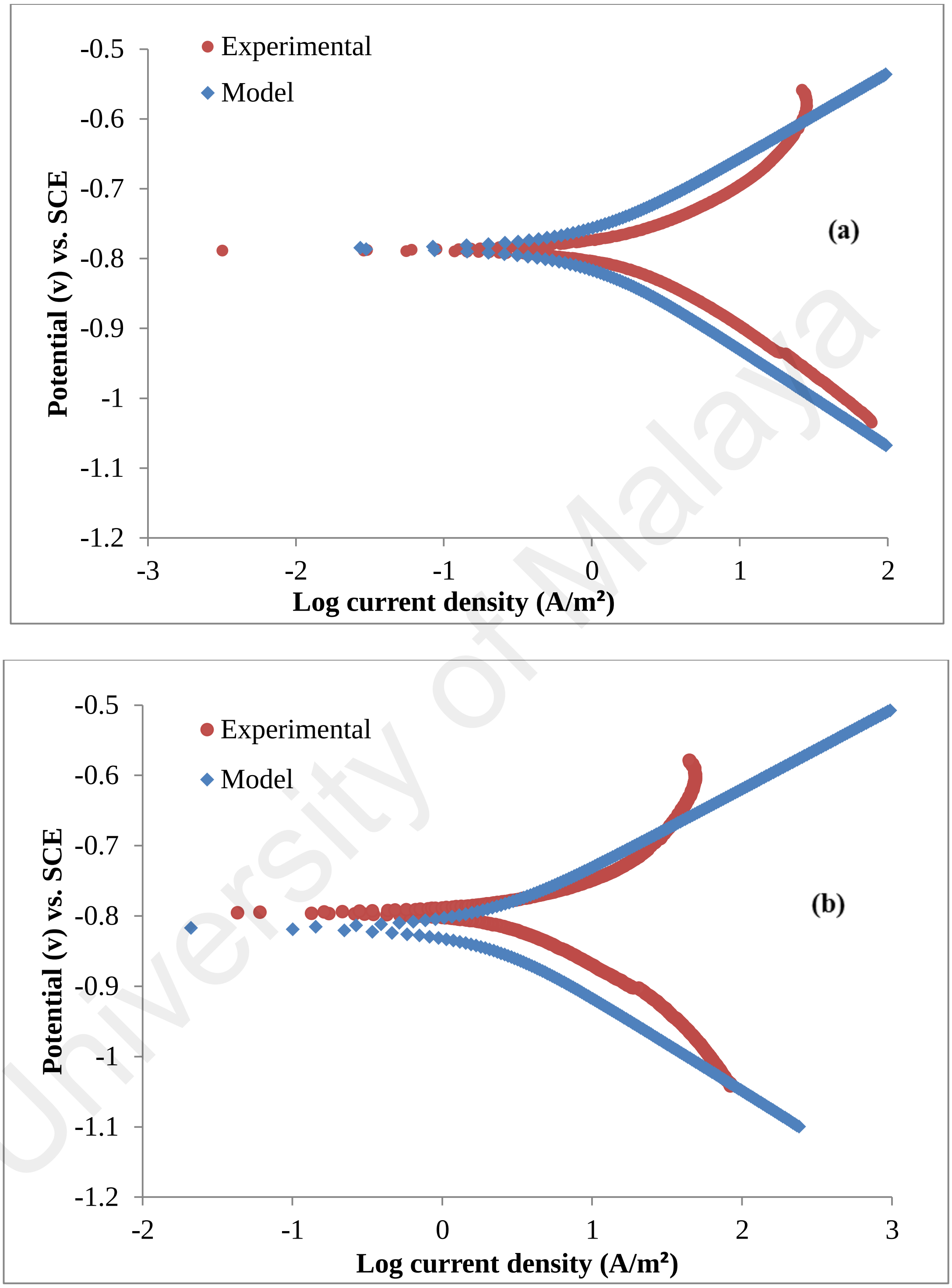

Figure 4.13: Comparison of simulated and experimental (Brahim, 2007) polarization curves. (a) 1.98M DEA + 0.01M PZ with CO_2 loading =0.71 (mol CO_2/ mol alkalinity) at 40 °C (b) 1.98M DEA + 0.01M PZ with CO_2 loading =0.67 (mol CO_2/ mol alkalinity) at 60 °C

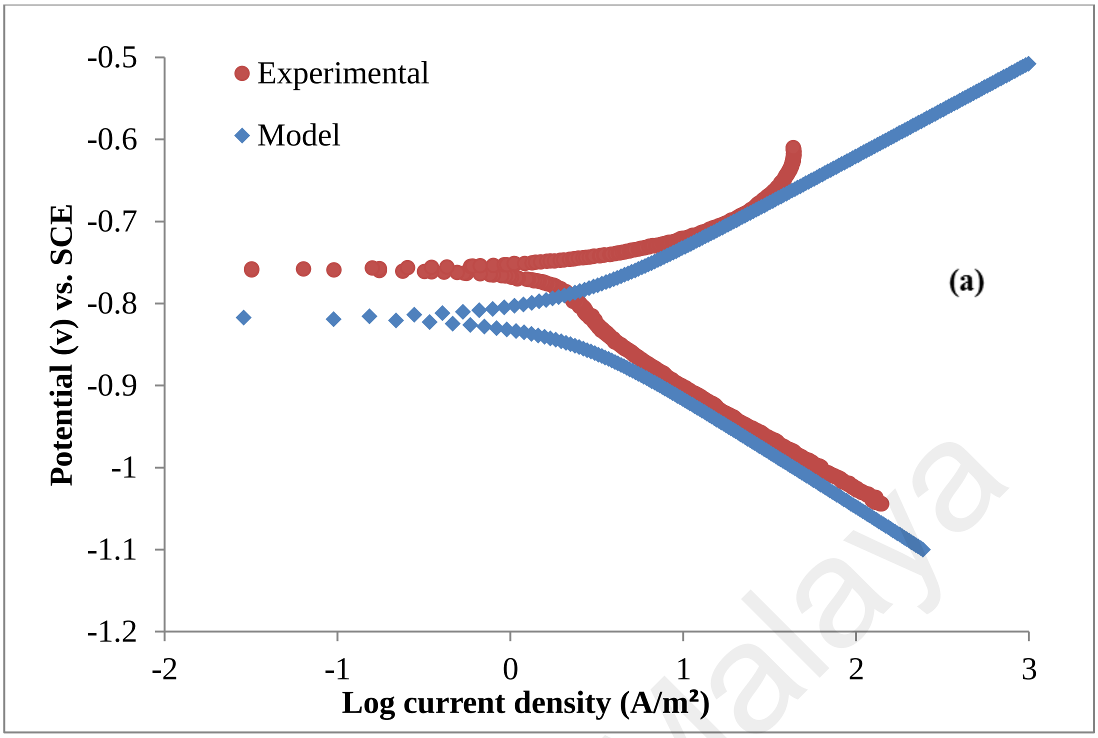

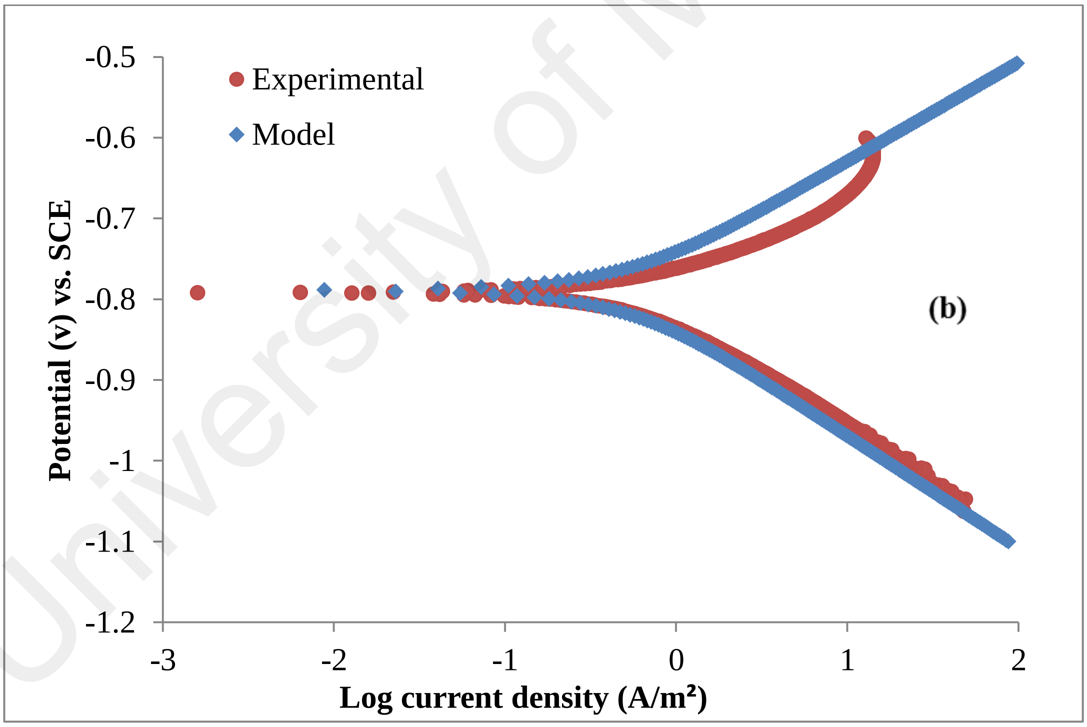

Figure 4.14: Comparison of simulated and experimental (Brahim, 2007) polarization curves. (a) 1.9M DEA + 0.05M PZ with CO_2 loading =0.66 (mol CO_2/ mol alkalinity) at 60 °C (b) 1.8M DEA + 0.1M PZ with CO_2 loading =0.54 (mol CO_2/ mol alkalinity) at 40°C

Table 4.3: Comparison of corrosion data from the model with experimental data for activated MDEA system

Conditions for simulation		Experimental Data Brahim (2007)		Model this work		δ^a	δ^b
System	CO_2 Partial Pressure kPa	E_{corr}(V)	CR(mm/yr)	E_{corr}(V)	CR(mm/yr)		
MDEA – 2M,40 °C	0.96	-0.842	0.220	-0.822	0.177	2.412	19.51
	9.53	-0.803	0.843	-0.828	0.779	3.215	7.62
	47.72	-0.795	1.305	-0.816	1.489	2.643	14.06
	95.61	-0.790	1.755	-0.804	1.716	1.762	2.23
MDEA – 2M,60 °C	0.83	-0.856	0.460	-0.838	0.154	2.117	66.57
	8.31	-0.824	1.154	-0.850	0.807	3.155	30.11
	41.37	-0.823	1.746	-0.845	2.089	2.625	19.63
	82.91	-0.816	2.229	-0.837	2.815	2.607	26.29
MDEA – 2M,80 °C	0.55	-0.863	0.103	-0.841	0.113	2.526	9.18
	5.56	-0.859	1.185	-0.861	0.609	0.194	48.57
	27.57	-0.841	1.473	-0.865	1.829	2.889	24.14
	55.48	-0.845	2.920	-0.863	2.829	2.135	3.10
MDEA–PZ,1.98–0.01 M 40 °C	0.96	-0.849	0.25	-0.82	0.17	3.28	34.73
	9.53	-0.798	0.60	-0.83	0.69	4.04	15.37
	47.72	-0.798	1.28	-0.82	1.36	2.82	6.23
	95.61	-0.788	1.65	-0.81	1.60	2.73	2.98
MDEA–PZ,1.98–0.01 M 60 °C	0.83	-0.856	0.37	-0.84	0.15	2.19	58.28
	8.31	-0.828	0.73	-0.85	0.74	2.52	2.00
	41.37	-0.829	1.63	-0.85	1.85	2.06	13.75
	82.91	-0.816	2.02	-0.84	2.52	2.94	24.73
MDEA–PZ,1.98–0.01 M 80 °C	0.55	-0.863	0.31	-0.84	0.12	2.46	61.45
	5.56	-0.859	0.95	-0.86	0.60	0.06	37.24
	27.57	-0.824	1.66	-0.86	1.70	4.83	2.24
	55.48	-0.842	2.35	-0.86	2.56	2.32	8.79

Where E_{corr}= Corrosion potential, CR =Corrosion rate , $\delta^{a} = \frac{|E_{corr(Cal.)}-E_{corr(Exp.)}|}{E_{corr(Exp.)}} \times 100$, $\delta_{AAD} = 2.45\%$, $\delta^{b} = \frac{|\mathrm{CR}_{(Cal.)}-\mathrm{CR}_{(Exp.)}|}{\mathrm{CR}_{(Exp.)}} \times 100$, $\delta_{AAD} = 24.47\%$

Table 4.3 (continued): Comparison of corrosion data from the model with experimental data for activated MDEA system

Conditions for simulation		Experimental Data Brahim (2007)		Model this work		δ^a	δ^b
System	P_{CO2} (kPa)	E_{corr}(V)	CR(mm/yr)	E_{corr}(V)	CR(mm/yr)		
MDEA–PZ,1.9–0.05 M 40 °C	0.96	-0.838	0.28	-0.82	0.16	2.62	41.49
	9.53	-0.815	0.490	-0.83	0.65	1.28	33.55
	47.72	-0.788	1.442	-0.82	1.26	3.42	12.57
	95.61	-0.789	1.316	-0.80	1.48	1.89	12.75
MDEA–PZ,1.9–0.05 M 60 °C	0.83	-0.853	0.255	-0.84	0.17	1.98	34.45
	8.31	-0.841	0.627	-0.85	0.74	0.57	18.56
	41.37	-0.806	1.686	-0.84	1.79	4.50	6.18
	82.91	-0.820	1.700	-0.84	2.41	1.94	41.86
MDEA–PZ,1.9–0.05 M 80 °C	0.55	-0.832	0.179	-0.85	0.14	1.57	23.97
	5.56	-0.828	0.887	-0.86	0.64	3.70	27.78
	27.57	-0.825	1.557	-0.86	1.72	4.37	10.69
	55.48	-0.841	2.019	-0.86	2.57	2.21	27.07
MDEA–PZ,1.8–0.1 M 40 °C	0.96	-0.785	0.209	-0.81	0.16	3.28	23.13
	9.53	-0.791	0.440	-0.82	0.61	3.43	38.76
	47.72	-0.784	1.456	-0.81	1.15	3.14	20.93
	95.61	-0.789	1.167	-0.80	1.35	1.18	15.52
MDEA–PZ,1.8–0.1 M 60 °C	0.83	-0.868	0.274	-0.83	0.18	4.00	33.02
	8.31	-0.834	0.503	-0.84	0.75	0.96	48.27
	41.37	-0.828	1.705	-0.84	1.72	1.17	1.13
	82.91	-0.821	1.236	-0.83	2.29	1.22	85.46
MDEA–PZ,1.8–0.1 M 80 °C	0.55	-0.857	0.167	-0.85	0.16	1.05	5.07
	5.56	-0.833	0.813	-0.86	0.69	3.08	14.78
	27.57	-0.839	1.484	-0.86	1.77	2.29	19.00
	55.48	-0.837	1.830	-0.86	2.56	2.27	39.85

Where E_{corr}= Corrosion potential, CR =Corrosion rate , $\delta^{a} = \frac{|E_{corr(Cal.)}-E_{corr(Exp.)}|}{E_{corr(Exp.)}} \times 100$, $\delta_{AAD} = 2.45\%$, $\delta^{b} = \frac{|\mathrm{CR}_{(Cal.)}-\mathrm{CR}_{(Exp.)}|}{\mathrm{CR}_{(Exp.)}} \times 100$, $\delta_{AAD} = 24.47\%$

Table 4.4: Comparison of corrosion data from the model with experimental data for activated DEA system

Conditions for simulation		Experimental Data Brahim (2007)		Model		Error	
System	P_{CO2} (kPa)	E_{corr}(V)	CR(mm/yr)	E_{corr}(V)	CR(mm/yr)	δ^a	δ^b
DEA – 2M,40 °C	0.96	-0.8100	0.2120	-0.78	0.17	3.62	11.637
	9.53	-0.7838	0.7950	-0.79	0.53	0.50	22.645
	47.72	-0.7688	1.0330	-0.79	1.03	2.22	13.756
	95.61	-0.7655	1.3140	-0.78	1.30	2.14	12.065
DEA – 2M,60 °C	0.83	-0.8089	0.4830	-0.82	0.18	1.29	60.642
	8.31	-0.8063	1.4990	-0.82	0.70	2.00	47.027
	41.37	-0.7994	1.3490	-0.82	1.54	2.64	31.711
	82.91	-0.7939	2.2210	-0.82	2.06	2.99	7.147
DEA – 2M,80 °C	0.55	-0.8865	0.1880	-0.85	0.15	4.64	17.810
	5.56	-0.8486	1.1060	-0.85	0.75	0.46	35.858
	27.57	-0.7952	4.4690	-0.85	2.12	6.97	58.028
	55.48	-0.7918	4.6370	-0.85	3.16	7.08	40.794
DEA–PZ,1.98–0.01 M 40 °C	0.96	-0.8154	0.2290	-0.78	0.17	4.22	26.61
	9.53	-0.7760	0.7380	-0.79	0.54	1.52	27.06
	47.72	-0.7887	0.7640	-0.79	1.03	0.36	35.08
	95.61	-0.7678	1.2870	-0.78	1.30	1.84	0.99
DEA–PZ,1.98–0.01 M 60 °C	0.83	-0.8248	0.5600	-0.82	0.18	0.62	67.85
	8.31	-0.8169	0.8700	-0.82	0.71	0.69	18.88
	41.37	-0.8029	1.6300	-0.82	1.55	2.20	4.98
	82.91	-0.7955	2.4300	-0.82	2.07	2.79	14.82

Where E_{corr}= Corrosion potential, CR =Corrosion rate , $\delta^{a} = \frac{|E_{corr(Cal.)} - E_{corr(Exp.)}|}{E_{corr(Exp.)}} \times 100$, $\delta_{AAD} = 3.58\%$, $\delta^{b} = \frac{|\mathrm{CR}_{(Cal.)} - \mathrm{CR}_{(Exp.)}|}{\mathrm{CR}_{(Exp.)}} \times 100$, $\delta_{AAD} = 26.37\%$

Table 4.4 (continued): Comparison of corrosion data from the model with experimental data for activated DEA system

Conditions for simulation		Experimental Data Brahim (2007)		Model		Error	
System	P_{CO2} (kPa)	E_{corr}(V)	CR(mm/yr)	E_{corr}(V)	CR(mm/yr)	δ^a	δ^b
DEA–PZ,1.98–0.01 M 80 °C	0.55	-0.8281	0.450	-0.84	0.15	1.90	65.89
	5.56	-0.8168	1.3630	-0.85	0.67	4.25	51.08
	27.57	-0.8159	3.0710	-0.85	1.69	4.30	44.93
	55.48	-0.8173	2.9950	-0.85	2.41	3.90	19.40
DEA–PZ,1.9–0.05 M 40 °C	0.96	-0.8168	0.2410	-0.78	0.18	4.28	26.42
	9.53	-0.7708	0.6510	-0.79	0.55	2.27	14.95
	47.72	-0.7662	0.9460	-0.79	1.05	2.58	10.64
	95.61	-0.7699	1.2600	-0.78	1.31	1.53	4.28
DEA–PZ,1.9–0.05 M 60 °C	0.83	-0.7979	0.4240	-0.82	0.20	2.94	53.65
	8.31	-0.8006	0.9520	-0.82	0.74	2.85	22.78
	41.37	-0.7785	1.9890	-0.82	1.59	5.45	20.20
	82.91	-0.7593	1.7180	-0.82	2.11	7.71	22.76
DEA–PZ,1.9–0.05 M 80 °C	0.55	-0.7960	0.2780	-0.85	0.18	6.59	36.65
	5.56	-0.7959	0.8930	-0.85	0.71	7.23	20.05
	27.57	-0.7916	2.4230	-0.85	1.76	7.62	27.32
	55.48	-0.7802	2.9700	-0.85	2.49	8.92	7.91

Where E_{corr}= Corrosion potential, CR =Corrosion rate, $\delta^{a} = \frac{|E_{corr(Cal.)} - E_{corr(Exp.)}|}{E_{corr(Exp.)}} \times 100$, $\delta_{AAD} = 3.58\%$, $\delta^{b} = \frac{|\mathrm{CR}_{(Cal.)} - \mathrm{CR}_{(Exp.)}|}{\mathrm{CR}_{(Exp.)}} \times 100$, $\delta_{AAD} = 26.37\%$

Table 4.4 (continued): Comparison of corrosion data from the model with experimental data for activated DEA system

Conditions for simulation		Experimental Data Brahim (2007)		Model		Error	
System	P_{CO2} (kPa)	E_{corr}(V)	CR(mm/yr)	E_{corr}(V)	CR(mm/yr)	δ^{a}	δ^{b}
DEA–PZ,1.8–0.1 M 40 °C	0.96	-0.7801	0.2263	-0.78	0.19	0.40	16.04
	9.53	-0.7919	0.4700	-0.79	0.57	0.35	22.10
	47.72	-0.7569	1.2900	-0.79	1.07	3.85	17.28
	95.61	-0.7676	1.2100	-0.78	1.33	1.79	9.84
DEA–PZ,1.8–0.1 M 60 °C	0.83	-0.7638	0.2529	-0.82	0.22	7.83	12.98
	8.31	-0.7969	0.8500	-0.82	0.78	3.46	8.62
	41.37	-0.8032	1.9500	-0.82	1.63	2.28	16.44
	82.91	-0.7897	1.4700	-0.82	2.16	3.58	46.72
DEA–PZ,1.8–0.1 M 80 °C	0.55	-0.7977	0.0700	-0.85	0.20	7.04	66.92
	5.56	-0.7977	0.8351	-0.86	0.78	7.31	6.28
	27.57	-0.8190	2.4930	-0.85	1.85	4.17	25.93
	55.48	-0.8206	2.9700	-0.85	2.60	3.66	12.34

Where E_{corr}= Corrosion potential, CR =Corrosion rate , $\delta^{a} = \frac{|E_{corr(Cal.)} - E_{corr(Exp.)}|}{E_{corr(Exp.)}} \times 100$, $\delta_{AAD} = 3.58\%$, $\delta^{b} = \frac{|\mathrm{CR}_{(Cal.)} - \mathrm{CR}_{(Exp.)}|}{\mathrm{CR}_{(Exp.)}} \times 100$, $\delta_{AAD} = 26.37\%$

4.2.2 Polarization curve behaviors

4.2.2.1 CO_2 loading effects

The simulation study for MDEA-PZ (1.6 + 0.2) M and DEA-PZ (1.6 + 0.2) M solution was carried out at different CO_2 loadings (0.21, 0.45 and 0.65) and (0.32, 0.50 and 0.62) (mol CO_2 /mol alkalinity) for each system, respectively at constant temperature (40 ^{o} C). Figure 4.15 and 4.16 showed that as the CO_2 loading increased, the anodic and cathodic polarization curves shifted to the right where corrosion currents were greater. Moreover, the higher i_{corr} obtained due to the increase in concentration and i_o of oxidizing agents responsible for the corrosion of carbon steel in both systems. An increase in the CO_2 loading led to the increase in i_{corr} and corrosion rate, while the change in E_{corr} was minimal. This suggests that the increase in CO_2 loading enhances both the rate of iron dissolution and rate of oxidizing agent reduction. The enhancement in the rate of oxidizer reduction is dedicated to the increase in dissociation rate of protonated alkanolamine ion ($MDEAH^+$, PZH^+ and $DEAH^+$) and bicarbonate (HCO_3^-) in the bulk activated MDEA and activated DEA solutions when increasing the CO_2 loading.

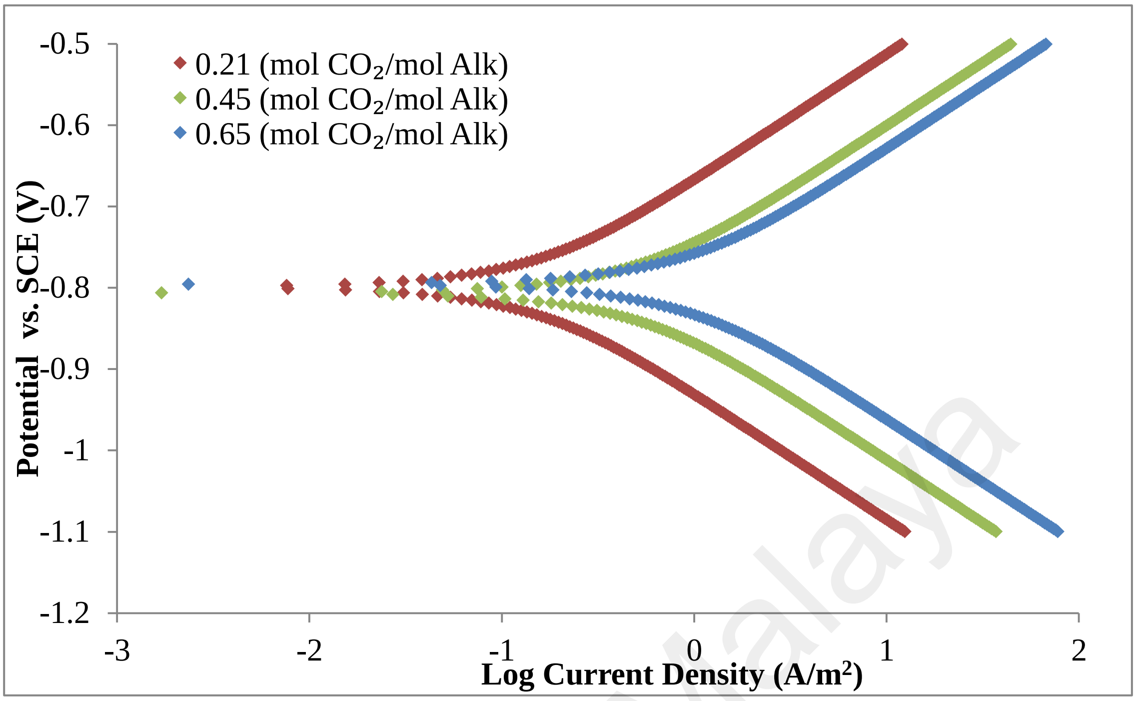

Figure 4.15: Effect of CO_2 loading on simulated polarization curves of carbon steel from the model in aqueous carbonated solution of (1.6 M MDEA +0.2 M PZ) at 40 °C.

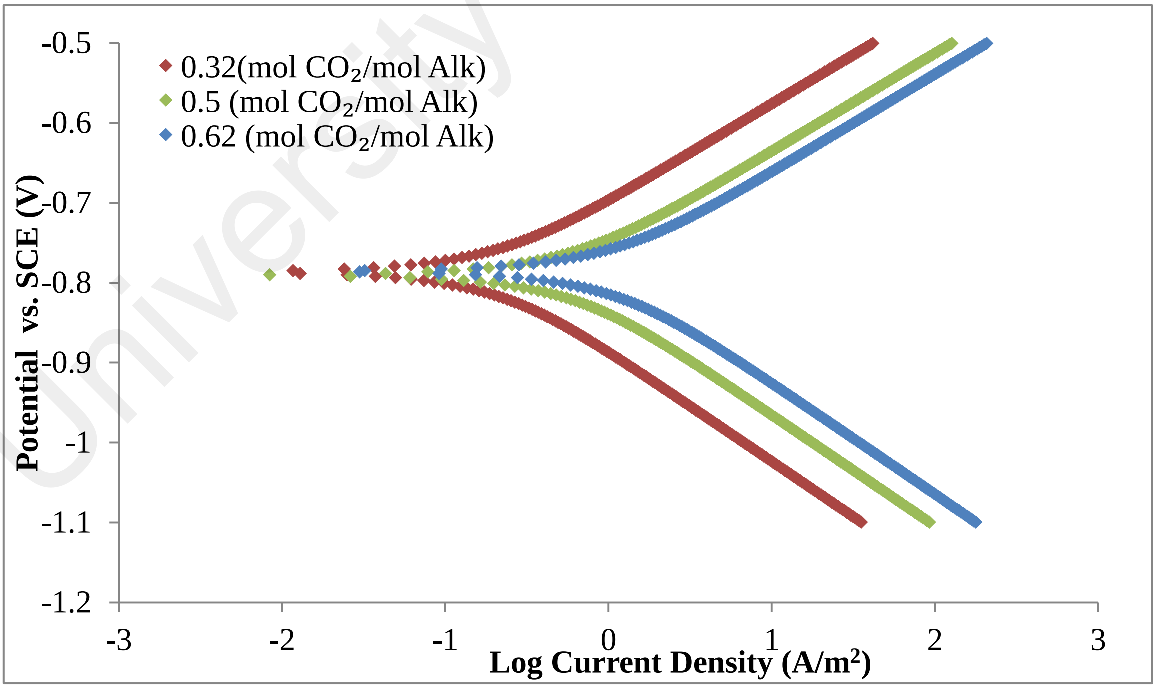

Figure 4.16: Effect of CO_2 loading on simulated polarization curves of carbon steel from the model in aqueous carbonated solution of (1.6 M DEA +0.2 M PZ) at 40 °C.

4.2.2.2 Effects of solution temperature

Corrosion of carbon steel was simulated for 2 M total alkalinity of aqueous MDEA-PZ and DEA-PZ solutions at 15 kPa partial pressure of CO_2 and at three different temperature (313.15, 333.15 and 353.15) K. As shown in the Figure 4.17 and 4.18 an increase in the solution temperature led to the increase in corrosion current and subsequently corrosion rate, while decreasing the corrosion potential. The corrosion potential shifted slightly towards high corrosion direction is of significance for low to high solution temperature. The increase in corrosion current is due to the nature of corrosion kinetics, at higher temperature, rates of corrosion reactions (both iron dissolution and reduction of oxidizing agents) are accelerated, resulting in the increase of corrosion current and subsequently corrosion rate. The anodic polarization curve shifted to the right where the current values are greater for both systems. The change in β_a and β_c values implies that the corrosion mechanism vary with the solution temperature in the MDEA-PZ system, while in the DEA-PZ system these changes were minimal due to the symmetric factor value in each system.

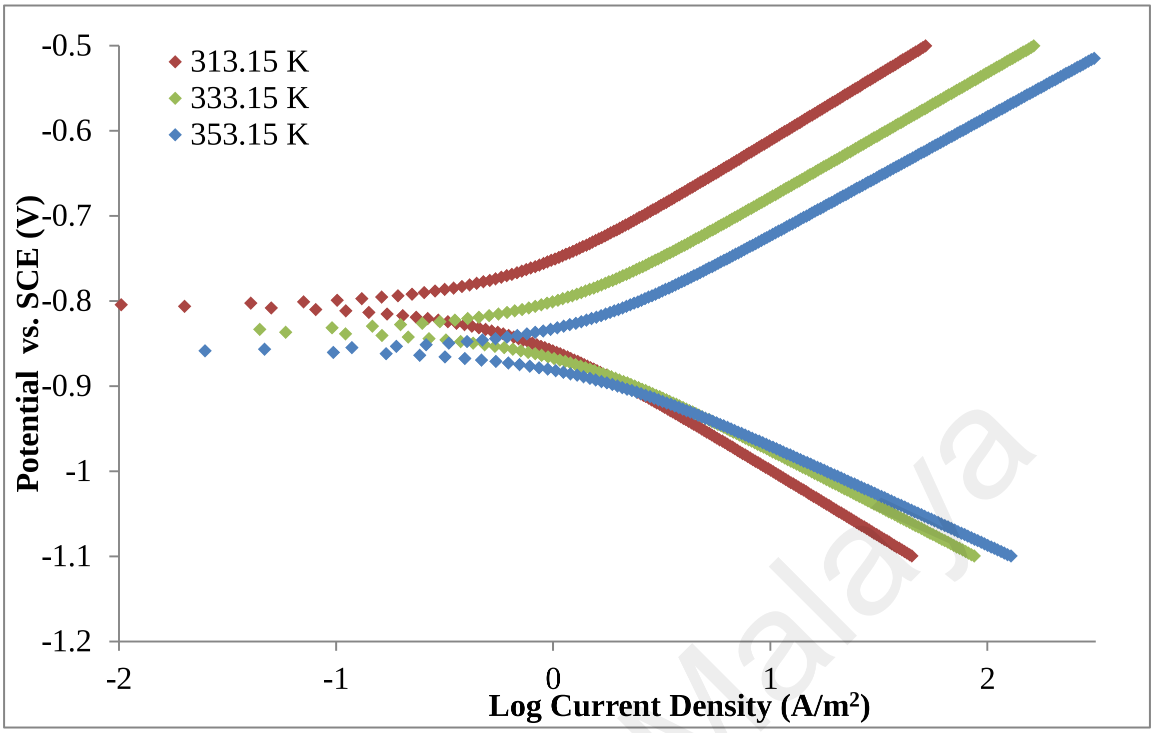

Figure 4.17: Effect of solution temperature on simulated polarization curves based model 1.6M MDEA + 0.2M PZ at low CO_2 loading

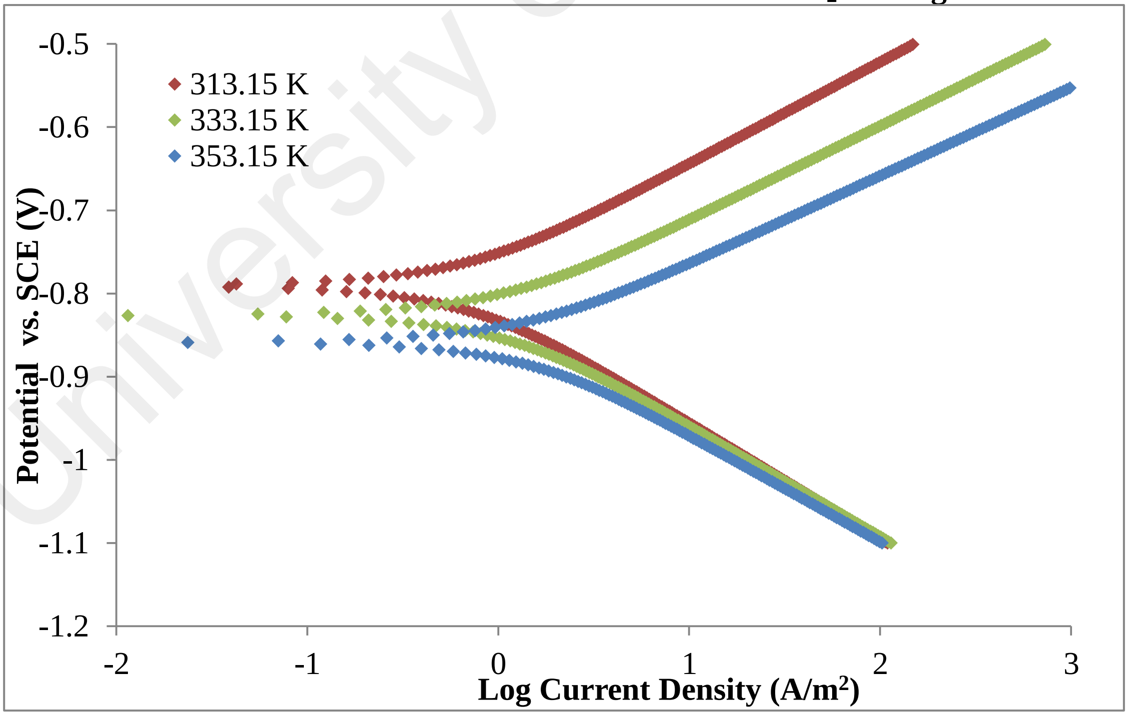

Figure 4.18: Effect of solution temperature on simulated polarization curves based model 1.6M DEA + 0.2M PZ at low CO_2 loading

4.2.2.3 Activator concentration effects

The effect of activator concentration on the corrosion of carbon steel was simulated for three different PZ concentrations (0.1, 0.5 and 0.95 M) for total alkalinity 2 M at 15 kPa partial pressure of CO_2 and 313.15 K solution temperature. As shown in Figure 4.19 for MDEA-PZ system, the increase in the PZ concentration shifted the anodic polarization curves in the direction of lesser current densities, reflecting a slight decrease in corrosion rate accompanied with the increase in corrosion potential. The slight decrease in corrosion current is due to the decrease in HCO_3^- concentration led to the decrease in exchange current density of iron dissolution with respect to concentration of HCO_3^-. Figure 4.20 for DEA-PZ system showed that as the PZ concentration increased, the anodic polarization curve slightly shifted towards higher corrosion current thereby increasing corrosion rate.

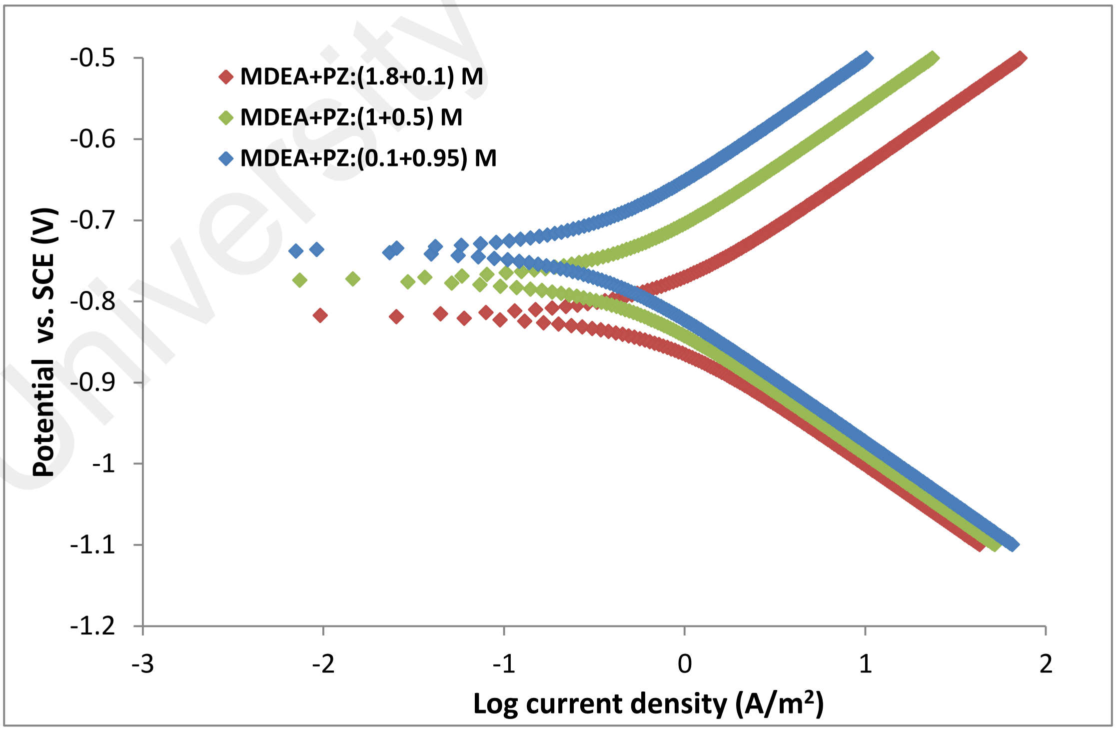

Figure 4.19: Effect of PZ concentration on simulated polarization curves based model at 15 kPa partial pressure of CO_2 and 313.15 K.

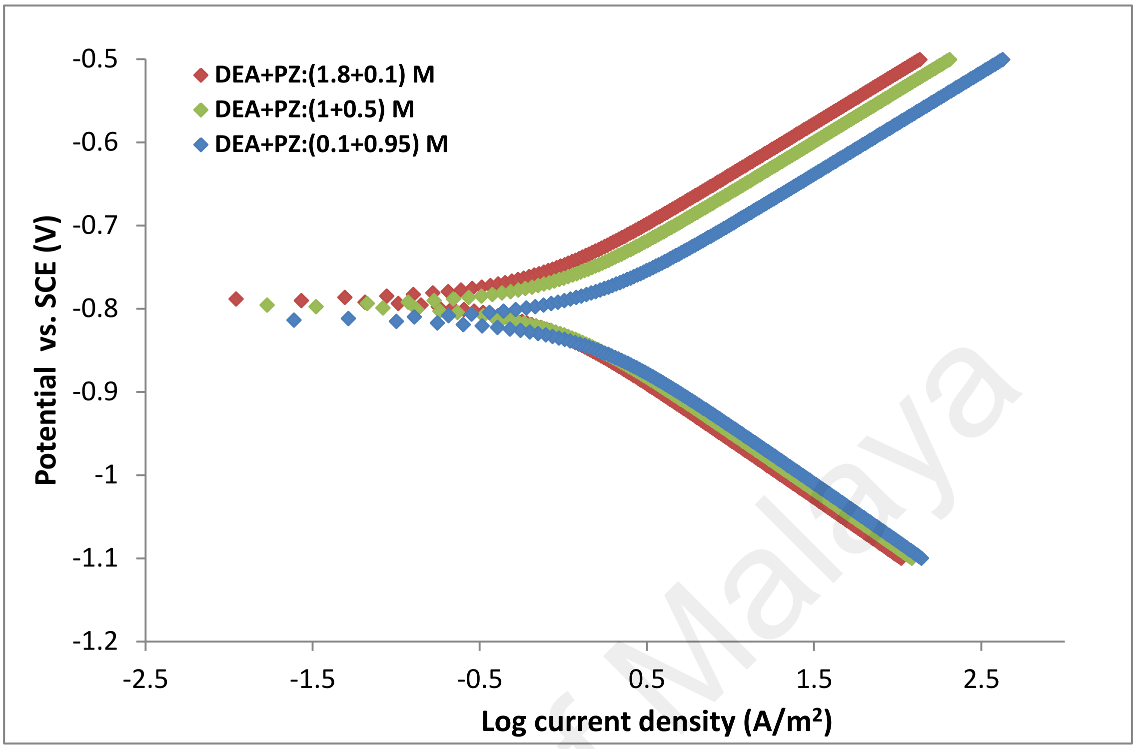

Figure 4.20: Effect of PZ concentration on simulated polarization curves based model at 15 kPa partial pressure of CO_2 and 313.15 K.

4.3 Simulation results of corrosion rate

The corrosivity of carbon steel in carbonated solution of activated MDEA and activated DEA systems is typically influenced by the process parameters. The parametric effect on corrosion behavior was simulated by carrying out the electrochemical corrosion model. The corrosion database generated will help in the selection of proper amine systems suitable for carbon dioxide absorption processes in terms of minimum corrosion difficulties. All tested parameters are presented in the following sections:

4.3.1 Effect of CO_2 loading on corrosion rate

The effect of CO_2 loading on the corrosivity of carbon steel, were simulated with six different concentrations of base alkanolamine (MDEA,DEA) and activator (PZ) at low absorption temperature. Figure 4.21 and 4.22 show that the CO_2 loading has a significant effect on corrosion rate of carbon steel. A high CO_2 loading the solution is more corrosive than that at low CO_2 loading. The corrosion rate was seen to increase with the increase of CO_2 loadings of solution for both systems activated MDEA and activated DEA as depicted in Figure 4.21 and 4.22. As shown in Figure 4.21 the corrosion rate was increased for (MDEA+ PZ):(1.8+0.1) M system at 313.15 K, from 0.166 to 1.358 mm/yr with the increase of CO_2 loading from 0.185 to 0.77 (mol CO_2 /mol alkalinity) and for (DEA+PZ): (1.8+0.1) M system (Figure 4.22), the corrosion rate increased from 0.176 to 1.213 mm/yr on increasing the CO_2 loading from 0.321 to 0.704 (mol CO_2 /mol alkalinity). Such increase in corrosion rate is due to the increase in dissolved CO_2 to form bicarbonate and protonated amine, which induces more iron dissolution, which in turn can accelerate the corrosion process. This is evidenced by greater cathodic current densities at particular CO_2 loading in Figure 4.15 and 4.16. Similar results with respect to bicarbonate and protonated amine concentrations effect on carbon steel corrosion rate has investigated by Choi *et al.* (2012) in their work on carbonated aqueous MDEA system's corosivity. They concluded that corrosion rate of carbon steel increased with increasing in HCO_3^- and $MDEAH^+$ concentrations under different test conditions. Furthermore, Deli Duan *et al.* (2013) evaluated the corrosion properties of carbon steel in 50 wt% MDEA systems at 50 °C with different CO_2 partial pressures. They found under the absorber conditions, the addition of CO_2 in MDEA systems significantly increased the corrosion rate and changed behavior from a passive to an active state. They also concluded that the dominant cathodic reactions in aqueous carbonated MDEA system are HCO_3^- and $MDEAH^+$ reduction reactions.

Labbe *et al.* (2004) reported that acids react with amine by a proton transfer reaction due to the availability of a free electron pair on the nitrogen atom. The protonated amine ions are acids, in that they can provide protons for the corrosion reaction. The corroding metal reacts with the most abundant acid in the solution. In the case of DEA solutions, Shahid & Faisal, (2009) found that $DEAH^+$ ions are much more concentrated than the hydrogen ions and, therefore, the mechanism of metal dissolution for DEA solutions corrosion can be best represented by the reduction reaction of $DEAH^+$. They reported that the increase in corrosion rate is the formation of more DEAH+ ions in solution; the greater amount of $DEAH^+$ ions will be the dissolution of iron.

Although the corrosion mechanism is believed to be different in MDEA-PZ and DEA-PZ, the two activated amine systems showed an increase in corrosion rate with increasing CO_2 loading. This is believed to be due to the concentration of HCO_3^- in the systems, the oxidizing agent is the bicarbonate ion for the two carbonated system. Gray et al. (1989) suggested that in CO_2 corrosion, the charge transfer controlled bicarbonate ion reduction could be the dominant cathodic reaction at pH 6 through 10. Hamada *et al.*, (2014) reported that corrosion rate of carbon steel in DEA+ K_2CO_3 solution increases with increasing CO_2 loading. They concluded that the rate controlling step of carbon steel corrosion in the solution is the liquid phase diffusion of HCO_3^- across the diffusion layer formed at the metal-solution interface. Frolova *et al.* (1997) investigated the effect of bicarbonate ion concentration on corrosion rate of low and high strength steel in 1 N sodium carbonate solutions. They reported that the corrosion rate increases with increasing bicarbonate concentration. Banks (1967) has found that high corrosion rate in carbonate system is due to high bicarbonate concentration.

At low CO_2 partial pressure the addition of PZ concentration yields higher amount of HCO_3^-, which in turn dissociates and due to the increasing in CO_2 loading, the increasing in CO_2 loading drives the corrosion process to proceed faster, thus causing an increase in corrosion rate according to the corrosion reaction between iron and bicarbonate in reaction (4.1) (Davies & Burstein, 1980), the greater the amount of bicarbonate, the higher the amount of dissolved iron. This results in a higher corrosion rate. With this principle, the corrosion rate in MDEA-PZ is therefore greater than DEA-PZ systems at low CO_2 loading as shown in Figure 4.23.

$$Fe^{+2} + HCO_3^- \rightleftharpoons FeCO_3 + H^+ \tag{4.1}$$

At high CO_2 partial pressure the addition of PZ concentration in the MDEA-PZ system leads to decrease the concentration of bicarbonate in the solution and then decrease the corrosion rate while in the system DEA-PZ, the addition of PZ concentration to the solution leads to increasing in the bicarbonate concentration even the CO_2 loading decrease that is causing the increasing in corrosion rate. This is believed to be due to the formation of carbamate when reacting with CO_2. This carbamate will be converted into bicarbonate by hydrolysis based on reaction (3.12) and increasing the concentration of bicarbonate in the DEA-PZ system.

Chakma & Meisen (1986) studied the influence of CO_2 partial pressure on corrosion rate of carbon steel in aqueous carbonated of DEA solutions at 100 °C. They investigated the effect of CO_2 partial pressure on corrosion rate of a 30% undegraded DEA solution at 100 °C using weight loss tests. At CO_2 partial pressure of 1.38 MPa, the corrosion rate was 0.61 mm/yr, and increased to 0.8 mm/yr at CO_2 partial pressure of 4.13 MPa, then they concluded that DEA solutions are more corrosive in the presence of carbon dioxide, this is the probable reason that all experiments were carried out at 100 °C and atmospheric pressure so that solutions were nearly boiling and the presence of vapor bubbles enhanced the corrosion rates.

Most of the investigations were focused on the corrosivity of the degradation products of conventional alkanolamines especially DEA, McNab *et al.* (1971), Blanc *et al.* (1982) and Chakma *et al.* (1984), few corrosion studies can be found dealing with amine blends. Dawudo and Meisen, (1996) tested 50 wt% amine solutions ranging from 100% MDEA to 100% DEA with various blends at 120 ^{o}C to 180 ^{o}C and 374 psia of CO_2 partial pressure. They concluded that MDEA/DEA blends require more maintenance to keep the MDEA/DEA ratio from changing. They concluded that MDEA was the most resistant, followed by MEA and then DEA.

Veawab *et al.* (1999) studied the influence of process parameters on corrosion behavior in sterically hindered amine – CO_2 systems. They concluded that corrosiveness in AMP is mainly due to CO_2 loading in the liquid solution. It increases significantly with temperature and CO_2 loading. Corrosion rate is affected by AMP concentration, in comparison with MEA system. AMP apparently induces less corrosiveness at elevated temperature. Furthermore, de Waard and Milliams (1975a) correlated CO_2 partial pressure to corrosion rate for temperatures ranging from 15 to 60 ^{o}C. They found the relationship between corrosion rate and CO_2 partial pressure exponential and the exponent is 0.67. Ikeda *et al.* (1983), Schmitt *et al.* (1983) and Videm *et al.* (1989) have found similar power laws between corrosion rate and CO_2 partial pressure with the exponent ranging from 0.5 to 0.8.

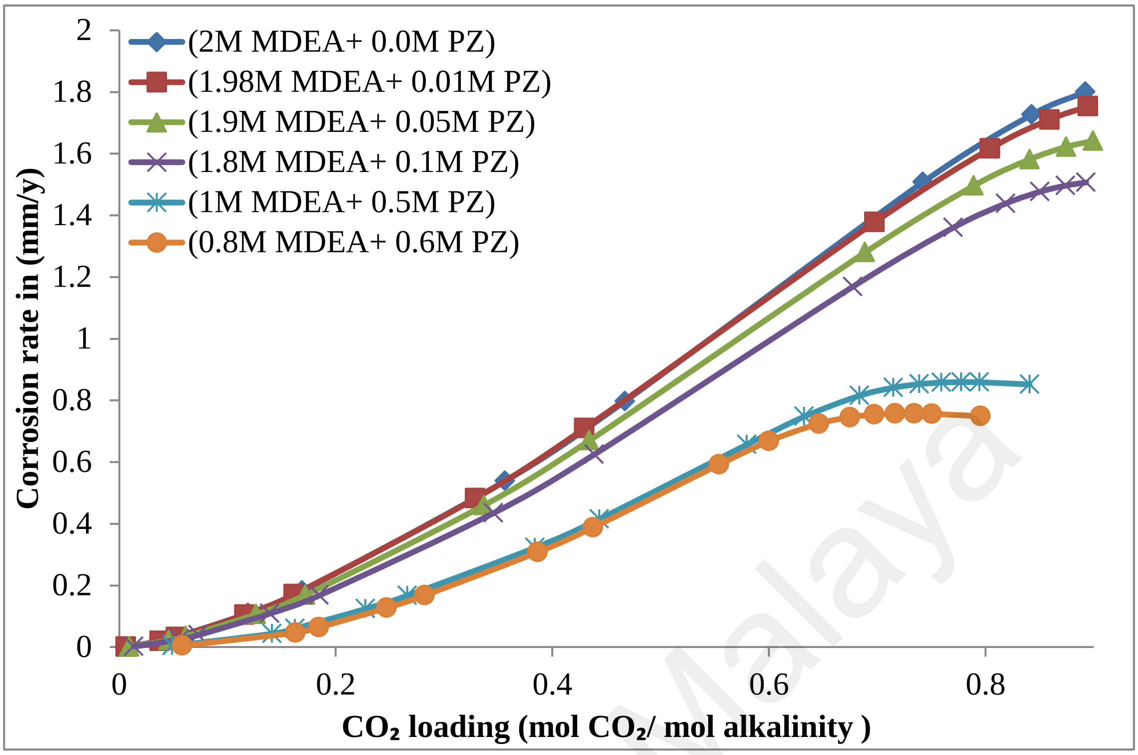

Figure 4.21: Effect of CO_2 loading on corrosion rate of carbon steel for MDEA-PZ system at 313.15 K.

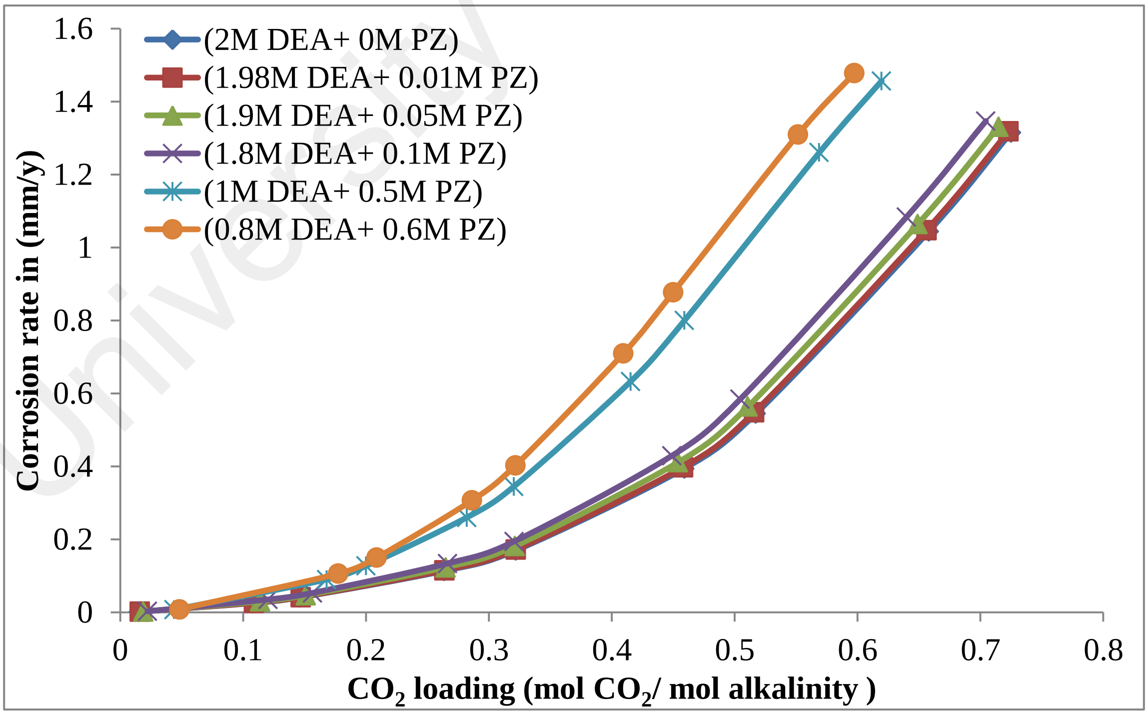

Figure 4.22: Effect of CO_2 loading on corrosion rate of carbon steel for DEA-PZ system at 313.15 K.

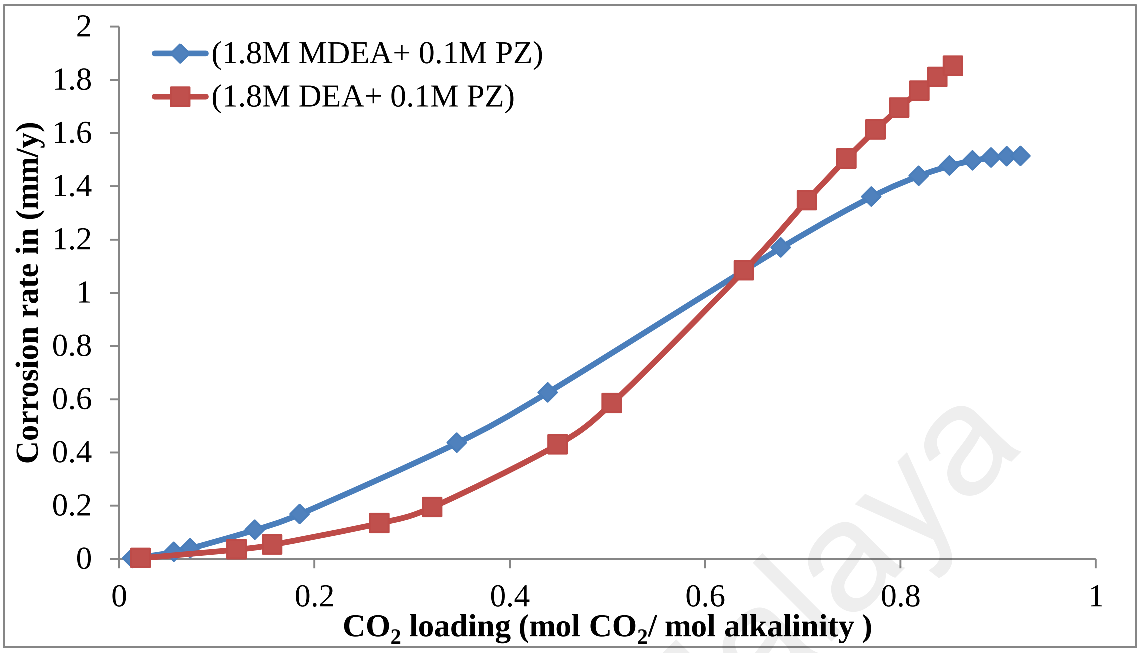

Figure 4.23: Effect of CO_2 loading in both activated MDEA and activated DEA at 313.15 K.

4.3.2 Effect of solution temperature on corrosion rate

The rate of every chemical reaction is sensitive to temperature. Undoubtedly, it is the same for the corrosion rate being an electrochemical reaction. The effect of temperature on the rate of a chemical reaction follows the Arrhenius equation (4.2):

$$k = A \times e^{\left(\frac{-E_a}{RT}\right)} \tag{4.2}$$

Where; k is the rate constant, *A* is the frequency factor, E_a is the activation energy, T is the temperature and R is the universal gas constant. It is evident that an increase in temperature leads to an increase the rate of reaction. According to this theory the increase of the rate of corrosion may be expected when the temperature is increased. It is known that electrochemical process of corrosion consists of two mutually conditioning coupled reactions anodic oxidation of iron, and cathodic reduction of oxidizing agents. The corroding system composition is heterogeneous, which consists of solid carbon steel, liquid electrolyte and dissolved gaseous carbon dioxide reactants. The temperature and the reactants concentration are significant factor for a chemical reaction rate.

In this section, the effect of solution temperature on carbon steel corrosion rate was investigated by simulating six different concentrations of activated MDEA and activated DEA at different solution temperature. For MDEA-PZ and DEA-PZ system low CO_2 loadings range from 0.007 to 0.33 mole of CO_2 per mole of alkalinity and 0.01 to 0.36 mole of CO_2 per mole of alkalinity, respectively. While the high CO_2 loading range was from 0.14 to 0.89 mole of CO_2 per mole of alkalinity for MDEA-PZ system and from 0.17 to 0.77 mole of CO_2 per mole of alkalinity for DEA-PZ system. The increase of solution temperature will result in a decrease of the CO_2 loading in both systems and thereby decrease the concentration of oxidizing agent in the solution which the corrosion process dependence on the flow of oxidizing agent to carbon steel solution interface. The corrosion results as illustrated in Figure 4.24 to 4.27, showed that the solution temperature has a considerable effect on corrosion rate, an increase in solution temperature led to increase in corrosion rate. This can be explained by the dependence of reaction kinetics on temperature. It is well established that the reaction rate increases with temperature. Therefore, the increase in temperature increases rates of metal dissolution and oxidizer reduction, thereby accelerating the corrosion process.

In the absence of any precipitation and corrosion product layer formation in the carbonated activated MDEA and activated DEA systems, temperature accelerates the kinetics of all the processes involved in a corroding system: electrochemical reactions, chemical reactions, transport processes, etc. Hence, the final corrosion rate also increases with temperature as indicated in Figure 4.24 through Figure 4.27, as is expected. The corrosion rate, which is under charge-transfer control at initial temperature, becomes mass-transfer limiting current controlled at higher temperatures.

The trend shown in this work agrees strongly with literature data in relation to corrosion rate of carbon steel in carbonated solution. Eustaquio *et al.* (2008) studied the corrosion rate of carbon steel in aqueous systems composed of MDEA, DEA and their mixtures at 393.15 K. Their results for carbon steel corrosion rate are noticed higher than that obtained for the same mixtures at 373.15 K by Chakma & Meisen, (1986). The effect of increasing corrosion rate with increases of temperature can also be observed in the work of Veawab *et al.* (1999) for aqueous solutions of AMP. This difference is in agreement with the observation made by Maddox (1982), that the corrosion rate in aqueous amine systems increases as the temperature increases, furthermore the results of Frolova *et al.* (1997) reported that upon an increase in temperature from 20 to 80 °C, the corrosion rate increased twice in pure carbonate-bicarbonate solution.

Soosaiprakasam & Veawab, (2008) studied the effect of temperature on carbon steel corrosion rate. Their results showed that carbon steel corrodes at a lower rate at 40 °C rather than at 80 °C. They found that this is attributed to the lower rate of iron dissolution and oxidizer reduction which are evidenced by the lower anodic and cathodic current densities. They observed that the differences in anodic Tafel slopes between low and high temperatures suggest different mechanisms for iron dissolution. They also, detected that the pH of the solution is higher at 40 °C than at 80 °C, this higher alkalinity may partly contributes to the lower iron corrosion rate at the lower temperature. Furthermore, Zheng *et al.* (2015) studied the effect of CO_2 loading on corrosion rate of A106 carbon steels in 30 wt% of MEA solution. They found the initial corrosion were significantly higher in the solutions, which it is increased with increasing CO_2 loading.

The data in Figure 4.24 for MDEA-PZ, showed that at low solution temperature (below 60 °C), the corrosion rate sharply increases with increasing temperature, and then slightly decreased when the temperature is around or above 80 °C. This is because an increase in solution temperature accelerates the corrosion process primarily causing the concentration of Fe^{2+} increases considerably with solution temperature. The increasing amount of Fe^{2+} at the carbon steel surface leads to the higher values of electrode parameters for oxidation reaction, especially i_o, resulting in the shift of anodic polarization curve in the positive direction of current density. Values of i_o and E_{rev} are rather insensitive to the changes in solution temperature for reductions of oxidizing agents. As a result, the cathodic polarization curve in this case also changed.

The increase in solution temperature could have one opposing effect as shown in the Figure 4.25, with increase in the temperature the viscosity of solution decreases with a consequence increase in corrosive species diffusivity according to the Stokes-Einstein equation, decreased pathways for corrosive species to reach the surface of carbon steel, which leads to high carbon steel dissolution. The corrosion rate continued at a gradually constant value than the initial corrosion rate. The temperature dependence of the viscosity for carbonated aqueous solutions of MDEA-PZ at a given CO_2 loading and a given concentration of PZ and MDEA, exponentially decrease with increasing temperature, the effect of decreasing viscosity with increases of temperature for carbonated aqueous solutions of MDEA-PZ can be found in the work by (Fu *et al.*, 2013).

The data in the Figure 4.26 and 4.27 for carbonated aqueous solution of DEA-PZ, showed that the corrosion rate of carbon steel increased with increasing in solution temperature at low and high CO_2 loading, this behavior could be ascribed to the low concentration of carbamate in the solution at low CO_2 loading. For high CO_2 loading range, the corrosion rate of carbon steel has increased with increasing temperature. This is due to high concentration of carbamate in the carbonated solution. The carbamates are responsible for the formation of iron chelate, which contributes to the increase in corrosion rate, by increasing oxidizing agent concentration (mainly HCO_3^-) in the solution. Sartori & Savage, (1983) concluded that the low carbamate stability increases the formation of the bicarbonate and maintains a high concentration of free amine in solution; this is due to the stability of carbamate in DEA less than that of MEA as reported by Mahajani & Danckwerts, (1982). Because of the similarity in the mechanism of CO_2 absorption in primary and secondary alkanolamine, it is worth mentioning that the statement of Tomoe *et al.* (1997), on primary amine carbamates that they are strong chelating agents and can form a soluble chelate compound with Fe^{2+}. They attributed this behavior to the mechanism of CO_2 absorption in primary amines. Also due to higher viscosity of the fluid that makes the diffusion of the electrochemical species (involved in corrosion phenomenon) between the electrodes strenuous. It is expected that at high temperature and high CO_2 loading, the CO_2 mass transfer rate, is positively affected via the increased driving force to increase corrosion rate in DEA-PZ as shown in Figure 4.27.

The results for corrosion rate of carbon steel at different solution temperature in carbonated aqueous solution of MDEA-PZ and DEA-PZ in Figure 4.28 showed that at low CO_2 loading the corrosion rate of carbon steel in 1.8M DEA+0.1M PZ more corrosive than 1.8M MDEA+0.1M PZ. This is because at low loading the concentration of oxidizing agents responsible for corrosion rate in the DEA-PZ higher in quantities than the oxidizing agents in the MDEA-PZ as shown in the Figure 4.29.

On the other hand, the effect of temperature on corrosion rate in carbonated DEA-PZ show a significant flow-sensitivity than MDEA-PZ. Teng *et al.* (1994) found that the DEA solution has higher activation energy for flow than MDEA. They suggested that could be due to the stronger hydrogen bonding from the hydrogen in DEA than the methyl group in MDEA.

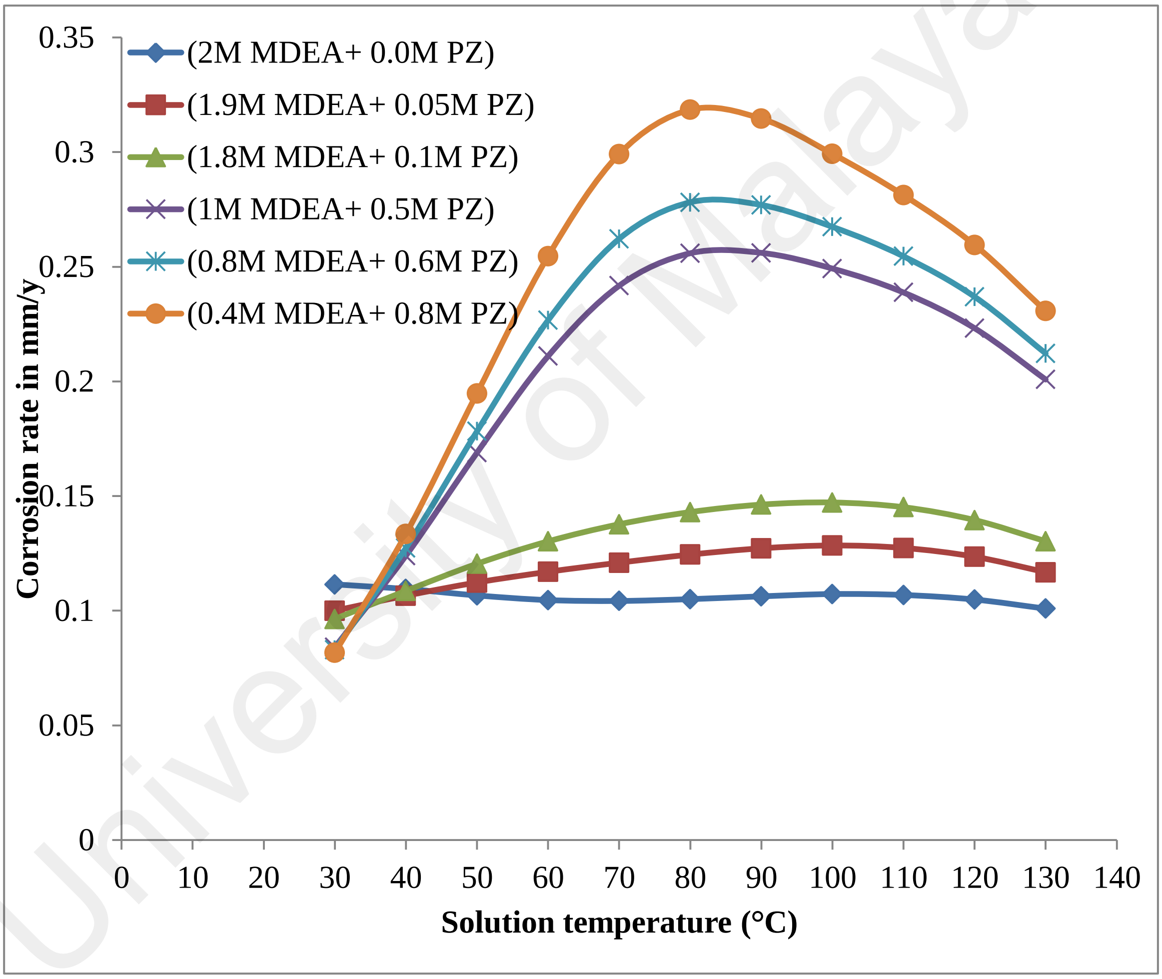

Figure 4.24: Effect of solution temperature on corrosion rate of carbon steel for system MDEA-PZ at low CO_2 loading

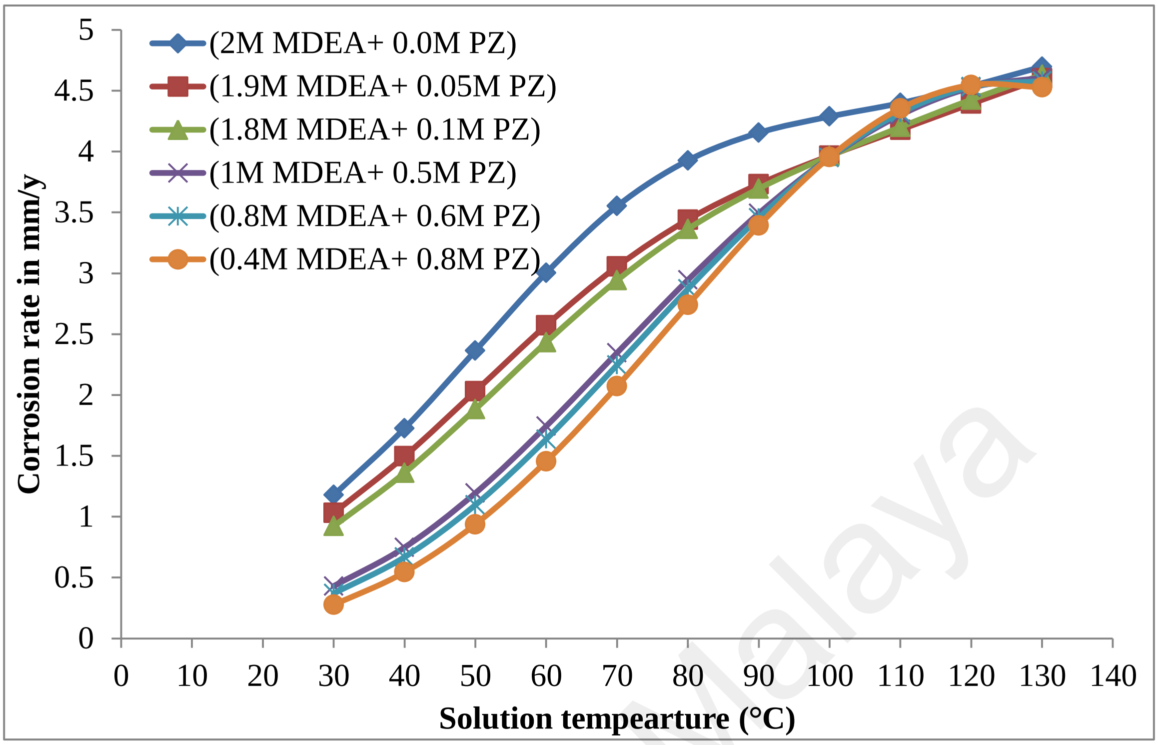

Figure 4.25: Effect of solution temperature on corrosion rate of carbon steel for system MDEA-PZ at high CO_2 loading.

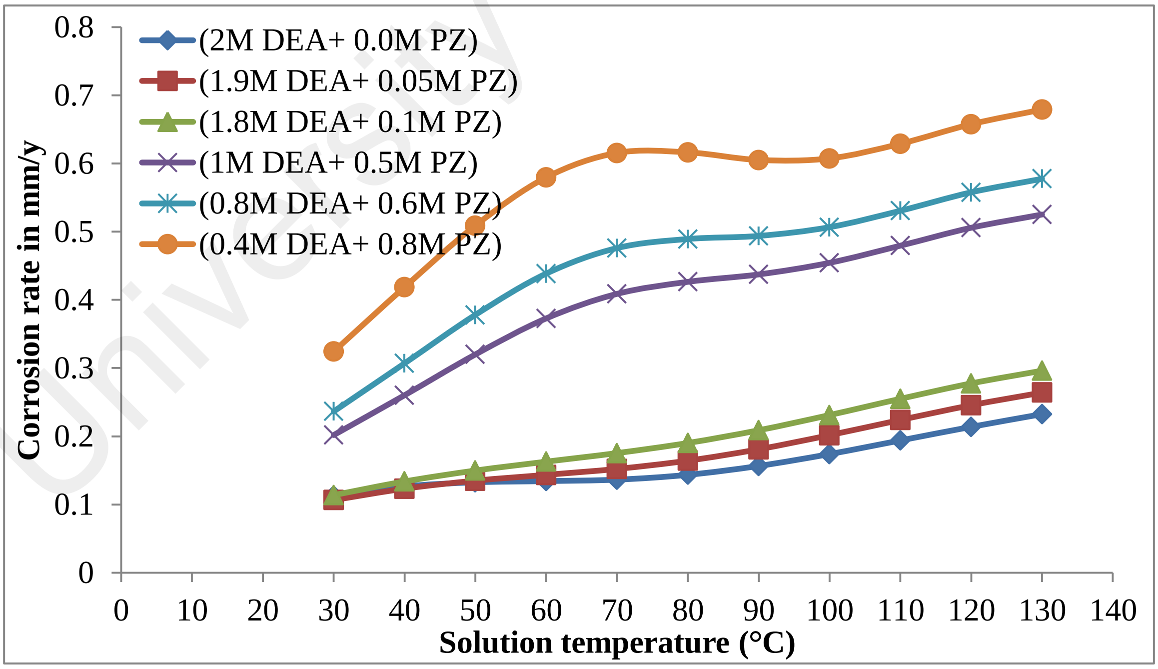

Figure 4.26: Effect of solution temperature on corrosion rate of carbon steel for system DEA-PZ at low CO_2 loading

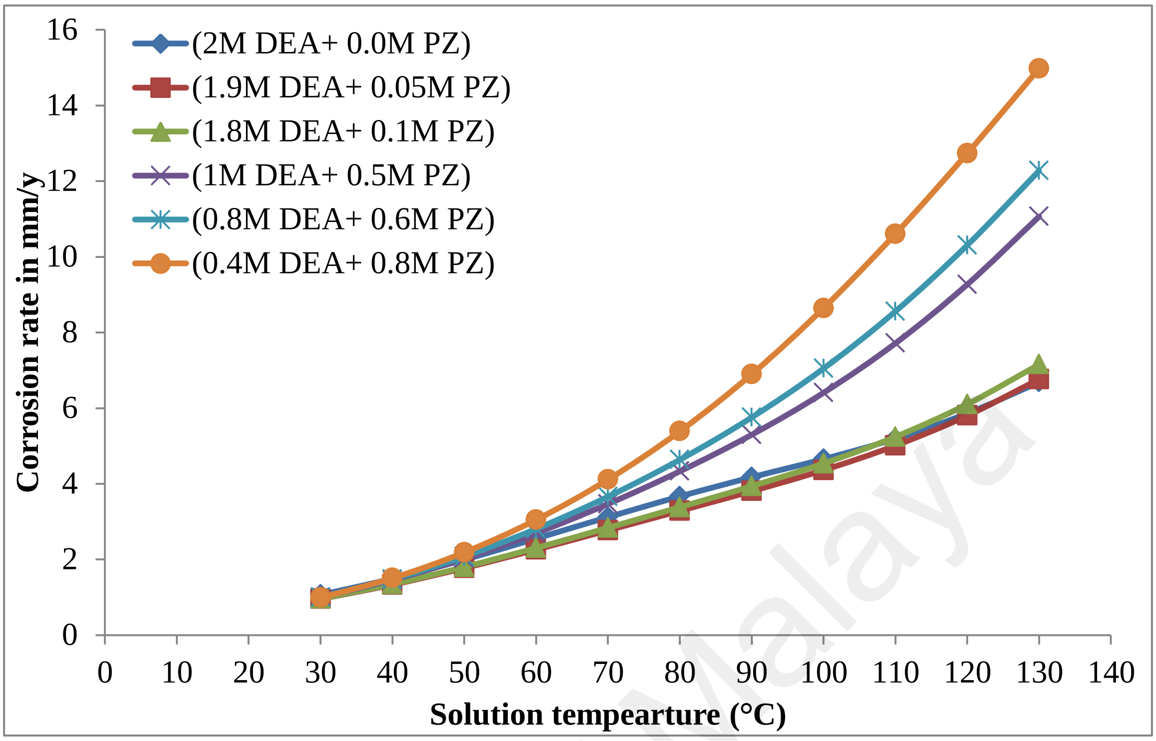

Figure 4.27: Effect of solution temperature on corrosion rate of carbon steel for system DEA-PZ at high CO_2 loading.

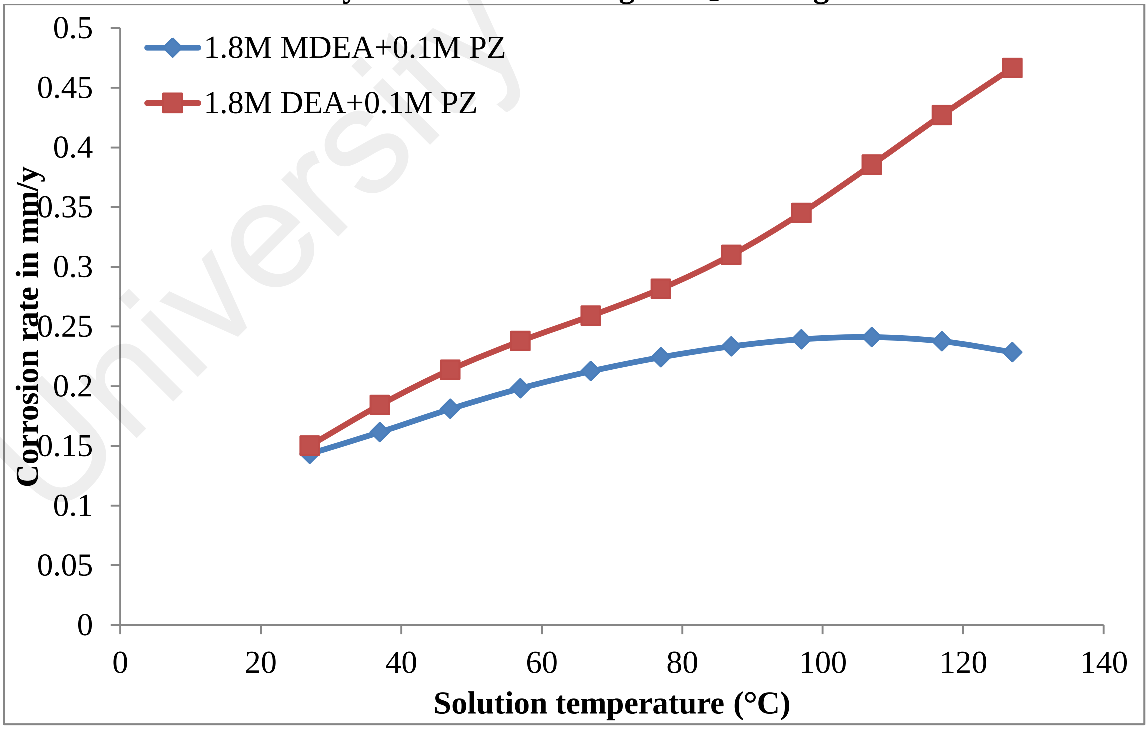

Figure 4.28: Effect of solution temperature on corrosion rate of carbon steel for 1.8M MDEA+0.1M PZ and 1.8M MDEA+0.1M PZ at low CO_2 loading.

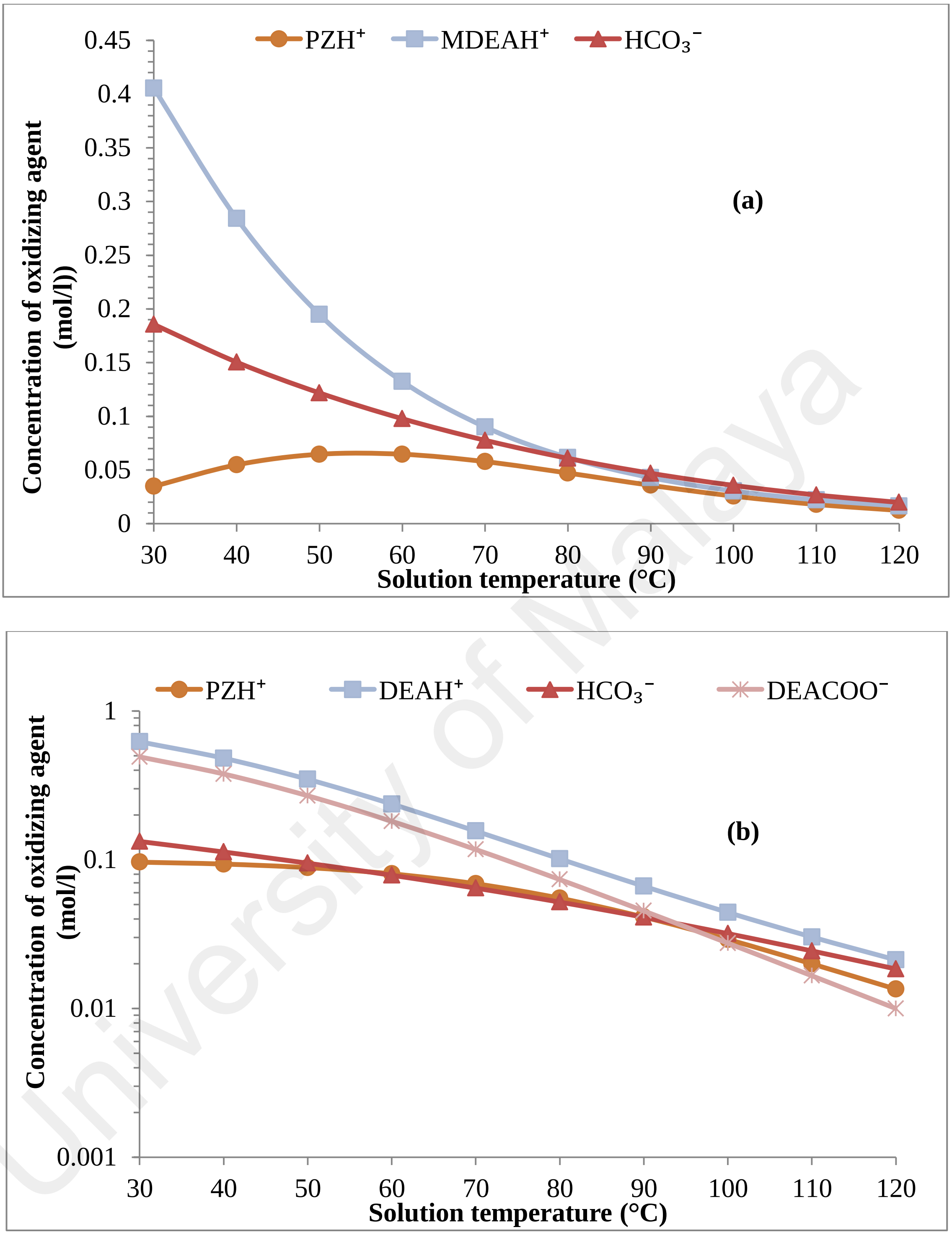

Figure 4.29: Effect of solution temperature on concentrations of oxidizing agents at low CO_2 loading for the systems (a) 1.8M MDEA+0.1M PZ (b) 1.8M DEA+0.1M PZ

4.3.3 Effect of activator concentration on corrosion rate

PZ is a cyclic secondary alkanolamine with two amine groups, which can involve in multiple reactions with CO_2, has some attractive advantage such as a low oxidation rate in the presence of ion Fe, a fast CO_2 absorption rate, a low thermal degradation rate up to 150 °C, low regeneration energy (Freeman, 2011; Freeman, Davis, *et al.*, 2010; Freeman, Dugas, *et al.*, 2010). This make PZ an attractive alternative solvent even with some disadvantage such as high viscosity and a narrow solubility window in lean CO_2 capture solutions, which could preclude its use as a single operational process solvent. Moreover, PZ has been routinely reported to be an effective promoter of the absorption rate in CO_2 capture solutions (Ali & Aroua, 2004; Cullinane, 2005; Dang, 2000). Corrosion of carbon steel in some of these blends has been conducted (Nainar & Veawab, 2009; Zhao *et al.*, 2011).

The effect of PZ concentration on carbon steel corrosion rate was simulated for 2 M total alkalinity of solution for three different solution temperatures at different CO_2 loading. Results in Figure 4.30 and 4.31 showed that at low CO_2 loading the corrosion rate of carbon steel increased with the increase in PZ concentration at the three solution temperature due to the increase in oxidizing agent concentrations for both systems. At low conditions of CO_2 partial pressure and solution temperature the effect of PZ on MDEA and DEA as activator to increase the CO_2 loading which increasing in HCO_3^- and protonated amine concentrations in both systems which led to increase the corrosion rate. Whereas at high CO_2 loading the corrosion rate of carbon steel decreased in the MDEA-PZ system, this is because of the decrease in the HCO_3^- concentration which is the main oxidizing agent affecting the corrosion process of carbon steel as shown in the Figure 4.32. While in the system DEA-PZ, the corrosion rate of carbon steel increased with the increase of PZ concentration at high CO_2 loading as shown in the Figure 4.31.

This is due to the increase in concentration of HCO_3^- from dissolved CO_2 and from hydrolysis DEA carbamate as shown in Figure 4.32. It could be other mechanism which has an impact on chelating proprieties of the iron complex, which is believed to increase the corrosion rate in carbonated DEA solution.

According to the experimental results by (Zheng *et al.*, 2014), the role of piperazine in reducing the corrosion rate of carbon steel, such 30 wt.% PZ at 0.4 (mol CO_2 /mol alkalinity) at 80 ^oC is completely different from the corrosion rate with carbon steels in similar solutions of 50 wt.% MDEA with 0.13 (mol CO_2 /mol alkalinity) and 30 wt.% MEA with 0.43 (mol CO_2 /mol alkalinity). They concluded that due to the two reasons, the corrosion product layer on the carbon steel surface was found to be highly dense and stable. One of the other possible reasons for a low corrosion rate is the low degradation rate of PZ, especially in cases with low oxygen content, which led to fewer corrosive species that were reported to be an important factor in increasing the corrosion rate of carbon steel in MEA solution loaded with CO_2.

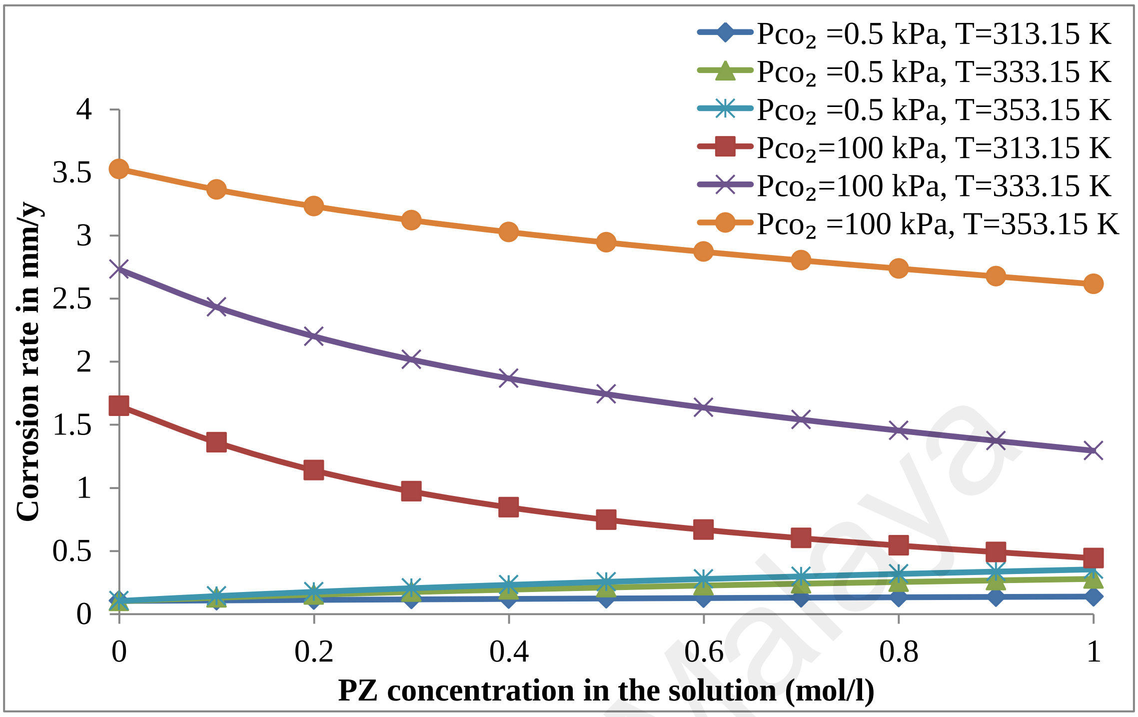

Figure 4.30: Effect of PZ concentration on corrosion rate of carbon steel at low and high CO_2 loading at different solution temperature for system MDEA-PZ.

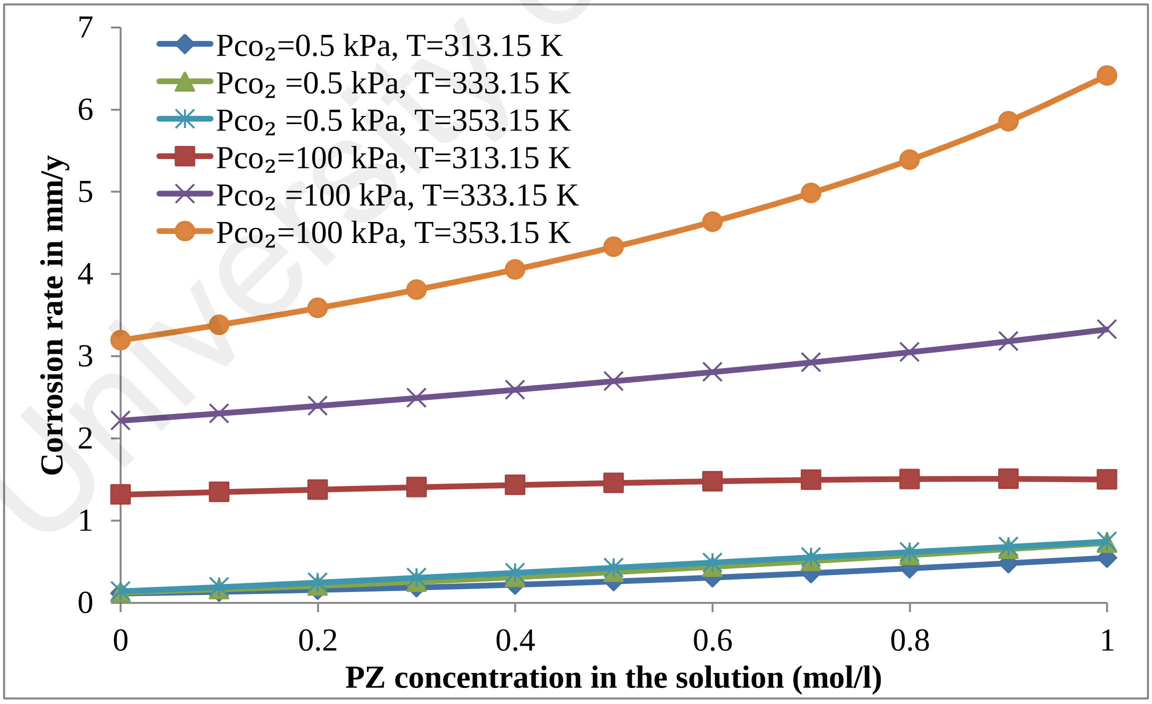

Figure 4.31: Effect of PZ concentration on corrosion rate of carbon steel at low and high CO_2 loading at different solution temperature for system DEA-PZ.

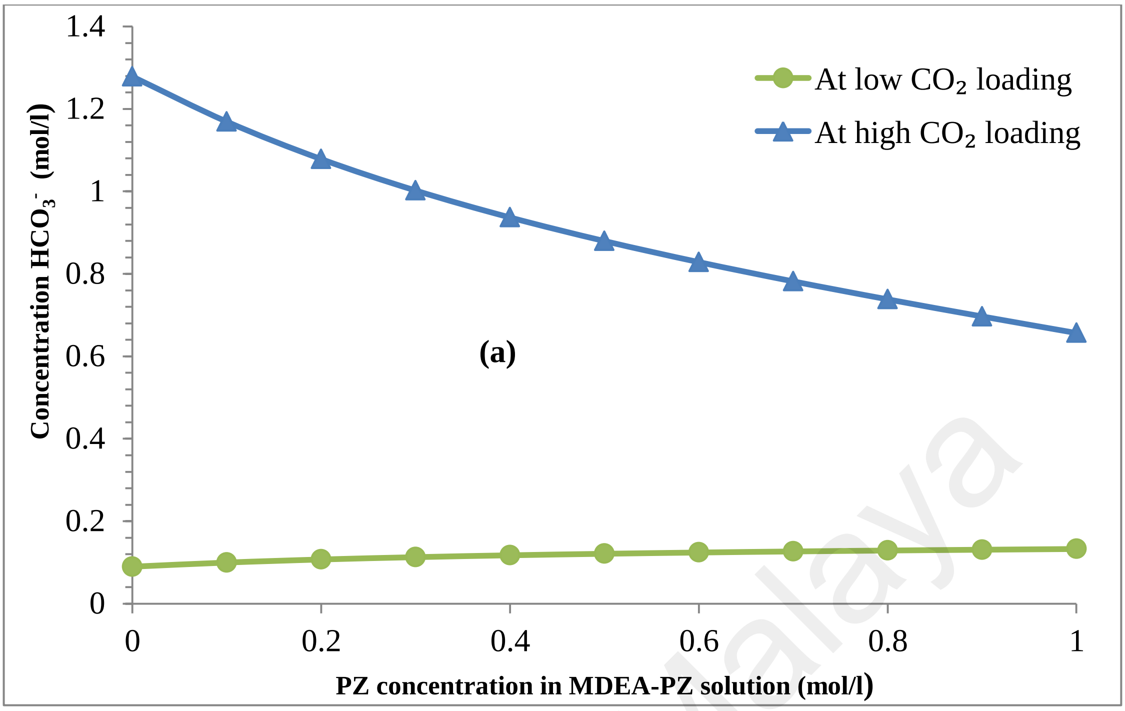

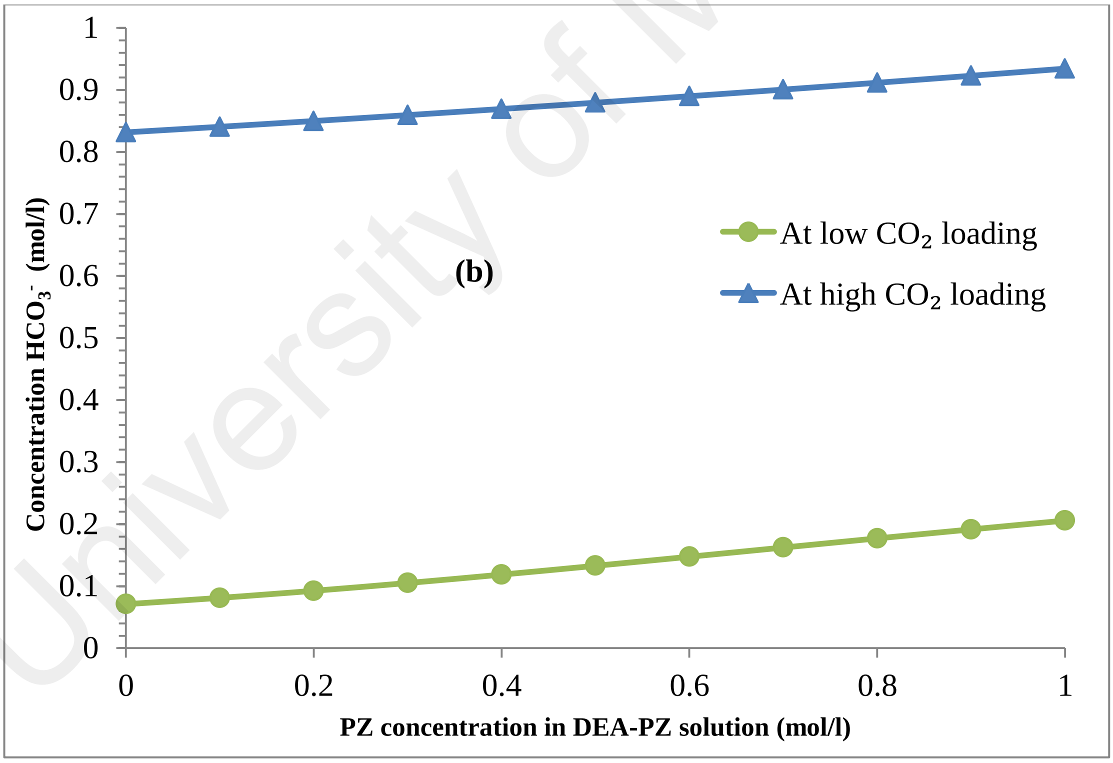

Figure 4.32: Effect of PZ concentration on concentration of HCO_3^- in the bulk solution of (a) MDEA-PZ system (b) DEA-PZ system at 333.15 K

4.3.4 Activated Amine type with piperazine

The results reveal corrosion behavior under a practical condition where CO_2 loading in each amine system vary depending upon the CO_2 solubility. The results shown in Figure 4.34 and 4.35 indicate that the amine type has an effect on the system corrosiveness. Corrosion rate in the DEA-PZ system was greater than MDEA-PZ system at high conditions. This is due to the difference in the amount of bicarbonate ion which is an oxidizing agent in these systems. At the low CO_2 loading, the system MDEA-PZ system contains greater amount of bicarbonate and protonated amine in comparison with DEA-PZ system.

At low operating conditions (CO_2 loading, solution temperature and activator concentration) the corrosion rate of carbon steel in DEA-PZ system was less than that in MDEA-PZ system as shown in the Figure 4.34. But at high operating conditions, the piperazine carbamate take place, resulting in piperazine carbamate and also formation of piperazine di-carbamate. These species might not have actively participated in the corrosion reactions and could be one of the possible reasons for the high corrosiveness of the DEA-PZ system while the effect of DEA carbamate in the solution is shown in the Figure 4.35.

Solutions composed of activated MEA by PZ were tested in Nainar & Veawab, (2009) showed more corrosion than in pure MEA. A great deal of attention is also given to the activated solutions of tertiary amines. Corrosion in MDEA using piperazine as activator solution was studied in Zhao *et al.* (2011), showing the same detrimental impact of CO_2 loading and temperature in MEA solutions.

4.3.5 Concentration of oxidizing agent

To determine which oxidizing agents play an important role in corrosivity of activated MDEA and activated DEA systems, the quantity of oxidizing agents participating in the corrosion process were considered. Based on the literature, the oxidizing agents in aqueous amine-CO_2 systems are H_2O (Veawab & Aroonwilas, 2002);(Benamor & Al-Marri, 2014) , HCO_3^- (Benamor & Al-Marri, 2014; Choi *et al.*, 2012; Duan *et al.*, 2013; Guo & Tomoe, 1999; Veawab & Aroonwilas, 2002), protonated amine (Kohl & Nielsen, 1997);(Guo & Tomoe, 1998);(Choi *et al.*, 2012; Duan *et al.*, 2013) and carbamate ions (Tomoe & Sato, 1997);(Guo & Tomoe, 1998). Hydronium ions were reported to play an insignificant role in the corrosion process of aqueous MEA-CO_2 systems (Veawab & Aroonwilas, 2002); (Najumudeen, 2012), aqueous DEA-CO_2 (Benamor & Al-Marri, 2014), aqueous MDEA-CO_2 systems (Duan *et al.*, 2013) and this was also confirmed by the pH data of single and blend amine system by the study of Gunasekaran (2012). The overall CO_2 absorption reaction with aqueous activated MDEA and activated DEA solution results in different amounts of protonated amine, HCO_3^- and carbamate as shown in Figure 4.33 that PZH^+ concentration was higher in DEA-PZ than in MDEA-PZ.

The studies on CO_2 solubility and absorption rate in pure piperazine suggested that the piperazine carbamate stability constant is comparable to that of other secondary amines such as DEA (Bishnoi & Rochelle, 2000). Thus, the concentration of carbamate species can be expected to have higher effect on corrosion rate for DEA-PZ system than MDEA-PZ system. Hence, it was found that DEA-PZ system is more corrosive than MDEA-PZ system.

The concentration of bicarbonate as in DEA-PZ is less than that in MDEA-PZ, as shown in Figure 4.21 and 4.22. The concentration of HCO_3^- in (1.8M MDEA+0.1M PZ) is in the range between 0.0044 to 1.41 mol/l and in (1.8M DEA+0.1M PZ) is in range 0.0043 to 1.04 mol/l at same condition of CO_2 partial pressure and temperature. The high corrosion rate in DEA-PZ compared to that of MDEA-PZ at same conditions is due to low bicarbonate concentration, and also the impact of carbamates species which hinder the film formation at the metal surface.

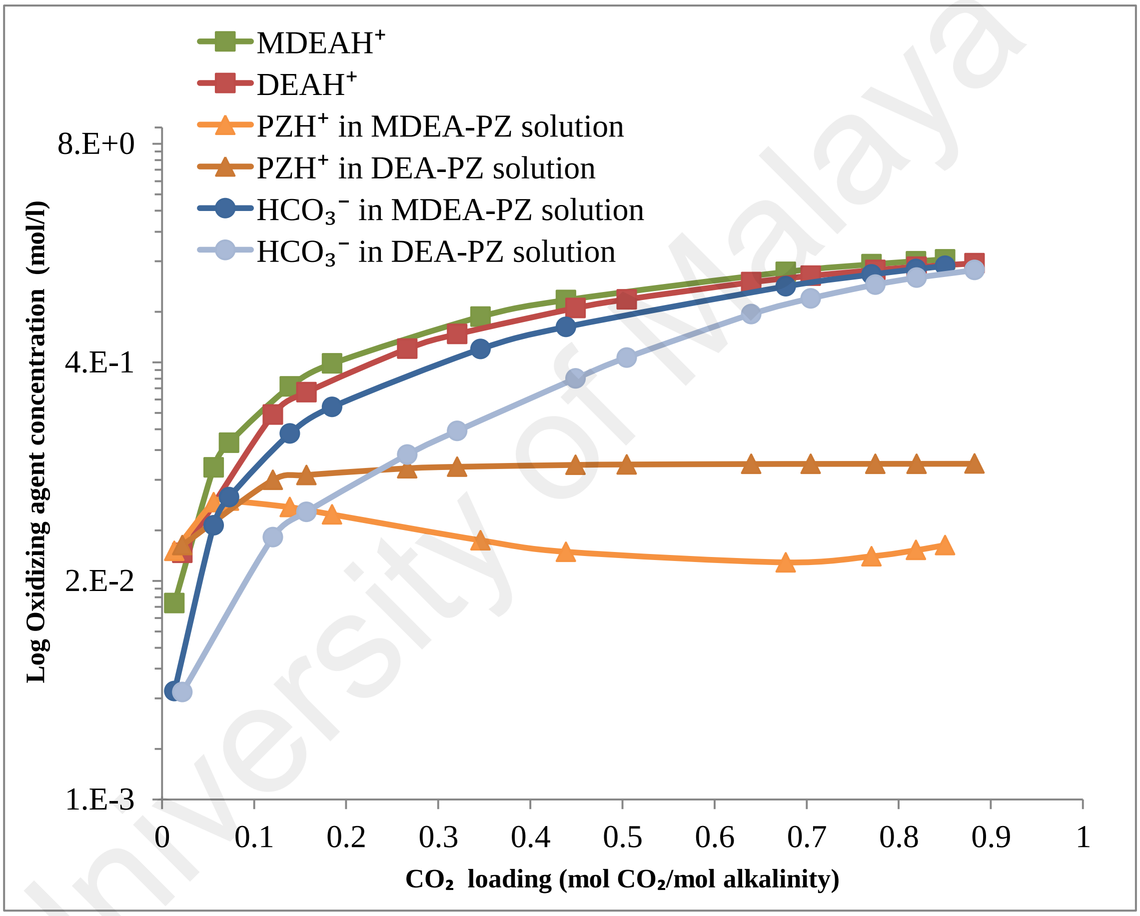

Figure 4.33: Prediction of oxidizing agents concentration in (1.8 MDEA+0.1 PZ) M and (1.8 DEA + 0.1 PZ) M; T=333.15 K.

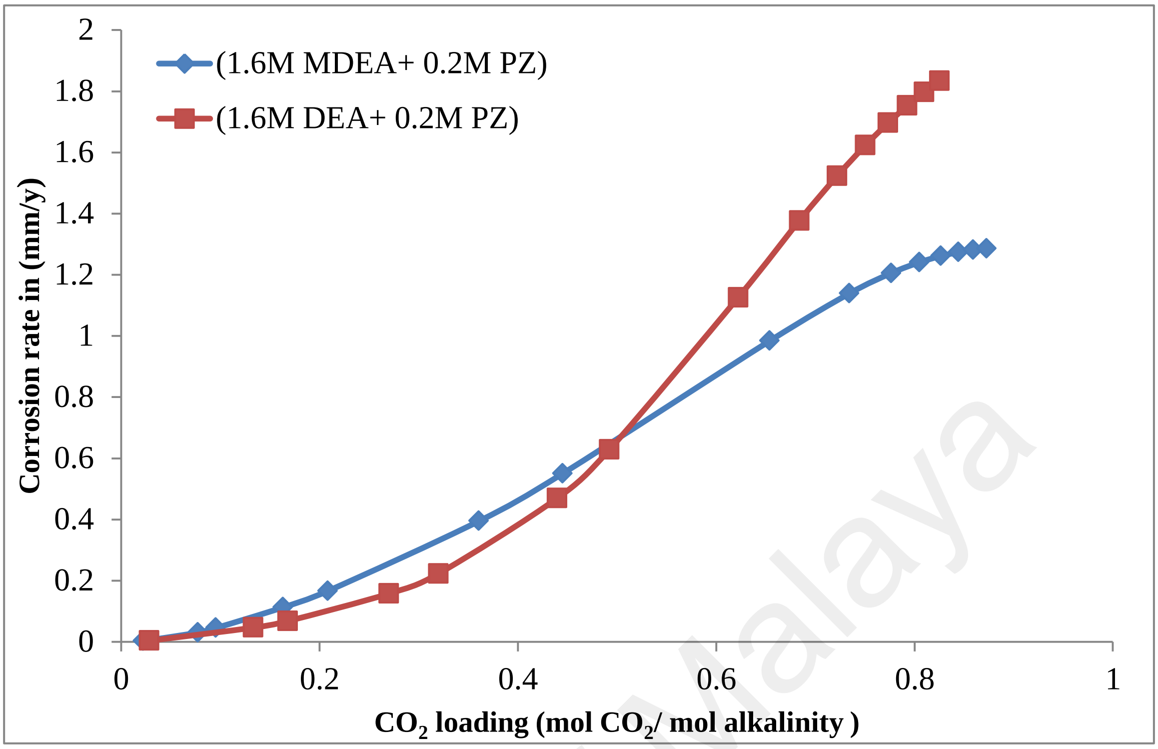

Figure 4.34: Prediction corrosion rate of MDEA-PZ and DEA-PZ at low operating conditions

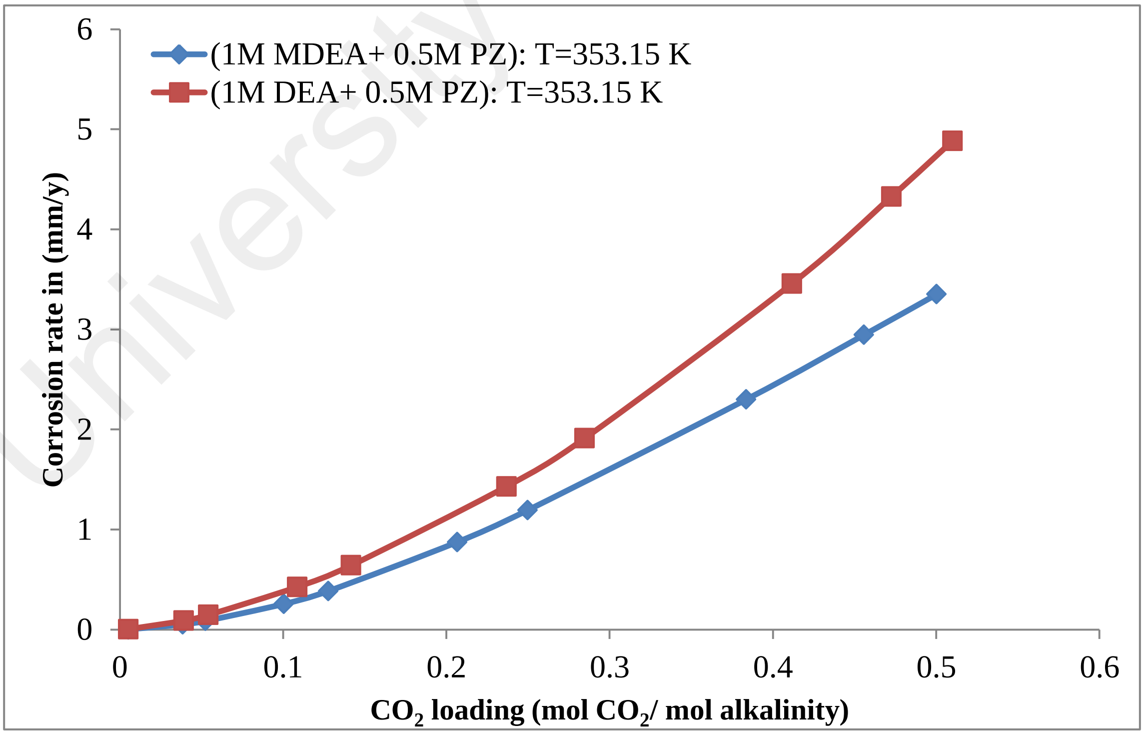

Figure 4.35: Prediction corrosion rate of MDEA-PZ and DEA-PZ at high operating conditions

CHAPTER 5: CONCLUSION AND RECOMMENDATIONS

5.1 Conclusion

A mechanistic corrosion model for carbon steel in aqueous carbonated solution of activated MDEA and activated DEA was successfully developed. The model was validated with the corrosion rate data obtained from the literature. The model showed that the capacity to predict changes in species concentration, CO_2 loading, solution pH and corrosion behavior under variety of operating conditions. The following are important findings construed from the model simulations in this work:

- Measure corrosion rate in MDEA-PZ and DEA-PZ.
- The use of the vapour-liquid equilibrium e-NRTL model to develop corrosion model yields higher accuracy for corrosion rate prediction.
- Corrosion rate of carbon steel in activated amine systems is greatly influenced by CO_2 loading, solution temperature and activator concentration.
- Hydronium ion H_3O^+ contributed least to the carbon steel corrosion rate for both activated MDEA and activated DEA systems, compared to the others oxidizing agents (H_2O, HCO_3^-, PZH^+, $MDEAH^+$ and $DEAH^+$).
- The relative contribution of bicarbonate, protonated amine and water reduction to the corrosion current depends on activator concentration. At low activator concentration, bicarbonate and protonated amine reduction contribution are important compared to the contribution of water reduction.
- The corrosivity order of carbonated aqueous activated amine for carbon steel was governed mainly by their CO_2 absorption capacity, at high CO_2 loading lead to high corrosion rate.

- CO_2 loading effect on the kinetics of the anodic and cathodic reactions. HCO_3^- reduction is more sensitive to the CO_2 loading than other oxidizing agents.
- Solution temperature alters the kinetic of the iron dissolution but slightly effected the cathodic reactions.
- The effect of the activator concentration on the carbon steel corrosion rate is pronounced for both systems. For MDEA-PZ the carbon steel corrosion rate decreasing with increasing activator concentration while the DEA-PZ system the carbon steel corrosion rate increases with increases activator concentration.

5.2 Recommendations for Future work

The present work serves as a guideline for the selection of suitable absorption solvent in terms of corrosivity. Study of the corrosivity of aqueous activated MDEA-PZ and activated DEA-PZ systems has more room for improvement, and further research. The present work can be further strengthened by focusing on the followings suggestions:

- Effect of oxygen ingress on the corrosivity of the systems.
- Effect of containments such as degradation products and impurities.
- The corrosion model can be extended to take into account the film formation and growth by implementing the solubility limits for $FeCO_3$ in the amine solution.
- For model validation, more experimental data are needed under various flow conditions.
- Inclusion of amines carbamates as oxidizing agents and studying their effect on the corrosion rate.

- The current model has been developed for MDEA-PZ and DEA-PZ systems. However, it could be extended to any alkanolamine with PZ, provided all the vapor-liquid equilibrium data are available.
- Fundamental studies of kinetics of electrochemical reactions could help to achieve more accurate corrosion rate data.
- Investigate the exchange current density of oxidizing agent and the reaction order for each system.

REFERENCES

Ali, B. S. (2007). *Carbon dioxide absorption and its corrosity in aqueos solutions of activated diethanolamine and methyldiethanolamnine and their mixture.* (Doctor of Philosophy), University of Malaya, Kuala Lumpur Malaysia.

Ali, B. S., & Aroua, M. (2004). Effect of piperazine on CO_2 loading in aqueous solutions of MDEA at low pressure. *International journal of thermophysics, 25*(6), 1863-1870.

Anderko, A. (2010). Modeling of aqueous corrosion In R. A. Cottis, M. J. Graham, R. Lindsay, S. B. Lyon, J. A. Richardson, J. D. Scantlebury, & F. H. Stott (Eds.), *Shreir's Corrosion series* (4 ed., Vol. 2): Elsevier Amsterdam.

Austgen, D. M. (1989). *A model of vapor-liquid equilibria for acid gas-alkanolamine-water systems.* (Doctor of Philosophy), University of Texas at Austin.

Austgen, D. M., Rochelle, G. T., & Chen, C. C. (1991). Model of vapor-liquid equilibria for aqueous acid gas-alkanolamine systems. 2. Representation of hydrogen sulfide and carbon dioxide solubility in aqueous MDEA and carbon dioxide solubility in aqueous mixtures of MDEA with MEA or DEA. *Industrial & Engineering Chemistry Research, 30*(3), 543-555.

Austgen, D. M., Rochelle, G. T., Peng, X., & Chen, C. C. (1989). Model of vapor-liquid equilibria for aqueous acid gas-alkanolamine systems using the electrolyte-NRTL equation. *Industrial & Engineering Chemistry Research, 28*(7), 1060-1073.

Bard, A. J., & Faulkner, L. R. (1980). *Electrochemical methods: fundamentals and applications* (Vol. 2): Wiley New York.

Benamor, A., & Al-Marri, M. J. (2014). Modeling Analysis of Corrosion Behavior of Carbon Steel in CO_2 Loaded Amine Solutions. *International Journal of Chemical Engineering and Applications, 5*(4), 353.

Bishnoi, S., & Rochelle, G. T. (2000). Absorption of carbon dioxide into aqueous piperazine: reaction kinetics, mass transfer and solubility. *Chemical Engineering Science, 55*(22), 5531-5543.

Bishnoi, S., & Rochelle, G. T. (2002). Thermodynamics of piperazine/methyldiethanolamine/water/carbon dioxide. *Industrial & Engineering Chemistry Research, 41*(3), 604-612.

Blomen, E., Hendriks, C., & Neele, F. (2009). Capture technologies: improvements and promising developments. *Energy Procedia, 1*(1), 1505-1512.

Bockris, J. M., Drazic, D., & Despic, A. (1961). The electrode kinetics of the deposition and dissolution of iron. *Electrochimica Acta, 4*(2), 325-361.

Bockris, J. M., & Reddy, A. K. (1970). *Modern electrochemistry: an introduction to an interdisciplinary area. Vol. 1*: Plenum Press.

Bockris, J. O. M., & Khan, S. U. (2013). *Surface electrochemistry: a molecular level approach*: Springer Science & Business Media.

Bower, V. E., Robinson, R. A., & Bates, R. G. (1962). Acidic dissociation constant and related thermodynamic quantities for diethanolammonium ion in water from 0 to 50° C. *J. Res. Natl. Bur. Stand. A, 66*, 71-75.

Brelvi, S., & O'connell, J. (1972). Correspondling states correlations for liquid compressibility and partial molal volumes of gases at infinite dilution in liquids. *AIChE journal, 18*(6), 1239-1243.

Chakma, A. (1995). An energy efficient mixed solvent for the separation of CO_2. *Energy conversion and management, 36*(6), 427-430.

Chakma, A. (1997). CO_2 capture processes—opportunities for improved energy efficiencies. *Energy conversion and management, 38*, S51-S56.

Chakma, A., & Meisen, A. (1986). Corrosivity of diethanolamine solutions and their degradation products. *Industrial & engineering chemistry product research and development, 25*(4), 627-630.

Chen, C. C., & Evans, L. B. (1986). A local composition model for the excess Gibbs energy of aqueous electrolyte systems. *AIChE journal, 32*(3), 444-454.

Choi, Y.-S., Nešić, S., Duan, D., & Jiang, S. (2012). *Mechanistic Modeling of Carbon Steel Corrosion in a MDEA-Based CO_2 Capture Process.* Paper presented at the Corrosion 2012.

Closmann, F., Nguyen, T., & Rochelle, G. T. (2009). MDEA/Piperazine as a solvent for CO_2 capture. *Energy Procedia, 1*(1), 1351-1357.

Critchfield, J. E. (1988). *CO_2 absorption/desorption methyldiethanolamine solutions promoted with monoethanolamine and diethanolamine: mass transfer and reaction kinetics.* (Doctor of Philosophy), University of Texas at Austin.

Cullinane, J. T. (2005). *Thermodynamics and kinetics of aqueous piperazine with potassium carbonate for carbon dioxide absorption.* (Doctor of Philosophy), The University of Texas at Austin, Austin.

Dang, H. (2000). *CO_2 absorption rate and solubility in monoethanolamine/piperazine/water.* (master), University of Texas at Austin.

Dang, H., & Rochelle, G. T. (2003). CO_2 absorption rate and solubility in monoethanolamine/piperazine/water. *Separation science and technology, 38*(2), 337-357.

Dash, S. K., & Bandyopadhyay, S. S. (2013). Carbon dioxide capture: absorption of carbon dioxide in piperazine activated concentrated aqueous 2-amino-2-methyl-1-propanol. *Journal of Clean Energy Technologies, 1*(3), 185-188.

Dash, S. K., & Bandyopadhyay, S. S. (2016). Studies on the effect of addition of piperazine and sulfolane into aqueous solution of N-methyldiethanolamine for CO_2 capture and VLE modelling using eNRTL equation. *International Journal of Greenhouse Gas Control, 44*, 227-237.

Dash, S. K., Samanta, A., Samanta, A. N., & Bandyopadhyay, S. S. (2011). Vapour liquid equilibria of carbon dioxide in dilute and concentrated aqueous solutions of piperazine at low to high pressure. *Fluid phase equilibria, 300*(1), 145-154.

Davies, D., & Burstein, G. (1980). The effects of bicarbonate on the corrosion and passivation of iron. *Corrosion, 36*(8), 416-422.

Dawodu, O. F., & Meisen, A. (1994). Solubility of carbon dioxide in aqueous mixtures of alkanolamines. *Journal of Chemical and Engineering Data, 39*(3), 548-552.

de Waard, C., & Lotz, U. (1993). *Prediction of CO_2 Corrosion of Carbon Steel.* Paper presented at the Corrosion-National Association of Corrosion Engineers Annual Conference.

de Waard, C., Lotz, U., & Dugstad, A. (1995). *Influence of Liquid Flow Velocity on CO_2 Corrosion: A Semi-Empirical Model.* Paper presented at the Corrosion-National Association of Corrosion Engineers Annual Conference.

de Waard, C., Lotz, U., & Milliams, D. (1991). Predictive model for CO_2 corrosion engineering in wet natural gas pipelines. *Corrosion, 47*(12), 976-985.

de Waard, C., & Milliams, D. (1975). Carbonic acid corrosion of steel. *Corrosion, 31*(5), 177-181.

Derks, P., Hogendoorn, J., & Versteeg, G. (2010). Experimental and theoretical study of the solubility of carbon dioxide in aqueous blends of piperazine and N-methyldiethanolamine. *The Journal of Chemical Thermodynamics, 42*(1), 151-163.

Derks, P., Kleingeld, T., Van Aken, C., Hogendoorn, J., & Versteeg, G. (2006). Kinetics of absorption of carbon dioxide in aqueous piperazine solutions. *Chemical Engineering Science, 61*(20), 6837-6854.

Derks, P. W., Hamborg, E. S., Hogendoorn, J., Niederer, J. P., & Versteeg, G. F. (2008). Densities, viscosities, and liquid diffusivities in aqueous piperazine and aqueous (piperazine+ N-methyldiethanolamine) solutions. *Journal of Chemical & Engineering Data, 53*(5), 1179-1185.

Dingman, J., Allen, D., & Moore, T. (1966). Minimize corrosion in MEA units. *Hydrocarbon processing, 45*(9), 285-&.

Duan, D., Choi, Y.-S., Jiang, S., & Nešic, S. (2013). Corrosion Mechanism of Carbon Steel in MDEA-Based CO_2 Capture Plants. *CORROSION/2013, paper*(51313-02345).

DuPart, Bacon, T., & Edwards, D. (1993). Understanding corrosion in alkanolamine gas treating plants. *Hydrocarbon processing, 72*(5), 89-94.

DuPart, Bacon, T. R., & Edwards, D. J. (1991). *Understanding and preventing corrosion in alkanolamine gas treating plants.* Paper presented at the Proceedings of the 41st Laurance Reid Gas Conditioning Conference.

Eisenberg, M., Tobias, C., & Wilke, C. (1954). Ionic mass transfer and concentration polarization at rotating electrodes. *Journal of the Electrochemical Society, 101*(6), 306-320.

Feng, Z., Jing-Wen, M., Zheng, Z., You-Ting, W., & Zhi-Bing, Z. (2012). Study on the absorption of carbon dioxide in high concentrated MDEA and ILs solutions. *Chemical Engineering Journal, 181*, 222-228.

Figueroa, J. D., Fout, T., Plasynski, S., McIlvried, H., & Srivastava, R. D. (2008). Advances in CO_2 capture technology—the US Department of Energy's Carbon Sequestration Program. *International Journal of Greenhouse Gas Control, 2*(1), 9-20.

Fosbøl, P. L., Thomsen, K., & Stenby, E. H. (2009). *Improving mechanistic CO_2 corrosion models.* Paper presented at the Corrosion 2009.

Freeman, S. A. (2011). Thermal degradation and oxidation of aqueous piperazine for carbon dioxide capture.

Freeman, S. A., Davis, J., & Rochelle, G. T. (2010). Degradation of aqueous piperazine in carbon dioxide capture. *International Journal of Greenhouse Gas Control, 4*(5), 756-761.

Freeman, S. A., Dugas, R., Van Wagener, D. H., Nguyen, T., & Rochelle, G. T. (2010). Carbon dioxide capture with concentrated, aqueous piperazine. *International Journal of Greenhouse Gas Control, 4*(2), 119-124.

Fu, D., Qin, L., & Hao, H. (2013). Experiment and model for the viscosity of carbonated piperazine-N-methyldiethanolamine aqueous solutions. *Journal of Molecular Liquids, 186*, 81-84.

Gileadi, E. (1993). *Electrode kinetics for chemists, chemical engineers, and materials scientists*: Capstone.

Goldberg, R. N., Kishore, N., & Lennen, R. M. (2002). Thermodynamic quantities for the ionization reactions of buffers. *Journal of physical and chemical reference data, 31*(2), 231-370.

Guo, X.-P., & Tomoe, Y. (1999). The effect of corrosion product layers on the anodic and cathodic reactions of carbon steel in CO_2-saturated MDEA solutions at 100 ^oC. *Corrosion Science, 41*(7), 1391-1402.

Guo, X., & Tomoe, Y. (1998). Electrochemical behavior of carbon steel in carbon dioxide-saturated diglycolamine solutions. *Corrosion, 54*(11), 931-939.

Haji-Sulaiman, M., Aroua, M., & Benamor, A. (1998). Analysis of equilibrium data of CO_2 in aqueous solutions of DEA, MDEA and their mixtures using the modified Kent Eisenberg model. *Trans Chem E, 76*, 961-968.

Helle, H. (1995). *Corrosion control in alkanolamine gas treating: Absorber corrosion*. Retrieved from

Kadiwala, S., Rayer, A. V., & Henni, A. (2010). High pressure solubility of carbon dioxide (CO_2) in aqueous piperazine solutions. *Fluid phase equilibria, 292*(1), 20-28.

Kaesche, H. (1985). Metallic corrosion. *H. Kaesche, Translated by R. A. Rapp, published 1985 by NACE, 498*.

Keller, A., Kammiller, R., Veatch, F., Cummings, A., Thompsen, J., & Mecum, S. (1992). *Heat-stable salt removal from amines by the HSSX process using ion exchange.* Paper presented at the Proceedings of Laurance Reid Gas Conditioning Conference. Norman, OK, USA (2–4 March).

Kohl, A. L., & Nielsen, R. (1997). *Gas purification*: Gulf Professional Publishing.

Krawczyk, L. S., Martin, C. W., & Pearce, R. L. (1984). Inhibitors for Acid gas conditioning solutions: Google Patents.

Landolt, D. (2007). *Corrosion and surface chemistry of metals*: CRC Press.

Lee, J. I., Otto, F. D., & Mather, A. E. (1972). Solubility of carbon dioxide in aqueous diethanolamine solutions at high pressures. *Journal of Chemical and Engineering Data, 17*(4), 465-468.

Lee., K.-L., J.,. (2004). A mechanistic modeling of carbon dioxide corrosion of mild steel in the presence of hydrogen sulfide. *Doctor of Philosophy College of Engineering and Technology of Ohio University*.

Lin, C., Kim, Y., Niedrach, L., & Ramp, K. (1996). Electrochemical corrosion potential models for boiling-water reactor applications. *Corrosion, 52*(8), 618-625.

Liu, H.-B., Zhang, C.-F., & Xu, G.-W. (1999). A study on equilibrium solubility for carbon dioxide in methyldiethanolamine-piperazine-water solution. *Industrial & Engineering Chemistry Research, 38*(10), 4032-4036.

Mandal, B., Guha, M., Biswas, A., & Bandyopadhyay, S. (2001). Removal of carbon dioxide by absorption in mixed amines: modelling of absorption in aqueous

MDEA/MEA and AMP/MEA solutions. *Chemical Engineering Science, 56*(21), 6217-6224.

Mock, B., Evans, L., & Chen, C. C. (1986). Thermodynamic representation of phase equilibria of mixed-solvent electrolyte systems. *AIChE journal, 32*(10), 1655-1664.

Mofarahi, M., Khojasteh, Y., Khaledi, H., & Farahnak, A. (2008). Design of CO_2 absorption plant for recovery of CO_2 from flue gases of gas turbine. *Energy, 33*(8), 1311-1319.

Moioli, S., & Pellegrini, L. A. (2015). Improved rate-based modeling of the process of CO_2 capture with PZ solution. *Chemical Engineering Research and Design, 93*, 611-620.

Mondal, M. K. (2009). Solubility of Carbon Dioxide in an aqueous blend of Diethanolamine and Piperazine†. *Journal of Chemical & Engineering Data, 54*(9), 2381-2385.

Mondal, M. K., Balsora, H. K., & Varshney, P. (2012). Progress and trends in CO_2 capture/separation technologies: a review. *Energy, 46*(1), 431-441.

Nainar, M., & Veawab, A. (2009). Corrosion in CO_2 capture unit using MEA-piperazine blends. *Energy Procedia, 1*(1), 231-235.

Najumudeen, A. (2012). *Development of a mechanistic corrosion model for carbon steel in MEA-based CO_2 absorption process.* (Master), University of Regina.

Nešić, S. (2007). Key issues related to modelling of internal corrosion of oil and gas pipelines–A review. *Corrosion Science, 49*(12), 4308-4338.

Nešić, S., Lee, J., & Ruzic, V. (2002). A mechanistic model of iron carbonate film growth and the effect on CO_2 corrosion of mild steel. *Corrosion/02, Paper*(02237).

Nesic, S., Nyborg, R., Stangeland, A., & Nordsveen, M. (2001). *Mechanistic Modeling for CO_2 Corrosion with Protective Iron Carbonate Films.* Paper presented at the Corrosion 2001.

Nešić, S., Postlethwaite, J., & Olsen, S. (1996). An electrochemical model for prediction of corrosion of mild steel in aqueous carbon dioxide solutions. *Corrosion, 52*(4), 280-294.

Nyborg, R. (2002). *Overview of CO_2 corrosion models for wells and pipelines.* Paper presented at the Corrosion 2002.

Poling, B. E., Prausnitz, J. M., & O'connell, J. P. (2001). *The properties of gases and liquids* (Vol. 5): McGraw-Hill New York.

Posey, M. L., & Rochelle, G. T. (1997). A thermodynamic model of methyldiethanolamine-CO2-H2S-water. *Industrial & Engineering Chemistry Research, 36*(9), 3944-3953.

Poulson, B. (1983). Electrochemical measurements in flowing solutions. *Corrosion Science, 23*(4), 391-430.

Poulson, B. (1993). Advances in understanding hydrodynamic effects on corrosion. *Corrosion Science, 35*(1), 655-665.

Renon, H., & Prausnitz, J. M. (1968). Local compositions in thermodynamic excess functions for liquid mixtures. *AIChE journal, 14*(1), 135-144.

Rinprasertmeechai, S., Chavadej, S., Rangsunvigit, P., & Kulprathipanja, S. (2012). Carbon dioxide removal from flue gas using amine-based hybrid solvent absorption. *World Academy of Science, Engineering and Technology, 64*(2012), 410-414.

Rowley, R. L., Adams, M. E., Marshall, T. L., Oscarson, J. L., Wilding, W. V., & Anderson, D. J. (1997). Measurement of diffusion coefficients important in modeling the absorption rate of carbon dioxide into aqueous N-methyldiethanolamine. *Journal of Chemical & Engineering Data, 42*(2), 310-317.

Rowley, R. L., Adams, M. E., Marshall, T. L., Oscarson, J. L., Wilding, W. V., & Anderson, D. J. (1998). Measurement of the absorption rate of carbon dioxide into aqueous diethanolamine. *Journal of Chemical & Engineering Data, 43*(3), 427-432.

Russell, M., Wortham, G., & Lawson, D. (1999). *Experiences with combined corrosion effects on stainless steel due to chlorides and* H_2S. Retrieved from

Sadegh, N. (2012). Acid Gas Removal from Natural Gas with Alkanolamines: A Modeling and Experimental Study. *Technical University of Denmark, DK-2800 Lyngby, Denmark.*

Samanta, A., & Bandyopadhyay, S. (2007). Kinetics and modeling of carbon dioxide absorption into aqueous solutions of piperazine. *Chemical Engineering Science, 62*(24), 7312-7319.

Schutt, H. U., & Lyle, F. F. (1998). CO_2/H_2S *Corrosion Under Wet Gas Pipeline Conditions in the Presence if Bicarbonate, Chloride, and Oxygen*. Paper presented at the Corrosion 98.

Sidi-Boumedine, R., Horstmann, S., Fischer, K., Provost, E., Fürst, W., & Gmehling, J. (2004). Experimental determination of carbon dioxide solubility data in aqueous alkanolamine solutions. *Fluid phase equilibria*, *218*(1), 85-94.

Smith, R., & Younger, A. (1972). *Operating experiences of Canadian diethanolamine plants*. Paper presented at the Proceedings of Gas Conditioning conference, 22nd Annual.

Snijder, E. D., te Riele, M. J., Versteeg, G. F., & Van Swaaij, W. (1993). Diffusion coefficients of several aqueous alkanolamine solutions. *Journal of Chemical and Engineering Data*, *38*(3), 475-480.

Soave, G. (1972). Equilibrium constants from a modified Redlich-Kwong equation of state. *Chemical Engineering Science, 27*(6), 1197-1203.

Soosaiprakasam, I. (2007). *Corrosion Inhibition Performance of Copper Carbonate in Carbon Dioxide Absorption Process Using Aqueous Solution of Monoethanolamine.* (Master), University of Regina.

Spencer, C. F., & Danner, R. P. (1973). Prediction of bubble-point density of mixtures. *Journal of Chemical and Engineering Data*, *18*(2), 230-234.

Tomoe, Y., & Sato, K. (1997). *Uneven distribution of metallic ions in deposits precipitated in the Koshijihara DGA CO_2 removal units*. Retrieved from

Vahidi, M., Matin, N. S., Goharrokhi, M., Jenab, M. H., Abdi, M. A., & Najibi, S. H. (2009). Correlation of CO_2 solubility in N-methyldiethanolamine+ piperazine aqueous solutions using extended Debye–Hückel model. *The Journal of Chemical Thermodynamics, 41*(11), 1272-1278.

Veawab, A. (2001). *Corrosion and corrosion control in CO_2 absorption process using aqueous amine solutions.*

Veawab, A., & Aroonwilas, A. (2002). Identification of oxidizing agents in aqueous amine–CO_2 systems using a mechanistic corrosion model. *Corrosion Science, 44*(5), 967-987.

Veawab, A., Tontiwachwuthikul, P., & Chakma, A. (1999). Corrosion behavior of carbon steel in the CO_2 absorption process using aqueous amine solutions. *Industrial & Engineering Chemistry Research, 38*(10), 3917-3924.

Vetter, K. J. (2013). *Electrochemical kinetics: theoretical aspects*: Elsevier.

Videm, K., & Dugstad, A. (1989). Corrosion of carbon steel in an aqueous carbon dioxide environment. I: solution effects. *Materials performance, 28*(3), 63-67.

Wagner, C., & Traud, W. (1938). Z. Elektrochem. angew. physik. *Chem*, *44*, 391.

Wang, S., & Nesic, S. (2003). *On coupling CO_2 corrosion and multiphase flow models.* Paper presented at the Corrosion 2003.

Wattanaphan, P. (2012). *Studies and Prevention of Carbon Steel Corrosion and Solvent Degradation During Amine-Based CO_2 Capture from Industrial Gas Streams.* (Doctor of Philosophy), University of Regina

Weiland, R. H., Dingman, J. C., Cronin, D. B., & Browning, G. J. (1998). Density and viscosity of some partially carbonated aqueous alkanolamine solutions and their blends. *Journal of Chemical & Engineering Data, 43*(3), 378-382.

Wilke, C., & Chang, P. (1955). Correlation of diffusion coefficients in dilute solutions. *AIChE journal, 1*(2), 264-270.

Williams, E., & Leckie, H. (1968). Corrosion and its prevention in a monoethanolamine gas treating plant. *MATER PROTECT, 7*(7), 21-25.

Yang, L. (2008). *Techniques for corrosion monitoring*: Elsevier.

Zhao, B., Sun, Y., Yuan, Y., Gao, J., Wang, S., Zhuo, Y., & Chen, C. (2011). Study on corrosion in CO_2 chemical absorption process using amine solution. *Energy Procedia, 4*, 93-100.

Zheng, L., Landon, J., Zou, W., & Liu, K. (2014). Corrosion Benefits of Piperazine As an Alternative CO_2 Capture Solvent. *Industrial & Engineering Chemistry Research, 53*(29), 11740-11746.

LIST OF PUBLICATIONS

Research Publication

1. Lubna Ghalib, Brahim Si Ali, Wan Mohd Ashri, Shaukat Mazari" Effect of piperazine on solubility of carbon dioxide using aqueous di-ethanolamine" Fluid Phase Equilibria (2016) 414, 1-13.
2. Lubna Ghalib, Brahim Si Ali, Shaukat Mazari ,Wan Mohd Ashri, Idris Mohamed Saeed " Effect of piperazine on CO_2 corrosion mechanism of carbon steel in activated MDEA solutions" Accepted in international journal of electrochemical science.
3. Lubna Ghalib, Brahim Si Ali, Wan Mohd Ashri, Shaukat Mazari, Idris Mohamed Saeed " Modeling the effect of Piperazine on CO_2 loading in MDEA/PZ mixture" Fluid Phase Equilibria.(under review)

Conference Publication

1. Lubna Ghalib, Brahim Si Ali, Shaukat Mazari ,Wan Mohd Ashri, Idris Mohamed Saeed" Mechanistic Model for prediction of corrosion rate in aqueous carbonated solution of activated Methyldiethanolamine" International Journal of Chemical & Environmental Engineering (IJCEE), December 2015,Volume 6, No. 6.
2. Salaheddine Kassab, Lubna Ghalib, Brahim Si Ali,Wan Mohd Ashri," Developing an Artificial neural network model to predict carbon steel's corrosion potential in carbonated solution mixture of amines" International Congress on Technology- Engineering and science, International Conference on Chemistry, Chemical & Petrochemical Engineering, At Kuala Lumpur, 13-14 FEBRUARY 2016.

APPENDIX A

MATLAB CODE

A.1 MDEA-PZ system

```
clear all
format long
clc
% program  to calculate carbon steel corrosion CO2-H2O-PZ-MDEA blend amine
% Basis:1 liter of solution
%-------------species concentration at the bulk ------------------------
%x(1)= xH2O
%x(2)= xCO2
%x(3)= xPZ
%x(4)= MDEA
%x(5)= PZH+
%x(6)= MDEAH+
%x(7)= H3O+
%x(8)= HCO3-
%x(9)= CO3-2
%x(10)= OH-
%x(11)= PZCOO-
%x(12)= PZ(COO-)2
%x(13)= H+PZCOO-
%x(14)= Fe2+
%------------------------input condition to evaluate model----------------
T=353.15;
molmdea=1.8;
molpz=0.1;
Pco2=100;
%------------- physical properties [ H2O CO2 PZ MDEA]----------
R=8.314;
Tc=[647.3 304.2 638.0 677];
Pc=[22048 7376 6870 3880];
Vc=[0.0559 0.0939  0.23 0.3932];
mwt=[18.02 86.13 119.16];
w=[0.344 0.225 0.8 1.242];
zra=[0.2432 0.20 0.192];
%---------Renormalize mole fractions  in the solution ----------
molamine=2*molpz + molmdea;
molh2o=55.5;
mol=[molh2o molpz molmdea];
totmol=molh2o+molpz+molmdea;
xtot=mol./totmol;
mass=mol.*mwt;
totmass=sum(mass);
wtfr=mass./totmass
totmwt=sum(xtot.*mwt);
%----------Rackett equation modified calculate molar volume of mixed solvent-
Pcs=Pc(:,[1,3,4]);
```

```
Tcs=Tc(:,[1,3,4]) ;
Vcs=Vc(:,[1,3,4]);
zram=sum(xtot.*zra);
Vcsm=sum(xtot.*Vcs);
O=(xtot.*Vcs)/Vcsm;
Tcsm=sum(O.*Tcs);
Trsm=T/Tcsm;
Vsm= R*sum(xtot.*(Tcs./Pcs))*zram.^(1+(1-Trsm)^(2/7));
ds=totmwt/Vsm;
%-------------calculate mixed solvent Dielectric constant -----------------
Ds(1)=88.36+33030*(inv(T)-inv(273.15));
Ds(2)=4.253+1532.2*(inv(T)-inv(298.15));
Ds(3)=24.76+8989*(inv(T)-inv(273.15));
Dm=sum(Ds.*(xtot.*mwt)/totmwt);
%------------- Antoine equation ---------------------------------
VP(1)=exp(72.55-7206.7/T-7.1385*log(T)+4.05e-06*T^2)/1000;
VP(2)=exp(72.82912-3403.28/T+9.49e-03*T-8.56*log(T)+2.91e-16*T^6)/1000;
VP(3)=exp(70.503-7914.5/T -6.6461*log(T)+5.21e-18*T^6)/1000;
VP(4)=exp(26.137-7588.5/T)/1000;
%----- equilibrium constant as function of Temperature based on mole fraction -----------
-------
k1=exp(132.899-(13445.9/T)-(22.477*log(T)));
k2=exp(231.465-(12092.1/T)-(36.782*log(T)));
k3=exp(216.049-(12431.7/T)-(35.482*log(T)));
k4=exp(-9.6416-(5008.4/T);
k5=exp(466.497+(1614.5/T)-(97.540*log(T))+0.2471*T);
k6=exp(6.822-(6066.9/T)-(2.290*log(T))+0.0036*T);
k7=exp(-11.563+(1769.4/T)-(1.467*log(T))+0.0024*T);
k8=exp(-83.490-(819.7/T)+10.9756*log(T));
Hco2=inv(1000)*exp(170.7126-8477.711/T-21.95743*log(T)+0.005781*T);
%----------------enter initial guess for equilibrium mole fraction at the bulk
x(1)=xtot(1);
x(2)=Pco2/Hco2;
Af=k6;
Bf=(k6*xtot(3) + k6*xtot(2) + k4*k6*x(1) + k6*k8*x(1) + k4*k5*x(1)*x(2));
Cf=(k4*k6*x(1)*xtot(3) - k1*k6*x(1)^2 + k6*k8*x(1)*xtot(2) + k4*k6*k8*x(1)^2 -
k2*k6*x(1)^2*x(2) + k4*k5*x(1)*x(2)*xtot(3) + k4*k5*k6*x(1)^2*x(2) +
k4*k5*k8*x(1)^2*x(2));
Df=(k4*k5*k6*k8*x(1)^3*x(2) - k1*k6*k8*x(1)^3 - k2*k4*k5*x(1)^3*x(2)^2 -
k1*k4*k5*x(1)^3*x(2) - 2*k2*k3*k6*x(1)^3*x(2) - k2*k4*k6*x(1)^3*x(2) -
k2*k6*k8*x(1)^3*x(2) - k1*k4*k6*x(1)^3 + k4*k5*k6*x(1)^2*x(2)*xtot(3) -
k4*k5*k6*x(1)^2*x(2)*xtot(2) + k4*k5*k6*k7*x(1)^3*x(2)^2);
Ef=(k4*k5*k6*k7*k8*x(1)^4*x(2)^2 - 2*k2*k3*k4*k6*x(1)^4*x(2) -
k1*k4*k5*k6*x(1)^4*x(2) - k1*k4*k5*k8*x(1)^4*x(2) - 2*k2*k3*k6*k8*x(1)^4*x(2)
- k2*k4*k6*k8*x(1)^4*x(2) - 2*k2*k3*k4*k5*x(1)^4*x(2)^2 -
k2*k4*k5*k6*x(1)^4*x(2)^2 - k2*k4*k5*k8*x(1)^4*x(2)^2 - k1*k4*k6*k8*x(1)^4 +
k4*k5*k6*k7*x(1)^3*x(2)^2*xtot(3) - 2*k4*k5*k6*k7*x(1)^3*x(2)^2*xtot(2) -
k4*k5*k6*k8*x(1)^3*x(2)*xtot(2)) ;
Ff=(- 2*k2*k3*k4*k5*k6*x(1)^5*x(2)^2 - 2*k2*k3*k4*k5*k8*x(1)^5*x(2)^2 -
k1*k4*k5*k6*k7*x(1)^5*x(2)^2 - k2*k4*k5*k6*k7*x(1)^5*x(2)^3 -
```

```
k2*k4*k5*k6*k8*x(1)^5*x(2)^2 - 2*k2*k3*k4*k6*k8*x(1)^5*x(2) -
k1*k4*k5*k6*k8*x(1)^5*x(2) - 2*k4*k5*k6*k7*k8*x(1)^4*x(2)^2*xtot(2)) ;
Gf=(- 2*k2*k3*k4*k5*k6*k7*x(1)^6*x(2)^3 - 2*k2*k3*k4*k5*k6*k8*x(1)^6*x(2)^2
- k1*k4*k5*k6*k7*k8*x(1)^6*x(2)^2 - k2*k4*k5*k6*k7*k8*x(1)^6*x(2)^3);
Hf=- 2*k2*k3*k4*k5*k6*k7*k8*x(1)^7*x(2)^3;


fun=[Af Bf Cf Df Ef Ff Gf Hf];
sol=roots(fun);
x(7)=max(sol(find(imag(sol)==0 & sol > 0)));
x(10)=k1*x(1)^2/x(7);
x(8)=k2*x(2)*x(1)^2/x(7);
x(9)=k3*x(8)*x(1)/x(7);
x(3)=xtot(2)/((k5*x(2))/k6 + x(7)/(k4*x(1)) + (k5*x(1)*x(2))/x(7) +
(k5*k7*x(1)^2*x(2)^2)/x(7)^2 + 1);
x(5)=x(3)*x(7)/(k4*x(1));
x(11)=k5*x(3)*x(2)*x(1)/x(7);
x(13)=x(11)*x(7)/(k6*x(1));
x(12)=k7*x(11)*x(2)*x(1)/x(7);
x(4)=(k8*x(1)*xtot(3))/(x(7) + k8*x(1));
x(6)=x(4)*x(7)/(k8*x(1));

err=1 ;
while err>0.00000001;
%--------------Gamma for Pitzer-Debye-Huckell and Born correction -----------------------
-
% charge species  [H2O;CO2;PZ;MDEA ;PZH+ MDEAH+ ; H3O+; HCO3-;CO3-2 ;
OH- ;PZCOO-;PZ(COO-)2;H+PZCOO-]
z=[0,0,0,0,1,1,1,-1,-2,-1,-1,-2,0] ;
e0=8.854e-12 ;
Na = 6.0221415e23;
rho=14.9  ;
Qe=-1.602e-19;
kb=1.38e-23 ;
ra = 3e-10*ones(1,size(z,2));
Ix=0.5*sum(x.*z.^2);
A_phi=1/3*(2*pi*Na*ds/totmwt*1000)^0.5*(Qe^2/(4*pi)/e0/Dm/kb/T)^1.5;
lnGamma_PDH=-A_phi*(2*z'.^2/rho*log(1+rho*Ix^0.5)+(z'.^2*Ix^0.5-
2*Ix^1.5)/(1+rho*Ix^0.5));
lnGamma_Born=Qe^2/2/kb/T*(1/Dm-1/Ds(1))*(z.^2./ra)'*10^-2  ;
lnGammaLR=lnGamma_PDH+lnGamma_Born ;
%--------------calculate activity coefficient term e-NRTL ------------
mca=[sum(z==0);sum(z>0);sum(z<0)];
    m=(z==0).*(1:size(z,2)) ;
        m=m(m~=0);
    c=(z>0).*(1:size(z,2));
        c=c(c~=0);
    a=(z<0).*(1:size(z,2));
        a=a(a~=0);
 Cj=[1;1;1;1;1;1;1;1;2;1;1;2;1] ;
  Xj=x'.*Cj;
```

```
  cTotal=sum(Xj(c));
  aTotal=sum(Xj(a));
  alpha1=0.2 ;
  alpha3=0.1;
  alpha_AM=[0.2*ones(mca(3),1),0.1*ones(mca(3),mca(1)-1)];
  alpha_CM=[0.2*ones(mca(2),1),0.1*ones(mca(2),mca(1)-1)];
  alpha_CAM=[0.2*ones(mca(2)*mca(3),1),0.1*ones(mca(2)*mca(3),mca(1)-1
  tau_CAM=[ones(mca(2)*mca(3),1)*-4,ones(mca(2)*mca(3),1)*-
8,ones(mca(2)*mca(3),mca(1)-2)*-2];

tau_MCA=[ones(mca(2)*mca(3),1)*8,ones(mca(2)*mca(3),1)*15,ones(mca(2)*mca(3),
mca(1)-2)*10];
  tau_MM=zeros(mca(1),mca(1));
  G_MM=exp(-alpha1*tau_MM);
  G_CAM=exp(-alpha_CAM.*tau_CAM);
  G_MCA=exp(-alpha_CAM.*tau_MCA);
  tauCprimeA_CA=zeros(mca(2),mca(2)*mca(3));
  tauCAprime_CA=zeros(mca(3),mca(2)*mca(3));
  GCprimeA_CA=exp(-alpha3*tauCprimeA_CA);
  GCAprime_CA=exp(-alpha3*tauCAprime_CA);
  temp1c=(Xj(c)*ones(1,mca(3)))';
  PsudoI_1=repmat(eye(mca(3),mca(3)),1,mca(2));
  c_sparse=(ones(mca(3),1)*temp1c(1:mca(2)*mca(3))).*PsudoI_1;
  temp1a=ones(mca(3),1)*(1:mca(2)) ;
  temp2a=temp1a(1:mca(2)*mca(3))+(0:mca(2):(mca(2)*mca(3)-1)*mca(2));
  temp1a=zeros(mca(2),mca(2)*mca(3));
  temp1a(temp2a)=1;
  PsudoI_2=temp1a;
  a_sparse=repmat(Xj(a)',mca(2),mca(2)).*PsudoI_2;
  PsudoI_3=repmat(eye(mca(2),mca(2)),mca(1),1);
  temp1m=ones(mca(2),1)*Xj(m)';
  temp2m=zeros(mca(1)*mca(2),1);
  temp2m(1:end)=temp1m(1:end);
  m_sparse1=(temp2m*ones(1,mca(2))).*PsudoI_3;
m_sparse2=repmat(eye(mca(3),mca(3)),1,mca(1)).*(ones(mca(3),1)*reshape(ones(mca(
3),1)*Xj(m)',1,mca(1)*mca(3)));
  temp1=ones(mca(1),1)*(1:mca(2));
  temp2=temp1(1:mca(2)*mca(1))+(0:mca(2):(mca(2)*mca(1)-1)*mca(2));
  temp1=zeros(mca(2),mca(2)*mca(1));
  temp1(temp2)=1;
  PsudoI_5=temp1;
  m_sparse3=PsudoI_5.*repmat(Xj(m)',mca(2),mca(2));

 G_AM=(c_sparse*G_CAM)/cTotal;
 G_CM=(a_sparse*G_CAM)/aTotal;
 tau_AM=-log(G_AM)./alpha_AM;
 tau_CM=-log(G_CM)./alpha_CM;
 MC_ACtemp1=reshape(tau_MCA,mca(3),mca(1)*mca(2));
 MC_ACtemp2=reshape(tau_CAM,mca(3),mca(1)*mca(2));
 tauMC_AC=ones(mca(3),1)*tau_CM(1:end)-MC_ACtemp2+MC_ACtemp1;
 AM_ACtemp1=repmat(tau_AM,mca(2),1)-tau_CAM+tau_MCA;
```

```
 AM_ACtemp2=AM_ACtemp1;
 tauAM_AC=reshape(AM_ACtemp2,mca(2),mca(1)*mca(3));
 GMC_AC=exp(-alpha3*tauMC_AC);
 GAM_AC=exp(-alpha3*tauAM_AC);
  lnGammaInfinity=zeros(sum(mca),1);
  lnGammaSym=zeros(sum(mca),1);
GtOverG_1=(Xj(m)'*(tau_MM.*G_MM)+Xj(a)'*(tau_AM.*G_AM)+Xj(c)'*(tau_CM.*
G_CM))./(Xj(m)'*G_MM+Xj(a)'*G_AM+Xj(c)'*G_CM);
GtOverG_2=((GCAprime_CA.*tauCAprime_CA)*a_sparse'+(tauMC_AC.*GMC_AC)
*m_sparse1)./(GCAprime_CA*a_sparse'+cTotal+GMC_AC*m_sparse1);
  GtOverG_2ca= reshape(repmat(GtOverG_2,mca(3),1),mca(3),mca(3)*mca(2));
GtOverG_3=((c_sparse*(GCprimeA_CA.*tauCprimeA_CA)'+m_sparse2*(tauAM_AC.
*GAM_AC)')./(c_sparse*GCprimeA_CA'+aTotal+m_sparse2*GAM_AC'))';
  M_term1=GtOverG_1;
  M_term2=((G_MM.*(tau_MM-
ones(mca(1),1)*GtOverG_1))*(Xj(m)./((Xj(m)'*G_MM+Xj(a)'*G_AM+Xj(c)'*G_CM)'
)))';
   temp1mc=ones(mca(2),1)*(1:mca(1));
    temp2mc=temp1mc(1:mca(1)*mca(2))+(0:mca(1):(mca(1)*mca(2)-1)*mca(1));
    temp1mc=zeros(mca(1),mca(1)*mca(2));
    temp1mc(temp2mc)=1 ;
    PsudoI_4=temp1mc;
M_term3=sum((((Xj(a)/aTotal)*ones(1,mca(1)*mca(2))).*(repmat(Xj(c)',mca(3),mca(1
)).*GMC_AC)./(repmat(GCAprime_CA*a_sparse'+cTotal+GMC_AC*m_sparse1,1,mc
a(1))).*(tauMC_AC-repmat(GtOverG_2,1,mca(1))))*PsudoI_4',1) ;
    temp1ma=ones(mca(3),1)*(1:mca(1)) ;
    temp2ma=temp1ma(1:mca(1)*mca(3))+(0:mca(1):(mca(1)*mca(3)-1)*mca(1));
    temp1ma=zeros(mca(1),mca(1)*mca(3)) ;
    temp1ma(temp2ma)=1;
    PsudoI_6=temp1ma;
M_term4=sum((((Xj(c)/cTotal)*ones(1,mca(1)*mca(3))).*(repmat(Xj(a)',mca(2),mca(1
)).*GAM_AC)./repmat(GAM_AC*m_sparse2'+GCprimeA_CA*c_sparse'+aTotal,1,mc
a(1)).*(tauAM_AC-repmat(GtOverG_3,1,mca(1))))*PsudoI_6',1);
  lnGammaInfinity(m)=(tau_MM(1,:)+G_MM(1,:).*tau_MM(1,:))';
C_term1=Xj(a)'*(((GCAprime_CA.*tauCAprime_CA)*a_sparse'+(GMC_AC.*tauMC_
AC)*m_sparse1)./(GCAprime_CA*a_sparse'+cTotal+GMC_AC*m_sparse1))/aTotal;
C_term2=sum((ones(mca(2),1)*(Xj(m)'./(Xj(m)'*G_MM+Xj(a)'*G_AM+Xj(c)'*G_CM
))).*(G_CM.*(tau_CM-ones(mca(2),1)*GtOverG_1)),2)';
  C_term4=Xj(a)'*reshape((Xj(c)'*(GCprimeA_CA.*(tauCprimeA_CA-
repmat(GtOverG_3,1,mca(2)))./repmat((c_sparse*GCprimeA_CA'+aTotal+m_sparse2*
GAM_AC')',1,mca(2))))',mca(3),mca(2))/cTotal ;
  temp1cc=reshape(Xj(a)'*tauMC_AC,mca(2),mca(1))/aTotal+tau_CM.*G_CM ;
  lnGammaInfinity(c)=temp1cc(:,1);
   clear temp1 ;
  for i=1:mca(2);
    temp1(:,i)=(i:mca(2):mca(2)*mca(3)-mca(2)+i)' ;
  end
Ind_Vector1=reshape(reshape(temp1,mca(2)*mca(3),1)*ones(1,mca(1))+ones(mca(2)*
mca(3),1)*(0:mca(2)*mca(3):mca(2)*mca(3)*(mca(1)-1)),mca(2)*mca(3)*mca(1),1);
```

```
 Atemp6=zeros(mca(2)*mca(3),1) ;
Atemp6(Ind_Vector1(1:mca(2)*mca(3)))=GCAprime_CA*a_sparse'+cTotal+GMC_AC
*m_sparse3';
 Atemp7=reshape((Atemp6*ones(1,mca(3)))',mca(2)*mca(3),mca(3))';
 A_term1=Xj(c)'*GtOverG_3/cTotal;
 A_term2=sum((G_AM.*(tau_AM-
ones(mca(3),1)*GtOverG_1)).*(ones(mca(3),1)*(Xj(m)'./(Xj(m)'*G_MM+Xj(a)'*G_A
M+Xj(c)'*G_CM))),2)';
 A_term4= Xj(c)'*(reshape(((GCAprime_CA.*(tauCAprime_CA-
GtOverG_2ca))./Atemp7)'*Xj(a),mca(3),mca(2))/aTotal)';
lnGammaInfinity(a)=(Xj(c)'*tauAM_AC(:,1:mca(3))/cTotal)'+(tau_AM(:,1).*G_AM(:,
1));
lnGammaSym(m)=M_term1+M_term2+M_term3+M_term4 ;
lnGammaSym(c)=C_term1+C_term2+C_term4;
lnGammaSym(a)=A_term1+A_term2+A_term4;
lnGammaSR=((z+(z==0))'.*(lnGammaSym-lnGammaInfinity)+lnGammaLR) ;
Gamma=exp(lnGammaSR);
g=Gamma;
% ----------- calculate truly values of mole fraction ------------------------
Anew=(g(10)*g(11)*g(12)*g(13)*g(3)*g(4)*g(7)^6*g(8)*g(9)*k6);
Bnew=(g(10)*g(11)*g(12)*g(13)*g(3)*g(4)*g(7)^6*g(8)*g(9)*k6*xtot(3) +
g(10)*g(11)*g(12)*g(13)*g(3)*g(4)*g(7)^6*g(8)*g(9)*k6*xtot(2) +
g(1)*g(10)*g(11)*g(12)*g(13)*g(4)*g(5)*g(7)^5*g(8)*g(9)*k4*k6*x(1) +
g(1)*g(10)*g(11)*g(12)*g(13)*g(3)*g(6)*g(7)^5*g(8)*g(9)*k6*k8*x(1) +
g(1)*g(10)*g(11)*g(12)*g(2)*g(3)*g(4)*g(5)*g(7)^5*g(8)*g(9)*k4*k5*x(1)*x(2));
Cnew=(g(1)^2*g(10)*g(11)*g(12)*g(13)*g(5)*g(6)*g(7)^4*g(8)*g(9)*k4*k6*k8*x(1)
^2 - g(1)^2*g(11)*g(12)*g(13)*g(3)*g(4)*g(7)^5*g(8)*g(9)*k1*k6*x(1)^2 -
g(1)^2*g(10)*g(11)*g(12)*g(13)*g(2)*g(3)*g(4)*g(7)^5*g(9)*k2*k6*x(1)^2*x(2) +
g(1)*g(10)*g(11)*g(12)*g(13)*g(4)*g(5)*g(7)^5*g(8)*g(9)*k4*k6*x(1)*xtot(3) +
g(1)*g(10)*g(11)*g(12)*g(13)*g(3)*g(6)*g(7)^5*g(8)*g(9)*k6*k8*x(1)*xtot(2) +
g(1)^2*g(10)*g(12)*g(13)*g(2)*g(3)*g(4)*g(5)*g(7)^4*g(8)*g(9)*k4*k5*k6*x(1)^2*x
(2) +
g(1)^2*g(10)*g(11)*g(12)*g(2)*g(3)*g(5)*g(6)*g(7)^4*g(8)*g(9)*k4*k5*k8*x(1)^2*x
(2) +
g(1)*g(10)*g(11)*g(12)*g(2)*g(3)*g(4)*g(5)*g(7)^5*g(8)*g(9)*k4*k5*x(1)*x(2)*xtot
(3));
Dnew=(g(1)^3*g(10)*g(11)*g(13)*g(2)^2*g(3)*g(4)*g(5)*g(7)^3*g(8)*g(9)*k4*k5*k
6*k7*x(1)^3*x(2)^2 -
g(1)^3*g(11)*g(12)*g(13)*g(3)*g(6)*g(7)^4*g(8)*g(9)*k1*k6*k8*x(1)^3 -
g(1)^3*g(10)*g(11)*g(12)*g(2)^2*g(3)*g(4)*g(5)*g(7)^4*g(9)*k2*k4*k5*x(1)^3*x(2)
^2 -
2*g(1)^3*g(10)*g(11)*g(12)*g(13)*g(2)*g(3)*g(4)*g(7)^4*g(8)*k2*k3*k6*x(1)^3*x(
2) -
g(1)^3*g(10)*g(11)*g(12)*g(13)*g(2)*g(4)*g(5)*g(7)^4*g(9)*k2*k4*k6*x(1)^3*x(2)
-
g(1)^3*g(10)*g(11)*g(12)*g(13)*g(2)*g(3)*g(6)*g(7)^4*g(9)*k2*k6*k8*x(1)^3*x(2)
- g(1)^3*g(11)*g(12)*g(2)*g(3)*g(4)*g(5)*g(7)^4*g(8)*g(9)*k1*k4*k5*x(1)^3*x(2) -
g(1)^3*g(11)*g(12)*g(13)*g(4)*g(5)*g(7)^4*g(8)*g(9)*k1*k4*k6*x(1)^3 +
g(1)^3*g(10)*g(12)*g(13)*g(2)*g(3)*g(5)*g(6)*g(7)^3*g(8)*g(9)*k4*k5*k6*k8*x(1)^
3*x(2) +
g(1)^2*g(10)*g(12)*g(13)*g(2)*g(3)*g(4)*g(5)*g(7)^4*g(8)*g(9)*k4*k5*k6*x(1)^2*x
```

```
(2)*xtot(3) -
g(1)^2*g(10)*g(12)*g(13)*g(2)*g(3)*g(4)*g(5)*g(7)^4*g(8)*g(9)*k4*k5*k6*x(1)^2*x
(2)*xtot(2));
Enew=(g(1)^4*g(10)*g(11)*g(13)*g(2)^2*g(3)*g(5)*g(6)*g(7)^2*g(8)*g(9)*k4*k5*k6
*k7*k8*x(1)^4*x(2)^2 -
2*g(1)^4*g(10)*g(11)*g(12)*g(13)*g(2)*g(4)*g(5)*g(7)^3*g(8)*k2*k3*k4*k6*x(1)^4
*x(2) -
2*g(1)^4*g(10)*g(11)*g(12)*g(13)*g(2)*g(3)*g(6)*g(7)^3*g(8)*k2*k3*k6*k8*x(1)^4
*x(2) -
g(1)^4*g(10)*g(11)*g(12)*g(13)*g(2)*g(5)*g(6)*g(7)^3*g(9)*k2*k4*k6*k8*x(1)^4*x
(2) -
g(1)^4*g(12)*g(13)*g(2)*g(3)*g(4)*g(5)*g(7)^3*g(8)*g(9)*k1*k4*k5*k6*x(1)^4*x(2)
-
g(1)^4*g(11)*g(12)*g(2)*g(3)*g(5)*g(6)*g(7)^3*g(8)*g(9)*k1*k4*k5*k8*x(1)^4*x(2)
-
2*g(1)^4*g(10)*g(11)*g(12)*g(2)^2*g(3)*g(4)*g(5)*g(7)^3*g(8)*k2*k3*k4*k5*x(1)^
4*x(2)^2 -
g(1)^4*g(10)*g(12)*g(13)*g(2)^2*g(3)*g(4)*g(5)*g(7)^3*g(9)*k2*k4*k5*k6*x(1)^4*
x(2)^2 -
g(1)^4*g(10)*g(11)*g(12)*g(2)^2*g(3)*g(5)*g(6)*g(7)^3*g(9)*k2*k4*k5*k8*x(1)^4*
x(2)^2 -
g(1)^3*g(10)*g(12)*g(13)*g(2)*g(3)*g(5)*g(6)*g(7)^3*g(8)*g(9)*k4*k5*k6*k8*x(1)^
3*x(2)*xtot(2) -
g(1)^4*g(11)*g(12)*g(13)*g(5)*g(6)*g(7)^3*g(8)*g(9)*k1*k4*k6*k8*x(1)^4 +
g(1)^3*g(10)*g(11)*g(13)*g(2)^2*g(3)*g(4)*g(5)*g(7)^3*g(8)*g(9)*k4*k5*k6*k7*x(
1)^3*x(2)^2*xtot(3) -
2*g(1)^3*g(10)*g(11)*g(13)*g(2)^2*g(3)*g(4)*g(5)*g(7)^3*g(8)*g(9)*k4*k5*k6*k7*
x(1)^3*x(2)^2*xtot(2));
Fnew=(-
2*g(1)^5*g(10)*g(12)*g(13)*g(2)^2*g(3)*g(4)*g(5)*g(7)^2*g(8)*k2*k3*k4*k5*k6*x(
1)^5*x(2)^2 -
2*g(1)^5*g(10)*g(11)*g(12)*g(2)^2*g(3)*g(5)*g(6)*g(7)^2*g(8)*k2*k3*k4*k5*k8*x(
1)^5*x(2)^2 -
g(1)^5*g(10)*g(11)*g(13)*g(2)^3*g(3)*g(4)*g(5)*g(7)^2*g(9)*k2*k4*k5*k6*k7*x(1)
^5*x(2)^3 -
g(1)^5*g(10)*g(12)*g(13)*g(2)^2*g(3)*g(5)*g(6)*g(7)^2*g(9)*k2*k4*k5*k6*k8*x(1)
^5*x(2)^2 -
g(1)^5*g(11)*g(13)*g(2)^2*g(3)*g(4)*g(5)*g(7)^2*g(8)*g(9)*k1*k4*k5*k6*k7*x(1)^
5*x(2)^2 -
2*g(1)^5*g(10)*g(11)*g(12)*g(13)*g(2)*g(5)*g(6)*g(7)^2*g(8)*k2*k3*k4*k6*k8*x(1
)^5*x(2) -
g(1)^5*g(12)*g(13)*g(2)*g(3)*g(5)*g(6)*g(7)^2*g(8)*g(9)*k1*k4*k5*k6*k8*x(1)^5*
x(2) -
2*g(1)^4*g(10)*g(11)*g(13)*g(2)^2*g(3)*g(5)*g(6)*g(7)^2*g(8)*g(9)*k4*k5*k6*k7*
k8*x(1)^4*x(2)^2*xtot(2));
Gnew=(-
2*g(1)^6*g(10)*g(11)*g(13)*g(2)^3*g(3)*g(4)*g(5)*g(7)*g(8)*k2*k3*k4*k5*k6*k7*
x(1)^6*x(2)^3 -
2*g(1)^6*g(10)*g(12)*g(13)*g(2)^2*g(3)*g(5)*g(6)*g(7)*g(8)*k2*k3*k4*k5*k6*k8*
x(1)^6*x(2)^2 -
g(1)^6*g(10)*g(11)*g(13)*g(2)^3*g(3)*g(5)*g(6)*g(7)*g(9)*k2*k4*k5*k6*k7*k8*x(1
```

```
)^6*x(2)^3 -
g(1)^6*g(11)*g(13)*g(2)^2*g(3)*g(5)*g(6)*g(7)*g(8)*g(9)*k1*k4*k5*k6*k7*k8*x(1)
^6*x(2)^2);
Hnew=-
2*g(1)^7*g(10)*g(11)*g(13)*g(2)^3*g(3)*g(5)*g(6)*g(8)*k2*k3*k4*k5*k6*k7*k8*x(
1)^7*x(2)^3;

funnew=[Anew Bnew Cnew Dnew Enew Fnew Gnew Hnew];
solnew=roots(funnew);
xnew(7)=max(solnew(find(imag(solnew) == 0)));
xnew(2)=Pco2/(Hco2);
xnew(1)=1-(x(2)+x(3)+x(4)+x(5)+x(6)+x(7)+x(8)+x(9)+x(10)+x(11)+x(12)+x(13));
xnew(10)=k1*(xnew(1)*g(1))^2/(g(7)*xnew(7)*g(10));
xnew(8)=k2*xnew(2)*g(2)*(xnew(1)*g(1))^2/(xnew(7)*g(7)*g(8));
xnew(9)=k3*xnew(8)*g(8)*xnew(1)*g(1)/(g(7)*xnew(7)*g(9));
xnew(3)=xtot(2)/((g(2)*g(3)*k5*xnew(2))/(g(13)*k6) +
(g(3)*g(7)*xnew(7))/(g(1)*g(5)*k4*xnew(1)) +
(g(1)*g(2)*g(3)*k5*xnew(1)*xnew(2))/(g(11)*g(7)*xnew(7)) +
(g(1)^2*g(2)^2*g(3)*k5*k7*xnew(1)^2*xnew(2)^2)/(g(12)*g(7)^2*xnew(7)^2) + 1);
xnew(5)=xnew(3)*g(3)*xnew(7)*g(7)/(k4*xnew(1)*g(1)*g(5));
xnew(11)=k5*xnew(3)*g(3)*xnew(2)*g(2)*xnew(1)*g(1)/(xnew(7)*g(7)*g(11));
xnew(13)=xnew(11)*g(11)*xnew(7)*g(7)/(k6*xnew(1)*g(1)*g(13));
xnew(12)=k7*xnew(11)*g(11)*x(2)*g(2)*xnew(1)*g(1)/(xnew(7)*g(7)*g(12));
xnew(4)=(g(1)*g(6)*k8*xnew(1)*xtot(3))/(g(4)*g(7)*xnew(7) +
g(1)*g(6)*k8*xnew(1));
xnew(6)=xnew(4)*g(4)*xnew(7)*g(7)/(k8*xnew(1)*g(1)*g(6));
err=max(abs((xnew-x)/xnew));
x=xnew;
end
Alk=(x(2)+x(8)+x(9)+x(11)+2*x(12)+x(13))*totmol/molamine
con=x.*totmol;
PH=-log10(con(7))
%----------------- Faraday constant----------------
Fa=96485;
%-----------standard Gibbs free energy of reaction at T(K) (kJ/mole)
Gro(1)=T*((0/298)+0*(inv(T)-inv(298)));
Gro(2)=T*((118/298)+29.8*(inv(T)-inv(298)));
Gro(3)=T*((159.8/298)+111.6*(inv(T)-inv(298)));
Gro(4)=T*((111.09/298)+ 85.78*(inv(T)-inv(298)));
Gro(5)=T*((98.4614/298)+73.8574*(inv(T)-inv(298)));
Gro(6)=T*((91.53/298)+89.1*(inv(T)-inv(298)));
%-----standard electrode potential at T(K)(J/C=V) SCE -------------
Eo(1)=(-Gro(1)*1000/(2*Fa))-0.244;
Eo(2)=(-Gro(2)*1000/(2*Fa))-0.244;-
Eo(3)=(-Gro(3)*1000/(2*Fa))-0.244;
Eo(4)=(-Gro(4)*1000/(2*Fa))-0.244;
Eo(5)=(-Gro(5)*1000/(2*Fa))-0.244;
Eo(6)=(-Gro(6)*1000/(2*Fa))-0.244;
%---------------- parameters ---------------------
MFe=55.845;
dFe=7874;
```

```
MFeco3=115.8;
dFeco3=3960;
rpm=600*0.104719755;c
dia=0.005;
Ve=rpm*dia/2;
%------ Viscosity of solution at T -----------
Vir_H2O=1.002e-3;
Vi_H2O=Vir_H2O*10^((1.3272*(293.15-T)-0.001053*(293.15-T)^2)/(T+105));%H2O
at T
Vir=Vir_H2O*(((-
0.1944*wtpr(2)+0.4315)*298.15+(80.684*wtpr(2)+2889.1))*(Alk*(0.0106*wtpr(2)+0*
298.15-0.2141)+1)*wtpr(2))/298.15^2;
Vi=Vi_H2O*(((-
0.1944*wtpr(2)+0.4315)*T+(80.684*wtpr(2)+2889.1))*(Alk*(0.0106*wtpr(2)+0*T-
0.2141)+1)*wtpr(2))/T^2;
Re=ds*Ve*dia/Vi;
%----- initial concentration of Fe+2 in the bulk of solution -------
Imm=0.5*sum(con.*z.^2);
Ksp=10^(-59.3498-0.041377*T-2.1963/T+24.5724*log10(T)+2.518*(Imm)^0.5-
0.657*(Imm));
Iron=Ksp/con(9) ;
totmol2=totmol+Iron;
U=x.*totmol2;
U(14)=Iron;
%-----Diffusivity of species at any T m2/s ----------
Di(1)=9.31e-9*(T/298.15)*(Vir/Vi);
Di(2)=1.11e-9*(T/298.15)*(Vir/Vi);
Di(3)=1.0e-9*(T/298.15)*(Vir/Vi);
Di(4)=exp(-13.672-2160.9/T-19.263e-5*U(5));
Di(5)=exp(-13.088+2360.7/T-24.727e-5*U(6));
Di(6)=7.2e-10*(T/298.15)*(Vir/Vi);
%----- mass transfer coefficients  (m/sec)-----------
km(1)=0.0791*Re^0.7*(Vi/(ds))^0.356*Di(1)^0.644/dia;
km(2)=0.0791*Re^0.7*(Vi/(ds))^0.356*Di(2)^0.644/dia;
km(3)=0.0791*Re^0.7*(Vi/(ds))^0.356*Di(3)^0.644/dia;
km(4)=0.0791*Re^0.7*(Vi/(ds))^0.356*Di(4)^0.644/dia;
km(5)=0.0791*Re^0.7*(Vi/(ds))^0.356*Di(5)^0.644/dia;
km(6)=0.0791*Re^0.7*(Vi/(ds))^0.356*Di(6)^0.644/dia;
%--------reversible electrode potential at any conc.(J/C=V)-------
Erev(1)=Eo(1)-((R*T)/(2*Fa))*log((U(1))^2/(U(7))^2);
Erev(2)=Eo(2)-((R*T)/(2*Fa))*log((U(9))^2/(U(8))^2);
Erev(3)=Eo(3)-((R*T)/(2*Fa))*log((U(10))^2/(U(1))^2);
Erev(4)=Eo(4)-((R*T)/(2*Fa))*log((U(3))^2/(U(5))^2);
Erev(5)=Eo(5)-((R*T)/(2*Fa))*log((U(4))^2/(U(6))^2);
Erev(6)=Eo(6)-((R*T)/(2*Fa))*log(1/(U(14)));
%---- limiting current density (diffusion current) (A/m2) --------
Ilim(1)=2e+3*Fa*km(1)*U(7);
Ilim(2)=2e+3*Fa*km(2)*U(8);
Ilim(3)=2e+3*Fa*km(3)*U(1);
Ilim(4)=2e+3*Fa*km(4)*U(5) ;
Ilim(5)=2e+3*Fa*km(5)*U(6) ;
```

```
Ilim(6)=2e+3*Fa*km(6)*U(14);
%---------exchange current density ( A/m^2)  ---------------
Io(1)=0.05*sqrt(U(7)/1e-4)*exp((-30000/R)*(1/T-1/298.15));
Io(2)=0.15*sqrt(U(8)/0.5)*exp((-50000/R)*(1/T-1/323.15));
Io(3)=3e-5*sqrt(U(1)/55.5)*exp((-30000/R)*(1/T-1/293.15));
Io(4)=0.15*(U(5)/0.63)*exp((-20000/R)*(1/T-1/323.15));
Io(5)=0.15*(U(6)/0.63)*exp((-20000/R)*(1/T-1/323.15));
Io(6)=0.53*sqrt(10^-9.1/U(7))*(U(8))^2*exp((-40000/R)*(1/T-1/323.15));
%--------------Tafel slope-------------------------
beta_ox=(R*T)/((0.0025*T - 0.3829)*Fa);
beta=(R*T)/((0.005*T - 1.165)*Fa);
%---------Calculate Ecorr & Icorr ----------------
Iex=-1 ;
Eapp=min(Erev);
while Iex <= 1e-6
    Eapp=Eapp+0.00001;
%---- Activation + Concentration polarization A/m^2 ---------------
Ic(1)=inv(inv((Io(1)*exp(-(Eapp-Erev(1))/beta)))+inv(Ilim(1)));
Ic(2)=inv(inv((Io(2)*exp(-(Eapp-Erev(2))/beta)))+inv(Ilim(2)));
Ic(3)=inv(inv((Io(3)*exp(-(Eapp-Erev(3))/beta)))+inv(Ilim(3)));
Ic(4)=inv(inv((Io(4)*exp(-(Eapp-Erev(4))/beta)))+inv(Ilim(4)));
Ic(5)=inv(inv((Io(5)*exp(-(Eapp-Erev(5))/beta)))+inv(Ilim(5)));
Ired=sum(Ic);
Iox=(Io(6)*exp((Eapp-Erev(6))/beta_ox));
Iex=Iox-Ired ;
end
Ecorr=Eapp;
Icorr=Iox
CR=1.155*(Icorr);
AA(ii,1)=Pco2;
AA(ii,2)=PH;
AA(ii,3)=Alk;
AA(ii,4)=Ecorr;
AA(ii,5)=CR
%-----------------graph plotting-------------------------
% Figure 1~Iex vs Eapp
SR=0.0018;
E=[-1.1:SR:-0.5];
 for j=1:length(E)
 %----cathodic current for each reaction A/m^2 ---------------
Ic(1)=inv(inv((Io(1)*exp(-(E(j)-Erev(1))/beta)))+inv(Ilim(1)));
Ic(2)=inv(inv((Io(2)*exp(-(E(j)-Erev(2))/beta)))+inv(Ilim(2)));
Ic(3)=inv(inv((Io(3)*exp(-(E(j)-Erev(3))/beta)))+inv(Ilim(3)));
Ic(4)=inv(inv((Io(4)*exp(-(E(j)-Erev(4))/beta)))+inv(Ilim(4)));
Ic(5)=inv(inv((Io(5)*exp(-(E(j)-Erev(5))/beta)))+inv(Ilim(5)));
Ired=sum(Ic);
Iox=(Io(6)*exp((E(j)-Erev(6))/beta_ox));
Iex=Iox-Ired;

 BB(j,1)=E(j);
 BB(j,2)=abs(Iex);
```

```
 BB(j,3)=abs(Ired);
 BB(j,4)=abs(Iox);
 BB(j,5)=abs(Ic(1));
 BB(j,6)=abs(Ic(2));
 BB(j,7)=abs(Ic(3));
 BB(j,8)=abs(Ic(4));
 BB(j,9)=abs(Ic(5));
   end
y1=BB(:,1);
x1=log10(BB(:,2));
x2=log10(BB(:,3));
x3=log10(BB(:,4));
x4=log10(BB(:,5));
x5=log10(BB(:,6));
x6=log10(BB(:,7));
x7=log10(BB(:,8));
x8=log10(BB(:,9));
figure (1)
plot(x1,y1,'.',x3,y1,'-.r',x4,y1,'-.m',x5,y1,'-.y',x6,y1,'-.c',x7,y1,'-.g',x8,y1,'-.k')
title('Potential applied vs. current density ')
legend('Iex','Fe+2','H3O+','HCO3-','H2O','PZH+','MDEAH+')
xlabel('Log Iapp ( A/m2)')
ylabel('E(V) vs SCE')
```

A.2 DEA-PZ system

```
clear all
format long
clc
% program  to calculate carbon steel corrosion at mixture CO2-H2O-PZ-DEA blend amine
%Basis:1 liter of solution
%--------------species concentration at the bulk -------------------------
%x(1)= xH2O
%x(2)= xCO2
%x(3)= xPZ
%x(4)= DEA
%x(5)= PZH+
%x(6)= DEAH+
%x(7)= H3O+
%x(8)= HCO3-
%x(9)= CO3-2
%x(10)= OH-
%x(11)= PZCOO-
%x(12)= DEACOO-
%x(13)= PZ(COO-)2
%x(14)= H+PZCOO-
%-------------------------input condition to evaluate model----------------
T=353.15;
moldea=1.8;
molpz=0.1;
PPco2=100;
%------------- physical properties [ H2O CO2 PZ DEA]---------
R=8.314;
Tc=[647.3 304.2 638.0 715.0];
Pc=[22048 7376 6870 3270];
Vc=[0.0559 0.0939  0.31 0.3490];
mwt=[18.02 86.13 105.14];
w=[0.344 0.225 0.4138 1.046];
zra=[0.2432 0.20 0.20];
%---------Renormalize mole fractions in the solution ----------------
molamine=2*molpz + moldea;
molh2o=55.5;
mol=[molh2o molpz moldea];
totmol=molh2o+molpz+moldea;
xtot=mol./totmol;
mass=mol.*mwt;
totmass=sum(mass);
wtfr=mass./totmass
totmwt=sum(xtot.*mwt);
%----------Rackett equation modified calculate molar volume of mixed solvent
Pcs=Pc(:,[1,3,4]);
Tcs=Tc(:,[1,3,4]) ;
Vcs=Vc(:,[1,3,4]);
zram=sum(xtot.*zra);
```

```
Vcsm=sum(xtot.*Vcs);
O=(xtot.*Vcs)/Vcsm;
Tcsm=sum(O.*Tcs);
Trsm=T/Tcsm;
Vsm= R*sum(xtot.*(Tcs./Pcs))*zram.^(1+(1-Trsm)^(2/7));
ds=totmwt/Vsm;
%-------------calculate mixed solvent Dielectric constant ---------------
Ds(1)=78.65+31989*(inv(T)-inv(298.15));
Ds(2)=4.253+1532.2*(inv(T)-inv(298.15));
Ds(3)=28.01+9277*(inv(T)-inv(273.15));
Dm=sum(Ds.*(xtot.*mwt)/totmwt);
%------------- Antoine equation ----------------------------------
VP(1)=exp(72.55-7206.7/T-7.1385*log(T)+4.05e-06*T^2)/1000;
VP(2)=exp(72.82912-3403.28/T+9.49e-03*T-8.56*log(T)+2.91e-16*T^6)/1000;
VP(3)=exp(70.503-7914.5/T -6.6461*log(T)+5.21e-18*T^6)/1000;
VP(4)=exp(286.01-20360/T-40.4*log(T)+ 0.032378*T)/1000;
%----- equilibrium constant as a function of Temperature based on mole fraction ---------
---------
k1=exp(132.899-(13445.9/T)-(22.477*log(T)));
k2=exp(231.465-(12092.1/T)-(36.782*log(T)));
k3=exp(216.049-(12431.7/T)-(35.482*log(T)));
k4=exp(-9.6416-(5008.4/T);
k5=exp(466.497+(1614.5/T)-(98.540*log(T))+0.2471*T);
k6=exp(6.822-(6066.9/T)-(2.290*log(T))+0.0036*T);
k7=exp(-11.563+(1769.4/T)-(1.467*log(T))+0.0024*T);
k8=exp(-13.3373-(4218.71/T)+0.009872*T);
k9=exp(16.5027-(4068.76/T)-1.5027*log(T));

Hco2=exp(170.7126-8477.711/T-21.95743*log(T)+0.005781*T)/1000;
%---------------enter initial guess for equilibrium mole fraction at the bulk -----------
x(1)=xtot(1);
x(2)=Pco2/Hco2;
Af= k6*k9;
Bf= k6*k9*xtot(3) + k6*k9*xtot(2) + k4*k6*k9*x(1) + k6*k8*k9*x(1) +
k4*k5*k9*x(1)*x(2);
Cf= k4*k6*k9*x(1)*xtot(3) - k1*k6*k9*x(1)^2 + k6*k8*k9*x(1)*xtot(2) +
k4*k6*k8*k9*x(1)^2 + k2*k6*k8*x(1)^2*x(2) - k2*k6*k9*x(1)^2*x(2) +
k4*k5*k9*x(1)*x(2)*xtot(3) + k4*k5*k6*k9*x(1)^2*x(2) +
k4*k5*k8*k9*x(1)^2*x(2);
Df= k2*k4*k6*k8*x(1)^3*x(2) - k1*k6*k8*k9*x(1)^3 - k1*k4*k5*k9*x(1)^3*x(2) -
2*k2*k3*k6*k9*x(1)^3*x(2) - k1*k4*k6*k9*x(1)^3 - k2*k4*k6*k9*x(1)^3*x(2) -
k2*k6*k8*k9*x(1)^3*x(2) - k2*k6*k8*x(1)^2*x(2)*xtot(3) +
k2*k6*k8*x(1)^2*x(2)*xtot(2) + k2*k4*k5*k8*x(1)^3*x(2)^2 -
k2*k4*k5*k9*x(1)^3*x(2)^2 + k4*k5*k6*k7*k9*x(1)^3*x(2)^2 +
k4*k5*k6*k8*k9*x(1)^3*x(2) + k4*k5*k6*k9*x(1)^2*x(2)*xtot(3) -
k4*k5*k6*k9*x(1)^2*x(2)*xtot(2);
Ef= k2*k4*k5*k6*k8*x(1)^4*x(2)^2 - k1*k4*k6*k8*k9*x(1)^4 -
k1*k2*k6*k8*x(1)^4*x(2) - 2*k2*k3*k4*k5*k9*x(1)^4*x(2)^2 -
k2^2*k6*k8*x(1)^4*x(2)^2 - k2*k4*k5*k6*k9*x(1)^4*x(2)^2 -
k2*k4*k5*k8*k9*x(1)^4*x(2)^2 - k2*k4*k5*k8*x(1)^3*x(2)^2*xtot(3) -
2*k2*k3*k4*k6*k9*x(1)^4*x(2) - k1*k4*k5*k6*k9*x(1)^4*x(2) -
```

```
k1*k4*k5*k8*k9*x(1)^4*x(2) - 2*k2*k3*k6*k8*k9*x(1)^4*x(2) -
k2*k4*k6*k8*k9*x(1)^4*x(2) - k2*k4*k6*k8*x(1)^3*x(2)*xtot(3) -
k4*k5*k6*k8*k9*x(1)^3*x(2)*xtot(2) + k4*k5*k6*k7*k8*k9*x(1)^4*x(2)^2 +
k4*k5*k6*k7*k9*x(1)^3*x(2)^2*xtot(3) - 2*k4*k5*k6*k7*k9*x(1)^3*x(2)^2*xtot(2);
Ff= k2*k4*k5*k6*k7*k8*x(1)^5*x(2)^3 - k2^2*k4*k5*k8*x(1)^5*x(2)^3 -
k2^2*k4*k6*k8*x(1)^5*x(2)^2 - k1*k2*k4*k5*k8*x(1)^5*x(2)^2 -
k1*k2*k4*k6*k8*x(1)^5*x(2) - 2*k2*k3*k4*k6*k8*k9*x(1)^5*x(2) -
k1*k4*k5*k6*k8*k9*x(1)^5*x(2) - 2*k2*k3*k4*k5*k6*k9*x(1)^5*x(2)^2 -
2*k2*k3*k4*k5*k8*k9*x(1)^5*x(2)^2 - k1*k4*k5*k6*k7*k9*x(1)^5*x(2)^2 -
2*k2^2*k3*k6*k8*x(1)^5*x(2)^2 - k2*k4*k5*k6*k7*k9*x(1)^5*x(2)^3 -
k2*k4*k5*k6*k8*k9*x(1)^5*x(2)^2 - k2*k4*k5*k6*k8*x(1)^4*x(2)^2*xtot(3) -
k2*k4*k5*k6*k8*x(1)^4*x(2)^2*xtot(2) -
2*k4*k5*k6*k7*k8*k9*x(1)^4*x(2)^2*xtot(2);
Gf= - 2*k2^2*k3*k4*k5*k8*x(1)^6*x(2)^3 - 2*k2^2*k3*k4*k6*k8*x(1)^6*x(2)^2 -
k2^2*k4*k5*k6*k8*x(1)^6*x(2)^3 - k1*k2*k4*k5*k6*k8*x(1)^6*x(2)^2 -
k2*k4*k5*k6*k7*k8*x(1)^5*x(2)^3*xtot(3) -
2*k2*k4*k5*k6*k7*k8*x(1)^5*x(2)^3*xtot(2) -
2*k2*k3*k4*k5*k6*k7*k9*x(1)^6*x(2)^3 - 2*k2*k3*k4*k5*k6*k8*k9*x(1)^6*x(2)^2
- k1*k4*k5*k6*k7*k8*k9*x(1)^6*x(2)^2 - k2*k4*k5*k6*k7*k8*k9*x(1)^6*x(2)^3 ;
Hf= - 2*k2^2*k3*k4*k5*k6*k8*x(1)^7*x(2)^3 -
k2^2*k4*k5*k6*k7*k8*x(1)^7*x(2)^4 - k1*k2*k4*k5*k6*k7*k8*x(1)^7*x(2)^3 -
2*k2*k3*k4*k5*k6*k7*k8*k9*x(1)^7*x(2)^3 ;
If= - 2*k2^2*k3*k4*k5*k6*k7*k8*x(1)^8*x(2)^4;

fun=[Af Bf Cf Df Ef Ff Gf Hf If];
sol=roots(fun);
x(7)=max(sol(find(imag(sol)==0 & sol > 0)));
x(10)=k1*x(1)^2/x(7);
x(8)=k2*x(2)*x(1)^2/x(7);
x(9)=k3*x(8)*x(1)/x(7);
x(3)=xtot(2)/((k5*x(2))/k6 + x(7)/(k4*x(1)) + (k5*x(1)*x(2))/x(7) +
(k5*k7*x(1)^2*x(2)^2)/x(7)^2 + 1);
x(5)=x(3)*x(7)/(k4*x(1));
x(11)=k5*x(3)*x(2)*x(1)/x(7);
x(14)=x(11)*x(7)/(k6*x(1));
x(13)=k7*x(11)*x(1)*x(2)/x(7);
x(4)=(k8*k9*x(1)*x(7)*xtot(3))/(k2*k8*x(2)*x(1)^2 + k8*k9*x(1)*x(7) + k9*x(7)^2);
x(6)=x(4)*x(7)/(k8*x(1));
x(12)=x(4)*x(8)/(k9*x(1));
err=1 ;
while err>0.00000001;
%----------------Gamma for Pitzer-Debye-Huckell and Born correction---------------------
-------
% charge species  [H2O;CO2;PZ;DEA ;PZH+ DEAH+ ; H3O+; HCO3-;CO3-2 ; OH-
;PZCOO-;DEACOO-;PZ(COO-)2;H+PZCOO-]
z=[0,0,0,0,1,1,1,-1,-2,-1,-1,-1,-2,0] ;
e0=8.854e-12 ;
Na = 6.0221415e23;
rho=14.9  ;
Qe=-1.602e-19;
kb=1.38e-23 ;
```

```
ra = 3e-10*ones(1,size(z,2));
Ix=0.5*sum(x.*z.^2);
A_phi=1/3*(2*pi*Na*ds/totmwt*1000)^0.5*(Qe^2/(4*pi)/e0/Dm/kb/T)^1.5;
lnGamma_PDH=-A_phi*(2*z'.^2/rho*log(1+rho*Ix^0.5)+(z'.^2*Ix^0.5-
2*Ix^1.5)/(1+rho*Ix^0.5));
lnGamma_Born=Qe^2/2/kb/T*(1/Dm-1/Ds(1))*(z.^2./ra)'*10^-2  ;
lnGammaLR=lnGamma_PDH+lnGamma_Born ;
%--------------calculate activity coefficient term e-NRTL ------------------
mca=[sum(z==0);sum(z>0);sum(z<0)];
    m=(z==0).*(1:size(z,2)) ;
        m=m(m~=0);
    c=(z>0).*(1:size(z,2));
        c=c(c~=0);
    a=(z<0).*(1:size(z,2));
        a=a(a~=0);
Cj=[1;1;1;1;1;1;1;1;2;1;1;1;2;1] ;
  Xj=x'.*Cj;
  cTotal=sum(Xj(c));
  aTotal=sum(Xj(a));

  alpha1=0.2 ;
  alpha3=0.1;
  alpha_AM=[0.2*ones(mca(3),1),0.1*ones(mca(3),mca(1)-1)];
  alpha_CM=[0.2*ones(mca(2),1),0.1*ones(mca(2),mca(1)-1)];
  alpha_CAM=[0.2*ones(mca(2)*mca(3),1),0.1*ones(mca(2)*mca(3),mca(1)-1)];
  tau_CAM=[ones(mca(2)*mca(3),1)*-4,ones(mca(2)*mca(3),1)*-
8,ones(mca(2)*mca(3),mca(1)-2)*-2];
tau_MCA=[ones(mca(2)*mca(3),1)*8,ones(mca(2)*mca(3),1)*15,ones(mca(2)*mca(3),
mca(1)-2)*10];
  tau_MM=zeros(mca(1),mca(1));
  G_MM=exp(-alpha1*tau_MM);
  G_CAM=exp(-alpha_CAM.*tau_CAM);
  G_MCA=exp(-alpha_CAM.*tau_MCA);
  tauCprimeA_CA=zeros(mca(2),mca(2)*mca(3));
  tauCAprime_CA=zeros(mca(3),mca(2)*mca(3));
  GCprimeA_CA=exp(-alpha3*tauCprimeA_CA);
  GCAprime_CA=exp(-alpha3*tauCAprime_CA);
  temp1c=(Xj(c)*ones(1,mca(3)))';
  PsudoI_1=repmat(eye(mca(3),mca(3)),1,mca(2));
  c_sparse=(ones(mca(3),1)*temp1c(1:mca(2)*mca(3))).*PsudoI_1;
  temp1a=ones(mca(3),1)*(1:mca(2)) ;
  temp2a=temp1a(1:mca(2)*mca(3))+(0:mca(2):(mca(2)*mca(3)-1)*mca(2));
  temp1a=zeros(mca(2),mca(2)*mca(3));
  temp1a(temp2a)=1;
  PsudoI_2=temp1a;
  a_sparse=repmat(Xj(a)',mca(2),mca(2)).*PsudoI_2;
  PsudoI_3=repmat(eye(mca(2),mca(2)),mca(1),1);
  temp1m=ones(mca(2),1)*Xj(m)';
  temp2m=zeros(mca(1)*mca(2),1);
  temp2m(1:end)=temp1m(1:end);
```

```
  m_sparse1=(temp2m*ones(1,mca(2))).*PsudoI_3;
m_sparse2=repmat(eye(mca(3),mca(3)),1,mca(1)).*(ones(mca(3),1)*reshape(ones(mca(
3),1)*Xj(m)',1,mca(1)*mca(3)));
  temp1=ones(mca(1),1)*(1:mca(2));
  temp2=temp1(1:mca(2)*mca(1))+(0:mca(2):(mca(2)*mca(1)-1)*mca(2));
  temp1=zeros(mca(2),mca(2)*mca(1));
  temp1(temp2)=1;
  PsudoI_5=temp1;
  m_sparse3=PsudoI_5.*repmat(Xj(m)',mca(2),mca(2));
 G_AM=(c_sparse*G_CAM)/cTotal;
 G_CM=(a_sparse*G_CAM)/aTotal;
 tau_AM=-log(G_AM)./alpha_AM;
 tau_CM=-log(G_CM)./alpha_CM;
 MC_ACtemp1=reshape(tau_MCA,mca(3),mca(1)*mca(2));
 MC_ACtemp2=reshape(tau_CAM,mca(3),mca(1)*mca(2));
 tauMC_AC=ones(mca(3),1)*tau_CM(1:end)-MC_ACtemp2+MC_ACtemp1;
 AM_ACtemp1=repmat(tau_AM,mca(2),1)-tau_CAM+tau_MCA;
 AM_ACtemp2=AM_ACtemp1;
 tauAM_AC=reshape(AM_ACtemp2,mca(2),mca(1)*mca(3));
 GMC_AC=exp(-alpha3*tauMC_AC);
 GAM_AC=exp(-alpha3*tauAM_AC);
  lnGammaInfinity=zeros(sum(mca),1);
  lnGammaSym=zeros(sum(mca),1);
GtOverG_1=(Xj(m)'*(tau_MM.*G_MM)+Xj(a)'*(tau_AM.*G_AM)+Xj(c)'*(tau_CM.*
G_CM))./(Xj(m)'*G_MM+Xj(a)'*G_AM+Xj(c)'*G_CM);
GtOverG_2=((GCAprime_CA.*tauCAprime_CA)*a_sparse'+(tauMC_AC.*GMC_AC)
*m_sparse1)./(GCAprime_CA*a_sparse'+cTotal+GMC_AC*m_sparse1);
  GtOverG_2ca= reshape(repmat(GtOverG_2,mca(3),1),mca(3),mca(3)*mca(2));
GtOverG_3=((c_sparse*(GCprimeA_CA.*tauCprimeA_CA)'+m_sparse2*(tauAM_AC.
*GAM_AC)')./(c_sparse*GCprimeA_CA'+aTotal+m_sparse2*GAM_AC'))';
  M_term1=GtOverG_1;
  M_term2=((G_MM.*(tau_MM-
ones(mca(1),1)*GtOverG_1))*(Xj(m)./((Xj(m)'*G_MM+Xj(a)'*G_AM+Xj(c)'*G_CM)'
)))';
    temp1mc=ones(mca(2),1)*(1:mca(1));
    temp2mc=temp1mc(1:mca(1)*mca(2))+(0:mca(1):(mca(1)*mca(2)-1)*mca(1));
    temp1mc=zeros(mca(1),mca(1)*mca(2));
    temp1mc(temp2mc)=1 ;
    PsudoI_4=temp1mc;
M_term3=sum((((Xj(a)/aTotal)*ones(1,mca(1)*mca(2))).*(repmat(Xj(c)',mca(3),mca(1
)).*GMC_AC)./(repmat(GCAprime_CA*a_sparse'+cTotal+GMC_AC*m_sparse1,1,mc
a(1))).*(tauMC_AC-repmat(GtOverG_2,1,mca(1))))*PsudoI_4',1) ;
    temp1ma=ones(mca(3),1)*(1:mca(1)) ;
    temp2ma=temp1ma(1:mca(1)*mca(3))+(0:mca(1):(mca(1)*mca(3)-1)*mca(1));
    temp1ma=zeros(mca(1),mca(1)*mca(3)) ;
    temp1ma(temp2ma)=1;
    PsudoI_6=temp1ma;
M_term4=sum((((Xj(c)/cTotal)*ones(1,mca(1)*mca(3))).*(repmat(Xj(a)',mca(2),mca(1
)).*GAM_AC)./repmat(GAM_AC*m_sparse2'+GCprimeA_CA*c_sparse'+aTotal,1,mc
a(1)).*(tauAM_AC-repmat(GtOverG_3,1,mca(1))))*PsudoI_6',1);
```

```
  lnGammaInfinity(m)=(tau_MM(1,:)+G_MM(1,:).*tau_MM(1,:))';
C_term1=Xj(a)'*(((GCAprime_CA.*tauCAprime_CA)*a_sparse'+(GMC_AC.*tauMC_
AC)*m_sparse1)./(GCAprime_CA*a_sparse'+cTotal+GMC_AC*m_sparse1))/aTotal;
C_term2=sum((ones(mca(2),1)*(Xj(m)'./(Xj(m)'*G_MM+Xj(a)'*G_AM+Xj(c)'*G_CM
))).*(G_CM.*(tau_CM-ones(mca(2),1)*GtOverG_1)),2)';
  C_term4=Xj(a)'*reshape((Xj(c)'*(GCprimeA_CA.*(tauCprimeA_CA-
repmat(GtOverG_3,1,mca(2)))./repmat((c_sparse*GCprimeA_CA'+aTotal+m_sparse2*
GAM_AC')',1,mca(2))))',mca(3),mca(2))/cTotal ;
  temp1cc=reshape(Xj(a)'*tauMC_AC,mca(2),mca(1))/aTotal+tau_CM.*G_CM ;
  lnGammaInfinity(c)=temp1cc(:,1);
   clear temp1 ;
  for i=1:mca(2);
    temp1(:,i)=(i:mca(2):mca(2)*mca(3)-mca(2)+i)' ;
  end
Ind_Vector1=reshape(reshape(temp1,mca(2)*mca(3),1)*ones(1,mca(1))+ones(mca(2)*
mca(3),1)*(0:mca(2)*mca(3):mca(2)*mca(3)*(mca(1)-1)),mca(2)*mca(3)*mca(1),1);
 Atemp6=zeros(mca(2)*mca(3),1) ;

Atemp6(Ind_Vector1(1:mca(2)*mca(3)))=GCAprime_CA*a_sparse'+cTotal+GMC_AC
*m_sparse3';
 Atemp7=reshape((Atemp6*ones(1,mca(3)))',mca(2)*mca(3),mca(3))';
 A_term1=Xj(c)'*GtOverG_3/cTotal;
 A_term2=sum((G_AM.*(tau_AM-
ones(mca(3),1)*GtOverG_1)).*(ones(mca(3),1)*(Xj(m)'./(Xj(m)'*G_MM+Xj(a)'*G_A
M+Xj(c)'*G_CM))),2)';
 A_term4= Xj(c)'*(reshape(((GCAprime_CA.*(tauCAprime_CA-
GtOverG_2ca))./Atemp7)'*Xj(a),mca(3),mca(2))/aTotal)';
lnGammaInfinity(a)=(Xj(c)'*tauAM_AC(:,1:mca(3))/cTotal)'+(tau_AM(:,1).*G_AM(:,
1));
lnGammaSym(m)=M_term1+M_term2+M_term3+M_term4 ;
lnGammaSym(c)=C_term1+C_term2+C_term4;
lnGammaSym(a)=A_term1+A_term2+A_term4;
lnGammaSR=((z+(z==0))'.*(lnGammaSym-lnGammaInfinity)+lnGammaLR) ;
Gamma=exp(lnGammaSR);
g=Gamma;
% ----------- calculate truly values of mole fraction ------------------------
Anew=(g(10)*g(11)*g(12)*g(13)*g(14)*g(3)*g(4)*g(7)^7*g(8)*g(9)*k6*k9);
Bnew=(g(10)*g(11)*g(12)*g(13)*g(14)*g(3)*g(4)*g(7)^7*g(8)*g(9)*k6*k9*xtot(3) +
g(10)*g(11)*g(12)*g(13)*g(14)*g(3)*g(4)*g(7)^7*g(8)*g(9)*k6*k9*xtot(2) +
g(1)*g(10)*g(11)*g(12)*g(13)*g(14)*g(4)*g(5)*g(7)^6*g(8)*g(9)*k4*k6*k9*x(1) +
g(1)*g(10)*g(11)*g(12)*g(13)*g(14)*g(3)*g(6)*g(7)^6*g(8)*g(9)*k6*k8*k9*x(1) +
g(1)*g(10)*g(11)*g(12)*g(13)*g(2)*g(3)*g(4)*g(5)*g(7)^6*g(8)*g(9)*k4*k5*k9*x(1)
*x(2)) ;
Cnew=(g(1)^2*g(10)*g(11)*g(12)*g(13)*g(14)*g(5)*g(6)*g(7)^5*g(8)*g(9)*k4*k6*k
8*k9*x(1)^2 -
g(1)^2*g(11)*g(12)*g(13)*g(14)*g(3)*g(4)*g(7)^6*g(8)*g(9)*k1*k6*k9*x(1)^2 -
g(1)^2*g(10)*g(11)*g(12)*g(13)*g(14)*g(2)*g(3)*g(4)*g(7)^6*g(9)*k2*k6*k9*x(1)^2
*x(2) +
g(1)*g(10)*g(11)*g(12)*g(13)*g(14)*g(4)*g(5)*g(7)^6*g(8)*g(9)*k4*k6*k9*x(1)*xto
t(3) +
g(1)*g(10)*g(11)*g(12)*g(13)*g(14)*g(3)*g(6)*g(7)^6*g(8)*g(9)*k6*k8*k9*x(1)*xto
```

```
t(2) +
g(1)^2*g(10)*g(11)*g(13)*g(14)*g(2)*g(3)*g(4)*g(6)*g(7)^5*g(8)*g(9)*k2*k6*k8*x(
1)^2*x(2) +
g(1)*g(10)*g(11)*g(12)*g(13)*g(2)*g(3)*g(4)*g(5)*g(7)^6*g(8)*g(9)*k4*k5*k9*x(1)
*x(2)*xtot(3) +
g(1)^2*g(10)*g(12)*g(13)*g(14)*g(2)*g(3)*g(4)*g(5)*g(7)^5*g(8)*g(9)*k4*k5*k6*k9
*x(1)^2*x(2) +
g(1)^2*g(10)*g(11)*g(12)*g(13)*g(2)*g(3)*g(5)*g(6)*g(7)^5*g(8)*g(9)*k4*k5*k8*k9
*x(1)^2*x(2));
Dnew=(g(1)^3*g(10)*g(11)*g(13)*g(2)^2*g(3)*g(4)*g(5)*g(6)*g(7)^4*g(8)*g(9)*k2*
k4*k5*k8*x(1)^3*x(2)^2 -
g(1)^3*g(11)*g(12)*g(13)*g(14)*g(3)*g(6)*g(7)^5*g(8)*g(9)*k1*k6*k8*k9*x(1)^3 -
g(1)^3*g(10)*g(11)*g(12)*g(13)*g(2)^2*g(3)*g(4)*g(5)*g(7)^5*g(9)*k2*k4*k5*k9*x
(1)^3*x(2)^2 -
2*g(1)^3*g(10)*g(11)*g(12)*g(13)*g(14)*g(2)*g(3)*g(4)*g(7)^5*g(8)*k2*k3*k6*k9*
x(1)^3*x(2) -
g(1)^3*g(10)*g(11)*g(12)*g(13)*g(14)*g(2)*g(4)*g(5)*g(7)^5*g(9)*k2*k4*k6*k9*x(
1)^3*x(2) -
g(1)^3*g(10)*g(11)*g(12)*g(13)*g(14)*g(2)*g(3)*g(6)*g(7)^5*g(9)*k2*k6*k8*k9*x(
1)^3*x(2) -
g(1)^3*g(11)*g(12)*g(13)*g(2)*g(3)*g(4)*g(5)*g(7)^5*g(8)*g(9)*k1*k4*k5*k9*x(1)^
3*x(2) -
g(1)^3*g(11)*g(12)*g(13)*g(14)*g(4)*g(5)*g(7)^5*g(8)*g(9)*k1*k4*k6*k9*x(1)^3 +
g(1)^3*g(10)*g(11)*g(13)*g(14)*g(2)*g(4)*g(5)*g(6)*g(7)^4*g(8)*g(9)*k2*k4*k6*k8
*x(1)^3*x(2) -
g(1)^2*g(10)*g(11)*g(13)*g(14)*g(2)*g(3)*g(4)*g(6)*g(7)^5*g(8)*g(9)*k2*k6*k8*x(
1)^2*x(2)*xtot(3) +
g(1)^2*g(10)*g(11)*g(13)*g(14)*g(2)*g(3)*g(4)*g(6)*g(7)^5*g(8)*g(9)*k2*k6*k8*x(
1)^2*x(2)*xtot(2) +
g(1)^3*g(10)*g(11)*g(12)*g(14)*g(2)^2*g(3)*g(4)*g(5)*g(7)^4*g(8)*g(9)*k4*k5*k6*
k7*k9*x(1)^3*x(2)^2 +
g(1)^3*g(10)*g(12)*g(13)*g(14)*g(2)*g(3)*g(5)*g(6)*g(7)^4*g(8)*g(9)*k4*k5*k6*k8
*k9*x(1)^3*x(2) +
g(1)^2*g(10)*g(12)*g(13)*g(14)*g(2)*g(3)*g(4)*g(5)*g(7)^5*g(8)*g(9)*k4*k5*k6*k9
*x(1)^2*x(2)*xtot(3) -
g(1)^2*g(10)*g(12)*g(13)*g(14)*g(2)*g(3)*g(4)*g(5)*g(7)^5*g(8)*g(9)*k4*k5*k6*k9
*x(1)^2*x(2)*xtot(2)) ;
Enew=(g(1)^4*g(10)*g(13)*g(14)*g(2)^2*g(3)*g(4)*g(5)*g(6)*g(7)^3*g(8)*g(9)*k2*
k4*k5*k6*k8*x(1)^4*x(2)^2 -
g(1)^4*g(10)*g(11)*g(13)*g(14)*g(2)^2*g(3)*g(4)*g(6)*g(7)^4*g(9)*k2^2*k6*k8*x(
1)^4*x(2)^2 -
g(1)^4*g(11)*g(13)*g(14)*g(2)*g(3)*g(4)*g(6)*g(7)^4*g(8)*g(9)*k1*k2*k6*k8*x(1)^
4*x(2) -
2*g(1)^4*g(10)*g(11)*g(12)*g(13)*g(2)^2*g(3)*g(4)*g(5)*g(7)^4*g(8)*k2*k3*k4*k5
*k9*x(1)^4*x(2)^2 -
g(1)^4*g(10)*g(12)*g(13)*g(14)*g(2)^2*g(3)*g(4)*g(5)*g(7)^4*g(9)*k2*k4*k5*k6*k
9*x(1)^4*x(2)^2 -
g(1)^4*g(10)*g(11)*g(12)*g(13)*g(2)^2*g(3)*g(5)*g(6)*g(7)^4*g(9)*k2*k4*k5*k8*k
9*x(1)^4*x(2)^2 -
2*g(1)^4*g(10)*g(11)*g(12)*g(13)*g(14)*g(2)*g(4)*g(5)*g(7)^4*g(8)*k2*k3*k4*k6*
k9*x(1)^4*x(2) -
```

```
2*g(1)^4*g(10)*g(11)*g(12)*g(13)*g(14)*g(2)*g(3)*g(6)*g(7)^4*g(8)*k2*k3*k6*k8*
k9*x(1)^4*x(2) -
g(1)^4*g(10)*g(11)*g(12)*g(13)*g(14)*g(2)*g(5)*g(6)*g(7)^4*g(9)*k2*k4*k6*k8*k9
*x(1)^4*x(2) -
g(1)^4*g(12)*g(13)*g(14)*g(2)*g(3)*g(4)*g(5)*g(7)^4*g(8)*g(9)*k1*k4*k5*k6*k9*x
(1)^4*x(2) -
g(1)^4*g(11)*g(12)*g(13)*g(2)*g(3)*g(5)*g(6)*g(7)^4*g(8)*g(9)*k1*k4*k5*k8*k9*x
(1)^4*x(2) -
g(1)^4*g(11)*g(12)*g(13)*g(14)*g(5)*g(6)*g(7)^4*g(8)*g(9)*k1*k4*k6*k8*k9*x(1)^
4 -
g(1)^3*g(10)*g(11)*g(13)*g(2)^2*g(3)*g(4)*g(5)*g(6)*g(7)^4*g(8)*g(9)*k2*k4*k5*k
8*x(1)^3*x(2)^2*xtot(3) -
g(1)^3*g(10)*g(11)*g(13)*g(14)*g(2)*g(4)*g(5)*g(6)*g(7)^4*g(8)*g(9)*k2*k4*k6*k8
*x(1)^3*x(2)*xtot(3) +
g(1)^4*g(10)*g(11)*g(12)*g(14)*g(2)^2*g(3)*g(5)*g(6)*g(7)^3*g(8)*g(9)*k4*k5*k6*
k7*k8*k9*x(1)^4*x(2)^2 +
g(1)^3*g(10)*g(11)*g(12)*g(14)*g(2)^2*g(3)*g(4)*g(5)*g(7)^4*g(8)*g(9)*k4*k5*k6*
k7*k9*x(1)^3*x(2)^2*xtot(3) -
2*g(1)^3*g(10)*g(11)*g(12)*g(14)*g(2)^2*g(3)*g(4)*g(5)*g(7)^4*g(8)*g(9)*k4*k5*k
6*k7*k9*x(1)^3*x(2)^2*xtot(2) -
g(1)^3*g(10)*g(12)*g(13)*g(14)*g(2)*g(3)*g(5)*g(6)*g(7)^4*g(8)*g(9)*k4*k5*k6*k8
*k9*x(1)^3*x(2)*xtot(2)) ;
Fnew=(g(1)^5*g(10)*g(11)*g(14)*g(2)^3*g(3)*g(4)*g(5)*g(6)*g(7)^2*g(8)*g(9)*k2*
k4*k5*k6*k7*k8*x(1)^5*x(2)^3 -
g(1)^5*g(10)*g(11)*g(13)*g(14)*g(2)^2*g(4)*g(5)*g(6)*g(7)^3*g(9)*k2^2*k4*k6*k8
*x(1)^5*x(2)^2 -
g(1)^5*g(10)*g(11)*g(13)*g(2)^3*g(3)*g(4)*g(5)*g(6)*g(7)^3*g(9)*k2^2*k4*k5*k8*
x(1)^5*x(2)^3 -
g(1)^5*g(11)*g(13)*g(2)^2*g(3)*g(4)*g(5)*g(6)*g(7)^3*g(8)*g(9)*k1*k2*k4*k5*k8*
x(1)^5*x(2)^2 -
g(1)^5*g(11)*g(13)*g(14)*g(2)*g(4)*g(5)*g(6)*g(7)^3*g(8)*g(9)*k1*k2*k4*k6*k8*x
(1)^5*x(2) -
2*g(1)^5*g(10)*g(12)*g(13)*g(14)*g(2)^2*g(3)*g(4)*g(5)*g(7)^3*g(8)*k2*k3*k4*k5
*k6*k9*x(1)^5*x(2)^2 -
2*g(1)^5*g(10)*g(11)*g(12)*g(13)*g(2)^2*g(3)*g(5)*g(6)*g(7)^3*g(8)*k2*k3*k4*k5
*k8*k9*x(1)^5*x(2)^2 -
g(1)^5*g(10)*g(11)*g(12)*g(14)*g(2)^3*g(3)*g(4)*g(5)*g(7)^3*g(9)*k2*k4*k5*k6*k
7*k9*x(1)^5*x(2)^3 -
g(1)^5*g(10)*g(12)*g(13)*g(14)*g(2)^2*g(3)*g(5)*g(6)*g(7)^3*g(9)*k2*k4*k5*k6*k
8*k9*x(1)^5*x(2)^2 -
g(1)^5*g(11)*g(12)*g(14)*g(2)^2*g(3)*g(4)*g(5)*g(7)^3*g(8)*g(9)*k1*k4*k5*k6*k7
*k9*x(1)^5*x(2)^2 -
2*g(1)^5*g(10)*g(11)*g(12)*g(13)*g(14)*g(2)*g(5)*g(6)*g(7)^3*g(8)*k2*k3*k4*k6*
k8*k9*x(1)^5*x(2) -
g(1)^5*g(12)*g(13)*g(14)*g(2)*g(3)*g(5)*g(6)*g(7)^3*g(8)*g(9)*k1*k4*k5*k6*k8*k
9*x(1)^5*x(2) -
2*g(1)^5*g(10)*g(11)*g(13)*g(14)*g(2)^2*g(3)*g(4)*g(6)*g(7)^3*g(8)*k2^2*k3*k6*
k8*x(1)^5*x(2)^2 -
g(1)^4*g(10)*g(13)*g(14)*g(2)^2*g(3)*g(4)*g(5)*g(6)*g(7)^3*g(8)*g(9)*k2*k4*k5*k
6*k8*x(1)^4*x(2)^2*xtot(3) -
g(1)^4*g(10)*g(13)*g(14)*g(2)^2*g(3)*g(4)*g(5)*g(6)*g(7)^3*g(8)*g(9)*k2*k4*k5*k
```

```
6*k8*x(1)^4*x(2)^2*xtot(2) -
2*g(1)^4*g(10)*g(11)*g(12)*g(14)*g(2)^2*g(3)*g(5)*g(6)*g(7)^3*g(8)*g(9)*k4*k5*k
6*k7*k8*k9*x(1)^4*x(2)^2*xtot(2));
Gnew=(-
2*g(1)^6*g(10)*g(11)*g(13)*g(14)*g(2)^2*g(4)*g(5)*g(6)*g(7)^2*g(8)*k2^2*k3*k4*
k6*k8*x(1)^6*x(2)^2 -
2*g(1)^6*g(10)*g(11)*g(13)*g(2)^3*g(3)*g(4)*g(5)*g(6)*g(7)^2*g(8)*k2^2*k3*k4*k
5*k8*x(1)^6*x(2)^3 -
g(1)^6*g(10)*g(13)*g(14)*g(2)^3*g(3)*g(4)*g(5)*g(6)*g(7)^2*g(9)*k2^2*k4*k5*k6*
k8*x(1)^6*x(2)^3 -
g(1)^6*g(13)*g(14)*g(2)^2*g(3)*g(4)*g(5)*g(6)*g(7)^2*g(8)*g(9)*k1*k2*k4*k5*k6*
k8*x(1)^6*x(2)^2 -
2*g(1)^6*g(10)*g(11)*g(12)*g(14)*g(2)^3*g(3)*g(4)*g(5)*g(7)^2*g(8)*k2*k3*k4*k5
*k6*k7*k9*x(1)^6*x(2)^3 -
2*g(1)^6*g(10)*g(12)*g(13)*g(14)*g(2)^2*g(3)*g(5)*g(6)*g(7)^2*g(8)*k2*k3*k4*k5
*k6*k8*k9*x(1)^6*x(2)^2 -
g(1)^6*g(10)*g(11)*g(12)*g(14)*g(2)^3*g(3)*g(5)*g(6)*g(7)^2*g(9)*k2*k4*k5*k6*k
7*k8*k9*x(1)^6*x(2)^3 -
g(1)^6*g(11)*g(12)*g(14)*g(2)^2*g(3)*g(5)*g(6)*g(7)^2*g(8)*g(9)*k1*k4*k5*k6*k7
*k8*k9*x(1)^6*x(2)^2 -
g(1)^5*g(10)*g(11)*g(14)*g(2)^3*g(3)*g(4)*g(5)*g(6)*g(7)^2*g(8)*g(9)*k2*k4*k5*k
6*k7*k8*x(1)^5*x(2)^3*xtot(3) -
2*g(1)^5*g(10)*g(11)*g(14)*g(2)^3*g(3)*g(4)*g(5)*g(6)*g(7)^2*g(8)*g(9)*k2*k4*k5
*k6*k7*k8*x(1)^5*x(2)^3*xtot(2));
Hnew=(-
2*g(1)^7*g(10)*g(13)*g(14)*g(2)^3*g(3)*g(4)*g(5)*g(6)*g(7)*g(8)*k2^2*k3*k4*k5*
k6*k8*x(1)^7*x(2)^3 -
g(1)^7*g(10)*g(11)*g(14)*g(2)^4*g(3)*g(4)*g(5)*g(6)*g(7)*g(9)*k2^2*k4*k5*k6*k7
*k8*x(1)^7*x(2)^4 -
g(1)^7*g(11)*g(14)*g(2)^3*g(3)*g(4)*g(5)*g(6)*g(7)*g(8)*g(9)*k1*k2*k4*k5*k6*k7
*k8*x(1)^7*x(2)^3 -
2*g(1)^7*g(10)*g(11)*g(12)*g(14)*g(2)^3*g(3)*g(5)*g(6)*g(7)*g(8)*k2*k3*k4*k5*k
6*k7*k8*k9*x(1)^7*x(2)^3) ;
Inew=-
2*g(1)^8*g(10)*g(11)*g(14)*g(2)^4*g(3)*g(4)*g(5)*g(6)*g(8)*k2^2*k3*k4*k5*k6*k
7*k8*x(1)^8*x(2)^4;

funnew=[Anew Bnew Cnew Dnew Enew Fnew Gnew Hnew Inew];
solnew=roots(funnew);
xnew(7)=max(solnew(find(imag(solnew) == 0)));
xnew(2)=Pco2/(Hco2);
xnew(1)=1-
(x(2)+x(3)+x(4)+x(5)+x(6)+x(7)+x(8)+x(9)+x(10)+x(11)+x(12)+x(13)+x(14));
xnew(10)=k1*xnew(1)^2*g(1)^2/(xnew(7)*g(7)*g(10));
xnew(8)=k2*xnew(2)*g(2)*xnew(1)^2*g(1)^2/(xnew(7)*g(7)*g(8));
xnew(9)=k3*xnew(8)*g(8)*xnew(1)*g(1)/(xnew(7)*g(7)*g(9));
xnew(3)=xtot(2)/((g(2)*g(3)*k5*xnew(2))/(g(14)*k6) +
(g(3)*g(7)*xnew(7))/(g(1)*g(5)*k4*xnew(1)) +
(g(1)*g(2)*g(3)*k5*xnew(1)*xnew(2))/(g(11)*g(7)*xnew(7)) +
(g(1)^2*g(2)^2*g(3)*k5*k7*xnew(1)^2*xnew(2)^2)/(g(13)*g(7)^2*xnew(7)^2) + 1);
xnew(5)=xnew(3)*g(3)*xnew(7)*g(7)/(k4*xnew(1)*g(1)*g(5));
```

```
xnew(11)=k5*xnew(3)*g(3)*xnew(2)*g(2)*xnew(1)*g(1)/(xnew(7)*g(7)*g(11));
xnew(14)=xnew(11)*g(11)*xnew(7)*g(7)/(k6*xnew(1)*g(1)*g(14));
xnew(13)=k7*xnew(11)*g(11)*xnew(1)*g(1)*xnew(2)*g(2)/(xnew(7)*g(7)*g(13));
xnew(4)=(g(1)*g(12)*g(6)*g(7)*k8*k9*xnew(1)*xnew(7)*xtot(3))/(g(2)*g(4)*g(6)*k2
*k8*xnew(2)*g(1)^2*xnew(1)^2 + g(12)*g(6)*k8*k9*g(1)*g(7)*xnew(1)*xnew(7) +
g(12)*g(4)*k9*g(7)^2*xnew(7)^2);
xnew(6)=xnew(4)*g(4)*xnew(7)*g(7)/(k8*xnew(1)*g(1)*g(6));
xnew(12)=xnew(4)*g(4)*xnew(8)*g(8)/(k9*xnew(1)*g(1)*g(12));
err=max(abs((xnew-x)/xnew));
x=xnew;
end
Alk=(x(2)+x(8)+x(9)+x(11)+x(12)+2*x(13)+x(14))*totmol/molamine
con=x.*totmol
PH=-log10(con(7))
%----------------- Faraday constant----------------
Fa=96485;
%-----------standard Gibbs free energy of reaction at T(K) (kJ/mole)
Gro(1)=T*((0/298)+0*(inv(T)-inv(298)));
Gro(2)=T*((118/298)+29.8*(inv(T)-inv(298)));
Gro(3)=T*((160/298)+109.5134*(inv(T)-inv(298)));
Gro(4)=T*((111.09/298)+ 85.78*(inv(T)-inv(298)));
Gro(5)=T*((101.364/298)+85.6*(inv(T)-inv(298)));
Gro(6)=T*((91.53/298)+89.1*(inv(T)-inv(298)));
%-----standard electrode potential at T (V) SCE -------------
Eo(1)=(-Gro(1)*1000/(2*Fa))-0.244;
Eo(2)=(-Gro(2)*1000/(2*Fa))-0.244;
Eo(3)=(-Gro(3)*1000/(2*Fa))-0.244;
Eo(4)=(-Gro(4)*1000/(2*Fa))-0.244;
Eo(5)=(-Gro(5)*1000/(2*Fa))-0.244;
Eo(6)=(-Gro(6)*1000/(2*Fa))-0.244;
%---------------- parameters ----------------------
MFe=55.845;
dFe=7874;
MFeco3=115.8;
dFeco3=3960;
rpm=600*0.104719755;
dia=0.005;
Ve=rpm*dia/2;
%------ Viscosity of solution at T -----------
Vir=[1.002e-3];
Vi(1)=Vir(1)*10^((1.3272*(293.15-T)-0.001053*(293.15-T)^2)/(T+105));
Re=ds*Ve*dia/Vi;
%----- initial concentration of Fe+2 in the bulk of solution -------
Imm=0.5*sum(con.*z.^2);
Ksp=10^(-59.3498-0.041377*T-2.1963/T+24.5724*log10(T)+2.518*(Imm)^0.5-
0.657*(Imm));
Iron=Ksp/con(9) ;
totmol2=totmol+Iron;
U=x.*totmol2;
U(15)=Iron;
%-----Diffusivity of species at any T m2/s ----------
```

```
Di(1)=9.31e-9*(T/298.15)*(Vir/Vi);
Di(2)=1.11e-9*(T/298.15)*(Vir/Vi);
Di(3)=1.0e-9*(T/298.15)*(Vir/Vi);
Di(4)=exp(-13.672-2160.9/T-19.263e-5*U(5));
Di(5)=exp(-13.268-2287.7/T-19.699e-5*U(6));
Di(6)=7.2e-10*(T/298.15)*(Vir/Vi);
%----- mass transfer coefficients  (m/sec)-----------
km(1)=0.0791*Re^0.7*(Vi/(ds))^0.356*Di(1)^0.644/dia;
km(2)=0.0791*Re^0.7*(Vi/(ds))^0.356*Di(2)^0.644/dia;
km(3)=0.0791*Re^0.7*(Vi/(ds))^0.356*Di(3)^0.644/dia
km(4)=0.0791*Re^0.7*(Vi/(ds))^0.356*Di(4)^0.644/dia;
km(5)=0.0791*Re^0.7*(Vi/(ds))^0.356*Di(5)^0.644/dia;
km(6)=0.0791*Re^0.7*(Vi/(ds))^0.356*Di(6)^0.644/dia;
%--------reversible electrode potential at any conc.(J/C=V)-------
Erev(1)=Eo(1)-((R*T)/(2*Fa))*log((U(1))^2/(U(7))^2);
Erev(2)=Eo(2)-((R*T)/(2*Fa))*log((U(9))^2/(U(8))^2);
Erev(3)=Eo(3)-((R*T)/(2*Fa))*log((U(10))^2/(U(1))^2);
Erev(4)=Eo(4)-((R*T)/(2*Fa))*log((U(3))^2/(U(5))^2);
Erev(5)=Eo(5)-((R*T)/(2*Fa))*log((U(4))^2/(U(6))^2);
Erev(6)=Eo(6)-((R*T)/(2*Fa))*log(1/(U(15)));
%---- limiting current density(diffusion current)(A/m2) --------
Ilim(1)=2e+3*Fa*km(1)*U(7);
Ilim(2)=2e+3*Fa*km(2)*U(8);
Ilim(3)=2e+3*Fa*km(3)*U(1);
Ilim(4)=2e+3*Fa*km(4)*U(5) ;
Ilim(5)=2e+3*Fa*km(5)*U(6) ;
Ilim(6)=2e+3*Fa*km(6)*U(15);
%---------exchange current density ( A/m2)  ---------------
Io(1)=0.05*sqrt(U(7)/1e-4)*exp((-30000/R)*(inv(T)-inv(298.15)));
Io(2)=0.15*sqrt(U(8)/0.5)*exp((-50000/R)*(1/T-1/323.15));
Io(3)=3e-5*sqrt(U(1)/55.5)*exp((-30000/R)*(1/T-1/293.15));
Io(4)=0.15*(U(5)/0.63)*exp((-20000/R)*(1/T-1/323.15));
Io(5)=0.15*(U(6)/0.63)*exp((-20000/R)*(1/T-1/323.15));
Io(6)=0.53*sqrt(10^(-9.1)/U(7))*(U(8))^2*exp((-40000/R)*(1/T-1/323.15)) ;
%--------------Tafel slope-------------------------
beta_ox=(R*T)/((0.0038*T - 0.6826)*Fa);
beta=(R*T)/((0.0025*T - 0.3325)*Fa);
%---------Calculate Ecorr & Icorr ----------------
Iex=-1 ;
Eapp=min(Erev);
while Iex <= 1e-6
   Eapp=Eapp+0.00001;
%---- Activation + Concentration polarization  A/m2 ---------------
Ic(1)=inv(inv((Io(1)*exp(-(Eapp-Erev(1))/beta)))+inv(Ilim(1)));
Ic(2)=inv(inv((Io(2)*exp(-(Eapp-Erev(2))/beta)))+inv(Ilim(2)));
Ic(3)=inv(inv((Io(3)*exp(-(Eapp-Erev(3))/beta)))+inv(Ilim(3)));
Ic(4)=inv(inv((Io(4)*exp(-(Eapp-Erev(4))/beta)))+inv(Ilim(4)));
Ic(5)=inv(inv((Io(5)*exp(-(Eapp-Erev(5))/beta)))+inv(Ilim(5)));
Ired=sum(Ic);
Iox=(Io(6)*exp((Eapp-Erev(6))/beta_ox));
Iex=Iox-Ired ;
```

```
end
Ecorr=Eapp;
Icorr=Iox
CR=1.155*(Icorr); % mm/yr.
AA(ii,1)=Pco2;
AA(ii,2)=PH;
AA(ii,3)=Alk;
AA(ii,4)=Ecorr;
AA(ii,5)=CR
end
%-----------------graph plotting-------------------------
% Figure 1~Iex vs Eapp
SR=0.0018;
E=[-1.1:SR:-0.5];
 for j=1:length(E)
 %----cathodic current for each reaction A/cm2 ---------------
Ic(1)=inv(inv((Io(1)*exp(-(E(j)-Erev(1))/beta)))+inv(Ilim(1)));
Ic(2)=inv(inv((Io(2)*exp(-(E(j)-Erev(2))/beta)))+inv(Ilim(2)));
Ic(3)=inv(inv((Io(3)*exp(-(E(j)-Erev(3))/beta)))+inv(Ilim(3)));
Ic(4)=inv(inv((Io(4)*exp(-(E(j)-Erev(4))/beta)))+inv(Ilim(4)));
Ic(5)=inv(inv((Io(5)*exp(-(E(j)-Erev(5))/beta)))+inv(Ilim(5)));
Ired=sum(Ic);
Iox=(Io(6)*exp((E(j)-Erev(6))/beta_ox));
Iex=Iox-Ired;

 BB(j,1)=E(j);
 BB(j,2)=abs(Iex);
 BB(j,3)=abs(Ired);
 BB(j,4)=abs(Iox);
 BB(j,5)=abs(Ic(1));
 BB(j,6)=abs(Ic(2));
 BB(j,7)=abs(Ic(3));
 BB(j,8)=abs(Ic(4));
 BB(j,9)=abs(Ic(5));
    end
y1=BB(:,1);
x1=log10(BB(:,2));
 x2=log10(BB(:,3));
x3=log10(BB(:,4));
x4=log10(BB(:,5));
x5=log10(BB(:,6));
x6=log10(BB(:,7));
x7=log10(BB(:,8));
x8=log10(BB(:,9));
figure (1)
plot(x1,y1,'.',x3,y1,'-.r',x4,y1,'-.m',x5,y1,'-.c',x6,y1,'-.b',x7,y1,'-.g',x8,y1,'-.k')
title('Potential applied vs. current density ')
legend('Iex','Fe+2','H3O+','HCO3-','H2O','PZH+','DEAH+')
xlabel('Log Iapp ( A/m2)')
ylabel('E(V) vs SCE')
```

APPENDIX B

COMPARISON BETWEEN PUBLISHED AND PREDICTED CO_2 LOADING IN AQUEOUS SOLUTIONS OF ACTIVATED MDEA AND ACTIVATED DEA

Table B.1: Comparison between published data from Liu et al. (1999) and predicted CO_2 loading in aqueous solution of 1.53 kmol/m3 MDEA + 0.17 kmol/m3 PZ at different temperature and pressure.

T(K)	P_{CO2} (kPa)	$\alpha_{CO_2 Exp.}$	$\alpha_{CO_2 Calc.}$	% Error
323.15	21.18	0.468	0.467	0.28
323.15	44	0.589	0.578	1.89
323.15	89.44	0.696	0.684	1.66
323.15	271.9	0.851	0.828	2.74
323.15	669.4	0.98	0.92	5.26
343.15	35.43	0.387	0.385	0.57
343.15	71.29	0.492	0.488	0.90
343.15	148.8	0.641	0.606	5.53
343.15	418.8	0.811	0.768	5.31
343.15	688.8	0.876	0.841	4.01

Table B.2: Comparison between published data from Liu et al. (1999) and predicted CO_2 loading in aqueous solution of 1.35 kmol/m3 MDEA + 0.35 kmol/m3 PZ at different temperature and pressure.

T(K)	P_{CO2} (kPa)	$\alpha_{CO_2 Exp.}$	$\alpha_{CO_2 Calc.}$	% Error
323.15	17.78	0.5	0.438	1.38
323.15	41.1	0.609	0.547	10.25
323.15	89.43	0.707	0.646	8.66
323.15	509.4	0.936	0.826	11.79
323.15	586.9	0.955	0.839	12.11
343.15	17.6	0.349	0.318	8.99
343.15	32.07	0.427	0.381	10.68
343.15	71.26	0.558	0.481	13.73
343.15	243.8	0.759	0.649	14.50
343.15	296.3	0.79	0.675	14.60

Table B.3: Comparison between published data from Liu et al. (1999) and predicted CO_2 loading in aqueous solution of 3.15 kmol/m3 MDEA + 0.35 kmol/m3 PZ at different temperature and pressure.

T(K)	P_{CO2} (kPa)	$\alpha_{CO_2 Exp.}$	$\alpha_{CO_2 Calc.}$	% Error
303.15	16.73	0.477	0.517	8.48
303.15	54.24	0.642	0.669	4.17
303.15	97.47	0.714	0.739	3.44
303.15	247.5	0.812	0.834	2.70
303.15	407.5	0.842	0.878	4.31
323.15	23.95	0.377	0.422	12.05
323.15	42.97	0.455	0.501	0.15
323.15	90.11	0.573	0.605	5.59
323.15	200.1	0.665	0.713	7.21
323.15	422.6	0.75	0.803	7.09
343.15	33.86	0.287	0.329	14.76
343.15	48.08	0.324	0.372	14.94
343.15	178	0.47	0.560	19.06
343.15	368	0.591	0.670	13.30
343.15	573	0.691	0.734	6.24
363.15	19.88	0.147	0.181	23.47
363.15	37.54	0.191	0.230	20.28
363.15	82.54	0.247	0.309	25.16
363.15	312.5	0.407	0.494	21.30
363.15	482.5	0.49	0.564	15.16

Table B.4: Comparison between published data from Liu et al. (1999) and predicted CO_2 loading in aqueous solution of 4.77 kmol/m3 MDEA + 0.53 kmol/m3 PZ at different temperature and pressure.

T(K)	P_{CO2} (kPa)	$\alpha_{CO_2 Exp.}$	$\alpha_{CO_2 Calc.}$	% Error
323.15	42.51	0.318	0.469	47.52
323.15	91.15	0.415	0.560	34.82
323.15	326.2	0.649	0.712	9.71
323.15	508.7	0.706	0.763	8.12
323.15	753.7	0.76	0.807	6.24
343.15	35.83	0.193	0.324	67.67
343.15	75.61	0.252	0.411	63.08
343.15	203.1	0.396	0.540	36.49
343.15	460.6	0.529	0.652	23.24
343.15	713.1	0.592	0.711	20.05

Table B.5: Comparison between published data from Liu et al. (1999) and predicted CO_2 loading in aqueous solution of 2.8 kmol/m3 MDEA + 0.7 kmol/m3 PZ at different temperature and pressure.

T(K)	P_{CO2} (kPa)	$\alpha_{CO_2 Exp.}$	$\alpha_{CO_2 Calc.}$	% Error
303.15	15.6	0.5	0.488	2.41
303.15	48.43	0.647	0.614	5.11
303.15	97.45	0.733	0.687	6.32
303.15	202.5	0.793	0.753	5.01
303.15	460	0.88	0.818	7.03
323.15	18.98	0.41	0.392	4.32
323.15	49.6	0.54	0.503	6.87
323.15	90.17	0.617	0.575	6.78
323.15	195.1	0.694	0.665	4.16
323.15	380.1	0.768	0.735	4.27
343.15	19.24	0.274	0.288	5.08
343.15	52.64	0.366	0.389	6.36
343.15	73.14	0.41	0.428	4.36
343.15	177.8	0.541	0.541	0.07
343.15	935.3	0.766	0.748	2.31
363.15	17.37	0.198	0.207	4.51
363.15	25.37	0.221	0.230	4.11
363.15	37.19	0.254	0.257	1.32
363.15	157.2	0.401	0.400	0.22
363.15	412.2	0.54	0.527	2.35

Table B.6: Comparison between published data from Liu *et al.* (1999) and predicted CO_2 loading in aqueous solution of 3.75 kmol/m^3 MDEA + 1.55 kmol/m^3 PZ at different temperature and pressure.

T(K)	P_{CO2} (kPa)	$\alpha_{CO_2 Exp.}$	$\alpha_{CO_2 Calc.}$	% Error
323.15	14.34	0.349	0.350	0.31
323.15	46.49	0.454	0.444	2.26
323.15	91.15	0.525	0.503	4.28
323.15	278.3	0.65	0.605	6.97
323.15	678.3	0.746	0.686	8.09
343.15	13.16	0.247	0 267	8.02
343.15	37.35	0.323	0.342	5.75
343.15	224.7	0.544	0.508	6.70
343.15	479.7	0.635	0.585	7.88
343.15	667.2	0.665	0.619	6.94

Table B.7: Comparison between published data from Jenab *et al.* (2005) and predicted CO_2 loading in aqueous solution of 3 kmol/m^3 MDEA + 0.36 kmol/m^3 PZ at different temperature and pressure.

T(K)	P_{CO2} (kPa)	$\alpha_{CO_2 Exp.}$	$\alpha_{CO_2 Calc.}$	% Error
313.15	33.99	0.4269	0.6027	41.17
313.15	73.98	0.63	0.7181	12.23
313.15	203.6	0.8365	0.8541	2.10
313.15	384.24	0.9148	0.9264	1.27
313.15	688.98	0.9686	0.9879	1.99
313.15	871.69	0.9872	1.0134	2.65
313.15	1030.27	0.9991	1.0325	3.34
313.15	1403.96	1.0364	1.0716	3.40
313.15	1810.74	1.0626	1.1094	4.41
313.15	2225.8	1.0935	1.1455	4.75
313.15	2869.07	1.1607	1.1987	3.27
313.15	3268.27	1.2067	1.2308	2.00
313.15	3850.87	1.2817	1.2770	0.37
328.15	42.95	0.2744	0.5172	88.49
328.15	95.35	0.4339	0.6422	48.02
328.15	102.94	0.4377	0.6544	49.50
328.15	220.84	0.6269	0.7719	23.13
328.15	357.35	0.7211	0.8403	16.53
328.15	601.42	0.8057	0.9084	12.74
328.15	845.49	0.8522	0.9507	11.56
328.15	1238.49	0.8979	0.9985	11.20
328.15	1641.82	0.9405	1.0362	10.17
328.15	1967.25	0.9727	1.0625	9.24
328.15	2452.63	1.0142	1.0982	8.28
328.15	2943.53	1.0552	1.1315	7.23
343.15	72.95	0.2823	0.4773	69.08
343.15	157.75	0.4286	0.6020	40.47
343.15	326.67	0.5893	0.7238	22.82
343.15	514.89	0.6889	0.7974	15.74
343.15	735.52	0.7603	0.8526	12.15
343.15	987.18	0.8085	0.8968	10.93
343.15	1245.73	0.8508	0.9314	9.47
343.15	1644.24	0.8909	0.9729	9.21
343.15	2014.48	0.9249	1.0044	8.60
343.15	2476.47	0.9462	1.0383	9.73
343.15	2922.5	0.9966	1.0674	7.11

Table B.8: Comparison between published data from Jenab *et al.* (2005) and predicted CO_2 loading in aqueous solution of 2.5 kmol/m^3 MDEA + 0.86 kmol/m^3 PZ at different temperature and pressure.

T(K)	P_{CO2} (kPa)	$\alpha_{CO_2 Exp.}$	$\alpha_{CO_2 Calc.}$	% Error
313.15	27.79	0.4268	0.6127	43.55
313.15	135.34	0.8063	0.8224	2.00
313.15	344.94	0.9426	0.9261	1.75
313.15	555.23	0.9903	0.9732	1.73
313.15	788.27	1.0234	1.0082	1.48
313.15	1059.23	1.0544	1.0402	1.34
313.15	1433.6	1.0842	1.0778	0.59
313.15	1825.91	1.1184	1.1133	0.46
313.15	2266.48	1.1607	1.1507	0.86
313.15	2810.47	1.2171	1.1952	1.80
313.15	3258.62	1.2606	1.2309	2.35
313.15	3938.43	1.3147	1.2843	2.31
313.15	27.79	0.4268	0.6127	43.55
328.15	38.82	0.3221	0.4420	37.21
328.15	106.38	0.529	0.5564	5.17
328.15	236	0.6854	0.6445	5.97
328.15	427.68	0.7846	0.7043	10.24
328.15	682.78	0.8516	0.7477	12.20
328.15	910.99	0.8821	0.7739	12.27
328.15	1281.92	0.9266	0.8059	13.02
328.15	1782.47	0.9746	0.8400	13.81
328.15	2108.59	0.9959	0.8594	13.70
328.15	2465.73	1.0258	0.8793	14.28
328.15	2990.42	1.0694	0.9070	15.19
328.15	38.82	0.3221	0.4420	37.21
343.15	41.23	0.2817	0.4622	64.08
343.15	99.83	0.45	0.5843	29.85
343.15	214.29	0.5896	0.6994	18.63
343.15	385.27	0.6968	0.7872	12.97
343.15	616.24	0.7769	0.8543	9.96
343.15	869.97	0.8284	0.9016	8.84
343.15	1276.75	0.8847	0.9534	7.77
343.15	1640.1	0.9073	0.9880	8.89
343.15	2014.48	0.9313	1.0176	9.27
343.15	2408.85	0.9545	1.0451	9.49
343.15	3023.17	1.0142	1.0832	6.80

Table B.9: Comparison between published data from Jenab *et al.* (2005) and predicted CO_2 loading in aqueous solution of 2.0 kmol/m^3 MDEA + 1.36 kmol/m^3 PZ at different temperature and pressure.

T(K)	P_{CO2} (kPa)	$\alpha_{CO_2 Exp.}$	$\alpha_{CO_2 Calc.}$	% Error
313.15	30.54	0.5611	0.6603	17.68
313.15	120.17	0.8261	0.8273	0.15
313.15	284.96	0.9588	0.9182	4.23
313.15	553.85	1.0131	0.9802	3.25
313.15	783.44	1.0547	1.0131	3.94
313.15	1152.99	1.023	1.0542	3.05
313.15	1703.87	1.1516	1.10	4.02
313.15	2063.09	1.195	1.1360	4.94
313.15	2495.38	1.2285	1.1716	4.63
313.15	2688.43	1.2561	1.1872	5.49
313.15	3168.99	1.2976	1.2254	5.56
313.15	3673.68	1.3613	1.2650	7.08
313.15	30.54	0.5611	0.6603	17.68
328.15	45.71	0.4597	0.6231	35.54
328.15	115.35	0.613	0.7437	21.33
328.15	233.25	0.7235	0.8323	15.04
328.15	535.23	0.8481	0.9262	9.21
328.15	750.34	0.8872	0.9619	8.42
328.15	1017.86	0.9273	0.9944	7.24
328.15	1306.74	0.9613	1.0225	6.36
328.15	1736.28	0.985	1.0576	7.37
328.15	2092.04	1.0064	1.0835	7.66
328.15	2548.64	1.0394	1.1145	7.23
328.15	2987.66	1.0675	1.1428	7.05
328.15	45.71	0.4597	0.6231	35.54
343.15	51.57	0.3811	0.5510	44.59
343.15	144.65	0.5603	0.6867	22.55
343.15	336.32	0.7202	0.8016	11.30
343.15	589.35	0.7929	0.8742	10.25
343.15	832.05	0.8354	0.9169	9.76
343.15	1311.22	0.9025	0.9729	7.80
343.15	1786.96	0.9359	1.0128	8.22
343.15	2149.61	0.9603	1.0384	8.13
343.15	2521.24	0.9817	1.0620	8.18
343.15	2996.97	1.025	1.0900	6.34
343.15	51.57	0.3811	0.5510	44.59

Table B.10: Comparison between published data from Brahim Si Ali (2007) and predicted CO_2 loading in aqueous solution of 2M MDEA at different temperature and pressure.

T(K)	P_{CO2} (kPa)	$\alpha_{CO_2 Exp.}$	$\alpha_{CO_2 Calc.}$	% Error
313.15	0.0963	0.0848	0.049	42.02
313.15	0.9595	0.1505	0.154	2.54
313.15	9.5612	0.4139	0.419	1.27
313.15	47.7218	0.7315	0.690	5.66
313.15	95.6116	0.8834	0.800	9.44
333.15	0.0836	0.0547	0.023	57.19
333.15	0.8307	0.0896	0.077	13.81
333.15	8.3073	0.2225	0.243	9.38
333.15	41.4526	0.4623	0.476	2.96
333.15	82.9052	0.6292	0.600	4.67
353.15	0.08	0.0299	0.012	60.51
353.15	0.5514	0.061	0.033	46.12
353.15	5.5475	0.1422	0.113	20.82
353.15	27.5697	0.24	0.252	4.99
353.15	55.4754	0.3413	0.346	1.47

Table B.11: Comparison between published data from Brahim Si Ali (2007) and predicted CO_2 loading in aqueous solution of 1.98M MDEA + 0.01M PZ at different temperature and pressure.

T(K)	P_{CO2} (kPa)	$\alpha_{CO_2 Exp.}$	$\alpha_{CO_2 Calc.}$	% Error
313.15	0.0961	0.088	0.051	41.59
313.15	0.9544	0.135	0.157	15.81
313.15	9.5444	0.404	0.420	4.10
313.15	47.5538	0.745	0.687	7.66
313.15	95.2756	0.858	0.796	7.29
333.15	0.0831	0.061	0.025	59.15
333.15	0.8307	0.086	0.079	.07
333.15	8.2569	0.231	0.245	5.91
333.15	41.2006	0.486	0.475	2.08
333.15	83.0731	0.632	0.599	5.14
353.15	0.056	0.057	0.010	81.86
353.15	0.5615	0.086	0.035	59.73
353.15	5.5475	0.113	0.115	0.98
353.15	27.5697	0.252	0.254	0.76
353.15	55.3075	0.353	0.347	1.63

Table B.12: Comparison between published data from Brahim Si Ali (2007) and predicted CO_2 loading in aqueous solution of 1.9M MDEA + 0.05M PZ at different temperature and pressure.

T(K)	P_{CO2} (kPa)	$\alpha_{CO_2 Exp.}$	$\alpha_{CO_2 Calc.}$	% Error
313.15	0.0958	0.095	0.060	36.93
313.15	0.9544	0.172	0.167	2.83
313.15	9.578	0.440	0.425	3.23
313.15	47.5538	0.752	0.679	9.73
313.15	95.7796	0.818	0.782	4.37
333.15	0.0829	0.064	0.030	52.60
333.15	0.8324	0.091	0.087	4.0
333.15	8.2905	0.247	0.253	2.46
333.15	41.2846	0.477	0.477	0.03
333.15	83.2411	0.625	0.596	4.64
353.15	0.0555	0.050	0.013	74.42
353.15	0.5531	0.059	0.040	33.03
353.15	5.5475	0.133	0.122	8.24
353.15	27.4858	0.232	0.260	12.28
353.15	55.6434	0.346	0.353	2.14

Table B.13: Comparison between published data from Brahim Si Ali (2007) and predicted CO_2 loading in aqueous solution of 1.8M MDEA + 0.1M PZ at different temperature and pressure.

T(K)	P_{CO2} (kPa)	$\alpha_{CO_2 Exp.}$	$\alpha_{CO_2 Calc.}$	% Error
313.15	0.0959	0.098	0.071	27.09
313.15	0.9511	0.183	0.180	1.96
313.15	9.5948	0.457	0.431	5.70
313.15	47.6378	0.712	0.669	6.11
313.15	95.7796	0.821	0.764	7.00
333.15	0.0836	0.066	0.037	43.23
333.15	0.8341	0.115	0.098	14. 3
333.15	8.3073	0.233	0.262	12.34
333.15	41.4526	0.487	0.479	1.64
333.15	83.409	0.604	0.592	1.93
353.15	0.0559	0.060	0.016	73.25
353.15	0.5548	0.067	0.046	30.50
353.15	5.5811	0.145	0.132	8.85
353.15	27.7377	0.267	0.269	0.85
353.15	55.4754	0.357	0.358	0.35

Table B.14: Comparison between published data from Vahidi *et al.* (2009) and predicted CO_2 loading in aqueous solution of 2 kmol/m^3 MDEA + 1.36 kmol/m^3 PZ at different temperature and pressure.

T(K)	P_{CO2} (kPa)	$\alpha_{CO_2 Exp.}$	$\alpha_{CO_2 Calc.}$	% Error
313.15	30.5	0.56	0.66	17.88
313.15	120.2	0.83	0.82	0.32
313.15	285	0.96	0.91	4.35
313.15	553.9	1.01	0.98	2.95
313.15	783.4	1.05	1.01	3.51
313.15	1153	1.08	1.05	2.39
313.15	1703	1.15	1.10	3.8
313.15	2063	1 2	1.13	5.33
313.15	2495	1.23	1.17	4.75
313.15	2688.4	1.26	1.18	5.78
313.15	3169	1.3	1.22	5.74
313.15	3673	1.36	1.26	6.99
328.15	45.7	0.46	0.62	35.45
328.15	115.4	0.61	0.74	21.93
328.15	233.3	0.72	0.83	15.61
328.15	535.2	0.85	0.92	8.96
328.15	750.3	0.89	0.96	8.08
328.15	1017.9	0.93	0.99	6.92
328.15	1306.7	0.96	1.02	6.51
328.15	1736.3	0.99	1.05	6.83
328.15	2092	1.01	1.08	7.28
328.15	2548.6	1.04	1.11	7.16
328.15	2987.7	1.07	1.14	6.80
343.15	51.6	0.38	0.55	45.03
343.15	144.7	0.56	0.68	22.62
343.15	336.3	0.72	0.80	11.33
343.15	589.4	0.79	0.87	10.66
343.15	832.1	0.84	0.91	9.16
343.15	1311.2	0.9	0.97	8.10
343.15	1787	0.94	1.01	7.74
343.15	2149.6	0.96	1.03	8.16
343.15	2521.2	0.98	1.06	8.37
343.15	2997	1.03	1.09	5.83

Table B.15: Comparison between published data from Vahidi *et al.* (2009) and predicted CO_2 loading in aqueous solution of 2.5 kmol/m^3 MDEA + 0.86 kmol/m^3 PZ at different temperature and pressure.

T(K)	P_{CO2} (kPa)	$\alpha_{CO_2 Exp.}$	$\alpha_{CO_2 Calc.}$	% Error
313.15	27.8	0.43	0.61	42.49
313.15	135.3	0.81	0.82	1.53
313.15	344.9	0.94	0.92	1.48
313.15	555.2	0.99	0.97	1.70
313.15	788.3	1.02	1.00	1.15
313.15	1059.2	1.05	1.04	0.93
313.15	1433.6	1.08	1.07	0.20
313.15	1825.9	1.12	1.11	0.60
313.15	2266.5	1.16	1.15	0.80
313.15	2810.5	1.22	1.19	2.03
313.15	3258.6	1.26	1.23	2.31
313.15	3938.4	1.31	1.28	1.96
328.25	38.8	0.32	0.55	73.23
328.25	106.4	0.53	0.69	31.72
328.25	236	0.69	0.80	17.23
328.25	427.7	0.78	0.88	13.34
328.25	682.8	0.85	0.93	10.43
328.25	911	0.88	0.97	10.41
328.25	1281.9	0.93	1.01	8.80
328.25	1782.5	0.97	1.05	8.72
328.25	2108.6	1	1.07	7.90
328.25	2465.7	1.03	1.10	7.19
328.25	2990.4	1.07	1.13	6.42
343.15	41.2	0.28	0.46	65.04
343.15	99.8	0.45	0.58	29.84
343.15	214.3	0.59	0.69	18.55
343.15	385.3	0.7	0.78	12.46
343.15	616.2	0.78	0.85	9.52
343.15	870	0.83	0.90	8.63
343.15	1276.8	0.88	0.95	8.34
343.15	1640.1	0.91	0.98	8.57
343.15	2014.5	0.93	1.01	9.42
343.15	2408.9	0.95	1.04	10.01
343.15	3023.2	1.01	1.08	7.25

Table B.16: Comparison between published data from Vahidi *et al.* (2009) and predicted CO_2 loading in aqueous solution of 3 kmol/m^3 MDEA + 0.36 kmol/m^3 PZ at different temperature and pressure.

T(K)	P_{CO2} (kPa)	$\alpha_{CO_2 Exp.}$	$\alpha_{CO_2 Calc.}$	% Error
313.15	34	0.43	0.54	26.36
313.15	74	0.64	0.64	1.19
313.15	203.6	0.84	0.77	8.25
313.15	384.2	0.91	0.83	8.11
313.15	689	0.97	0.89	8.06
313.15	871.7	0.99	0.91	7.59
313.15	1030.3	1	0.93	6.79
313.15	1404	1.04	0.96	6.98
313.15	1810.7	1.06	1.00	5.52
313.15	2225.8	1.09	1.03	5.14
313.15	2869.1	1.16	1.08	6.73
313.15	3268.3	1.21	1.11	8.19
313.15	3850.9	1.28	1.15	9.96
328.15	43	0.34	0.46	37.45
328.15	95.4	0.43	0.58	34.92
328.15	102.9	0.44	0.59	34.32
328.15	220.8	0.63	0.69	10.66
328.15	357.4	0.72	0.75	5.42
328.15	601.4	0.81	0.82	1.29
328.15	845.5	0.85	0.85	1.02
328.15	1238.5	0.9	0.90	0.21
328.15	1641.8	0.94	0.93	0.44
328.15	1967.3	0.97	0.96	1.06
328.15	2452.6	1.01	0.99	1.79
328.15	2943.5	1.06	1.02	3.58
343.15	36	0.28	0.34	21.29
343.15	157.8	0.43	0.54	26.47
343.15	326.7	0.59	0.65	10.80
343.15	514.9	0.69	0.72	4.38
343.15	735.5	0.76	0.77	1.33
343.15	987.2	0.81	0.81	0.01
343.15	1245.7	0.85	0.84	1.03
343.15	1644.2	0.89	0.87	1.26
343.15	2014.5	0.92	0.90	1.39
343.15	2476.5	0.95	0.93	1.28
343.15	2922.5	1	0.96	3.59

Table B.17: Comparison between published data from Derks *et al.* (2010) and predicted CO_2 loading in aqueous solution of 2.8 kmol/m^3 MDEA + 0.7 kmol/m^3 PZ at different temperature and pressure.

T(K)	P_{CO2} (kPa)	$\alpha_{CO_2 Exp.}$	$\alpha_{CO_2 Calc.}$	% Error
303	0.51	0.208	0.241	15.6
303	0.96	0.252	0.284	12.81
303	1.75	0.303	0.335	10.47
303	2.61	0.348	0.373	7.26
303	4.16	0.399	0.423	6.02
303	5.23	0.435	0.449	3.26
303	6.8	0.468	0.481	2.67
303	8.65	0.513	0.510	.53
303	10.2	0.537	0.531	1.08
303	9.4	0.518	0.521	0.54
303	10.7	0.523	0.537	2.74
303	15.2	0.573	0.583	1.78
303	25.7	0.664	0.653	1.60
303	36.1	0.681	0.699	2.63
303	32.1	0.689	0.683	0.84
303	38.9	0.708	0.709	0.12
303	56.4	0.758	0.757	0.08
303	73.7	0.79	0.791	0.14
303	70.4	0.784	0.785	0.18
303	93.8	0.818	0.820	0.28
303	96.9	0.815	0.824	1.12
303	100.1	0.837	0.828	1.08
323	0.68	0.127	0.158	24.67
323	1.05	0.155	0.175	13.16
323	2	0.19	0.207	9.03
323	3.19	0.233	0.236	1.15
323	4.68	0.255	0.263	3.10
323	6.99	0.31	0.295	4.76
323	8.37	0.323	0.311	3.70
323	19.7	0.418	0.396	5.18
323	32.8	0.483	0.454	6.03
323	45.8	0.541	0.493	8.81
323	60.3	0.584	0.527	9.85
323	69.5	0.61	0.544	10.87
323	84	0.636	0.567	10.91
323	94.5	0.657	0.581	11.60

Table B.18: Comparison between published data from Derks *et al.* (2010) and predicted CO_2 loading in aqueous solution of 0.5 kmol/m^3 MDEA + 1.5 kmol/m^3 PZ at different temperature and pressure.

T(K)	P_{CO2} (kPa)	$\alpha_{CO_2 Exp.}$	$\alpha_{CO_2 Calc.}$	% Error
298	0.25	0.502	0.471	6.19
298	1.02	0.64	0.551	13.96
298	1. 5	0.675	0.582	13.71
298	7.15	0.807	0.727	9.89
298	9.02	0.826	0.752	9.02
298	10.6	0.843	0.768	8.84
298	26.8	0.906	0.861	4.95
298	29.1	0.909	0.869	.44
298	53.7	0.943	0.920	2.48
298	81.1	0.965	0.949	1.67
298	80.1	0.967	0.948	1.96
298	102	0.978	0.964	1.45
298	110	0.984	0.969	1.57
313	0.45	0.465	0.466	0.26
313	1.38	0.555	0.525	5.42
313	3.76	0.649	0.601	7.47
313	9.24	0.74	0.686	7.24
313	8.1	0.731	0.673	7.93
313	9.7	0.749	0.691	7.68
313	20.1	0.817	0.769	5.90
313	36.9	0.865	0.832	3.78
313	38.8	0.87	0.837	3.76
313	59.2	0.9	0.878	2.48
313	64.1	0.906	0.885	2.33
313	79.8	0.921	0.904	1.86
313	80.8	0.923	0.905	1.96
313	96	0.934	0.919	1.60
313	98.8	0.936	0.921	1.57

Table B.19: Comparison between published data from Derks *et al.* (2010) and predicted CO_2 loading in aqueous solution of 4 kmol/m^3 MDEA + 0.6 kmol/m^3 PZ at different temperature and pressure.

T(K)	P_{CO2} (kPa)	$\alpha_{CO_2 Exp.}$	$\alpha_{CO_2 Calc.}$	% Error
313	0.72	0.123	0.169	37.76
313	0.9	0.126	0.181	43.80
313	2.07	0.178	0.234	3.50
313	2.7	0.189	0.254	34.43
313	4.36	0.232	0.294	26.67
313	5.24	0.25	0.310	24.15
313	7	0.283	0.338	19.31
313	7.33	0.284	0.342	20.47
313	9.38	0.31	0.367	18.29
313	8.65	0.312	0.359	14.91
313	12.6	0.327	0.397	21.50
313	12.8	0.339	0.399	17.69
313	25.3	0.426	0.474	11.22
313	39	0.498	0.523	5.09
313	39	0.504	0.523	3.84
313	58.4	0.568	0.57	0.41
313	60.4	0.578	0.574	0.65
313	78.5	0.621	0.605	2.61
313	80	0.632	0.607	3.95
313	89.7	0.638	0.620	2.77

Table B.20: Comparison between published data from Brahim Si Ali (2007) and predicted CO_2 loading in aqueous solution of 1M PZ at different temperature and pressure.

T(K)	P_{CO2} (kPa)	$\alpha_{CO_2 Exp.}$	$\alpha_{CO_2 Calc.}$	% Error
313.15	0.965	0.392	0.334	14.82
313.15	9.578	0.489	0.441	9.86
313.15	47.386	0.539	0.488	9.2
313.15	95.108	0.50	0.502	0.41
333.15	0.836	0.303	0.269	11.39
333.15	8.341	0.416	0.399	4.08
333.15	41.201	0.483	0.468	3.05
333.15	82.737	0.517	0.487	5.73
353.15	0.555	0.166	0.152	8.42
353.15	5.598	0.313	0.310	0.76
353.15	27.234	0.437	0.417	4.68
353.15	55.139	0.469	0.452	3.66

Table B.21: Comparison between published data from Najibi & Maleki (2013) and predicted CO_2 loading in aqueous solution of 2.0 kmol/m^3 MDEA + 0.3 kmol/m^3 PZ at different temperature and pressure.

T(K)	P_{CO2} (kPa)	$\alpha_{CO_2 Exp.}$	$\alpha_{CO_2 Calc.}$	% Error
363.15	32.6	0.221	0.244	10.51
363.15	48.3	0.263	0.281	6.66
363.15	73.1	0.312	0.325	4.17
363.15	87.4	0.331	0.346	4.59
363.15	152.2	0.384	0.419	9.23
363.15	189.3	0.402	0.451	12.21
383.15	28.5	0.176	0.169	.19
383.15	62.3	0.261	0.215	17.46
383.15	86.1	0.282	0.241	14.69
383.15	100.2	0.296	0.254	14.28
383.15	130.1	0.318	0.278	12.43
383.15	196.1	0.346	0.323	6.62
403.15	33.1	0.129	0.139	7.48
403.15	51.2	0.164	0.154	6.39
403.15	72.2	0.192	0.168	12.50
403.15	95	0.218	0.182	16.63
403.15	117.3	0.23	0.194	15.73
403.15	177	0.258	0.222	14.05
403.15	204	0.271	0.233	14.07
423.15	27.3	0.079	0.117	48.21
423.15	46.8	0.117	0.127	8.63
423.15	68.8	0.133	0.136	2.25
423.15	99.2	0.168	0.146	12.83
423.15	112	0.172	0.150	12.52
423.15	141.1	0.188	0.159	15.41

Table B.22: Comparison between published data from Najibi & Maleki (2013) and predicted CO_2 loading in aqueous solution of 3.0 kmol/m^3 MDEA + 0.3 kmol/m^3 PZ at different temperature and pressure.

T(K)	P_{CO2} (kPa)	$\alpha_{CO_2 Exp.}$	$\alpha_{CO_2 Calc.}$	% Error
363.15	32.6	0.221	0.244	10.51
363.15	48.3	0.263	0.281	6.66
363.15	73.1	0.312	0.325	4.17
363.15	87.4	0.331	0.346	4.59
363.15	152.2	0. 84	0.419	9.23
363.15	189.3	0.402	0.451	12.21
383.15	28.5	0.176	0.169	4.19
383.15	62.3	0.261	0.215	17.46
383.15	86.1	0.282	0.241	14.69
383.15	100.2	0.296	0.254	14.28
383.15	130.1	0.318	0.278	12.43
383.15	196.1	0.346	0.323	6.62
403.15	33.1	0.129	0.139	7.48
403.15	51.2	0.164	0.154	6.39
403.15	72.2	0.192	0.168	12.50
403.15	95	0.218	0.182	16.63
403.15	117.3	0.23	0.194	15.73
403.15	177	0.258	0.222	14.05
403.15	204	0.271	0.233	14.07
423.15	27.3	0.079	0.117	48.21
423.15	46.8	0.117	0.127	8.63
423.15	68.8	0.133	0.136	2.25
423.15	99.2	0.168	0.146	12.83

Table B.23: Comparison between published data from Najibi & Maleki (2013) and predicted CO_2 loading in aqueous solution of 1.6 kmol/m^3 MDEA + 0.7 kmol/m^3 PZ at different temperature and pressure.

T(K)	P_{CO2} (kPa)	$\alpha_{CO_2 Exp.}$	$\alpha_{CO_2 Calc.}$	% Error
363.15	35.3	0.349	0.296	15.16
363.15	63	0.432	0.342	20.81
363.15	91.2	0.491	0.376	23.36
363.15	112.4	0.532	0.397	25.33
363.15	146	0.601	0.425	29.27
363.15	204.3	0.65	0.463	28.76
383.15	30.3	0.242	0.238	1.52
383.15	52.3	0.294	0.265	9.78
383.15	80.6	0.349	0.291	16.62
383.15	102.1	0.383	0.307	19.82
383.15	186	0.463	0.355	23.25
403.15	26.3	0.166	0.210	26.25
403.15	41.3	0.207	0.224	8.20
403.15	50.4	0.225	0.231	2.59
403.15	67.3	0.249	0.242	3.00
403.15	89.5	0.275	0.253	7.94
403.15	111.3	0.308	0.263	14.61
403.15	176.3	0.34	0.287	15.56
423.15	31.4	0.163	0.203	24.25
423.15	52.6	0.208	0.216	3.84
423.15	78.9	0.225	0.227	0.93
423.15	110	0.231	0.237	2.52
423.15	152	0.258	0.247	4.16

Table B.24: Comparison between published data from Dash & Bandyopadhyay (2016) and predicted CO_2 loading in aqueous solution of 50 mass% MDEA at different temperature and pressure.

T(K)	P_{CO2} (kPa)	$\alpha_{CO_2 Exp.}$	$\alpha_{CO_2 Calc.}$	% Error
31	32.05	0.3946	0.5026	27.37
313	103.81	0.5966	0.6054	1.49
313	279.71	0.7758	0.7016	9.57
313	344.78	0.8346	0.7236	13.30
313	547.30	0 9132	0.7748	15.16
313	670.26	0.9571	0.7983	16.59
323	71.34	0.4373	0.5273	20.58
323	141.44	0.5484	0.5926	8.07
323	262.27	0.7004	0.6544	6.57
323	359.05	0.7698	0.6875	10.68
323	463.41	0.8307	0.7155	13.87
323	537.50	0.8610	0.7321	14.96
323	653.51	0.9078	0.7547	16.87
323	681.29	0.9128	0.7595	16.79
323	725.27	0.9157	0.7669	16.25
333	18.62	0.2044	0.2107	3.07
333	44.61	0.2875	0.2779	3.35
333	86.19	0.4107	0.3369	17.98
333	157.89	0.5614	0.3975	29.19
333	293.58	0.6892	0.4661	32.38
333	457.88	0.8037	0.5193	35.39
333	550.34	0.8451	0.5424	35.82

Table B.25: Comparison between published data from Dash & Bandyopadhyay (2016) and predicted CO_2 loading in aqueous solution of 48 mass% MDEA + 2 mass% PZ at different temperature and pressure.

T(K)	P_{CO2} (kPa)	$\alpha_{CO_2 Exp.}$	$\alpha_{CO_2 Calc.}$	% Error
313	8.13	0.2582	0.4262	65.05
313	23.99	0.3843	0.5127	33.42
313	50.04	0.4677	0.5688	21.60
313	115.25	0.6290	0.6344	0.85
313	257.79	0.7853	0 7034	10.44
313	489.87	0.9078	0.7637	15.87
313	523.1	0.9207	0.7702	16.35
313	878.89	1.0 39	0.8233	17.99
313	949.14	1.0248	0.8315	18.86
313	1052.54	1.0302	0.8428	18.20
313	1329.63	1.0511	0.8689	17.34
323	13.10	0.2624	0.4103	56.36
323	56.25	0.4253	0.5369	26.24
323	84.64	0.5005	0.5710	14.09
323	216.92	0.6645	0.6521	1.86
323	432.53	0.8321	0.7163	13.92
323	523.17	0.8923	0.7350	17.63
323	636.49	0.9078	0.7547	16.86
323	672.05	0.9182	0.7602	17.21
323	1029.83	0.9939	0.8053	18.97
323	1244.21	1.0302	0.8262	19.80
333	41.36	0.3205	0.4590	43.23
333	90.99	0.4097	0.5329	30.08
333	173.70	0.5193	0.5927	14.13
333	244.01	0.6316	0.6245	1.11
333	353.60	0.6917	0.6601	4.57
333	473.54	0.7724	0.6890	10.79
333	676.19	0.8321	0.7254	12.82
333	868.50	0.9262	0.7520	18.81
333	1122.85	0.9730	0.7801	19.82
333	1364.79	0.9884	0.8022	18.84

Table B.26: Comparison between published data from Dash & Bandyopadhyay (2016) and predicted CO_2 loading in aqueous solution of 45 mass% MDEA + 5 mass% PZ at different temperature and pressure.

T(K)	P_{CO2} (kPa)	$\alpha_{CO_2 Exp.}$	$\alpha_{CO_2 Calc.}$	% Error
313	10.34	0.344	0.50373	46.19
313	28.19	0.4430	0.56859	28.36
313	71.27	0.5847	0.62672	7.19
313	125.31	0.7047	0.66337	5.86
313	147.73	0.7465	0.67440	9.65
313	224.71	0.8142	0.70333	13.61
313	85.91	0.8610	0. 2050	16.32
313	407.37	0.9078	0.74653	17.76
313	538.54	0.9546	0.76778	19.57
313	602.64	0.9730	0.77654	20.19
313	671.98	0.9859	0.78515	20.36
313	781.65	1.0014	0.79732	20.38
313	1058.74	1.0457	0.82276	21.32
313	1298.61	1.0616	0.84087	20.79
323	12.41	0.3153	0.46762	48.31
323	41.84	0.4482	0.55685	24.24
323	118.83	0.6170	0.62907	1.96
323	139.44	0.6479	0.64027	1.17
323	213.68	0.7310	0.67071	8.25
323	322.52	0.8012	0.70106	12.50
323	382.69	0.8326	0.71401	14.24
323	417.71	0.8530	0.72073	15.51
323	458.37	0.8764	0.72791	16.95
323	481.95	0.8819	0.73183	17.01
323	557.36	0.9103	0.74328	18.35
323	713.96	0.9625	0.76325	20.70
323	899.52	0.9909	0.78248	21.04
323	1195.22	1.0377	0.80716	22.22
323	1358.58	1.0511	0.81875	22.11
333	49.46	0.3842	0.52630	37.00
333	76.51	0.4548	0.56035	23.21
333	591.41	0.8426	0.71985	14.57
333	678.26	0.8714	0.73128	16.08
333	7779.58	0.8973	1.02122	13.81
333	1091.83	0.9675	0.77249	20.16
333	1220.04	0.9859	0.78251	20.63
333	1327.56	1.0014	0.79027	21.08

Table B.27: Comparison between published data from Dash & Bandyopadhyay (2016) and predicted CO_2 loading in aqueous solution of 42 mass% MDEA + 8 mass% PZ at different temperature and pressure.

T(K)	P_{CO2} (kPa)	$\alpha_{CO_2 Exp.}$	$\alpha_{CO_2 Calc.}$	% Error
313	7.93	0.3764	0.5344	41.98
313	8.96	0.3948	0.5416	37.17
313	14.75	0.4535	0.5694	25.55
313	42.32	0.5708	0.6233	9.20
313	128.89	0.7608	0.6789	10.76
313	347.95	0.9176	0.7313	20.30
313	523.17	0.9640	0.7544	21.79
313	589.13	0.9785	0.7614	22.19
313	1007.04	1.0255	0.7956	22.42
313	1048.40	1.0349	0.7984	22.85
313	1300.68	1.0583	0.8141	23.07
313	1368.92	1.0654	0.8181	23.21
323	12.34	0.3540	0.5157	45.69
323	13.92	0.3660	0.5238	43.11
323	22.88	0.4190	0.5555	32.56
323	57.28	0.5357	0.6092	13.71
323	152.95	0.7052	0.6639	5.86
323	309.97	0.8240	0.7039	14.57
323	424.05	0.8770	0.7224	17.63
323	525.23	0.9128	0.7353	19.44
323	664.19	0.9399	0.7499	20.21
323	688.59	0.9546	0.7522	21.20
323	1015.32	0.9960	0.7781	21.88
323	1112.50	1.0107	0.7845	22.38
323	1426.82	1.0502	0.8030	23.54
333	20.40	0.3190	0.5023	57.45
333	23.99	0.3381	0.5142	52.11
333	36.33	0.3608	0.5437	50.69
333	89.54	0.4935	0.6030	22.20
333	210.65	0.6089	0.6562	7.78
333	269.51	0.6463	0.6715	3.90
333	346.02	0.7065	0.6872	2.73
333	406.06	0.7255	0.6973	3.89
333	629.46	0.8379	0.7257	13.39
333	743.05	0.8546	0.7368	13.79
333	749.18	0.8678	0.7373	15.04
333	1133.46	0.9874	0.7664	22.38
333	1329.91	1.0042	0.7783	22.49

Table B.28: Comparison between published data from Dash & Bandyopadhyay (2016) and predicted CO_2 loading in aqueous solution of 30 mass% MDEA at different temperature and pressure.

T(K)	P_{CO2} (kPa)	$\alpha_{CO_2 Exp.}$	$\alpha_{CO_2 Calc.}$	% Error
303	1.99	0.1779	0.2580	45.03
303	6.42	0.2587	0.4001	54.66
303	7.44	0.3269	0.4204	28.62
303	7.02	0.3573	0.4123	15.40
303	18.09	0.4638	0.5500	18.57
303	18.73	0.5646	0.5552	1.66
303	55.42	0.678	0.7172	5.78
303	34.0	0.7006	0.6454	7.88
303	49.64	0.7846	0.7012	10.62
303	92.60	0.7856	0.7886	0.38
303	102.91	0.8271	0.8025	2.98
303	76.05	0.8616	0.7619	11.57
303	95.01	0.9000	0.7920	12.00
303	623.51	0.9794	1.0007	2.17
313	2.91	0.1166	0.2326	99.46
313	8.68	0.2742	0.3609	31.64
313	11.46	0.2926	0.3991	36.41
313	19.53	0.3950	0.4773	20.84
313	28.59	0.4779	0.5360	12.17
313	47.50	0.5955	0.6158	3.41
313	66.81	0.6716	0.6691	0.37
313	61.90	0.6717	0.6572	2.16
313	82.25	0.7159	0.70	2.09
313	88.09	0.7620	0.7113	6.65
313	109.32	0.8391	0.7435	11.40
313	232.97	1.0089	0.8474	16.01
313	305.62	1.1997	0.8809	26.57
313	426.11	1.4036	0.9197	34.48
323	1.31	0.0602	0.1199	99.20
323	8.64	0.1334	0.2859	114.35
323	14.63	0.2621	0.3535	34.87
323	24.49	0.3490	0.4277	22.57
323	36.47	0.4306	0.4895	13.67
323	52.01	0.5088	0.5466	7.44
323	62.3	0.5639	0.5770	2.32
323	74.54	0.6088	0.6055	0.53
323	250.83	0.7325	0.7960	8.68
323	595.60	0.8351	0.9122	9.24
323	719.39	1.0071	0.9357	7.09
323	1039.90	1.1959	0.9811	17.96
323	1238.41	1.3607	1.0032	26.27
323	1306.65	1.4277	1.0102	29.24

Table B.29: Comparison between published data from Dash & Bandyopadhyay (2016) and predicted CO_2 loading in aqueous solution of 28 mass% MDEA + 2 mass% PZ at different temperature and pressure.

T(K)	P_{CO2} (kPa)	$\alpha_{CO_2 Exp.}$	$\alpha_{CO_2 Calc.}$	% Error
303	3.29	0.3182	0.3535	11.09
303	5.62	0.3764	0.4170	10.80
303	7.80	0.4446	0.4589	3.22
303	14.69	0.5575	0.5444	2.36
303	28.91	0.6879	0.6 94	7.04
303	69.09	0.8431	0.7594	9.92
303	88.93	0.8787	0.7922	9.85
303	101.77	0.8937	0.8091	9.47
313	1.85	0.1613	0.2363	46.48
313	10.55	0.3568	0.4236	18.73
313	28.86	0.5297	0.5638	6.44
313	44.97	0.6128	0.6289	2.63
313	63.37	0.6773	0.6792	0.28
313	80.31	0.7209	0.7133	1.05
313	91.70	0.7443	0.7322	1.62
323	5.59	0.2248	0.2815	25.20
323	19.54	0.3847	0.4306	11.95
323	36.66	0.4917	0.5208	5.91
323	45.32	0.543	0.5526	1.75
323	60.55	0.5973	0.5968	0.09
323	105.53	0.6670	0.6817	2.21
323	472.77	0.8857	0.8897	0.46
323	685.55	0.9898	0.9343	5.60
323	681.41	0.9976	0.9336	6.42
323	904.74	1.0843	0.9670	10.82
323	1066.03	1.2844	0.9865	23.19

Table B.30: Comparison between published data from Dash & Bandyopadhyay (2016) and predicted CO_2 loading in aqueous solution of 25 mass% MDEA + 5 mass% PZ at different temperature and pressure.

T(K)	P_{CO2} (kPa)	$\alpha_{CO_2 Exp.}$	$\alpha_{CO_2 Calc.}$	% Error
303	1.18	0.2958	0.3076	4.00
303	4.49	0.44 6	0.4337	3.32
303	13.41	0.6067	0.5620	7.37
303	26.34	0.7075	0.6478	8.44
303	44.46	0.7995	0.7151	10.56
303	63.36	0.8557	0.7597	11.22
303	82.46	0.8964	0.7919	11.66
303	90.49	0.9121	0.8031	11.95
303	99.29	0.9290	0.8140	12.37
313	0.42	0.1476	0.2051	39.00
313	2.81	0.2898	0.3290	13.54
313	9.68	0.4254	0.4563	7.28
313	20.24	0.5288	0.5473	3.51
313	35.44	0.6169	0.6211	0.68
313	52.76	0.6847	0.6745	1.49
313	74.99	0.7400	0.7215	2.51
313	90.27	0.7712	0.7459	3.29
323	1.01	0.1140	0.2170	90.28
323	4.47	0.2536	0.3180	25.40
323	7.49	0.3081	0.3666	18.99
323	12.93	0.3773	0.4259	12.88
323	21.49	0.4497	0.4875	8.41
323	32.49	0.513	0.5415	5.46
323	47.24	0.5756	0.5925	2.94
323	56.73	0.6078	0.6180	1.67
323	62.67	0.6298	0.6319	0.33
323	78.26	0.6783	0.6630	2.25
323	87.96	0.7116	0.6794	4.52

Table B.31: Comparison between published data from Dash & Bandyopadhyay (2016) and predicted CO_2 loading in aqueous solution of 22 mass% MDEA + 8 mass% PZ at different temperature and pressure.

T(K)	P_{CO2} (kPa)	$\alpha_{CO_2 Exp.}$	$\alpha_{CO_2 Calc.}$	% Error
303	0.37	0.1497	0.2140	42.96
303	1.08	0.2371	0.3504	47.77
303	2.51	0.3532	0.4168	18.00
303	4.49	0.4221	0.4703	11.41
303	5.68	0.4224	0.4936	16.86
303	12.15	0.5078	0.5746	13.16
303	21.02	0.590	0.6372	7.85
303	34.37	0.6623	0.6951	4.96
303	56.69	0.7456	0.7543	1.17
303	87.95	0.7909	0.8049	1.77
313	0.45	0.1481	0.2531	70.90
313	1.00	0.2258	0.2887	27.86
313	2.52	0.3256	0.3449	5.93
313	4.23	0.3849	0.3843	0.15
313	9.15	0.4831	0.4543	5.96
313	17.22	0.5682	0.5213	8.26
313	27.67	0.6358	0.5765	9.32
313	40.15	0.6899	0.6222	9.81
313	87.76	0.8065	0.7217	10.51
323	5.37	0.1501	0.2875	91.56
323	7.77	0.2554	0.4167	63.17
323	13.99	0.3704	0.4758	28.45
323	18.82	0.4255	0.5083	19.46
323	28.78	0.4959	0.5579	12.49
323	42.12	0.5574	0.6046	8.47
323	60.09	0.6209	0.6496	4.62
323	77.29	0.6614	0.6819	3.10
323	78.30	0.6737	0.6836	1.47
323	88.32	0.7135	0.6991	2.02
323	242.09	0.8439	0.8258	2.14
323	593.96	0.9632	0.9272	3.73
323	696.25	1.0 58	0.9442	10.57
323	1118.78	1.1874	0.9953	16.18
323	1246.29	1.2476	1.0074	19.25
393.2	21.7882	0.14	0.146	4.11
393.2	68.95	0.328	0.262	19.97
393.2	217.882	0.545	0.454	16.77
393.2	689.5	0.8	0.741	7.42
393.2	2178.82	1.165	1.183	1.54
393.2	6895	1.88	2.110	12.22
393.2	21.7882	0.14	0.146	4.11

Table B.31 (continued): Comparison between published data from Dash & Bandyopadhyay (2016) and predicted CO_2 loading in aqueous solution of 22 mass% MDEA + 8 mass% PZ at different temperature and pressure.

413.2	21.7882	0.03	0.082	72.21
413.2	68.95	0.2	0.154	23.16
413.2	217.882	0.42	0.288	31.37
413.2	689.5	0 698	0.534	23.43
413.2	2178.82	1.08	0.984	8.86
413.2	6895	1.8	1.927	7.06

Table B.32: Comparison between published data from Lee *et al.* (1972) and predicted CO_2 loading in aqueous solution of 0.5 N DEA at different temperature and pressure

T(K)	P_{CO2} (kPa)	$\alpha_{CO_2 Exp.}$	$\alpha_{CO_2 Calc.}$	% Error
273.15	0.6895	0. 8	0.614	9.69
273.15	2.17882	0.776	0.716	7.67
273.15	6. 95	0.875	0.826	5.59
273.15	21.7882	0.982	0.936	4.67
273.15	68.95	1.098	1.063	3.15
273.15	217.882	1.350	1.314	2.63
298.15	0.6895	0.475	0.452	4.90
298.2	2.17882	0 58	0.579	0.16
298.2	6.895	0.688	0.710	3.24
298.2	21.7882	0.802	0.839	4.58
298.2	68.95	0.925	0.960	3.84
298.2	217.882	1.065	1.110	4.27
298.2	689.5	1.368	1.445	5.59
298.2	2178.82	2.08	2.438	17.20
323.2	0.6895	0.302	0.243	19.41
323.2	2.17882	0.418	0.370	11.40
323.2	6.895	0.536	0.523	2.51
323.2	21.7882	0.662	0.685	3.47
323.2	68.95	0.803	0.843	4.94
323.2	217.882	0.963	0.997	3.54
323.2	689.5	1.180	1.225	3.78
323.2	2178.82	1.68	1.800	7.12
323.2	6895	2.695	3.561	32.15
348.2	0.6895	0.098	0.105	7.40
348.2	2.17882	0.212	0.182	14.13
348.2	6.895	0.34	0.300	11.74
348.2	21.7882	0.465	0.460	0.97
348.2	68.95	0.608	0.650	6.94
348.2	217.882	0.767	0.850	10.86

Table B.32 (continued): Comparison between published data from Lee *et al.* (1972) and predicted CO_2 loading in aqueous solution of 0.5 N DEA at different temperature and pressure

T(K)	P_{CO2} (kPa)	$\alpha_{CO_2 Exp.}$	$\alpha_{CO_2 Calc.}$	% Error
348.2	689.5	0.98	1.082	10.39
348.2	2178.82	1.361	1.51	11.21
348.2	6895	2.34	2.722	16.32
373.2	2.17882	0.058	0.081	39.41
373.2	6.895	0.165	0.145	12.32
373.2	21.7882	0.312	0.251	19.71
373.2	68 95	0.48	0.411	14.39
373.2	217.882	0.665	0.627	5.74
373.2	689.5	0.882	0.901	2.10
373.2	2178.82	1.24	1.320	6.47
373.2	6895	2.08	2.307	10.90

Table B.33: Comparison between published data from Lee *et al.*(1972) and predicted CO_2 loading in aqueous solution of 2 N DEA at different temperature and pressure

T(K)	P_{CO2} (kPa)	$\alpha_{CO_2 Exp.}$	$\alpha_{CO_2 Calc.}$	% Error
273.15	0.6895	0.543	0.510	6.08
273.15	2.17882	0.622	0.558	10.34
273.15	.895	0.708	0.616	13.05
273.15	21.7882	0.798	0.691	13.41
273.15	68.95	0.892	0.790	11.39
273.15	217.882	1.02	0.927	9.15
273.15	689.5	1. 35	1.155	1.77
273.15	2178.82	.285	1.694	31.79
298.2	0.6895	0.402	0.398	1.07
298.2	2.17882	0.48	0.473	1.47
298.2	6.895	0.568	0.545	4.13
298.2	21.7882	0.663	0.621	6.27
298.2	68.95	0.765	0.713	6.86
298.2	217.882	0.875	0.826	5.63
298.2	689.5	1.026	0.981	4.39
298.2	2178.82	1.172	1.261	7.63
298.2	6895	1.392	1.982	42.39
323.2	0.6895	0.258	0.217	15.81
323.2	2.17 82	0.34	0.314	7.74
323.2	6.895	0.44	0.415	5.63
323.2	21.7882	0.532	0.516	3.10
323.2	68.95	0.638	0.618	3.11
323.2	217.882	0.752	0.732	2.69
323.2	689.5	0.887	0.871	1.80

Table B.33 (continued): Comparison between published data from Lee *et al.*(1972) and predicted CO_2 loading in aqueous solution of 2 N DEA at different temperature and pressure

323.2	2178.82	1.053	1.079	2.44
348.2	0.6895	0.086	0.085	1.35
348.2	2.17882	0.163	0.146	10.20
348.2	6.895	0.248	0.236	4.81
348.2	21.7882	0.365	0.349	4.40
348.2	68.95	0.486	0.475	2.33
348.2	217.882	0.62	0.608	2.00
348.2	689.5	0.77	0.756	1.88
348.2	2178.82	0.947	0.949	0.21
348.2	6895	1.18	1.296	9.82
373.2	2.17882	0.035	0.057	63.21
373.2	6.895	0.112	0.103	7.59
373.2	21.7882	0.22	0.179	18.44
373.2	68.95	0.348	0.291	16.52
373.2	217.882	0.49	0.433	11.71
373.2	689.5	0.645	0.600	6.94
373.2	2178.82	0.83	0.807	2.77
373.2	6895	1.075	1.133	5.37
298.2	68.95	0.765	0.713	6.86
393.2	21.7882	0.1	0.094	6.21
393.2	68.95	0.212	0.168	20.92
393.2	217.882	0.343	0.283	17.47
393.2	689.5	0.507	0.446	12.12
393.2	2178.82	0.701	0.664	5.32
393.2	6895	0.946	0.998	5.47
413.2	68.95	0.093	0.091	2.08
413.2	217.882	0.23	0.167	27.20
413.2	689.5	0.395	0.296	24.99
413.2	2178.82	0.598	0.501	16.16
413.2	6895	0.84	0.842	0.23

Table B.34: Comparison between published data from Lee *et al.*(1972) and predicted CO_2 loading in aqueous solution of 5 N DEA at different temperature and pressure.

T(K)	P_{CO2} (kPa)	$\alpha_{CO_2 Exp.}$	$\alpha_{CO_2 Calc.}$	% Error
273.15	2.17882	0.493	0.511	3.6
273.15	6.895	0.551	0.533	3.30
273.15	21.78 2	0.61	0.563	7.75
273.15	68.95	0.673	0.607	9.75
273.15	217.882	0.746	0.677	9.31
273.15	689.5	0.822	0.792	3.65
273.1	2178.82	0.92	1.018	10.64
273.15	6895	1.02	1. 62	53.11

Table B.34 (continued): Comparison between published data from Lee *et al.*(1972) and predicted CO_2 loading in aqueous solution of 5 N DEA at different temperature and pressure.

298.15	0.6895	0.378	0.424	12.24
298.15	2.17882	0.43	0.467	8.55
298.15	6.895	0.49	0.500	2.02
298.15	21.7882	0.554	0.532	3.97
298.15	68.95	0.629	0.571	9.22
298.15	217.882	0.708	0.625	11.69
298.15	689.5	0.818	0.707	13.52
298.15	2178.82	0.919	0.846	7.89
298.15	6895	1.05	1.132	7.80
323.15	0.6895	0.24	0.266	10.89
323.15	2.17882	0.308	0.353	14.72
323.15	6.895	0.376	0.424	12.66
323.15	21.7882	0.444	0.478	7.67
323.15	68.95	0.525	0.526	0.18
323.15	217.882	0.608	0.578	4.91
323.15	689.5	0.702	0.647	7.83
323.15	2178.82	0.809	0.753	6.96
323.15	6895	0.94	0.947	0.78
348.15	0.6895	0.084	0.103	22.91
348.15	2.17882	0.158	0.176	11.66
348.15	6.895	0.23	0.270	17.41
348.15	21.7882	0.315	0.364	15.57
348.15	68.95	0.398	0.445	11.70
348.15	217.882	0.485	0.514	6.04
348.15	689.5	0.58	0.586	1.06
348.15	2178.82	0.691	0.680	1.63
348.15	6895	0.836	0.835	0.06
373.2	6.895	0.08	0.116	44.47
373.2	21.7882	0.164	0.197	19.94
373.2	68.95	0.265	0.299	12.86
373.2	217.882	0. 63	0.403	11.01
373.2	689.5	0.46	0.500	8.62
373.2	2178.82	0.587	0.601	2.47
373.2	6895	0.721	0.745	3.32
393.2	21.7882	0.073	0.097	32.58
393.2	68.95	0.153	0.172	12.21
393.2	217.882	0.253	0.276	9.01
393.2	689.5	0.355	0.394	11.08
393.2	2178.82	0.464	0.517	11.51
393.2	6895	0.602	0.669	11.07
413.2	217.882	0.122	0.157	28.90
413.2	689.5	0.241	0.265	9.93
413.2	2178.82	0.36	0.403	11.88
413.2	6895	0.515	0.574	11.37

Table B.35: Comparison between published data from Lee *et al.*(1972) and predicted CO_2 loading in aqueous solution of 6.5 N DEA at different temperature and pressure.

T(K)	P_{CO2} (kPa)	$\alpha_{CO_2 Exp.}$	$\alpha_{CO_2 Calc.}$	% Error
273.15	0.6895	0.485	0.493	1.58
273.15	2.17882	0.533	0.505	5.32
273.15	6.895	0.582	0.518	11.02
273.15	21.7882	0.638	0.536	15.96
273.15	68.95	0.695	0.564	18.80
273.15	217.882	0 758	0.610	19.52
273.15	689.5	0.833	0.689	17.26
273.15	2178.82	0.92	0.846	8.07
298.15	0.6895	0.372	0.446	19.82
298.15	2.17882	0.424	0.475	12.02
298.15	6.895	0.475	0.496	4.51
298.15	21.7882	0.524	0.516	1.48
298.15	68.95	0.587	0.540	7.95
298.15	217.882	0.65	0.575	11.55
298.15	689.5	0.737	0.630	14.53
298.15	2178.82	0.822	0.726	11.66
298.15	6895	0.932	0.924	0.81
323.15	2.17882	0.297	0.391	31.78
323.15	6.895	0.356	0.444	24.68
323.15	21.7882	0.419	0.481	14.72
323.15	68.95	0.484	0.511	5.63
323.15	217.882	0.555	0.544	1.95
323.15	689.5	0.638	0.589	7.70
323.15	2178.82	0.725	0.660	8.92
323.15	6895	0.84	0.795	5.39
348.15	0.6895	0.083	0.129	54.97
348.15	2.17882	0.157	0.218	38.59
348.15	6.895	0.225	0.316	40.54
348.15	21.7882	0.29	0.397	36.87
373.2	6.895	0. 78	0.141	80.53
373.2	21.7882	0.16	0.236	47.25
373.2	68.95	0.25	0.338	35.05
373.2	217.882	0.338	0.422	4.91
373.2	689.5	0.425	0.491	15.47
373.2	2178.82	0.528	0.559	5.88
373.2	6895	0.638	0.655	2.65
393.2	21.7882	0.065	0.115	76.22
323.15	2.17882	0.297	0.391	31.78
323.15	6.895	0.356	0.444	24.68
323.15	21.7882	0.419	0.481	14.72
323.15	68.95	0.484	0.511	5.63
323.15	217.882	0.555	0.544	1.95
323.15	689.5	0.638	0.589	7.70

Table B.35 (continued): Comparison between published data from Lee *et al.*(1972) and predicted CO_2 loading in aqueous solution of 6.5 N DEA at different temperature and pressure.

T(K)	P_{CO2} (kPa)	$\alpha_{CO_2 Exp.}$	$\alpha_{CO_2 Calc.}$	% Error
393.2	68.95	0.138	0.202	46.47
393.2	217.882	0.222	0.310	39.73
393.2	689.5	0.32	0.411	28.47
393.2	2178.82	0.423	0.501	18.32
393.2	6895	0.532	0.603	13.34
413.2	689.5	0.198	0.293	47.92
413.2	21 8.82	0.31	0.412	32.88
413.2	6895	0.44	0.536	21.81

Table B.36: Comparison between published data from Lee *et al.*(1972) and predicted CO_2 loading in aqueous solution of 8 N DEA at different temperature and pressure.

T(K)	P_{CO2} (kPa)	$\alpha_{CO_2 Exp.}$	$\alpha_{CO_2 Calc.}$	% Error
273.15	0.6895	0.483	0.494	2.21
273.1	2.17882	0.522	0.500	4.15
273.15	6.895	0.568	0.507	10.71
273.15	21.7882	0.617	0.516	16.31
273.15	68.9	0.668	0.531	20.52
273.15	217.882	0.728	0.556	23.61
273.15	689.5	0.782	0.603	22.87
273.15	2178.82	0.85	0.701	17.51
298.15	0.6895	0.368	0.464	26.21
298.15	2.17882	0.42	0.482	14.80
298.15	6.895	0.472	0.494	4.72
298.15	21.7882	0.525	0.505	3.88
298.15	68.95	0.58	0.517	10.94
298.15	217.882	0.64	0.534	16.54
298.15	689.5	0.702	0.564	19.62
298.15	2178.82	0.773	0.622	19.58
298.15	6895	0.855	0.747	12.68
323.15	0.6895	0.235	0.379	61.29
323.15	2.17882	0.298	0.430	44.40
323.15	6.895	0.355	0.463	30.30
323.15	21.7882	0.413	0.484	17.15
323.15	68.95	0.479	0.500	4.44
323.15	217.882	0.54	0.517	4.25
323.15	689.5	0.615	0.540	12.13
323.15	2178.82	0.68	0.581	14.61
323.15	6895	0.77	0.662	13.96
348.15	2.17882	0.156	0.295	89.15

Table B.36 (continued): Comparison between published data from Lee *et al.*(1972) and predicted CO_2 loading in aqueous solution of 8 N DEA at different temperature and pressure.

T(K)	P_{CO2} (kPa)	$\alpha_{CO_2 Exp.}$	$\alpha_{CO_2 Calc.}$	% Error
348.15	6.895	0.221	0.379	71.29
348.15	21.7882	0.29	0.432	49.09
348.15	68.95	0.362	0.468	29.19
348.15	217.882	0.435	0.494	13.51
348.15	689.5	0.52	0.519	0.21
348.15	2178.82	0.598	0.553	7.50
348.15	6895	0.683	0.616	9.88
373.2	6.895	0.077	0.105	36.45
373.2	21.7882	0.158	0.165	4.58
373.2	68.95	0.245	0.242	1.04
373.2	217.882	0.33	0.321	2.59
373.2	689.5	0.402	0.390	3.04
373.2	2178.82	0.499	0.448	10.15
373.2	6895	0.595	0.512	13. 8
393.2	217.882	0.2	0.366	82.76
393.2	689.5	0.29	0.435	50.10
393.2	2178.82	0.383	0.490	28.01
393.2	6895	0.485	0.552	13.77
413.2	2178.82	0.275	0.432	57.26
413.2	6895	0.4	0.511	27.81

Table B.37: Comparison between published data from Dawodu & Meisen (1994) and predicted CO_2 loading in aqueous solution of 4.2 M DEA at different temperature and pressure.

T(K)	P_{CO2} (kPa)	$\alpha_{CO_2 Exp.}$	$\alpha_{CO_2 Calc.}$	% Error
373.15	93	0.29	0.312	4.26
373.15	486	0.469	0.500	6.60
373.15	1110	0.595	0.605	1.69
373.15	2019	0.660	0.692	4.80
373.15	2660	0.684	0.737	7.74
373.15	3742	0.725	0.800	10.33

Table B.38: Comparison between published data from Haji-Sulaiman *et al.* (1998) and predicted CO_2 loading in aqueous solution of 2M DEA at different temperature and pressure.

T(K)	P_{CO2} (kPa)	$\alpha_{CO_2 Exp.}$	$\alpha_{CO_2 Calc.}$	% Error
303	0 098	0.183	0.21298	16.38
303	0.492	0.325	0.33951	4.47
303	1.119	0.388	0.40383	4.08
303	5.355	0.521	0.52005	0.18
303	10.726	0.591	0.57172	3.26
303	32.527	0.699	0.66052	5.51
303	54.213	0.73	0.70556	3.35
303	100.85	0.786	0.7649	2.68
313	0.095	0.172	0.143	16.41
313	0.474	0.278	0.260	6.32
313	1.039	0.32	0.326	2.02
313	5.265	0.459	0.464	1.18
313	10.665	0.538	0.523	2.68
313	32.147	0.597	0.618	3.59
313	53.829	0.662	0.665	0.53
313	104.727	0.727	0.730	0.46
323	0.09	0.133	0.091	31.16
323	0.449	0.152	0.184	21.56
323	1.04	0.272	0.251	7.64
323	5.11	0.398	0.395	0.67
323	10.035	0.473	0.458	3.04
323	30.358	0.546	0.563	3.18
323	50.763	0.611	0.613	0.38
323	98.17	0.688	0.680	1.13

Table B.39: Comparison between published data from Brahim Si Ali (2007) and predicted CO_2 loading in aqueous solution of 2M DEA at different temperature and pressure.

T(K)	P_{CO2} (kPa)	$\alpha_{CO_2\,Exp.}$	$\alpha_{CO_2\,Calc.}$	% Error
313.15	0.062	0.0	0.128	48.55
313.15	0.961	0.36	0.354	1.08
313.15	9.595	0.573	0.563	1.81
313.15	47.89	0.721	0.715	0.77
313.15	95.612	0.801	0.787	1.80
333.15	0.083	0.074	0.058	21.43
333.15	0.832	0.214	0.181	15.26
333.15	8.307	0.426	0.414	2.73
333.15	41.621	0.585	0.598	2.24
333.15	83.409	0.681	0.679	0.31
353.15	0.056	0.035	0.019	45.61
353.15	0.556	0.121	0.065	45.98
353.15	5.514	0.259	0.208	19.88
353.15	27.402	0.422	0.392	6.99
353.15	55.475	0.489	0.488	0.23

Table B.40: Comparison between published data from Brahim Si Ali (2007) and predicted CO_2 loading in aqueous solution of 1.98M DEA + 0.01M PZ at different temperature and pressure.

T(K)	P_{CO2} (kPa)	$\alpha_{CO_2\,Exp.}$	$\alpha_{CO_2\,Calc.}$	% Error
313.15	0.096	0.158	0.157	0.79
313.15	0.95948	0.342	0.353	3.29
313.15	9.59475	0.561	0.501	0.05
313.15	47.8898	0.711	0.713	0.31
313.15	95.4436	0.784	0.784	0.09
333.15	0.084	0.088	0.060	32.16
333.15	0.83241	0.206	0.182	11.60
333.15	8.32411	0.418	0.414	0.98
333.15	41.5366	0.584	0.596	2.01
333.15	83.0731	0.671	0.676	0.80
353.15	0.055	0.050	0.019	61.08
353.15	0.54972	0.104	0.066	36.62
353.15	5.54754	0.229	0.209	8.77
353.15	27.9057	0.387	0.395	2.04
353.15	55.8114	0.482	0.488	1.18

Table B.41: Comparison between published data from Brahim Si Ali (2007) and predicted CO_2 loading in aqueous solution of 1.9M DEA + 0.05M PZ at different temperature and pressure.

T(K)	P_{CO2} (kPa)	$\alpha_{CO_2 Exp.}$	$\alpha_{CO_2 Calc.}$	% Error
313.15	0.096	0.167	0.161	3.86
313.15	0.9578	0. 32	0.350	5.43
313.15	9.59475	0.55	0.554	0.26
313.15	47.7218	0.683	0.703	2.96
313.15	95.7796	0.763	0.773	1.32
333.15	0.084	0.088	0.064	26.73
333.15	0.82905	0.197	0.185	5.91
333.15	8.30731	0.413	0.411	0.56
333.15	41.6206	0.578	0.589	1.94
333.15	83.4091	0.665	0.668	0.46
353.15	0.056	0.068	0.022	67.62
353.15	0.5581	0.106	0.071	32.76
353.15	5.58114	0.232	0.213	8.32
353.15	27.8217	0.412	0.393	4.67
353.15	55.1395	0.489	0.482	1.28

Table B.42: Comparison between published data from Brahim Si Ali (2007) and predicted CO_2 loading in aqueous solution of 1.8M DEA + 0.1M PZ at different temperature and pressure.

T(K)	P_{CO2} (kPa)	$\alpha_{CO_2 Exp.}$	$\alpha_{CO_2 Calc.}$	% Error
313.15	0.096	0.193	0.165	14.26
313.15	0.95948	0.321	0.348	8.15
313.15	9.59475	0.538	0 545	1.32
313.15	47.7218	0.702	0.691	1.50
313.15	95.6116	0.772	0.759	1.62
333.15	0.083	0.097	0.070	27.75
333.15	0.83409	0.258	0.190	26.06
333.15	8.35771	0.431	0.408	5.49
333.15	41.2846	0.597	0.580	2.80
333.15	83.5771	0.652	0.658	0.99
353.15	0.056	0.060	0.025	58.63
353.15	0.55811	0.111	0.077	30.45
353.15	5.56434	0.252	0.217	13.95
353.15	27.7377	0.400	0.391	2.36
353.15	56.1473	0.501	0.480	4.22

Table B.43: Comparison between published data from Mondal (2009) and predicted CO_2 loading in aqueous solution of DEA + PZ.

Total amine concentration	ratio PZ	T(K)	P_{CO2} (kPa)	$\alpha_{CO_2 Exp.}$	$\alpha_{CO_2 Calc.}$	% Error
2	0.01	313	15.2	0.545	0.555	1.86
2	0.02	313	15.2	0.549	0.557	1.42
2	0.05	313	15.2	0.56	0.562	0.35
2	0.1	313	15.2	0.58	0.571	1.60
2	0.2	313	15.2	0.656	0.589	10.19
2.5	0 01	313	15.2	0.525	0.538	2.56
2.5	0.02	313	15.2	0.529	0.540	2.09
2.5	0 05	313	15.2	0.538	0.545	1.32
2.5	0.1	313	15.2	0.56	0.554	1.14
2.5	0.2	313	15.2	0.629	0.572	9.14
3	0.01	313	15.2	0.514	0.527	2.52
3	0.02	313	15.2	0.517	0.529	2.24
3	0.05	313	15.2	0.526	0.533	1.42
3	0.1	313	15.2	0.548	0.542	1.13
3	0.2	313	15.2	0.615	0.559	9.08
1	0.2	313	15.2	0.734	0.661	9.95
1.5	0.2	313	15.2	0.691	0.616	10.86
3.5	0.2	313	15.2	0.607	0.550	9.37
4	0.2	313	15.2	0.601	0.543	9.60
2	0.01	313	10.13	0.511	0.521	1.94
2	0.02	313	10.13	0.517	0.523	1.10
2	0.05	313	10.13	0.524	0.528	0.75
2	0.1	313	10.13	0.543	0.537	1.13
2	0.2	313	10.13	0.618	0.556	10.09
2	0.01	313	12.67	0.529	0.540	2.03
2	0.02	313	12.67	0.536	0.541	1.02
2	0.05	313	12.67	0.544	0.547	0.48
2	0.1	313	12.67	0.557	0.555	0.27
2	0.2	313	12.67	0.637	0.574	9.88
2	0.01	313	17.73	0.561	0.568	1.19
2	0.02	313	17.73	0.563	0.570	1.17
2	0.25	313	17.73	0.574	0.575	0.22
2	0.1	313	17.73	0.595	0.585	1.68
2	0.2	313	17.73	0.676	0.605	10.44
2	0.01	313	20.27	0.569	0.580	1.89
2	0.02	313	20.27	0.576	0.581	0.94
2	0.25	313	20.27	0.589	0.586	0.42
2	0.1	313	20.27	0.609	0.595	2.27
2	0.2	313	20.27	0.685	0.613	10.45
2	0.2	303	15.2	0.678	0.631	6.90
2	0.2	323	15.2	0.587	0.539	8.24
2	0.2	333	15.2	0.53	0.479	9.68
2	0.2	343	15.2	0.475	0.411	13.48
2	0.2	353	15.2	0.442	0.340	23.06

APPENDIX C

COMPARISON BETWEEN PUBLISHED AND PREDICTED SOLUTION PH

Table C.1: Comparison between published data from Brahim Si Ali (2007) and predicted solution pH for aqueous solution of 2M DEA.

T(K)	P_{CO2} (kPa)	$pH_{Exp.}$	$pH_{Calc.}$	% Error
313.15	0.961	9.3	8.65	7.01
313.15	9.595	8.72	8.05	7.6
313.15	47.89	8.25	7.58	8.07
313.15	95.612	7.09	7.36	3.87
333.15	0.832	9.1	8.71	4.24
333.15	8.307	8.49	8.12	4.35
333.15	41.621	.08	7.67	5.05
333.15	83.409	7.88	7.46	5.28
353.15	0.556	9.63	8.84	8.20
353.15	5.514	9	8.27	8.15
353.15	27.402	7.95	7.84	1.42
353.15	55.475	7.76	7.64	1.57

Table C.2: Comparison between published data from Brahim Si Ali (2007) and predicted solution pH for aqueous solution of 1.98M DEA + 0.01M PZ.

T(K)	P_{CO2} (kPa)	$pH_{Exp.}$	$pH_{Calc.}$	% Error
313.15	0.95948	9.24	8.65	6.38
313.15	9.59475	.59	8.05	6.28
313.15	47.8898	8.23	7.58	7.84
313.15	95.4436	7.99	7.3	7.82
313.15	0.83241	9.12	8.72	4.41
333.15	8.32411	8.57	8.12	5.23
333.15	41.5366	8.13	7.67	5.61
333.15	83.0731	7.87	7.47	5.13
353.15	0.54972	10.16	8.85	12.90
353.15	5.54754	8.87	8.27	6.79
353.15	27.9057	8.34	7.83	6.08
353.15	55.8114	8.22	7.64	7.09

Table C.3: Comparison between published data from Brahim Si Ali (2007) and predicted solution pH for aqueous solution of 1.9M DEA + 0.05M PZ.

T(K)	P_{CO2} (kPa)	$pH_{Exp.}$	$pH_{Calc.}$	% Error
313.15	0.9578	7.82	8.66	10.73
313.15	9.59475	8.13	8.06	0.92
313.15	47.7218	7.01	7.59	8.23
313.15	95.7796	7.38	7.36	0.22
333.15	0.82905	7.81	8.73	11.80
333.15	8.30731	8.27	8.13	1.72
333.15	41.6206	7.01	7.68	9.50
333.15	83.4091	7.5	7.47	0.45
353.15	0.5581	8.02	8.87	10.60
353.15	5.58114	8.73	8.28	5.18
353.15	27.8217	7.14	7.84	9.80
353.15	55.1395	7.74	7.64	1.23

Table C.4: Comparison between published data from Brahim Si Ali (2007) and predicted solution pH for aqueous solution of 1.8M DEA + 0.1M PZ.

T(K)	P_{CO2} (kPa)	$pH_{Exp.}$	$pH_{Calc.}$	% Error
313.15	0.95948	7.99	8.67	8.50
313.15	9.59475	7. 7	8.06	3.74
313.15	47.7218	6.81	7.59	11.44
313.15	95.6116	7.08	7.36	4.02
333.15	0.83409	7.9	8.75	10.71
333.15	8.35771	8.34	8.13	2.46
333.15	41.2846	7.02	7.68	9.44
333.15	83.5771	7.19	7.4	3.87
353.15	0.55811	7.92	8.90	12.35
353.15	5.56434	8.03	8.29	3.27
353.15	27.7377	7.08	7.85	10.85
353.15	56.1473	7.4	7.64	3.31

Table C.5: Comparison between published data from Brahim Si Ali (2007) and predicted solution pH for aqueous solution of 1M PZ.

T(K)	P_{CO2} (kPa)	$pH_{Exp.}$	$pH_{Calc.}$	% Error
313.15	0.965	8.49	8.93	5.13
313.15	9.578	7.73	8.24	6.65
313.15	47.386	6.31	7.64	21.16
313.15	95.108	6.9	7.36	6.66
333.15	0.836	8.49	8.99	5.93
333.15	8.341	7.74	8.36	8.04
333.15	41.201	6.54	7.81	19.41
333.15	82.737	6.82	7.54	10.50
353.15	0.555	8.57	9.14	6.68
353.15	5.598	8.09	8.55	5.70
353.15	27.234	6.71	8.06	20.16
353.15	55.139	7.07	7.81	10.49

Table C.6: Comparison between published data from Brahim Si Ali (2007) and predicted solution pH for aqueous solution of 2M MDEA.

T(K)	P_{CO2} (kPa)	$pH_{Exp.}$	$pH_{Calc.}$	% Error
313.15	0.9595	9.27	8.92	3.76
313.15	9.5612	9.04	8.41	6.97
313.15	47.7218	8.54	7.99	6.43
313.15	95.6116	7.15	7.78	8.75
333.15	0.8307	9.09	8.90	2.10
333.15	8.3073	8.72	8.38	3.85
333.15	41.4526	8.4	8.00	4.75
333.15	82.9052	8.23	7.82	5.00
353.15	0.5514	9.83	8.96	8.90
353.15	5.5475	8.49	8.44	0.64
353.15	27.5697	8.86	8.06	9.03
353.15	55.4754	8.6	7.89	8.24

Table C.7: Comparison between published data from Brahim Si Ali (2007) and predicted solution pH for aqueous solution of 1.98M MDEA + 0.01M PZ.

T(K)	**P_{CO2} (kPa)**	$pH_{Exp.}$	$pH_{Calc.}$	**% Error**
313.15	0.9544	9.55	8.92	6.61
313.15	9.5444	9 06	8.41	7.23
313.15	47.5538	8.55	7.99	6.61
313.15	95.2756	8.24	7.77	5.70
333.15	0.8307	9.36	8.90	4.92
333.15	8.2569	8.82	8.38	4.95
333.15	41.2 06	8.41	8.00	4.89
333.15	83.0731	7.83	7.81	0.2
353.15	0.5615	9.24	8.96	3.06
353.15	5.5475	8.92	8.44	5.42
353.15	27.5697	8.45	8.06	4.63
353.15	55.3075	8.45	7.89	6.63

Table C.8: Comparison between published data from Brahim Si Ali (2007) and predicted solution pH for aqueous solution of 1.9M MDEA + 0.05M PZ.

T(K)	**P_{CO2} (kPa)**	$pH_{Exp.}$	$pH_{Calc.}$	**% Error**
313.15	0.9544	7.86	8.90	13.26
313.15	9.578	8. 8	8.38	0.03
313.15	47.5538	6.88	7.96	15.69
313.15	95.7796	7.51	7.74	3.08
333.15	0.8324	7.87	8.90	13.11
333.15	8.2905	8.34	8.37	0.39
333.15	41.2846	6.99	7.98	14.20
333.15	83.2411	7.62	7.80	.30
353.15	0.5531	7.88	8.98	13.96
353.15	5.5475	8.35	8.44	1.08
353.15	27.4858	6.98	8.05	15.38
353.15	55.6434	7.62	7.88	3.41

Table C.9: Comparison between published data from Brahim Si Ali (2007) and predicted solution pH for aqueous solution of 1.8M MDEA + 0.1M PZ.

T(K)	P_{CO2} (kPa)	$pH_{Exp.}$	$pH_{Calc.}$	% Error
313.15	0.9511	7.8	8.88	13.91
313.15	9.5948	7.9	8.35	5.09
313.15	47.6378	6.75	7.93	17.44
313.15	95.7796	7.07	7.71	9.03
333.15	0.8341	7.78	8.90	14.43
333.15	8.3073	7.94	8.36	5.29
333.15	41.4526	6.9	7.96	15.40
333.15	83.409	7.13	7.77	9. 2
353.15	0.5548	7.83	9.00	14.91
353.15	5.5811	8.21	8.44	2.82
353.15	27.7377	6.98	8.04	15.25
353.15	55.4754	7.53	7.87	4.52

Table C.10: Comparison between published data from Derks *et al.* (2010) and predicted solution pH for aqueous solution of 4 kmol/m^3 MDEA + 0.6 kmol/m^3 PZ.

T(K)	P_{CO2} (kPa)	$pH_{Exp.}$	$pH_{Calc.}$	% Error
313	0.72	9.61	8.99	6.46
313	2.07	9.38	8.78	6.41
313	2.7	9.35	8.73	6.67
313	4.36	9.24	8.63	6.58
313	5.24	9.21	8.60	6.68
313	7	9.14	8.54	6.60
313	7.33	9.14	8.53	6.70
313	9.38	9.09	8.48	6.74
313	8.65	9.07	8.49	6.35
313	2.6	9.07	8.42	7.21
313	12.8	9.02	8.41	6.74
313	25.3	8.88	8.27	6.92
313	39	8.78	8.17	6.98
313	39	8.76	8.17	6.77
313	58.4	8.65	8.07	6.70
313	60.4	8.65	8.06	6.80
313	78.5	8.65	8.00	7.56
313	80	8.58	7.99	6.86
313	89.7	8.62	7.96	7.64

Table C.11: Comparison between published data from Derks *et al.* (2010) and predicted solution pH for aqueous solution of 2.8 kmol/m^3 MDEA + 0.7 kmol/m^3 PZ.

T(K)	P_{CO2} (kPa)	$pH_{Exp.}$	$pH_{Calc.}$	% Error
303	0.51	9.58	9.12	4.84
303	0.96	9.49	8.99	5.30
303	1.75	9.33	8.86	5.00
303	2.61	9.28	8.78	5.38
303	4.16	9.13	8.68	4.90
303	5.23	9.1	8.63	5.13
303	6.8	8.99	8.58	4.60
303	8.65	8.95	8.52	3.81
303	10.2	8.86	8.49	6.75
303	9.4	9.1	8.50	6 55
303	10.7	9.52	8.47	10.98
303	15.2	8.92	8.39	5.91
303	25.7	8.81	8.26	6.20
303	36.1	9.16	8.18	10.74
303	32.1	9.17	8.21	10.50
303	38.9	8.65	8.16	5.71
303	56.4	8.52	8.05	5.48
303	73.7	8.43	7.97	5.40
303	70.4	8.91	7.99	10.34
303	93.8	8.34	7.90	5.26
303	96.9	8.81	7.89	10.43
303	100.1	8.31	7.88	5.16
323	0.68	9.66	9.01	6.72
323	1.05	9.52	8.92	6.33
323	2	9.52	8.78	7.78
323	3.19	9.3	8.68	6.67
323	4.68	9.33	8.60	7.85
323	6.99	9.15	8.51	6.98
323	8.37	9.15	8.47	7.40
323	19.7	9.01	8.28	8.06
323	32.8	8.91	8.17	8.34
323	45.8	8.77	8.09	7.80
323	60.3	8.72	8.02	8.06
323	69.5	8.65	7.98	7.73
323	84	8.62	7.93	7.99
323	94.5	8.55	7.90	7.61

Table C.12: Comparison between published data from Derks *et al.* (2010) and predicted solution pH for aqueous solution of 0.5 kmol/m^3 MDEA + 1.5 kmol/m^3 PZ.

T(K)	P_{CO2} (kPa)	$pH_{Exp.}$	$pH_{Calc.}$	% Error
298	0.25	10.12	9.3149	7 96
298	1.02	9.68	8.9920	7.11
298	1. 5	9.57	8.8921	7.08
298	7.15	9.02	8.4993	5.77
298	9.02	8.98	8.4340	6.08
298	10.6	8.35	8.3875	0.45
298	26.8	8.02	8.0992	0.99
298	29.1	7.98	8.0718	1.15
298	53.7	7.75	7.8578	1.3
298	81.1	7.58	7.7047	1.65
298	80.1	7.58	7.7094	1.71
298	102	7.47	7.6168	1.96
298	110	7.44	7.5874	1.98
313	0.45	9.24	9.1580	0.89
313	1.38	8.97	8.9006	0.77
313	3.76	8.65	8.6597	0.11
313	9.24	8.34	8.4283	1.06
313	8.1	8.6	8.4634	1.59
313	9.7	8.55	8.4152	1.58
313	20.1	8.29	8.2097	0.97
313	36.9	8.05	8.0227	0.34
313	38.8	8.07	8.0065	0.79
313	59.2	7.91	7.8658	0.56
313	64.1	7.86	7.8384	0.27
313	79.8	7.79	7.7615	0.37
313	80.8	7.75	7.7570	0.09
313	96	7.88	7.6949	2.35
313	98.8	7.7	7.6844	0.20